Mechanical Design, 4D Printing, and Programming of Smart Composite Actuators

Mohammadreza Lalegani Dezaki

M.Sc., B.Sc.

A thesis submitted in partial fulfilment of the requirements of Nottingham Trent University for the degree of Doctor of Philosophy

September 2024

Declaration

Acknowledgement

I wish to express my sincere gratitude to the individuals whose guidance and support were instrumental in completing my PhD thesis.

I am deeply indebted to my director of study and supervisors for their invaluable expertise, patience, and unwavering encouragement. Mahdi Bodaghi's insightful contributions were essential in refining my research. His collective mentorship has been a cornerstone of my academic growth.

I am eternally grateful to my wife, Saghi, for her steadfast support and understanding throughout this challenging endeavour. Additionally, I would like to acknowledge the unconditional love and support of my family, Ayat, Mozhgan, Amin, and Atefeh, whose sacrifices have enabled me to pursue my academic goals. Their belief in my abilities has been an invaluable source of motivation.

I extend my appreciation to the PhD students and technicians within the Engineering department at Nottingham Trent University for their camaraderie and collaboration. The stimulating intellectual environment fostered by the department has significantly enriched my research experience. I would like to thank Nottingham Trent University for providing the necessary resources and a conducive academic environment to facilitate my research.

I am profoundly aware that this achievement would not have been possible without the collective support of those mentioned above.

LIST OF PUBLICATIONS

1. **Lalegani Dezaki M**, Bodaghi M. 2024. 4D printing and programming of continuous fibre-reinforced shape memory polymer composites. *European polymer journal*, 21010. Available at:1016/j.eurpolymj.2024.112988.

2. **Lalegani Dezaki M**, Zolfagharian A, Demoly F, Bodaghi M. 2024. Human–Material Interaction Enabled by Fused Filament Fabrication 4D Printing. *Advanced engineering materials*, 202410. Available at:1002/adem.202301917.

3. **Lalegani Dezaki M**, Bodaghi M. A Review of Recent Manufacturing Technologies for Sustainable Soft Actuators. 2024. *Int J of Precis Eng and Manuf -Green Tech*, 10(6):1661-171010. Available at: 1007/s40684-023-00533-4.

4. **Lalegani Dezaki M**, Bodaghi M. Magnetorheological elastomer-based 4D printed electroactive composite actuators. 2023. *Sensors and actuators. A. Physical*. ,349:11406310. Available at:1016/j.sna.2022.114063.

5. **Lalegani Dezaki M**, Bodaghi M. Sustainable 4D printing of magneto-electroactive shape memory polymer composites. 2023. *Int J Adv Manuf Technol*, 126(1-2):35-4810. Available at:1007/s00170-023-11101-0.

6. **Lalegani Dezaki M**, Bodaghi M. Shape memory meta-laminar jamming actuators fabricated by 4D printing. 2023. *Soft matter*, 19(12):2186-22310. Available at: 1039/d3sm00106g.

7. **Lalegani Dezaki M**, Sales R, Zolfagharian A, Yazdani Nezhad H, Bodaghi M. Soft pneumatic actuators with integrated resistive sensors enabled by multi-material 3D printing. 2023. *Int J Adv Manuf Technol*, 128(9-10):4207-422110. Available at:1007/s00170-023-12181-8.

8. **Lalegani Dezaki M**, Bodaghi M. Magnetically controlled bio-inspired elastomeric actuators with high mechanical energy storage. 2023. *Soft matter*, 19(16):315-33210. Available at:1039/d3sm00266g.

9. **Lalegani Dezaki M**, Bodaghi M, Serjouei A, Afazov S, Zolfagharian A. Soft Pneumatic Actuators with Controllable Stiffness by Bio-Inspired Lattice Chambers and Fused Deposition Modeling 3D Printing. 2023. *Advanced engineering materials*, 25(6):n Available at: /a10.1002/adem.202200797.

10. **Lalegani Dezaki M**, Bodaghi M, Serjouei A, Afazov S, Zolfagharian A. Adaptive reversible composite-based shape memory alloy soft actuators. 2022. *Sensors and actuators. A. Physical*., 345:11377910. Available at:1016/j.sna.2022.113779.

11. **Lalegani Dezaki M**, Bodaghi M. Soft Magneto-Responsive Shape Memory Foam Composite Actuators. 2022. *Macromolecular materials and engineering,* 307(11):n Available at: /a10.1002/mame.202200490.

12. **Lalegani Dezaki M**, Hatami S, Zolfagharian A, Bodaghi M. A pneumatic conveyor robot for color detection and sorting. 2022. *Cognitive robotics*, 2:60-7210. Available at:1016/j.cogr.2022.03.001.

13. Moradi M, **Lalegani Dezaki M**, Kheyri E, Rasouli SA, Aghaee Attar M, Bodaghi M. Simultaneous FDM 4D printing and magnetizing of iron-filled polylactic acid polymers. 2023. *Journal of magnetism and magnetic materials*, 568:17042510. Available at: 1016/j.jmmm.2023.170425.

14. Zolfagharian A, Gharaie S, Kouzani AZ, Lakhi M, Ranjbar S, **Lalegani Dezaki M**, Bodaghi M. Silicon-based soft parallel robots 4D printing and multiphysics analysis. 2022. *Smart materials and structures*,31(11):11503010. Available at:1088/1361-665X/ac976c.

Abstract

The rise of four-dimensional (4D) printing addressed the growing need for rapid and replicable prototyping of bespoke structures with intricate geometries. Smart materials explore advancements in the creation and control of soft, responsive, strong, and functional actuators designed for safe interaction with delicate environments. The mechanical design, programming, and 4D printing of stimuli-responsive shape memory polymers (SMPs) for smart composite actuators are the main areas of interest in this work. The activation of smart actuators can be done via temperature, electricity, magnetic fields, and pneumatic air in this study. This thesis aims to develop a method for designing and constructing smart composite actuators with customized geometrical, functional, and control properties. It leverages existing 4D printing techniques to fabricate actuators from SMPs and shape memory polymer composites (SMPCs).

The research investigates and controls the actuation of these 3D dynamic structures by manipulating the stimuli components. The study describes 4D-printed composite actuators with functionalities including remote programmability, precise controllability, shape manipulation, and shape locking. This work presents a novel approach to developing 4D-printed shape memory composite actuators using fused deposition modelling (FDM). This thesis delves into the selection of suitable materials for 4D printing smart composite actuators. It achieves this through a comprehensive review of existing 4D printing technologies, smart actuator designs, and identifying materials that excel in both printability and functionality. Also, the thesis specifically evaluates actuators, focusing on their material properties, fabrication methods, and responsiveness to various stimuli. This thesis also examines how FDM 4D printing is used to fabricate smart composite actuators. These actuators hold the potential for integration into various applications based on requirements.

Shape memory magneto-electroactive composite actuators are developed accordingly. These composite smart actuators offer remote programmability, enabling control over shape morphing and subsequent shape locking. It achieves this by utilizing 4D-printed SMPs/SMPCs as hinges, enabling the transformation of a planar sheet into a 3D structure. 4D-printed SMPC structures offer cost-effective, multi-stable designs that can be remotely programmed at high temperatures. These structures exhibit the capacity to repeatedly transition between predetermined temporary and permanent configurations. This prevents material waste and enables several designs in a single construction. Understanding magnetic response, SMPC mechanics, and the manufacturing concept form the basis of the strategy. Switchable multi-stable structures have the advantage of lowering material waste, effort, and energy consumption while boosting productivity in industries like packing.

Composite shape memory meta-laminar jamming (MLJ) actuators fabricated using negative air pressure and SMPs are developed as well. These MLJ actuators exhibit enhanced stiffness at both room and high temperatures when activated with negative air pressure. Additionally, they possess remote programmability and shape-locking functionalities. MLJ actuators have an advantage over traditional LJ actuators in that the actuator can be stimulated without a constant negative air pressure. The actuator is able to lift and hold objects with a variety of weights and shapes without the need for power input. This actuator has proven its adaptability in hypothetical uses by serving as both a gripper and an end-effector.

The final objectives of this thesis centre around the development of a fabrication method for 4D-printed SMPC actuators exhibiting high mechanical properties and dynamic responses. This groundbreaking method can be applied universally to all types of SMPC actuators, resulting in superior strength and durability. To achieve this, the research focuses on developing FDM 4D printing of SMPCs for continuous fibre-reinforced composite (CFRC) actuators. This approach paves the way for the development of robust shape memory smart composite actuators. The ability to modify the polymer matrix allows for actuation via diverse stimuli, exceeding the limitations of traditional SMPs in terms of strength. These results show how versatile 4D-printed CFRCs may be in a range of domains, including mechanical and biological sciences as well as human-material interaction. By minimising material use and waste, the approach promotes sustainability by creating goods that are lightweight and reusable.

This dissertation explores the synergy between mechanical design, 3D/4D printing, and the unique properties of SMPs/SMPCs. By leveraging FDM 4D printing with SMPCs, it presents novel composite actuators/structures with significantly expanded functionalities. By showcasing 4D printing's potential for practical uses, this study advances the field of smart actuators.

TABLE OF CONTENTS

LIST OF TABLES

LIST OF FIGURES

ABBREVIATIONS AND SYMBOLS

1D	One-dimensional
2D	Two-dimensional
3D	Three-dimensional
4D	Four-dimensional
AF	Aramid fibre
CF	Carbon fibre
CNF	Carbon nanofiber
CNT	Carbon nanotube
CAD	Computer-aided design
CAM	Computer-aided manufacturing
CFRC	Continuous fibre-reinforced composite
CPLA	Conductive polylactic acid
DMA	Dynamic mechanical analyser
DC	Direct current
DIW	Direct ink writing
EA	Energy absorption
EDS	Energy-dispersive spectroscopy
FGM	Functionally graded material
FDM	Fused deposition modelling
FG	Fibreglass
T_g	Glass transition temperature
LJ	Laminar jamming
LCE	Liquid crystal elastomer
MRE	Magnetorheological elastomer
MPLA	Magnetic polylactic acid
MLJ	Meta-laminar jamming
MM	Multi-material
PLA	Polylactic acid
PU	Polyurethane
PEU	Polyester urethane
PMMA	Polymethyl methacrylate
PIY	Print it Yourself
SEM	Scanning electron microscopy
SME	Shape memory effect
SMP	Shape memory polymer
SMPC	Shape memory polymer composite
SLS	Selective laser sintering
SEA	Specific energy absorption
SRM	Stimuli-responsive material
STL	Stereolithography
TPU	Thermoplastic polyurethane

Chapter 1

Introduction

This chapter covers the methods for gathering and analysing data as well as the study topic, aim, questions, and objectives. An outline of the thesis is also included.

1.1. Overview of four-dimensional (4D) printing

The inspiration for this research comes from the field of four-dimensional (4D) printing (Ge, Qi and Dunn 2013). Here, the "fourth dimension" signifies how three-dimensional (3D) printed objects can transform over time in response to external triggers like heat (Momeni, et al. 2017). 4D printing utilises the existing 3D printing methods to create stimuli-responsive materials (SRMs). This essentially involves designing, creating, and manipulating the dynamic behaviour of soft, active structures through 3D printing. Functional structures and devices are created directly from the printing process, bypassing the need for assembly. This eliminates challenges like tolerances, errors, and energy consumption common during assembly. Additionally, 4D printing allows for direct integration with other components during printing such as electronic parts (Shahbazi, et al. 2023). This eliminates design limitations when separate electronic components need to be assembled with different parts.

A two-step iterative procedure is used in the formal development of smart composite actuators. Model-based inquiry and tangible prototype fabrication are integrated into this process. Computer-aided design (CAD) software tools are usually used in the first design exploration stage (Regassa Hunde and Debebe Woldeyohannes 2022). While these techniques are very helpful during the design stage, they might not offer thorough knowledge in scenarios where complex interactions between the actuator and its surroundings occur. This is especially true for habitats like those that are difficult to reproduce or model, including those that are located underwater or on land, or those that are classified as terrestrial or aquatic. Rapid 3D/4D printing can be used to get around this restriction. This approach makes it easier to test different design modifications using real prototypes. Also, developing actuators with both appropriate mechanical qualities and actuation capabilities is the main goal in the field of this research.

Smart soft actuators offer a unique combination of adaptability and gentle interaction, allowing soft robots to safely handle fragile objects. Smart actuators have historically been produced using traditional methods like moulding and micro-moulding, but these approaches need manual device fabrication, additional post-processing and assembly procedures, and numerous iterations to reach optimal manufacturing maturity (Zolfagharian, et al. 2016). As a result, several academics are focusing on creating smart actuators that would fulfil the mechanical and control requirements of soft robots. 4D printing is an alternative way to create smart actuators that are suitable for a variety of uses (Kuang, et al. 2019). The range of actuation methods seen in 4D-printed actuators allows for their differentiation. These processes can be broadly classified into multiple subcategories, such as those that are stimulated by light (Leist and Zhou 2016), pH (Sadasivuni, Deshmukh and AlAli AlMaadeed 2019), electrical (Dong, X., et al. 2022), thermal (Bodaghi, M., Damanpack and Liao 2017), pneumatic (Zolfagharian, Mahmud, et al. 2020), and magnetic field (Zhang, Fenghua, et al. 2019).

The ability to create unique soft structures that can be 4D-printed in a single step can reduce the time needed between developing and installing smart actuators, which is another advantage of using 4D printing technology over traditional methods. Furthermore, they make

it possible to combine all actuator parts into one structure, doing away with the need for external joints, glue, and fasteners. This leads to a reduction in the number of distinct components, post-processing procedures, and manufacturing duration. During the printing process, 4D-printed smart actuators can be designed to incorporate actuation and particular functionality into printable objects. To produce tunable mechanical, electrical, and other functional qualities, strict control over the composition and dynamics of the material is therefore necessary.

Common materials utilized in the printing of smart actuators include hydrogels and elastomers (Peng, B., et al. 2021), shape memory polymers (SMPs) (Subash and Kandasubramanian 2020), liquid crystal elastomers (LCEs) (Chen, M., et al. 2023), and shape memory polymer composites (SMPCs) (Khalid, Arif, Noroozi, et al. 2022). Several 3D/4D printing techniques have been used to create smart actuators using these materials. The primary 4D printing techniques used to create smart soft actuators include fused deposition modelling (FDM) (Carrell, Gruss and Gomez 2020), direct ink writing (DIW) (Wan, et al. 2020), selective laser sintering (SLS) (Kafle, et al. 2021), vat photopolymerization (Andreu, et al. 2021), and inkjet printing (Nachimuthu and P.K. 2023). Each of these methods has special qualities and capacities for creating smart actuators. This thesis employed an FDM 3D/4D printing technique due to its versatility and capabilities.

The FDM method can fabricate complex structures with a wide range of materials, encompassing both rigid metallic materials and soft polymeric composite materials (Vyavahare, et al. 2020). Furthermore, it enables control over the resolution of the structures with an acceptable degree of precision. Notably, FDM was chosen due to its cost-effectiveness compared to alternative methods with similar capabilities. 3D/4D printing of SMPCs is appealing because of their potential responsiveness to a broad range of activation stimuli, higher strength compared to SMPs, and comparatively fast reaction time. SMPCs are a class of polymeric materials that exhibit a unique property. By providing a particular stimulus, they can be distorted into a transient shape and then stimulated to regain their original form. Different heat sources, including local energy absorption, uniform heating, and Joule heating, can cause heat-activated SMPCs to react. In homogenous sheets or laminated composites, SMPCs can produce discretely folded structures. This dissertation explores the use of SMPCs in 4D printing, considering the previously described advantages of FDM printing of SMPCs.

1.2. Study significance

A significant portion of the study is dedicated to mechanical design, programming, and controlling the stimuli-responsive actuators within the developed 4D-printed actuators. Previous studies showed a variety of amazing 4D-printed structures and tools with shape-changing capabilities. All these 4D-printed transformable constructions, however, were primarily intended for visual exposition and concentrated on showcasing shape memory potential. Moreover, FDM-produced SMPs exhibit inferior mechanical properties compared to those fabricated using alternative 3D printing methods. Furthermore, prior studies have explored the design of actuators from elastomeric materials like silicones, this work emphasizes the under-investigated area of fabrication using SMP and SMPC materials using the FDM procedure.

The focus lies on identifying and utilizing SMP/SMPC materials that are well-suited for FDM 4D printing applications. Following material selection, the research delves into the fabrication of composite actuators using 3D/4D printing. Selecting the SMP or SMPCs with the appropriate transition temperature, modulus range, shape-fixity ratio, shape-recovery ratio, and good mechanical properties is crucial to creating structures and devices with the intended functions. Consequently, a 3D printing method known as FDM is utilised since it works with a variety of thermoplastics. The dynamic structures that have been designed are triggered by heating, Joule heating, magnetic fields, and pneumatic systems. This research introduces a novel methodology for producing robust, dual-stimulus-responsive, 4D-printed composite actuators and their potential applications.

1.3. Aim and objectives

The primary goal of this research is to make use of 3D/4D printing technology to manufacture SMPCs and SMPs. To comprehend the behaviour of the selected materials, their mechanical properties are examined. The shape memory properties and shape memory effect (SME) characteristics of the selected materials are investigated by shape programming. Next, from design to final product with their applications, characterization, and control of specially designed 4D-printed composite actuators are finished. Meanwhile, the proposed research topic must be addressed since it would provide a novel way to custom design and control smart actuators produced in a single fabrication step using 3D printing technology. This study is divided into smaller tasks to visualise a trajectory route to achieving its goal. These are the tasks that need to be completed:

- Investigating SMP and SMPC, focusing on their mechanical properties.
- Assessing the printing conditions of responsive materials by adjusting the settings of the FDM 3D printer.
- Designing and developing an innovative FDM 4D-printed composite actuator.
- Incorporating a secondary stimulus alongside the heating actuation method. This would enable more versatile control over the actuator's behaviour.
- Improving the mechanical properties of the composite actuators. This could involve increased strength, stiffness, or other desired mechanical characteristics.
- Analysing the behaviour and programming of SMP/SMPC actuators.
- Investigating an identification model for the system to regulate the mechanical behaviour of the actuators.
- Activating SMP and SMPC materials through various external stimuli, including heat, electricity, magnetic fields, pneumatic air, or combinations thereof.
- Demonstrating the applications of the developed actuators.

1.4. Thesis structure

This thesis is made up of publications split into seven chapters. **Table 1.1** provides information on the flow and connections between the chapters to help the reader navigate the thesis. **Chapter 1** outlines the research question and offers a summary of the thesis. It delves into the application of 4D printing of composite actuators and their advantages. This chapter examines the aim, objectives, and requirements of 4D printing within the field of composite soft actuators. It highlights the custom functional geometry, controllability, and various applications of these actuators. **Chapter 2** explores the feasibility of using FDM 4D-printed actuators by reviewing recent advancements and relevant literature**.** It concludes by demonstrating how the development of novel composite actuators in this study enhances performance and mechanical properties. Also, it shows that SMPs and SMPCs in FDM are ideal candidates for this research. Furthermore, it identifies the incorporation of SMPCs with shape-locking features, multi-stimuli responsiveness, and increased strength as effective composite actuators for control purposes and various applications. In **Chapter 3,** the development of a 4D-printed composite actuator employing magnetorheological elastomer and electrical stimulation of SMPCs is examined. The actuators are characterized by examining crucial factors that influence their actuation performance, such as multi-stimulus

capabilities, shape change abilities, remote programming, and applications of the actuators. **Chapter 4** introduces 4D-printed electro-magneto active SMPC actuators, highlighting their shape-morphing and remote programming capabilities. The use of these actuators offers benefits such as reduced material usage, improved printing quality, greater design freedom, and minimized material waste. Moreover, **Chapter 5** investigates 4D-printed multi-stimulus meta-laminar jamming (MLJ) composite actuators, focusing on their features, remote programming capabilities, and shape-locking mechanisms. **Chapter 6** covers the programming of SMPC actuators with continuous fibre and FDM 4D printing, emphasising the reduction of material consumption and increase in strength and reusability. Since SMPs have low and poor mechanical properties, a method is developed to produce SMPCs with high mechanical strength. The applications of these printed SMPC actuators are discussed accordingly. The developed method can be used to develop all previous composite actuators. However, the actuators will be stronger and stiffer due to the existence of continuous fibre. The thesis is concluded in **Chapter 7** with a discussion of the importance of the main findings and recommendations for future study directions.

Table 1.1. Overview of thesis chapters

Chapter 1	
Introduction to the development of 4D-printed smart composite actuators	
Chapter 2	
Article 1: (Lalegani Dezaki and Bodaghi 2023b) Article 2: (Dezaki, et al. 2024)	A literature review on the feasibility of FDM 4D-printed SMP/SMPC actuators activated via heat, Joule heating, magnetic field, and air pressure
Chapter 3	
Article: (Lalegani Dezaki and Bodaghi 2023a)	Integration of magnetorheological elastomer into 4D-printed electroactive composites for remotely programmable dual-stimulus actuation
Chapter 4	
Article: (Lalegani Dezaki and Bodaghi 2023d)	Eco-friendly 4D printing of magneto-electroactive SMPC actuators including freeform design and shape-morphing abilities
Chapter 5	
Article: (Lalegani Dezaki and Bodaghi 2023c)	Shape memory meta-laminar jamming composite actuators fabricated via 4D printing: incorporating shape locking features and remote programming
Chapter 6	
Article: (Lalegani Dezaki and Bodaghi 2024)	Tailoring the behaviour of SMPCs through 4D printing and continuous fibre reinforcement
Chapter 7	
Concluding the thesis by discussing the findings from the chapters and outlining future directions	

Chapter 2
Literature review

This chapter reviews the literature on FDM 4D printing SMP and SMPC actuators. These actuators are activated through various stimuli, including thermal activation, Joule heating, magnetic fields, and pneumatic air supply. Additionally, this chapter identifies and discusses the research gaps present in these areas of study. This chapter is derived with permission, including figures, from a combination of two published articles as below, with relevant details added to clarify the purposes of this thesis (Lalegani Dezaki and Bodaghi 2023b, Dezaki, et al. 2024).

1. **Lalegani Dezaki M**, Zolfagharian A, Demoly F, Bodaghi M. Human–Material Interaction Enabled by Fused Filament Fabrication 4D Printing. Advanced engineering materials 202410.1002/adem.202301917.

2. **Lalegani Dezaki M**, Bodaghi M. A Review of Recent Manufacturing Technologies for Sustainable Soft Actuators. Int J of Precis Eng and Manuf -Green Tech 2023;10(6):1661-171010.1007/s40684-023-00533-4.

2.1. 4D printing

The considerable progress made in 3D printing techniques is the foundation for the development of 4D printing (Demoly, et al. 2021). Computer-controlled, layer-by-layer printing, guided by CAD, allows for the creation of a vast array of structures ranging from simple to highly intricate designs (Momeni, et al. 2017). It is possible to alter the structure of printed items such that they can change into new shapes by combining 3D printing techniques with active materials, using suitable mathematical modelling, and sequential energy stimulation (Yuan, Lu and Wang 2022). 4D printing offers several benefits over 3D printing, such as the faster development of smart and multi-materials (MM) and the production of multifunctional objects that better react to their surroundings (Kantaros, Ganetsos and Piromalis 2023b).

With the current state of technology, 4D printing can produce a much wider range of products than standard 3D printing (Tibbits 2014). With the use of 3D tools and external triggers, this cutting-edge technology makes it possible to change the shapes of materials (Spiegel, et al. 2022). According to research, a basic 3D structure can gradually transform into a more complex shape by combining smart materials with 3D printing techniques and exposing them to environmental conditions (Wang, J., et al. 2019). The elimination of complicated mechanical drive elements in actuation systems allows for the direct embedding of functional components into the materials, simplifying assembly, cutting down on the number of components required, and cutting production costs (Maurya, et al. 2022). In contrast to traditional manufacturing methods, this process excels in several areas: it is a streamlined, one-step operation; economically advantageous, especially for small-scale production; capable of producing exceptionally detailed outputs; remarkably efficient in material usage through recycling; entirely solvent-free; and necessitates minimal post-production refinement (Rastogi and Kandasubramanian 2019).

This technology incorporates important 3D printing properties such as controllability, reproducibility, and repeatability (George, et al. 2017). It also facilitates technological developments in fields like 3D modelling of new constructions. Because of these benefits,

4D printing is now a widely sought-after technology in engineering (Mitchell, et al. 2018). It is becoming a more and more popular option due to its capabilities, which have consistently pushed the frontiers of the design field. Innovative self-folding processes have dramatically curtailed production times and material usage by up to 87%, significantly accelerating the development of 3D prototypes (Ding, et al. 2018, Pingale, et al. 2023). Moreover, space can be saved during storage and transportation by utilising the shape-changing properties made possible by stimuli-responsive materials (Bodaghi, M., Damanpack and Liao 2017).

4D printing significantly accelerates the design and production of complex actuating components. As mentioned in **Chapter 1 (Section 1.1)**, there are several 3D printing processes available to create parts with shape memory properties. Using any of the mentioned methods for design and production has several benefits. Based on current research and reviews, 4D printing is mostly focused on biomedical and medical applications (Aufa, Ismail and Zaki Hassan 2023, Mathur, et al. 2023, Zeenat, et al. 2023), soft robotics (Mohammadi, et al. 2023, Khalid, Arif, Ahmed, et al. 2022), electrical devices (Huang, et al. 2021), wearable devices (McLellan, Sun and Naguib 2022), construction (Pacillo, et al. 2021), dentistry (Javaid, et al. 2022), and agriculture (Maraveas, Bayer and Bartzanas 2022).

Also, 4D printing has enabled the creation of highly customized, MM soft actuators with unprecedented high resolution and design freedom (Zolfagharian, et al. 2022, Khalid, Arif, Ahmed, et al. 2022). New prospects for soft actuators have been opened by this development, which could drastically change the way we make smart composite actuators (Jeong, et al. 2019). 4D printing empowers the creation of versatile actuators capable of morphing, transforming, deploying, and reconfiguring themselves, optimizing space, usability, and productivity (Ka ergis, Mitkus and Sinapius 2019). It revolutionizes domestic living by enabling the creation of adaptive furniture, intelligent storage systems, and seamlessly integrated home automation solutions that prioritize comfort, convenience, and personalization.

The importance of 4D printing for promoting composite actuator development is discussed at the outset of the study. After that, it explores how FDM 4D-printed SMPs and SMPCs are used for various purposes. The applicability of smart actuators is demonstrated with specific examples, and their potential for future expansion is evaluated. The analysis of 4D printing in smart constructions is noteworthy. The review also examines the possibilities of 4D printing methods which can reduce waste generation.

2.2. Why 4D printing?

Products are still made using conventional manufacturing techniques for a range of industrial uses (Pereira, Kennedy and Potgieter 2019). Despite their potential, these techniques face significant challenges, including high energy consumption and material wastage. Consequently, the pursuit of advanced technologies to propel 3D printing and other intelligent manufacturing methods forward continues unabated (CORREA, et al. 2017, de León, et al. 2023, Bazli, et al. 2023). Due to its widespread adoption across a variety of sectors and research fields, 4D printing has garnered significant attention from researchers in recent decades (Zhang, Zhizhou, Demir and Gu 2019). **Figure 2.1a**, which was taken from the Scopus database, shows the increase in publications on 4D printing between 2012 and 2022. There is a notable spike in publications from 2018 to 2022, suggesting strong development in this field, and the trend of modest rises persists. **Figure 2.1b** presents the top ten most prolific authors in the field of 4D printing, as determined by article frequency data extracted from the Scopus spanning the years 2012 to 2022. An expanded subject category list for 4D printing research is shown in **Figure 2.1c**. The percentage of 4D printing across multiple domains is shown by this analysis. Contents The most well-known fields that have made major contributions to 4D printing research are science and engineering. Moreover, **Figure 2.1d** illustrates the various nations' contributions to the field of 4D printing, with China topping the list with the largest percentage of research contributions.

Concerning 4D printing technology, which is growing due to its unique features that help reduce material waste, the information given provides insightful information (Kuang, et al. 2019). A wide range of sectors have shown a great deal of interest in 4D printing. It is anticipated that by 2025, 4D printing's market value will have increased to USD 488.02 million from USD 62.02 million in 2019 (Joshi, et al. 2020, Subash and Kandasubramanian 2020, Le Duigou, Antoine, et al. 2020). 3D products may be produced more quickly and with less material usage because of 4D printing's self-actuation and self-folding features. With its potential to improve manufacturing procedures, expedite production cycles, and maximise material utilisation across multiple industries, this technology is extremely promising. The information emphasises how 4D printing is being adopted more widely and how much research is being done on it, highlighting how it has the potential to transform industrial procedures and solve sustainability issues. The results indicate that 4D printing has attracted a lot of interest as a competitive substitute for traditional manufacturing methods, leading to funding and development for its advancement and use in areas such as soft robots. As technology evolves, it possesses the transformative power to reshape industries, foster environmental stewardship, and unlock unprecedented ways for creative design and production (Hartmann, Baumgartner and Kaltenbrunner 2021).

Moreover, 4D-printed products can autonomously adapt their shape within dynamic environments, significantly reducing the need for human intervention or complex mechanical systems (Yang, H. 2019). This advancement enables the regulation of form through self-actuation, self-folding, self-assembly, autonomous decision-making, and adaptive responses to external influences (Pinho, Buga and Piedade 2020, Pei and Loh 2018). Recent advancements in production processes have shifted the paradigm of 4D printing from design-centric to manufacturing-focused, enabling successful applications in

stimulus-responsive systems. The inherent reusability of 4D-printed objects offers potential for enhancing the circular economy of polymers and composites by reducing material waste (Zhang, Fenghua, et al. 2021, Lalegani Dezaki and Bodaghi 2023b). The material utilisation rate can be lowered by up to 70% by combining topology optimisation approaches with 3D printing. This indicates that a sizable percentage of the materials used in 4D printing can be recycled and used again, supporting a manufacturing strategy that is more resource-efficient and sustainable (Pinho, Buga and Piedade 2020). This investigation will shed light on the creative ways that 4D printing can be applied in novel contexts, fostering the creation of inventive environment solutions.

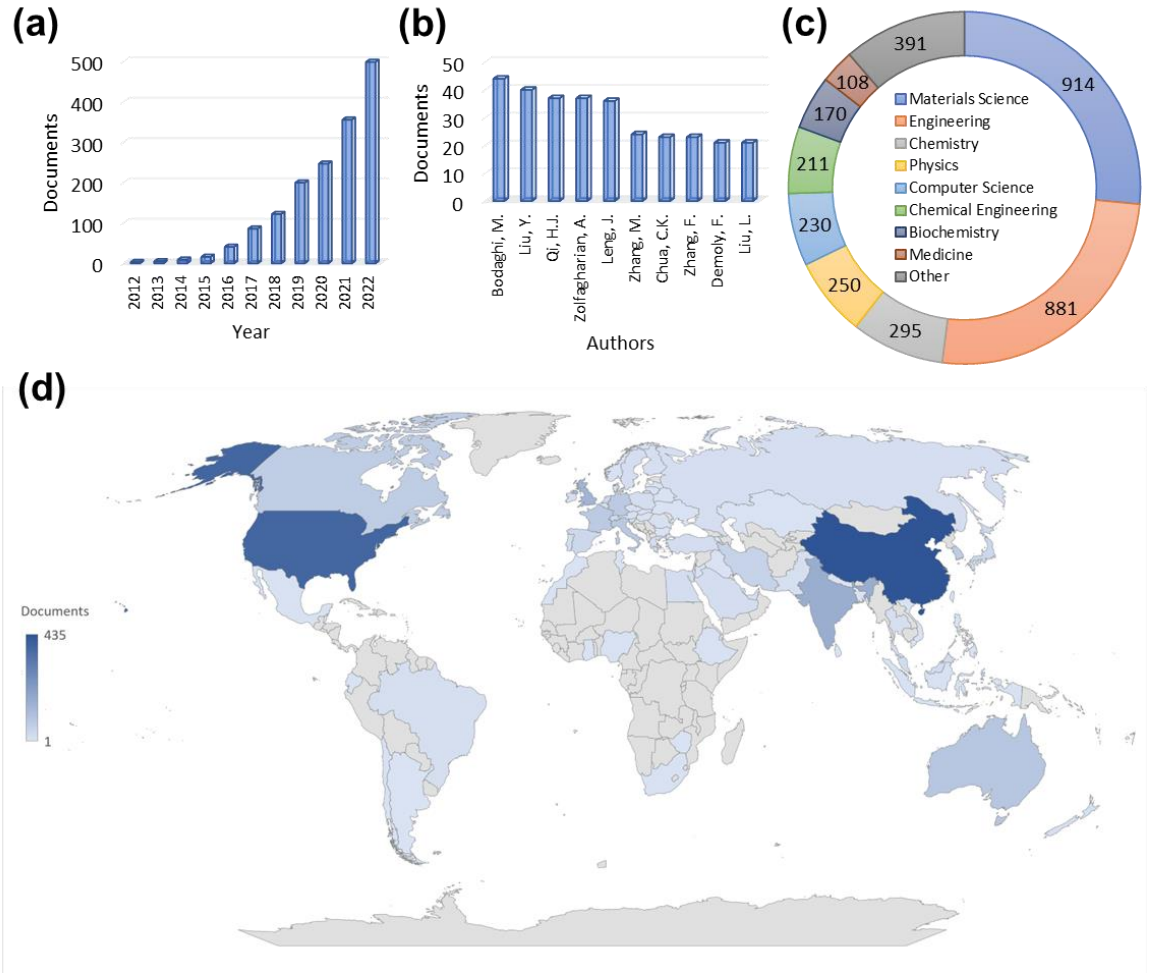

Figure 2.1. Figures illustrating important facets of the 4D printing field include (a) an increase in publications; (b) top writers in the field; (c) 4D printing application fields; and (d) nations that publish 4D printing research. Adapted with permission (Dezaki, et al. 2024).

2.3. FDM 4D printing

This thesis focuses on FDM printers, which operate by melting plastic filament and depositing it layer-by-layer to construct the desired object (Lalegani Dezaki, Mohd Ariffin and Hatami 2021). Finding affordable, high-quality 3D printers has gotten easier as their costs have dropped and their utility has increased. Given its versatility across numerous academic disciplines, the 3D printer stands out as an exceptionally adaptable and cost-effective laboratory asset (Roudný and Syrový 2022). To discover 4D printing's potential for these applications, it is necessary to first explore the notion.

Production of personalised and customised items that can be adapted to products is made possible by FDM 4D printing. This adaptability makes it possible to design one-of-a-kind actuators that precisely suit each user's needs. Furthermore, because FDM 4D printing does not require complicated tooling or moulds, which are usually needed in traditional manufacturing methods, it provides manufacturing at a lower cost (Vyavahare, et al. 2020). Because of its low cost, a greater number of users may afford it at a cheaper price compared to other 3D printing technologies. Additionally, FDM 4D printing enables the integration of several features into a single printed product. This makes it possible to develop smart products that integrate a variety of features and functionalities to improve performing tasks. Due to the rapid advancement and adoption of FDM 4D printing as a manufacturing method for various components, it has demonstrated potential for a wide array of applications. (Carrell, Gruss and Gomez 2020). Throughout educational institutions including schools, libraries, design studios, and even homes, desktop FDM 3D printers are becoming increasingly common (Wang, Q., et al. 2016).

FDM is an extrusion-based 3D printing process. As depicted in **Figure 2.2a**, an FDM printer employs an extruder to melt and deposit plastic filament layer by layer. The printer follows a precise path dictated by G-code instructions, gradually constructing the desired object from a stereolithography (STL) file. G-code is generated from a CAD model via a computer-aided manufacturing (CAM) process that slices the 3D model into layers and defines the toolpath. A pinch roller, driven by an electric or hydraulic motor, feeds the filament into the nozzle (Popescu, et al. 2018). The FDM process involves extruding molten plastic through a nozzle onto a build platform. This material solidifies upon contact, forming successive layers that collectively construct the 3D object from a two-dimensional (2D) layer. Various cooling techniques are employed to accelerate the solidification process.

Meanwhile, improving the quality of the product is an ongoing goal in all manufacturing procedures. The surface quality and mechanical qualities of the parts generated in the FDM process are determined by a multitude of criteria (Ka ergis, Mitkus and Sinapius 2019). Optimising the crucial parameters to reduce errors during the printing process is the key to achieving good quality. To avoid flaws and mistakes, it is essential to choose the best parameters (Lalegani Dezaki and Mohd Ariffin 2020). Numerous parameters significantly influence the outcome of FDM printing, including fill pattern, nozzle and bed temperatures, nozzle diameter, build orientation, layer thickness, infill density, extrusion and printing speeds, ambient temperature, and bed adhesion techniques (Solomon, Sevvel and Gunasekaran 2021, Lalegani Dezaki, et al. 2021, Dey and Yodo 2019). These variables are

vital in establishing the attributes and properties of parts. Hence, finding optimal conditions based on requirements and material properties is important.

Furthermore, kinematic mechanisms have been crucial in the development of tactile, dynamic objects and interfaces in the realm of actuators. The design and construction of spatial structures are complex due to intricate geometries, demanding assembly processes, and the inherent instability of joint connections caused by inevitable dimensional discrepancies between components (Calì, et al. 2012). It is possible to get around the difficulties and problems related to conventional FDM printing techniques by creating and utilising FDM 4D printing in conjunction with SMPs (Chen, Q., et al. 2020). This combination produces better printing processes and results by enabling more control and manipulation of the printed objects (Carrell, Gruss and Gomez 2020). With FDM 4D printing, SMPs can form intricate and dynamic structures because of their remarkable ability to return to their initial shape in response to stimuli (Nezhad, et al. 2022). Thus, this strategy provides a viable way to overcome the drawbacks and improve the FDM technique's overall printing experience.

2.3.1. Printing parameters

Several process parameters in FDM significantly influence the final product's surface quality and mechanical properties. Optimising these critical factors is paramount to minimising printing errors and achieving high-quality results. Selecting the ideal printing conditions to prevent defects throughout the process is crucial. Selecting the optimal range of variables is essential to avoid such defects and errors. Extensive research, employing both numerical and statistical methods, has been conducted to achieve accurate fabrication and high-quality specimens. A subsequent section will detail the main parameters impacting the final products.

A critical factor influencing the mechanical properties and stiffness of FDM-fabricated parts is the infill pattern. These patterns come in various geometries. The infill density, expressed as a percentage, dictates the final part's form, ranging from completely solid (100% infill) to entirely hollow (0% infill) (Lalegani Dezaki, et al. 2021). Common infill pattern shapes include cubic, linear, rectilinear, honeycomb, and wiggle. Also, nozzle temperature significantly impacts the printing process and layer adhesion. This parameter varies depending on the material's melting point, typically ranging from 170°C to 300°C. Improper nozzle temperature can negatively affect layer bonding.

Nozzle diameter significantly impacts both the surface finish and mechanical properties of the final product. Nozzle sizes typically range from 0.2 mm to 0.8 mm. While smaller nozzles generate parts with higher precision, they also require longer printing times (Lalegani Dezaki, Mohd Ariffin and Hatami 2021). Another crucial element for controlling the melted filament is the bed temperature. This parameter ranges from 0°C to 100°C, depending on the specific material properties. Build orientation is a significant factor in FDM printing. This parameter influences both mechanical properties and surface textures (Lalegani Dezaki and Mohd Ariffin 2020). Parts can be printed at various angles (0° to 180°) along the x, y, and z axes. It's important to note that the machine utilizes support structures

at angles perpendicular to the build orientation, which can affect part accuracy and surface finish.

Layer thickness defines the distance between the nozzle and the printing bed, essentially determining the width of each deposited layer. Maintaining the correct nozzle-to-bed distance is crucial as it directly correlates with the nozzle diameter. This parameter significantly impacts surface roughness and overall printing time. Layer thickness typically ranges from 0.06 mm to 0.6 mm, with smaller values resulting in higher quality prints but also longer printing times. Raster width refers to the width of the deposited material filament, while raster angle defines the orientation of the printing pattern within the x-direction. These parameters can influence warping and shrinkage in the final product (Vyavahare, et al. 2020).

The parameters represent the primary factors influencing the mechanical and surface quality of FDM printed parts. However, several other aspects play a significant role depending on the chosen printing parameters. These additional factors include surface layer pattern, wall thickness, support structure, and so on. Optimizing these additional factors alongside the core printing parameters is crucial for achieving the desired final product quality in FDM printing.

2.4. Overview of SMPs/SMPCs

The ability to undergo predictable form changes on demand is a unique trait of SMPs, known as the SME (Wang, L., et al. 2023). This property depends on the interaction of two systems that exist in the polymer: switching segments and net points. When activated, usually by applying heat, the SMP can be programmed to assume specific forms and then return to their original form. As the polymer network's memory element, the net points are always trying to reshape the SMP to its original configuration. These network points often manifest as increased polymer entanglement or crystallinity, thereby contributing to SME of SMPs (Mather, Luo and Rousseau 2009). Also, SMPCs are materials that combine the enhanced mechanical properties of composite materials with the unique properties of SMPs (Yu, Yuxuan, et al. 2022). When reinforcing fibres, fillers, and nanoparticles are added to the SMP matrix enhances the mechanical characteristics of the polymers—such as strength and stiffness—and enables customisation of the composite's response to external stimuli (Meng, H. and Li 2013, Meng, Q. and Hu 2009, Khalid, Arif, Noroozi, et al. 2022). Also, bio-derived reinforcement has better biodegradability and less density, which improves certain mechanical properties of SMP (Palaniyappan, et al. 2022, Song, et al. 2021, Palaniyappan, et al. 2023).

To keep the polymer in its intended structure, switching segments in SMPs/SMPCs is essential (Zhao, Q., Qi and Xie 2015). In comparison to the net points, these segments usually have a lower degree of entanglement. The switching segments of the polymer are the first to move when the triggering stimulus is applied. Because of their mobility, the SMPs/SMPCs can demonstrate their SME and alter shape as desired (Hu, G. and Bodaghi 2023). For shape memory functionality to be successfully integrated into SMPCs, the switching segments must exhibit a reversible transition from a static to a dynamic state. SMPs' SME allows them to be programmed into transient shapes and then return to their original form (Li, G. and Wang 2016). The behaviour of SMPs/SMPCs is characterised in this context by two key criteria. The form recovery index and shape fixity index are critical metrics for assessing shape memory performance (Aberoumand, et al. 2023). A SMP's ability to regain its original shape following the removal of a stimulus is measured by the shape recovery index. Conversely, the shape fixity index gauges a polymer's capacity to hold onto its predetermined form. These indices serve as essential benchmarks for comparing, characterizing, and selecting appropriate SMPs for diverse applications, providing critical insights into their shape memory behaviour.

The shape fixity index for SMP/SMPCs is determined by programming a rectangular sample into an elongated shape and subsequently measuring the residual tension upon stimulus removal (Rahmatabadi, et al. 2023). Conversely, the shape recovery index is calculated as a ratio of residual stress to the intended or anticipated stress. Similar to the shape fixity index, determining the residual stress of a recovered programmed rectangular sample is essential for calculating the shape recovery index in an SMP. The shape fixity index is calculated as the ratio of the difference between the intended strain and the recovered strain to the intended strain.

Due to their unique properties, these materials are ideally suited for applications requiring dynamic and adaptable structural modifications. The properties of the materials stated in 3D printing can change significantly in the context of 4D printing in reaction to outside stimuli

or environmental circumstances. These stimuli include a variety of elements, such as light (Leist and Zhou 2016), water (Cremonini, et al. 2023), pH (Muzaffar, et al. 2020), heat (Zhang, Quan, et al. 2015), electricity (Zolfagharian, et al. 2022), magnetic fields (Moradi, et al. 2023), and pneumatic (Zhang, Qiang, et al. 2021). These stimuli allow the actuator to be turned on to achieve the desired shape or to undergo shape morphing. The FDM approach is applied to the 4D printing of various polymers and composite materials. Polyurethane (PU) and polylactic acid (PLA) are two materials that are commonly used in FDM process. PLA is classified as a semi-crystalline SMP (Wang, W., et al. 2006, Zhang, Quan, Zhang and Hu 2016). PLA and PU can change shape in response to preprogrammed strain-temperature procedures (Jing, et al. 2015). Non-toxicity is one benefit of the PLA materials used in FDM (Mehrpouya, et al. 2021). This feature guarantees the safety of handling and using devices made with FDM 4D printing in residential settings. PLA is appropriate for a variety of uses because of its non-toxic nature (Zhang, Qian, et al. 2019). This functionality enhances user safety by allowing for effortless handling and interaction with 4D-printed objects without fear of injury.

Programming of SMPs/SMPCs is an important approach in 4D printing (see **Figure 2.2b**). FDM is used to shape the printed item during the hot programming process. The sample is heated above its glass transition temperature (T_g) to achieve a rubber-like state. It is then subjected to a load, cooled, and allowed to set in a temporary shape. Subsequent reheating restores the original shape. Alternatively, cold programming involves cooling the printed object to a strain-free glassy state before applying an external load to induce deformation. Upon load removal, residual plastic strain creates a temporary shape, known as the cold-programmed shape (Cerbe, et al. 2023). Final heating restores the sample to its original state. The printed structure incorporates both plastic strains induced by hot and cold programming, as well as intrinsic inelastic strains. The FDM technique's use of SMP/SMPC has been well-documented in earlier research studies (Ehrmann and Ehrmann 2021, Quiñonez, et al. 2021).

Also, an overview of FDM 4D printing's main objectives is shown in **Figure 2.2c**, which emphasises the technology's application in the production of composite actuators. The procedure starts by explaining 4D printing and exploring SMP material features. When repeatedly heated and cooled, these SMPs show a mechanical and thermal reaction. There's also a diagram of the FDM printer, which is the main machine used to make 4D-printed actuators. As seen in the image, a variety of stimuli can activate these printed objects which will be discussed further.

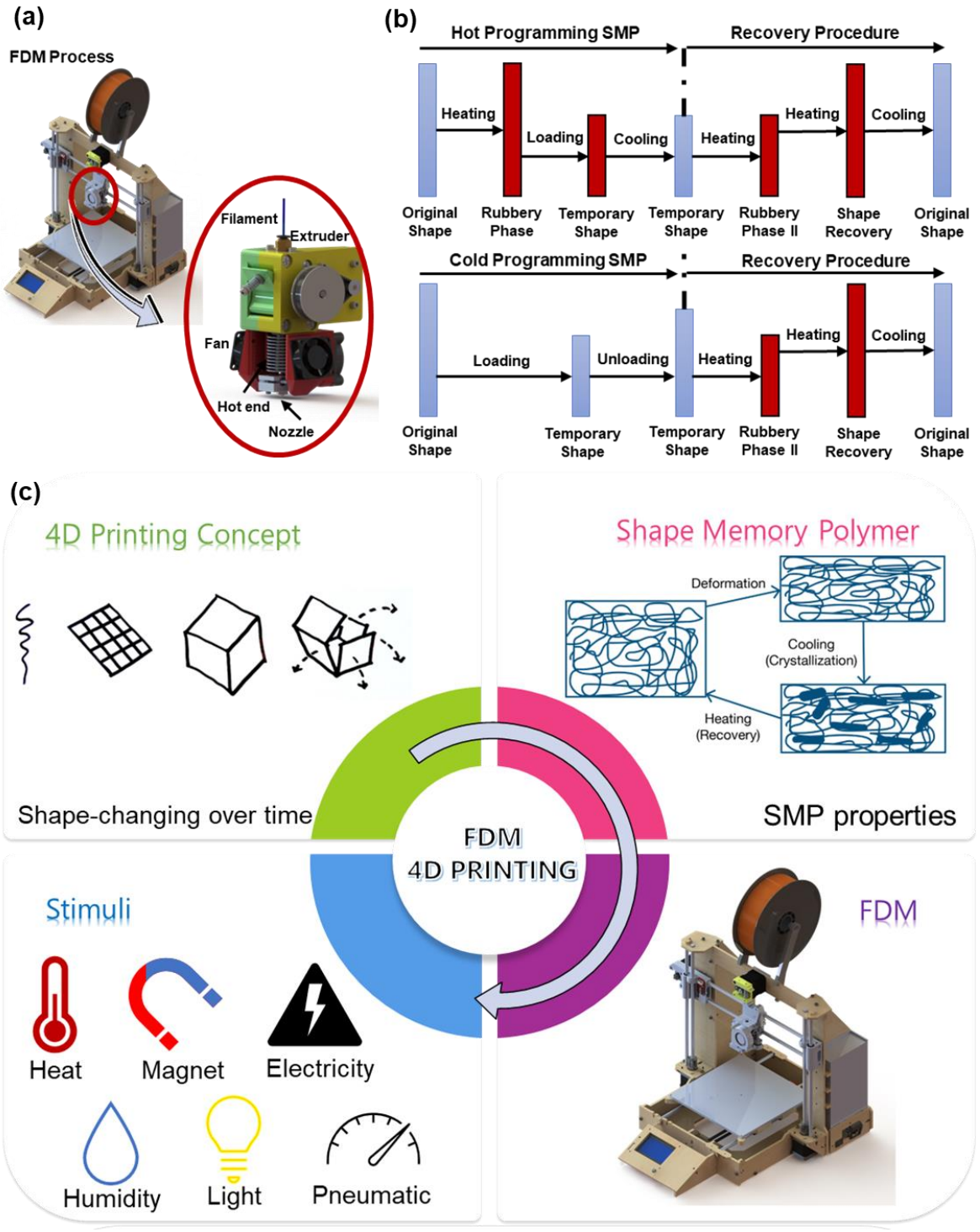

Figure 2.2. (a) The parts of an FDM 3D printer, encompassing the nozzle. (b) SMP material is programmed through hot and cold processes for 4D printing. (c) The steps involved in using SMP and FDM 4D printing to create actuators. Adapted with permission (Dezaki, et al. 2024).

2.5. Smart actuators

Over the past few decades, smart soft actuators have become increasingly widely used in a wide range of sectors and research fields. Actuators may deform and adapt to various shapes, surroundings, and applications since they are composed of soft and flexible materials (Li, M., et al. 2022). The manufacturing process for soft actuators varies depending on the specific actuator type and materials used. Every actuator follows a similar process from design to testing using various production methods. Depending on the materials and actuator type, different manufacturing techniques can be employed for smart actuators. All actuators go through the same broad procedures from design to testing using various production processes. There are categories into which the procedures can be separated including 3D printing (Zolfagharian, et al. 2016), 4D printing (Khalid, Arif, Ahmed, et al. 2022), casting and moulding (Jones, et al. 2021), textile processing (Fu, et al. 2022), electrospinning (Yu, Yue, et al. 2023), laser cutting (Hao, et al. 2022), origami/kirigami folding (Ai, et al. 2021), and electrowetting (Cole and Tang 2022).

Smart soft actuators can offer novel features including shape and environment adaptation, enhanced safety, comfort, and human-machine interaction because of their soft materials, flexible design, and creative control strategies (Yin, R., et al. 2021). Actuators are a rapidly expanding field that is becoming more complex and capable because of advances in electronics, materials science, and control engineering. Soft actuators, constructed from more pliable materials than traditional actuators, pose reduced risks to humans and other living beings. Their flexible design minimizes damage in collisions. Consuming less energy than rigid counterparts, soft actuators can be powered by various sources (as detailed in **Section 2.4**). Integrating smart materials like SMPs and SMPCs into soft actuators offers a promising approach. These materials enable the creation of highly adaptable, robust actuators capable of motion and deformation with minimal energy consumption, eliminating the need for conventional actuators or motors.

Researchers are increasingly focused on developing energy-efficient, environmentally friendly smart actuators. The ability of these actuators to mimic natural movement and motions is very useful in applications where precise movements are required. Various strategies can be employed to enhance soft actuator performance. Material selection is paramount. The following section provides an overview of the diverse soft actuator types explored in this thesis:

- *Shape memory actuators:* These actuators combine SMP/SMPC materials that have shape memory characteristics (Ren, et al. 2023). When subjected to temperature changes, these materials can experience reversible deformations, which allows the actuators to exhibit programmed and flexible movements. SRMs offer an environmentally friendly approach to creating morphing structures and biomedical devices by minimizing energy consumption during thermal activation (Oladapo, et al. 2023).
- *Electroactive soft actuators:* Electroactive polymers, which exhibit significant deformations in response to electrical stimuli, are used in soft actuators based on electroactive principles. A diverse array of soft actuators utilises electroactive polymeric materials, including those incorporating ionic and metallic components, dielectric properties, or conductive characteristics (Yang, Y. and Jiao 2023).

Additionally, Joule heating, which involves generating heat through electric current, can be utilised to enhance the actuation process. These actuators are lightweight, have minimal power consumption, and have good deformability, among many other advantages. Energy-efficient control systems and eco-friendly and biocompatible electro-active materials can be used to further boost sustainability.

- *Magnetic soft actuators:* These actuators precisely regulate movements and deformations by using magnetism. Flexible polymer matrices infused with magnetic components are subjected to external magnetic fields to instigate morphological and compositional transformations (Lin, D., et al. 2023). Characterized by their ability to generate significant force and displacement, operate without physical contact, and exhibit high positional accuracy, these actuators are indispensable components in the realms of biomedical engineering, human-machine interaction, and advanced robotics. Magnetic soft actuators provide outstanding controllability with environmentally friendly actuation by utilising different materials and optimising actuator designs (Yang, Z., et al. 2023).
- *Pneumatic actuators:* A fundamental approach to soft actuation relies on the application of pneumatic or hydraulic pressure to induce deformation. These actuators are fabricated from compliant materials, such as pneumatic chambers and elastomers, that exhibit volumetric changes in response to pressure fluctuations (Orozco, et al. 2023, Lalegani Dezaki, et al. 2023). Pneumatic and hydraulic soft actuators can provide energy-efficient and sustainable actuation by optimising actuator design and utilising eco-friendly fluids. Actuators like this are used in domains like robotics, prosthetics, and haptic interfaces, where precise and obedient movements are required (Zolfagharian, Mahmud, et al. 2020).

Actuators that are multi-responsive will result from combining the aforementioned stimuli. Multi-responsive actuators can be produced by developing materials or combining materials during the 3D printing process. Also, Multi-responsive actuators are available that react to heat, electricity, magnetic fields, and pneumatic air types (Liu, Yan, et al. 2021, Peng, X. and Wang 2018, Bowen, Rose and Morin 2021). Adaptability is higher for multi-responsive actuators than for mono-responsive actuators. Because of their adaptability to a variety of stimuli, they can operate well in a wider range of contexts by adjusting to changes in their environment. These benefits include better control, flexibility, efficiency, and functionality. Therefore, it is expected that multi-responsive actuators will have a profound effect on many sectors in the future, revolutionising their operations and changing their capacities.

2.6. FDM 4D printing SMPCs

Research on FDM 4D printing with SMPs like pure PLA has considered how the printed structure affects shape memory behaviour (Hosseinzadeh, Ghoreishi and Narooei 2023). The physical interactions within the polymer have allowed PLA to demonstrate shape memory properties. The printing sample structure is preserved by the physical interactions between PLA polymer strands. Entanglements can recover to their unstretched condition at their T_g which is roughly 60–70°C, when the material becomes very elastic, as the chains between these entanglements are bent and stretched into a temporary shape (Mehrpouya, et al. 2021). For example, A cost-effective and efficient 4D printing method using the multispeed FDM technique was proposed by Wang et al. (2023) (see **Figure 2.3a**). With this method, flat precursory patterns with graded built-in strain could be integrated, enabling quick and adaptable shapeshifting when heated. They could directly and highly accurately manufacture complicated 3D structures from flat precursory patterns by methodically optimising the printing parameters. PLA samples were printed at different printing speeds as part of the experiments carried out by the researchers. After that, these samples were heated to cause shape changes and produce intricate forms. This technique greatly lowers the 4D printing process complexity and construction time.

PLA is commonly described as a brittle material due to its prominence in 3D printing (Liu, Guang, Xiong and Zhou 2021). For this reason, research has been done on using PLA composite printing to enhance these mechanical qualities. Augmenting the structural robustness of printed constructs can be achieved through the advancement of FDM printing technology or the utilisation of composite and fibre/particle-reinforced printing methodologies. These composite materials consist of SMPs combined with a wide array of supplementary components, including ceramics, metallic particles, glass fibres, nanohydroxyapatite, carbon fibres (CF), fiberglass (FG), aramid fibre (AF), carbon black, natural fibres, wood fibres, and carbon nanotubes (CNTs) (Nugroho, et al. 2021, Yu, Wang Wang, et al. 2017, Wickramasinghe, Do and Tran 2020, Le Duigou, Antoine, et al. 2020). The printed parts that are produced have greater strength and durability because the printing material contains reinforcing fibres (Ram Kishore, et al. 2023). Beyond their role in augmenting the strength and reinforcement of the SMPs, these additives function as an active component that catalyses the shape changing capability (Liu, Y. and Chou 2020). Between 60% and 70% of polymers serve as the matrix for the majority of polymer-based composites, while the remaining 30% to 40% are composed of reinforcement material (Muthe, Pickering and Gauss 2022). The objectives of this study are to investigate SMPs and SMPCs, electroactive SMPCs, magnetic SMPCs, and pneumatic SMP actuators developed by the FDM process.

Yu et al. (2020) suggested a composite design that includes PLA and CF-reinforced PLA. The efficacy of the workflow was demonstrated by several imaginative design examples. At least 95% of the measured deformation accuracy was found, with a confidence interval of (0.972, 0.985). The workflow that is being shown, according to the authors, is very promising for a variety of applications and is essential in integrating geometry, material mechanism, and design (see **Figure 2.3b**) (Yu, Yuxuan, et al. 2022). In addition, there has been a notable increase in the use of composite materials in the field of 3D printing, particularly in the FDM process (Patel, et al. 2022, Baechle-Clayton, et al. 2022). In this perspective, PLA and its composites are one often used composite material that has found widespread uses in a variety

of industries (Joseph Arockiam, et al. 2022). These composite materials are perfect for producing a variety of products in industries because they have better mechanical qualities, increased functionality, and improved durability. The capacity to print using composite materials creates new opportunities for producing complex, personalised products that meet industry criteria (Mishra, Negi and Kar 2023).

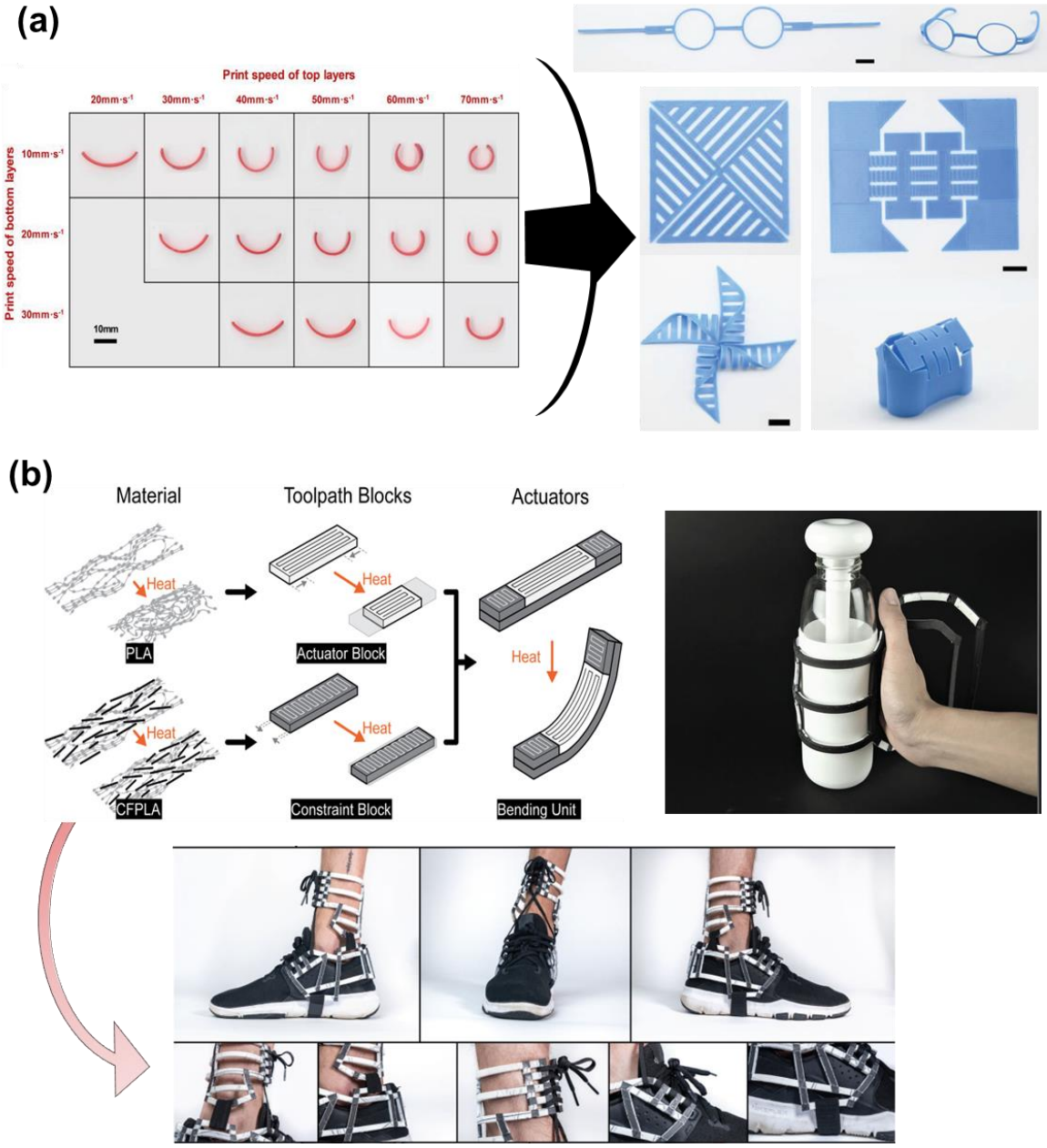

Figure 2.3. (a) The profiles of the PLA samples. During the fabrication process, different printing speed combinations were used to create the house, pinwheel and spectacle frame (scale bar: 10 mm). Adapted with permission (Wang, F., et al. 2023). (b) The arrangement of the polymer chains is the study's central idea. The white actuator blocks and grey constraint blocks exemplify anisotropic structures comprised of dual layers produced through disparate printing processes. An additional illustration shows a bending unit with limitations (grey) and actuators (white). This study includes the development of the bottle holder and shoe supporter design variations. Adapted with permission (Yu, Yuxuan, et al. 2020).

Moreover, one important strategy for improving the mechanical properties of SMPs made by FDM 4D printing is MM and functionally graded material (FGM) printing (Tamburrino, Graziosi and Bordegoni 2019, Espalin, et al. 2014, Kumar, et al. 2019, Pei, et al. 2017, Wen and Li 2021). Continuous fibre MM printing is also an alternative option to improve the mechanical properties of polymers (Kabir, Mathur and Seyam 2020, Parandoush and Lin 2017). Continuous fibre-reinforced composites (CFRCs) are printed in three dimensions using a 3D printing technique that combines in-situ impregnation with fibre tension in the FDM process (Liu, Guang, Xiong and Zhou 2021). CFRCs promote lightweight goods and enhance mechanical qualities while using less material (de Kergariou, et al. 2023, Yu, Yuxuan, et al. 2020). Numerous studies that have concentrated on MM 4D printing CFRCs have broadened the possible applications of SMPCs (Rafiee, Farahani and Therriault 2020, Wang, H., et al. 2023). The performance of printed CFRC metamaterials and their capacity for shape fixity and recovery were also the subject of research studies (Rafiee, Farahani and Therriault 2020, Wang, H., et al. 2023, Zeng, et al. 2022, Zhang, Yan, et al. 2021, Cheng, et al. 2021).

Zeng et al. (2020) investigated the electrically induced SME of 4D-printed PLA-based composites reinforced with continuous CF. By employing electric heating tests to monitor the shape recovery process, they demonstrated the effectiveness and reliability of resistance heating for this purpose, achieving a shape recovery rate exceeding 95% (Zeng, et al. 2021). Also, Dong et al. (2021) conducted a comprehensive analysis of the correlation between printing and structural factors on the mechanical behaviour and shape memory attributes of printed CF-reinforced composites composed of AF and PLA. Experiments showed that a mere 3.8% addition of fibre to the composite significantly increased its tensile strength by almost 300%. More fibre, however, harmed the composite's capacity to regain its shape, which in turn affected its shape-changing characteristics and shape recovery properties (see **Figure 2.4a**). Also, 4D-printed materials with localised form memory were the subject of research by Sun et al. (2019). They investigated using FGM layers to produce localised actuation. Also, they evaluated using varying concentrations of plasticiser to accomplish this. Researchers discovered that localised shape memory was produced using tri-layer FGM composites with increasing plasticiser content throughout the layers (see **Figure 2.4b**).

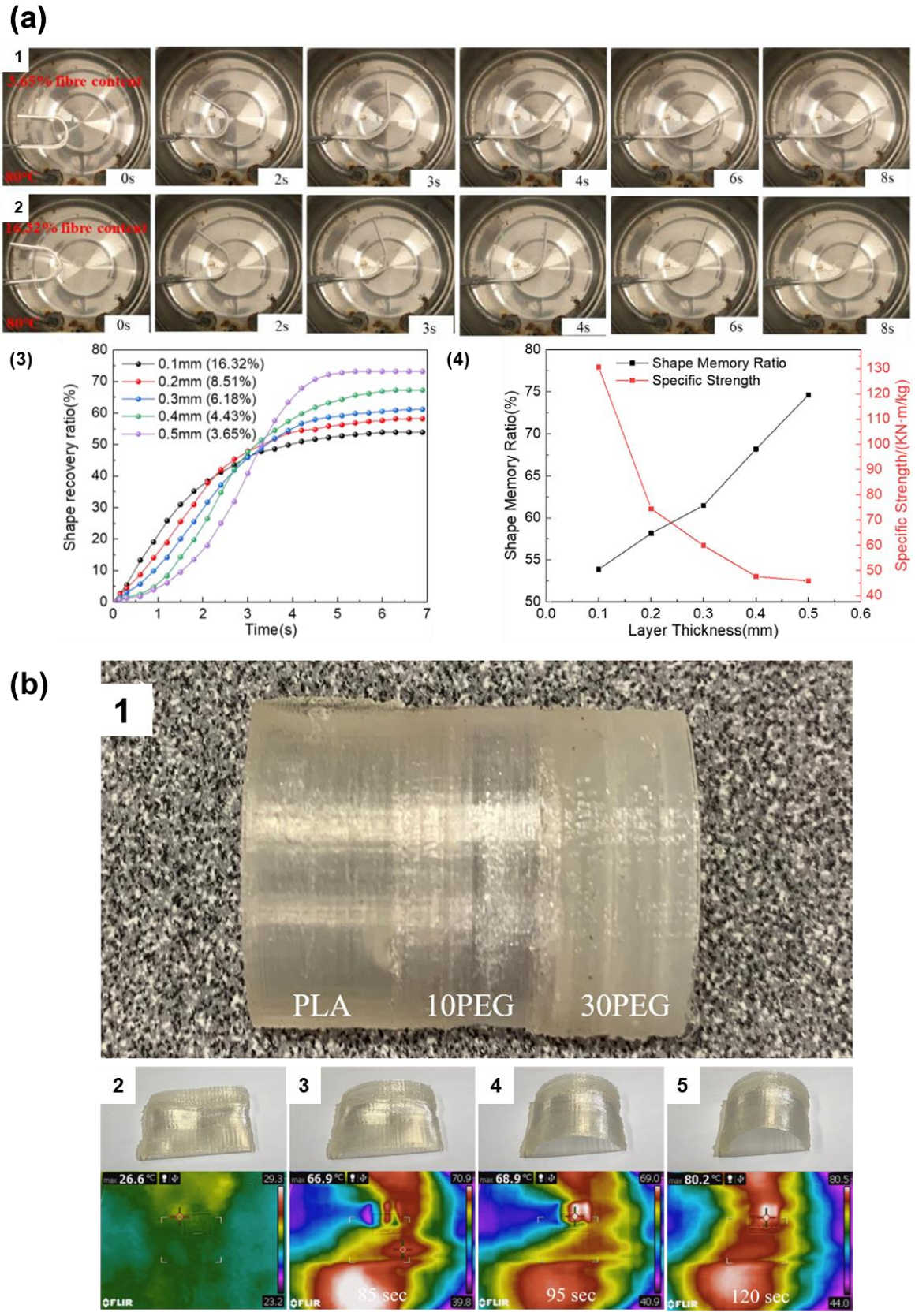

Figure 2.4. (a) Procedure for recovering the shape of AFSMPC composites having layers that are (1) 0.5 mm and (2) 0.1 mm thick. (3) Shape recovery ratio of CFRCs produced over time at varying printed layer thicknesses. (Note: 16.32% of fibre and a print layer thickness of 0.1 mm are indicated by the figure 0.1 mm (16.32%), and so on. (4) The specific strength and shape recovery ratio of printed cellular structures with varying printed layer thickness. Adapted with permission (Dong, K., et al. 2021). (b) Image 1 displays a 4D-printed SMPC

FGM. Shape recovery stages of FGM structure from 1 to 4. Adapted with permission (Sun, Y., et al. 2019).

2.6.1. Electroactive SMPCs

Electroactive SMPCs harness the Joule heating phenomenon to induce shape restoration, and mitigating the influence of external factors. Key advantages of these materials encompass superior filler dispersion, consistent heat distribution, remote controllability, and elevated driving efficiency (Dong, X., et al. 2022, Liu, Yanju, et al. 2009). The matrix material PLA is the most often utilised for electroactive SMPCs developed by the FDM process. Conductive fillers can be classified as zero-dimensional particles, one-dimensional fibres, or two-dimensional layers or films based on their morphologies. Furthermore, fillers fall into two main groups: metal and carbonaceous. Metal fillers include gold, silver, copper, and nickel. In contrast, carbonaceous fillers typically comprise CNTs, carbon nanofibers (CNFs), graphene, and carbon black (Liu, Wanwan, et al. 2018, Cho, et al. 2005, Li, M., et al. 2019). Zhang et al. (2018) created CNT-enriched PLA composite filaments. These filaments were then utilised to create the matching conductive 3D-printed parts using FDM technology. CNTs were discovered to be successfully maintained and stabilised on the filament surface during 3D printing. By using this method, the created 3D-printed components displayed an electrical conductivity that was noticeably higher than that of the conventional 3D-printed parts at the same loading of CNTs. This difference was roughly eight orders of magnitude.

Numerous methods are being developed to produce electroactive SMPCs (Garces, Irina Tatiana and Ayranci 2021, Meng, H. and Li 2013). Dong et al. (2022) utilised FDM technology to construct electroactive PLA/CNT-based composites for a spectrum of remotely operated smart devices. Intricate SMPC structures capable of assuming predefined 2D and 3D configurations under electrical excitation were investigated. Results demonstrated that elevating the CNT concentration improved the electrical, thermal, and shape recovery characteristics of the SMPCs, though these enhancements exhibited certain constraints as illustrated in **Figure 2.5a**. Also, bi-layer SMP/ conductive PLA (CPLA) structures to augment controllability and bending deflection were developed by Mitkus et al. (2022). Their research demonstrated a substantial reduction in resistance upon application of diverse activation voltages to the structure. Also, Wang et al. (Apr 21, 2018) introduced a cost-effective, electrically driven, reversible actuation and sensing technology based on CPLA and FDM. The potential of electroactive polymers was demonstrated by several uses for this recently created actuator.

Le Duigou et al. (2019) developed 4D-printed multi-responsive structural material, which combined a moisture-sensitive polymer with conductive carbon reinforcements. Pinecones and other natural actuators were made possible by the microstructure of these 4D-printed materials. These functional materials could be activated in two ways: passively by changes in the surrounding moisture content, or actively by electro-heating, which uses Joule effects to modify the moisture content of initially wet samples. Compared to other existing hygromorphs with the same responsiveness, this novel class of functional materials exhibited an actuation speed increase of a factor of 10. Passive cooling and moisture-driven actuation were activated in a fully reversible mode when the electrical heating was switched off. Also, Razzaq et al. (2023) developed thermoplastic blend-based electro-active triple-shape

composites for FDM 4D printing. Traditional melt processing techniques created composite blends containing multiwall CNTs (MWCNTs) as conductive fillers, polyester urethane (PEU), and PLA. The T_g of amorphous PLA (61 ± 1 °C) and the melting point of the PEU's crystallizable switching domain (T_m~50 ± 1 °C) were the basis for the two T_g found by thermal analysis. To show and measure the triple-shape effect, 3D models made of one or more materials were created. Electric current at varying voltages was applied to the resultant pieces to cause resistive heating. A thermomechanical programming process was used to train the printed demonstrators, and a step-by-step increase in voltage was used to achieve the triple-shape effect.

Alshebly et al. (Jan 1, 2022) fabricated four CPLA actuators at varying speeds, each powered by Joule heating. Increased printing speed correlated with greater bending. These structures transformed into active components when heated from 30 to 80 °C while conducting electricity. Also, Fallah et al. (2023) created a coaxial 3D printing process using CFRC SMPCs for 4D printing. The results indicated that mid-range feed rates (i.e., 150 mm/min and 200 mm/min) produced a higher fibre volume fraction and acceptable printability. Compared to pure PLA, the tensile and flexural modulus of CFRC samples with 6% CF volume fraction improved by 276 % and 246%, respectively. Also, significantly deformed structures showed 95% of shape recovery. Chen et al. (2021) employed FDM to produce SMPCs composed of continuous CF-reinforced PLA. This composite demonstrated outstanding electrothermal shape memory effect, rapid responsiveness to low-voltage stimuli, robust shape recovery force, and elevated strength. Most specimens attained a 90% shape recovery ratio after electrical thermal stimulation (see **Figure 2.5b**).

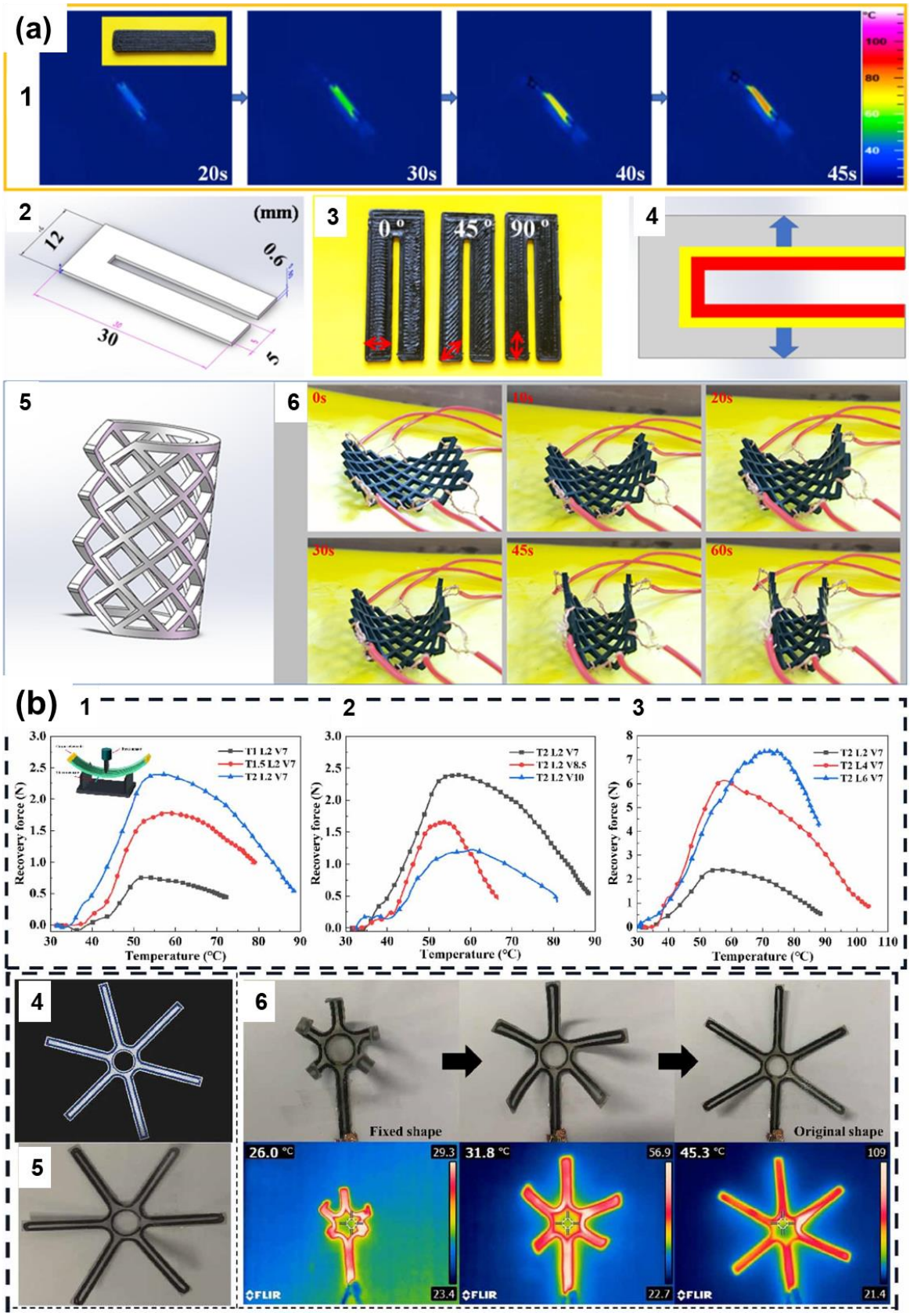

Figure 2.5. (a) The two-dimensional printed structures are as follows: (1) the heat distribution of the strip-shaped structure during the energisation process; (2) a U-shaped structure; (3) a U-shaped structure with varying directions of infill (0°, 45°, and 90°); and (4) the direction of heat diffusion inside the U-shaped structure. (5) External fixation stent model and (6) electroactive clamping procedure of the 4D-printed electroactive external fixation stent. Adapted with permission (Dong, X., et al. 2022). (b) The charts showing the shape recovery force versus temperature of 4D-printed CFRC PLA at three different

specimens (1) thicknesses, (2) voltages, and (3) CF layers. (4) A printed prototype and (5) a composite deployable claw device model. (6) The infrared pictures and photos of the claw device throughout the electrothermally triggered form recovery procedure. Adapted with permission (Chen, H., et al. 2021).

2.6.2. Magnetic SMPCs

Magnetic fields constitute a secure and dependable method for actuating SMPCs (Yue, et al. 2021, Bonifacich, et al. 2021). Magneto-active materials, created by embedding magnets or magnetic particles in PLA, offer many applications for soft actuators due to their magnetic field control advantages (Yarali, et al. 2022). Actuators, metamaterials, soft robotics, and medical devices are just a few of the industries that can benefit from the utilisation of magnetic materials (Chaudhary, et al. 2020). These materials can move dynamically and change form swiftly and reversibly in the presence of a magnetic field (Zhang, Chengqian, et al. 2021). Magnetic SMPs contain hard magnetic particles that have shown improved shape-manipulation capabilities. In a single material system, they can perform shape locking as well as reprogrammable, untethered, rapid, and reversible shape changes (van Vilsteren, Yarmand and Ghodrat 2021).

To achieve the required shape, SMPCs can be remotely stimulated and programmed. Zhao et al. (2019) printed a scaffold exhibiting magnetically induced shape recovery within 35 seconds when exposed to a 30 kHz magnetic field. Magnetic materials, possessing biodegradability, SME, remote controllability, and swift responsiveness, offer potential as occlusion devices for cardiac applications. Liu et al. (2023) produced SMPCs with good mechanical properties and magneto-responsive behaviour using a PLA, thermoplastic polyurethane (TPU), and Fe_3O_4 particle feedstock for 3D printing. The 3D-printed material demonstrated significant tensile strength and modulus, as well as a homogeneous distribution of magnetic particles throughout polymer mixtures, according to the findings. The printed actuators could be activated by heat or magnetic fields. It exhibited high heat generation efficiency due to its exceptional shape fix ratio, recovery rate, and rapid 40-second magnetic response. To construct smart actuators that could be fully recovered under a contactless magnetic field and programmed by an external force, the scientists printed and produced structures that resembled bionic flowers and honeycombs (see **Figure 2.6a**. Using three pedals with different Fe_3O_4 composites, the repair of the flower-bud structure could be controlled layer by layer.

The shape memory capabilities of 4D-printed PLA/Fe_3O_4 composite actuators were demonstrated by Zhang et al. (2019). A certain magnetic field and temperature were used to study the form recovery mechanism. A bone-shaped PLA/Fe_3O_4 structure (15% Fe_3O_4) was activated by a 27.5 kHz magnetic field. The results showed that there was great potential for 4D-printed magnetic structures to work in biological and medicinal applications (see **Figure 2.6b**). Riley et al. (2020) introduced a substantial improvement in the capacity of SMP structures to produce various stable shapes. Their method allowed for swift and reversible alterations to these shapes without the requirement of reprogramming. To activate snap-through remotely using magnetic fields, they combined PLA with magnetic PLA (MPLA). Also, Moradi et al. (2023) studied the effect of concurrent magnetization on the magneto-mechanical properties of active polymers created using 4D printing. The primary goal of the FDM technique in 4D printing was to magnetise MPLA material. Samples were magnetised

in different states of the magnetic field during the printing process. Specimens were printed in three different states: without magnets, at three angles of 0, 45, and 90° to the applied magnetic field, and with two magnets surrounding the printing area and one beneath it. The findings indicated that, in comparison to printed samples with and without a magnetic field, those on the magnet's edge were saturated in a higher specific magnetization. By applying a magnetic field, the specific magnetization in the magnetic field increased by 63.46% in the direction of the sample deposition. When a magnetic field was present and the sample was printed at a 0° angle along the tension direction, the strength increased by 21.4%. Using two magnets around the printing zone instead of one beneath it improved the mechanical properties of the printed sample, regardless of the effect of the printing angle. 4D printing with magnets under the printing bed at a 0° angle along the tension direction was the best printing method for achieving the necessary mechanical and magnetic properties.

Doostmohammadi et al. (2024) investigated 4D-printed magnetic SMPs using a composite of Fe_3O_4 nanoparticles, PLA, and polymethyl methacrylate (PMMA). The uniform dispersion of Fe_3O_4 nanoparticles and the high compatibility of PLA and PMMA phases, both crucial for the efficient transfer of heat during the shape memory process, were confirmed by field emission scanning electron microscopy. Achieving 100% shape fixity and 100% recovery in less than 85 seconds, 4D-printed magnetic SMP nanocomposites demonstrated remarkable mechanical qualities and quick, effective shape memory responses to both inductive and direct heating stimuli. Owing to their quick remote actuation, biocompatibility, and strong mechanical design, they were suggested as viable options for biomedical implants, particularly for the minimally invasive introduction of bone scaffolds. With their special benefits for applications requiring resilient, sensitive, and adaptable materials, magnetic SMPCs represent a promising new direction in smart materials technology. A multitude of advanced technical and medical applications can benefit greatly from composite materials due to their inherent strength, flexibility, and durability, as well as their ability to undergo considerable form changes in reaction to magnetic fields.

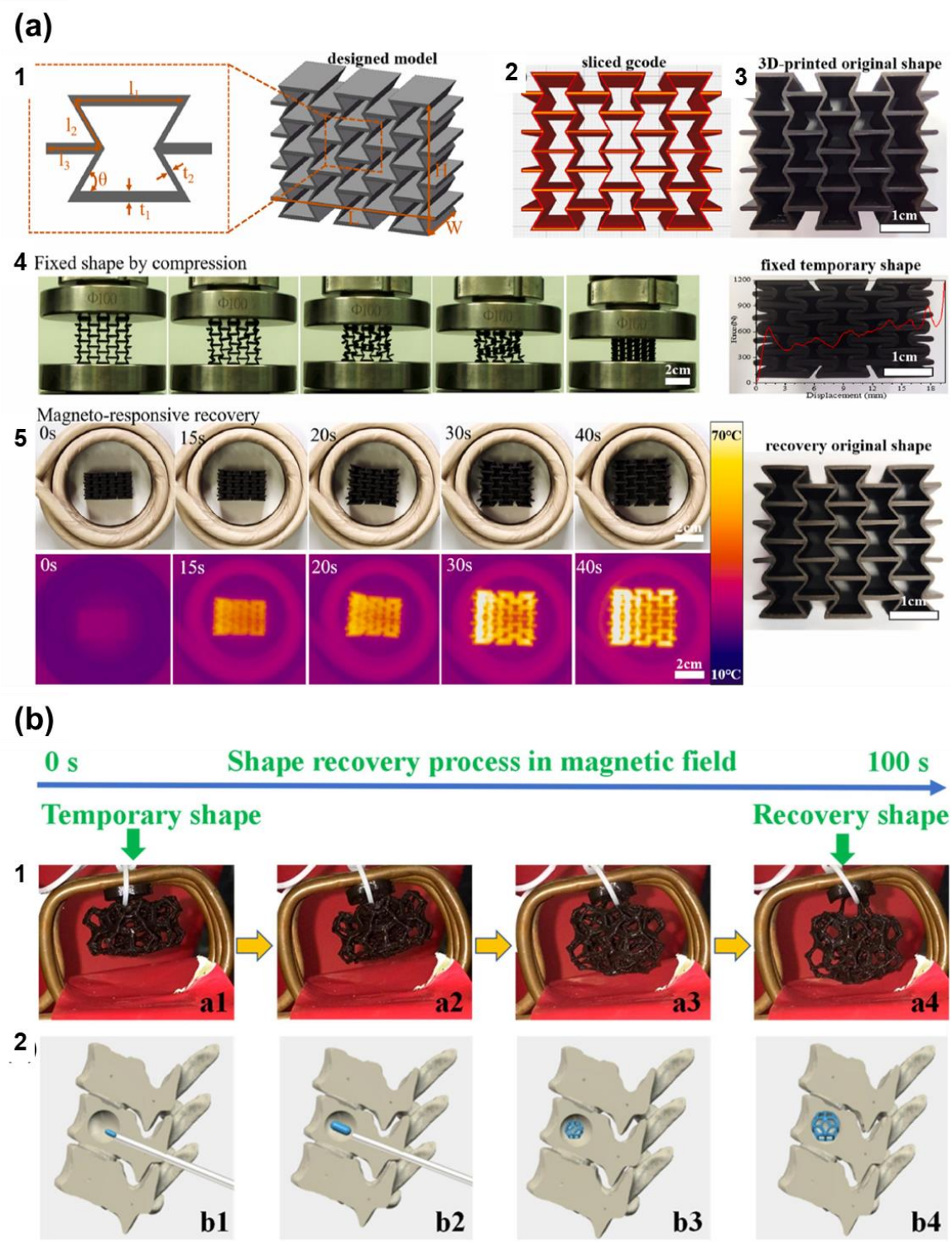

Figure 2.6. (a) (1) The reentrant structure's geometric design was (2) sliced using CURA software, (3) 3D printed parts, (4) fixed shape by compression (with a compression force-displacement curve as the inset curve), and (5) magneto-responsive shape memory method. Adapted with permission (Liu, Han, et al. 2023). (b) (1) The 4D-printed composite structure's shape recovery behaviour in a magnetic field; (2) A simulation illustrating the 4D structure's mechanism as a bone-mending tool. Adapted with permission (Zhang, Fenghua, et al. 2019).

2.6.3. Pneumatic actuators

Recently, the production of complex soft pneumatic actuators with high resolution and repeatability has been made possible by the promising technique known as 3D/4D printing (Lalegani Dezaki, et al. 2023, Zolfagharian, Mahmud, et al. 2020). Pneumatic actuators are inexpensive because solenoids and diaphragm pumps, two inexpensive parts, are used in them. These robots use soft pneumatic actuators made of pneumatic networks as well as fibre-reinforced actuators (Tawk and Alici 2021). These actuators can withstand large deformations and have excellent flexibility and safety. They can be made cheaply and have favourable power-to-weight ratios (Xavier, et al. 2022). Pneumatic actuators can be activated by either positive or negative pressure; vacuum actuators are particularly helpful in situations when volume is constrained (Hu, D., et al. Jul 2020). Printed pneumatic actuators can perform a variety of movements based on their features. These actuators are utilised in a variety of fields, including human-computer interaction, minimally invasive surgery, rehabilitation, senior citizen support, and manipulation of fragile materials (Hong, et al. May 2015, Sun, Z., Guo and Tang 2019).

Production of thermoplastic and elastomeric materials is possible under specific circumstances thanks to 3D printing technology. FDM is a more successful 3D printing technique since it requires far less post-processing and is more affordable and repeatable than other techniques. For example, EcoFlex 00–30 (Smooth-On) was extruded using a customised FDM printer to create the pneumatic actuators (J. Morrow, S. Hemleben and Y. Menguc 2017). The printed actuator and the mould-made technique were contrasted. Even though the method's initial viability was established, it was noted that the printed actuators considerably differed from the intended characteristics, especially in wall thickness, which decreased the force output and bending deflection. Also, a Print-it-Yourself (PIY) glove, a fully 3D-printed soft robotic hand exoskeleton for stroke patients, was designed and investigated in advance by Ang et al. (Sep 2017). FDM was used to fabricate the PIY glove employing consumer-based 3D printing technology to reduce fabrication costs and enable patients to 3D print rehabilitative and assistive equipment at home. Using a unique fold-based design of 3D-printed soft actuators, the PIY glove allowed for finger bending function. The PIY Glove was characterised by its grip force and range of motion, and fabrication recommendations were provided.

The FDM method and commercial TPU filaments have been used to 3D/4D print the inexpensive soft pneumatic actuators (Xavier, et al. 2022, Zolfagharian, Mahmud, et al. 2020, Lalegani Dezaki, et al. 2023). Meanwhile, pneumatic actuators can be developed using SMPs. PneuMesh is a novel truss-based shape-changing system that was 3D printed by Gu et al. (2022). It allowed for a variety of jobs to be performed while streamlining the design and building process. An air channel connection approach and a changeable constraint design were used by PneuMesh to achieve this. This allowed for the intricate shape-changing capabilities to be maintained with a marked decrease in the number of control units needed. Users can design the shape and motion of truss-based structure-changing machines and devices using a design tool developed that features real-time simulation. During the design session, seven participants demonstrated how PneuMesh can be used to create structures with a range of shapes and practical movements.

Additionally, Wang et al. (2023b) examined how 4D-printed thermoplastics with thermoformable and heat-deformable properties may be used to simplify the intricate human production process and increase the variety of blow moulding possibilities. They proposed PneuFab, a unique and democratised blow moulding technology made possible using temporal triggering techniques and FDM 3D-printed bespoke structures. They also developed and evaluated a design tool that allowed users to view the forms that were generated and change parameters until they achieved the desired designs. The objective was to increase accessibility and investigate the unexplored possibilities of digital blow moulding production by showcasing design spaces that included artefacts with intricate geometries and adjustable stiffness (refer to **Figure 2.7a**) (Wang, G., et al. 2023a).

Moreover, pneumatic actuators might vary based on the specifications. One useful method for giving robots the advantages of both rigid and soft designs is the use of variable stiffness pneumatic actuators (Fitzgerald, Delaney and Howard 2020). Jamming structures show promise for controlling changeable stiffness because of their ease of usage, affordability, flexibility, quick response, and customizability (Wang, Y., et al. 2021). The process of jamming involves the collapse of fluid-tight packaging that is loaded with different materials. By bringing the parts closer together, this movement creates friction, which in turn makes the device more stiff (Hwang, et al. 2022). The standard parts of jamming structures consist of a vacuum bag and internal components enclosed in the bag.

A vacuum pressure causes large normal forces to be created between internal components, and the ensuing frictional forces prevent the jamming structure from undergoing deformation. The rigidity of the structure can be dynamically modified by adjusting the pressure discrepancy between the interior and exterior of the vacuum bag (Yang, B., et al. 2021). Jamming structures have been widely employed to increase the stiffness of soft pneumatic actuators because of their ease of usage and safety (Aktaş, et al. 2021). Studies on jamming tactics based on different internal components have been reported (Gao, et al. 2020, Li, W., et al. May 30, 2021). The most often utilised internal part in laminar jamming (LJ) designs is a flexible yet inextensible sheet. They are usually lightweight and have a suction system that allows them to respond rapidly. innovative jamming structures, including those composed of particles and LJ materials, have also been developed (Ibrahimi, et al. 2021).

Narang et al. (2018) provided a quantitative analysis of the performance of a two-layer LJ actuator across all critical deformation phases. Soft machines can exhibit specific characteristics such as rigidity, damping, and kinematics that are usually associated with rigid robots. This is made possible by the incorporation of jamming structures into these machines. They showed how LJ can be used to lock the shape in the required position (see **Figure 2.7b**). For small and adaptable artificial muscles, Lin et al. (2020) created origami skeletons with adjustable stiffness. Controllable stiffness origami skeletons were created by merging the folding strategy of origami with an adjustable stiffness strategy, inspired by the activity strategy of a human limb. A cubic artificial muscle was constructed using layers of flexible sandpaper folded in an origami pattern and filled with LJ material. This device was powered by vacuum pressure and capable of a shape change.

Kwon et al. (2022) built a sandwich-structured jamming mechanism composed of a rubber-coated outer layer and an internal core with asymmetrical cellular properties. The low

bending modulus of the light anisotropic core allowed for remarkable structural compliance when the structure was not jammed but jamming made it quite rigid. In comparison to particle and liquid jet structures, the proposed structure exhibited superior strength-to-weight ratio and a more pronounced change in stiffness between jammed and unjammed states. Wang et al. (2020) employed an LJ structure to construct a tendon-driven soft robotic hand capable of adjusting stiffness. The LJ actuator independently modified the stiffness of individual actuator components, while a single tendon controlled the overall deformation.

Many of the shortcomings of conventional variable dampers are addressed by LJ, a helpful variable-impedance mechanism, according to Narang et al. (2018). Jamming structures' tunable stiffness properties showed that frequencies could be controlled, and their ability to modify damping had an impact on amplitudes. Innovative LJ actuators with increased strength were created for a variety of uses. Moreover, the results suggested that actuators with jamming features can tune to store or release energy according to the requirements. Also, Gerez et al. (2020) introduced a novel exoskeleton glove that utilizes LJ technology to enable independent finger spreading. This device incorporates adaptable stiffness regions on the glove's back to modify finger curvature and enhance grip stability. To further improve grasp security, an extendable auxiliary thumb was integrated into the design. The exoskeleton glove, a hybrid assistive device, greatly enhanced the user's grasping ability by applying the pressures required to do various daily tasks. Additionally, Willemstein et al. (2022) used the infill foam method to print structures with varying porosities and a coiling liquid rope to print a soft actuator. This grading allowed for the creation of rectangular frameworks with a variety of distortion sequences, including bending, shrinking, and folding.

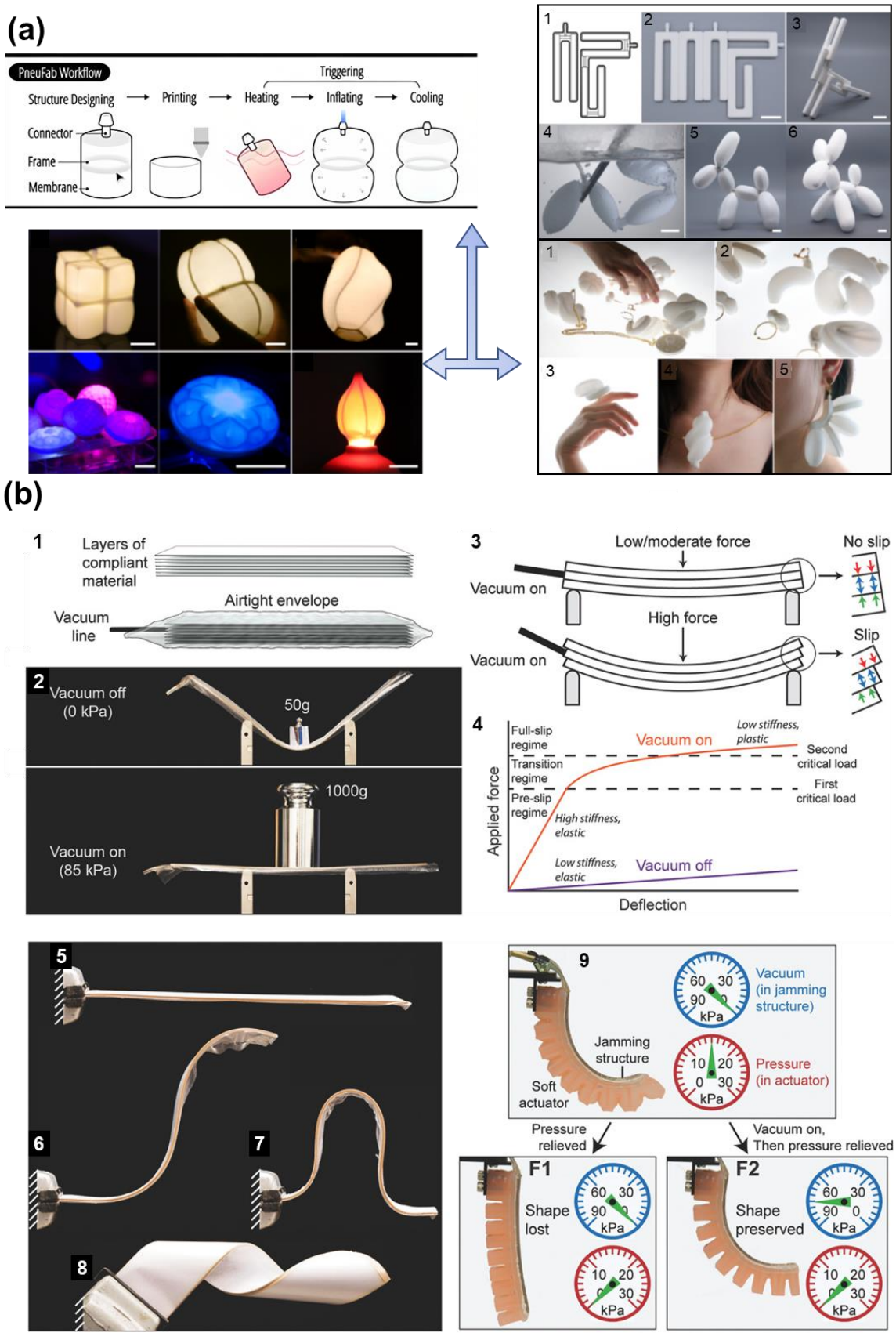

Figure 2.7. (a) The PneuFab manufacturing process, consists of heating, activating, and cooling processes for two modular balloon dog constructions and transformative lights, as shown by labels 1 through 6. The heating, activation, and cooling processes depicted in labels 1 through 5 can be applied in the jewellery industry. A length of 20 mm is represented by the scale bar in the picture (Wang, G., et al. 2023b). (b) Essential characteristics of LJ structures. (1) Diagram showing the structure of jamming. (2) There is minimal bending

stiffness in the structure when the vacuum is removed because the layers bend separately. With the vacuum activated, the structure exhibits great bending stiffness as the layers flex cohesively. (3) The layers are cohesive only up to a critical force when the vacuum is on, though. At specific spots along their interfaces, the layers slip due to longitudinal shear stress, which is significant for greater forces. (4) A brief overview of the mechanical behaviour of the LJ actuator. (5-8) Function of shape-locking demonstrated. After 20 layers of copy paper were twisted into different forms, a vacuum was applied, and the shape was always maintained in the jamming structure. (9) A pneumatic soft actuator was attached to a 20-layer jamming structure. To achieve the specified bending angle, the actuator was first pressurised to 16 kPa. F1) In the first test, the jamming structure was not vacuumed, and the actuator was depressurised. The composite structure instantly went back to being unaltered. F2) The jamming structure was first subjected to a vacuum pressure of 85 kPa, and the actuator was subsequently depressurised. The system maintained its shape with great accuracy (Narang, Vlassak and Howe 2018).

2.7. Summary and challenges

FDM 3D/4D printing is rather popular in many different areas now because of its track record of providing exceptional performance and consistent quality (Roudný and Syrový 2022). As previously said, this process has shown to be flexible, producing a wide range of final parts for different manufacturing sectors. The widely accepted and advantageous production process of FDM is the reason for its widespread use. From specialists to enthusiasts, this procedure is simple and accessible to anyone, enabling them to practically implement their ideas (van Manen, Janbaz and Zadpoor 2017, Ford and Minshall 2019). FDM offers several additional benefits in addition to consistent quality and performance.

Evaluations have been conducted regarding FDM 4D printing's ability to produce SMP/SMPCs. In contrast to conventional 3D printing, 4D printing adds an intriguing dimension by allowing time-dependent modifications to be made to a part's design and specifications. This allows for the construction of unique and dynamic structures. Despite its recent emergence, 4D printing shares fundamental similarities with its predecessor, 3D printing. Both processes construct objects layer-by-layer through the extrusion of molten thermoplastic material using a heated nozzle. However, 4D printing distinguishes itself by incorporating a time-dependent element, enabling printed objects to undergo transformative changes. This temporal dimension is achieved through careful selection and manipulation of specific printing materials (Kantaros, Ganetsos and Piromalis 2023a).

FDM 4D printing excels in producing intricate and dynamic structures, making it a valuable tool for the development of composite actuators (Carrell, Gruss and Gomez 2020, Bodaghi, M., et al. 2020). Through FDM 4D printing, objects can be engineered to react dynamically to user interactions, alterations in environmental conditions, or even physiological cues. This gives designers new freedom to craft intuitive and captivating user experiences. The shape or texture of FDM 4D-printed control interfaces, for example, may dynamically change based on the user's choices or usage conditions, making for a more engaging and customised interaction experience (Wang, Z., et al. 2023, Li, J., et al. 2023). Additionally, direct and seamless human-computer interactions can be made possible by FDM 4D printing by enabling the integration of interactive different components into actuators. Application of time variation in 4D printing may fundamentally change the end actuator's functionality and

design. This technology transcends the limitations of static objects, empowering them to dynamically adapt to their surroundings or specific stimuli. A new era of interactive and dynamic actuators is brought in by 4D printing with the introduction of the fourth dimension, time. With the potential to revolutionize countless industries, this groundbreaking innovation offers a wealth of opportunities for manufacturing and design.

The chapter makes the point that conventional 3D printing materials, such as PLA and its composites, can be employed as smart materials in 4D printing projects. Nevertheless, a major obstacle to 4D printing's advancement is the need to increase the range of easily accessible materials for this purpose. Expanding the range of printing possibilities is necessary for 4D printing to realise its full potential for printing SMPC actuators. Apart from selecting materials with good external response, some uses may require materials with specific responses to external stimuli. Also, users may encounter several challenges because 4D printing is still in its infancy, the most significant of which is the intricacy of building the structures necessary to enable the necessary transformation into a certain shape (Yang, H. 2019). To enable material programming to perform complex transformations, users may need to construct extra components. It becomes essential to employ multiple materials as well as special printing techniques and interfaces to accomplish movements. A combination of these problems results in the overall difficulties users face when utilising the potential of 4D printing technology (Demoly and André 2022) . Even though 4D-printed structures have shown they can change shape by using a range of materials and pre-designed internal tensions, SMP and shape-changing materials are now seen as the best options due to their increased usefulness. Nevertheless, low mechanical characteristics are a problem for SMPs like PLA. Therefore, it is essential to enhance the mechanical characteristics without compromising the shape memory properties.

FDM 4D printing offers new opportunities but also presents certain difficulties when used with SMPs and SMPCs. In the field of 4D printing, one significant drawback is the complex control needed for the transformation and shape changing. Comprehending the complicated thermomechanical properties of metals and ceramics is crucial for attaining accurate temporal regulation of their shape-morphing behaviour, as these properties might be fundamentally difficult. Conducting a smooth transition and remote programming of actuators can be difficult since different SMPCs have distinct phase transitions and thermal expansion coefficients. The brittle nature of SMPs, such as PLA, presents significant challenges for FDM 4D printing. Precise control over stress distribution is crucial during the transformation process to prevent structural failure. Moreover, the time-dependent nature of 4D printing introduces additional complexities in terms of printing parameters and material behaviour. To fully realize the potential of FDM 4D printing with SMP composites, substantial advancements in material science, temperature regulation, and design methodologies are imperative. To advance the sector, future material development initiatives ought to concentrate on a few key areas. Potential advancements in FDM 4D printing of SMP composites include reduced activation times, increased activation force, the ability to print with multiple materials, actuation from various positions, remote and targeted activation, lower activation temperatures, and the capacity to activate using multiple stimuli. In addition to advances in 3D printing technology, the development of state-of-the-art 4D materials is crucial. Among the basic mechanical properties of these materials that may be enhanced are strength, flexibility, and reusability. Additional performance indicators such as

electrical, thermal, or pneumatic actuation capabilities also enable the construction of multifunctional composite actuators. These improvements allow these materials to be applied to numerous manufacturing sectors.

4D-printed composite smart actuators have historically been primarily activated by various stimuli chosen according to their properties. Still, a lot of actuators need a continuous control system and a stable energy supply to provide the forces required for their intended movements (El-Atab, et al. 2020). While multi-responsive smart actuators hold the promise of wireless and sustainable operation through external stimuli, significant hurdles remain. These challenges include scalability limitations, susceptibility to environmental influences, and insufficient force output. Overcoming these obstacles is essential for realizing the full potential of this technology. Robotics and healthcare are only two of the industries that could undergo a radical transformation because of a novel technology called multi-responsive soft actuators. Multi-responsive actuators exhibit superior adaptability compared to their single-stimulus counterparts by responding to a wider spectrum of stimuli. Moreover, these actuators incorporate advanced features such as shape locking, which significantly enhances energy efficiency. By retaining their configuration without continuous energy input, shape locking optimizes actuator performance and minimises overall energy consumption (Lalegani Dezaki and Bodaghi 2023b).

By maximising performance and consuming less energy, they increase efficiency. For instance, these actuators can retain their shape without requiring extra energy thanks to the shape-locking process, which can increase their effectiveness and lower their total energy usage. Smart actuators can preserve their shape for an extended amount of time and save energy by using shape locking. A robotic gripper equipped with shape-locking capabilities can securely hold objects without consuming continuous energy to maintain a closed grip. This innovative approach significantly reduces the usage of energy and extends the gripper's operational lifespan (Arif, et al. 2022).

4D-printed actuators offer several sustainability advantages, including energy efficiency, adaptability, and the incorporation of waste-reducing materials. Nevertheless, the process necessitates specific materials and energy consumption, potentially incurring environmental disadvantages. A comprehensive life cycle assessment, encompassing disposal and recycling potential, is essential to ensure the sustainability benefits of these actuators outweigh their environmental impact (Khalid, et al. 2022).

Chapter 3

Magnetorheological elastomer-based 4D printed electroactive composite actuators

This chapter examines 4D-printed electroactive composite actuators based on magnetorheological elastomers, activated through electro-Joule heating and magnetic fields. It highlights research gaps and showcases the unique aspects of these actuators. This chapter covers the materials and methods, findings, and manufacturing processes with applications. All content is adapted with permission from the article published in Sensors and Actuators A: Physical by Elsevier.

- **Lalegani Dezaki M**, Bodaghi M. Magnetorheological elastomer-based 4D printed electroactive composite actuators. Sensors and actuators. A. Physical. 2023;349:11406310.1016/j.sna.2022.114063.

Chapter 2 covers the literature and introduction for this chapter comprehensively. The following introduction is quick summary of the chapter.

3.1. Introduction

The magnetically controlled motions of soft robots can be powered by soft actuators, which are made of elastomers and gels functionalized with magnetically active materials. Advancements in soft actuator technologies, including electroactive polymer, tough hydrogels, origami, 4D printing, and liquid metal-injected elastomers, have made it possible to create actuators with significantly better accomplishment (Li, M., et al. 2022). Magnetorheological elastomers (MRE), composed of a polymeric matrix reinforced with magnetic particles, exhibit the capacity to undergo alterations in their mechanical properties when subjected to an external magnetic field (Bernat, et al. 2022).

Given that magnetic fields are fast-acting, contactless, and generally safe for human health, using them to induce reactions seems like a good idea. MRE materials and composites are specifically defined as those that exhibit tunable rheological and viscoelastic properties, such as shear stress, yield stress, dynamic modulus, and damping, in response to an external magnetic field (Chung, Parsons and Zheng 2021). The magnetic resonance effect induces alterations in the composite's mechanical properties through magnetic interactions between particles within the surrounding matrix. This phenomenon results in the formation of chain-like structures that exhibit approximate alignment with the applied magnetic field. Most MREs are composed of 3–5 μm micron-sized particles with magnetic characteristics incorporated into a nonmagnetic medium (Díez, et al. 2021).

Magnetic forces can be employed to control how tightly a gripper holds an item, the movement of its grasping parts, and the rigidity of the surrounding material. The grippers designed by Xu et al. (2019) and Jiachen et al. (2017) were innovative in their use of external magnetic fields to precisely control and program the movement of their gripping arms. Skfivan et al. (Apr 2019) designed a gripper without fingers or joints, controlled by an electromagnet positioned at its core. The gripper's components were constructed from a magnetic material that could alter its rigidity and weight distribution based on adjustments to the electromagnet's strength.

Additionally, Carpenter et al. (2021) created a flexible magnetic actuator from strontium ferrite, which could be activated with minimal magnetic exposure. Iwasaki et al. (2020) designed a suction cup system with a central neodymium magnet, allowing for precise

manipulation of the cup's speed and position through magnetic field adjustments. The magnetic field served as a versatile tool for object control, managing both the suction cup's adhesion and release processes. Lalegani Dezaki et al. (2022) presented a new design for magneto-responsive SMP foam composites with excellent stability and reversibility. The fabrication process uses strontium ferrite magnetic particle-filled silicone resins and a thin layer of SMP foam on one side. The result is a versatile, lightweight gripper constructed from MRE composite, offering customizable magnetic patterns for precise manipulation. With a low magnetic field, it can grasp, hold, and move objects both horizontally and vertically. The SMP foam enhances stability more than magnetic elastomers alone by improving the contact surface and reducing weight by up to three times. This small, shape-recoverable gripper can lift objects up to eight times its own weight.

While MRE soft actuators offer numerous benefits, their activation and positional control necessitate a permanent magnet or a magnetic field. Additionally, the compatibility of electroactive 4D printing with MRE actuators remains unexplored. This chapter introduces a novel, lightweight, bi-stable actuator composed entirely of CPLA and MRE. This is the first instance of combining these materials to create a reversible composite activated by Joule heating under low magnetic field control. This study signifies the first demonstration of a remotely programmable bi-stable smart soft composite actuator actuated by a combined magnetic and Joule heating electric stimuli. Consequently, this research achieves the development of a bi-directional actuator by integrating MRE and 4D printing technology.

This chapter focuses on three key objectives: (1) identifying crucial design considerations, (2) proposing a conceptual design, and (3) comprehensively detailing the fabrication process for these novel MRE-SMP actuators. A streamlined production method promises faster actuator development for diverse applications. The implemented model and solution techniques are anticipated to facilitate the creation of lightweight, highly stable MRE-responsive Joule heating actuators with minimal contact area. As depicted in **Figure 3.1**, this chapter is structured to first explore the mechanical properties of CPLA. The shape-shifting properties and materials that are electroactive of printed CPLA are then demonstrated. After a detailed assessment of the produced actuator's possible uses, the integration of MRE with CPLAs is covered.

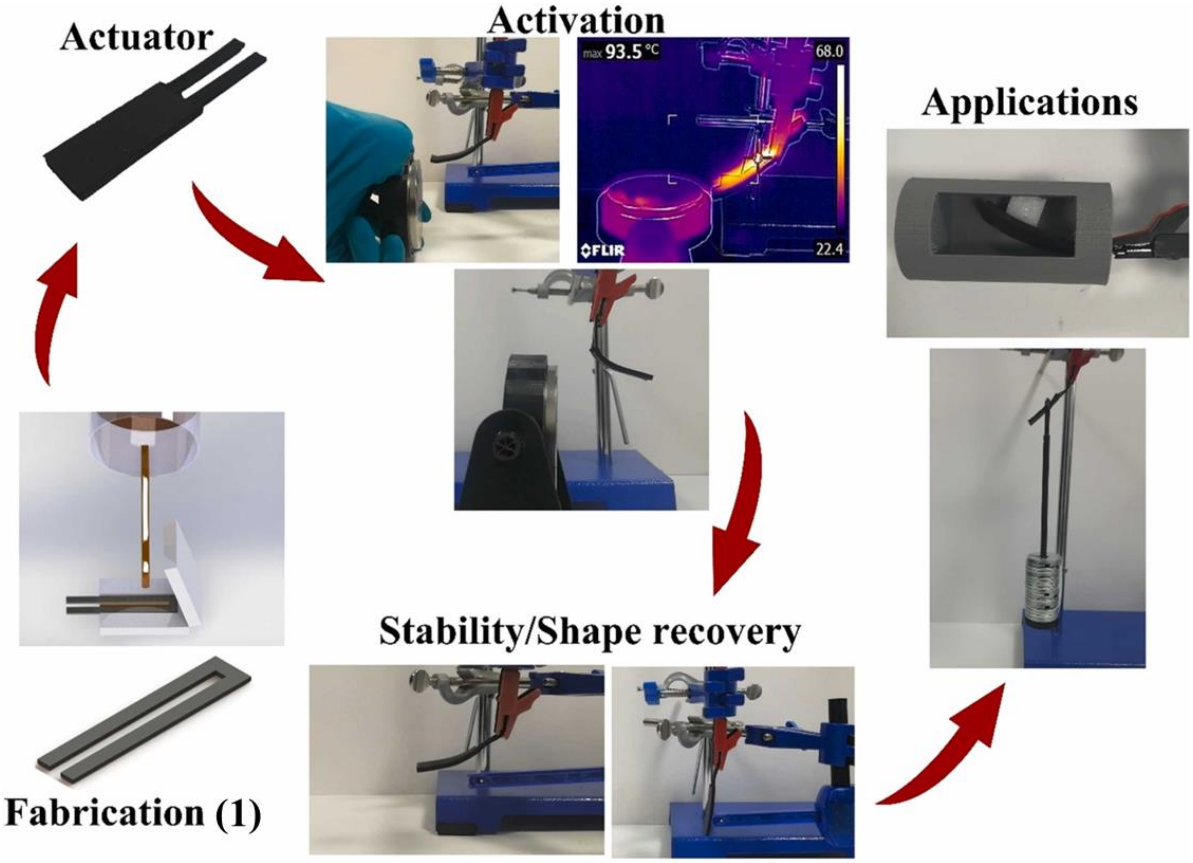

Figure 3.1. Images show the schematic processes involved in manufacturing and implementing the suggested actuator.

3.2. Materials and methods

3.2.1. Materials

This chapter explores the utilization of existing thermoplastic filaments, potentially incorporating functional additives, for FDM 4D printing. Commercially available black PLA filament from Creality was chosen for its affordability and well-documented SME among SMPs. Additionally, CPLA filament (Proto-Pasta, Proto Plant, USA), containing approximately 21 wt% of conductive carbon black, was employed due to its suitability for low-voltage devices. CPLA exhibits a significant decrease in Young's modulus upon being raised to 80°C from room temperature (Al-Rubaiai, et al. Sep 18, 2017). Scanning electron microscopy (SEM) using a JSM-7100F LV FEG SEM instrument was utilized to analyse the microstructure and characteristics of CPLA.

The second material investigated was strontium ferrite ($SrFe_{12}O_{19}$), a magnetic particle commercially available under the name UF-S2 (DOWA Electronics Materials). This chosen manufacturing method offers high adaptability, allowing for changes to the particles' size, shape, and chemical structure (Lalegani Dezaki and Bodaghi 2022). By examining the magnetic properties, mechanical properties, and deformation behaviour of composites incorporating different particle types, the potential of this design space can be explored. UF-S2 was selected due to its well-defined bimodal particle size distribution, with an average diameter of 1.3 μm. This powder's biocompatibility and ability to achieve magnetization within composites at relatively low magnetic fields make it particularly attractive for the development of soft actuators (Tripathi, et al. 2021, de Oliveira Barros, et al. 2022).

3.2.2. 4D printing process

All samples were created using an Ultimaker S3 FDM 3D printer equipped with two 0.4 mm nozzles. The design of the 3D-printed structure, detailed in **Figures 3.2a and 3.2b**, leverages the phase change properties of CPLA to achieve optimal heat distribution throughout the structure (Dong, X., et al. 2022, Mitkus, Cerbe and Sinapius 2022). Material properties related to CPLA's conductivity and resistance have been established in prior research (Beniak, et al. 2022, Stopforth 2021, Al-Rubaiai, et al. Sep 18, 2017). This design offers improved stability for MRE while maintaining its weight within a similar footprint. The structure's extended length facilitates better clamping and electrical connections. Printing parameters were set at 30°C for the hotbed and 210°C for printing temperature. A concentric infill pattern with a 100% fill rate was chosen to ensure internal continuity. To optimize printing quality, a layer height of 0.2 mm and no surface coating were employed. Additionally, a printing speed of 70 mm/s was selected to enhance actuation behaviour as reported (Alshebly and Nafea Jan 1, 2022). The 3D-printed structure serves as the core of the MRE, contributing to its stability. Furthermore, the electroactive properties of the CPLA material offer an alternative approach that eliminates the requirement for a magnetic field. By adjusting the size of the printed structure, the resistance of the CPLA component can be manipulated. This variation in resistance necessitates corresponding adjustments to the temperature distribution within the structure and the applied electrical current.

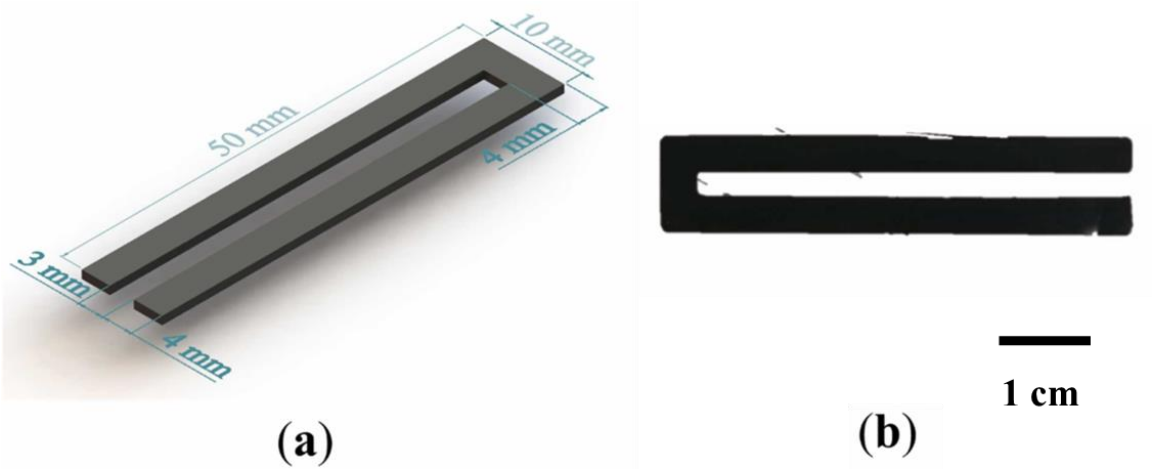

Figure 3.2. (a) A 3D model including the details of the structure, and (b) the core structure.

3.2.3. MRE-based 4D-printed composite

This research explores the potential of MREs as multifunctional materials for soft robotics applications. MREs exhibit promise as sensors, actuators, and even the building blocks for untethered robots capable of pick-and-place manoeuvres, gripping objects, and manipulating 3D shapes through remote control (Ze, et al. 2020, Ausanio, et al. 2014). The combination of MREs with 4D-printed structures is proposed as a method to create ultra-thin bistable shape memory actuators. This design approach allows for the customization of actuators based on specific performance requirements.

The fabrication process for MRE soft actuators is relatively straightforward. A homogeneous, viscous composite paste is produced by thoroughly mixing magnetic particles with a silicone resin (such as Ecoflex 00-30) using a mechanical stirrer. This paste typically comprises a high concentration (approximately 70%) of bimodal UF-S2 magnetic particles. The magnetic characteristics of the resulting films are determined by measuring the magnetic flux density perpendicular to the film's surface.

Moulds fabricated from PLA using FDM 3D printing are employed to shape the MRE paste. The formation of a conductive network within the composite increases its viscosity, hindering its flowability. Consequently, the paste requires squeezing during the casting process to ensure complete mould filling. The high viscosity of the paste makes air bubble removal challenging; however, their presence has a negligible effect on the material's magnetic responsiveness.

The inherent instability of the magnetic silicone composite films necessitates the continuous application of a magnetic field during the fabrication process. This field is crucial for maintaining the actuator's shape without compromising its stiffness or weight. To create a self-sustaining design without continuous magnetic field exposure, a printed core structure is integrated. This approach is particularly beneficial for developing shape memory composite smart actuators.

The fabrication of a composite actuator incorporating a 4D-printed core follows the process outlined in **Figure 3.3**. Silicone resin is applied to both the upper and lower surfaces of the 4D-printed structure during the curing phase, as shown in **Figures 3.3a and 3.3b**. The mould is initially filled with the magnetic resin. Subsequently, the magnetic paste is introduced, followed by the careful placement of the CPLA structure. To achieve the desired actuator thickness of 2.5 mm, additional magnetic resin is added. After shaping, the MRE composite is compressed with a plate and cured at room temperature for a minimum of 4 hours. A neodymium magnet is positioned on the mould during the curing process to maintain alignment (see **Figure 3.3c**).

A uniform out-of-plane magnetization is achieved using a square neodymium magnet. Permanent magnets positioned on the mould during the curing process are employed to magnetize the soft composite actuators. During the curing process, a square magnet (N42 grade, Magnet Expert Ltd.) is positioned at each extremity of the MRE composite film to optimise particle alignment with their magnetic easy axis parallel to the applied field. This approach results in a higher degree of magnetization compared to post-curing methods (Carpenter, et al. 2021). The resulting actuator measures 55 millimetres in length, 12 millimetres in width, and 2.5 millimetres in thickness (refer to **Figure 3.3d**).

The impact of the core structure on the actuator's stability and weight is assessed by analysing sample behaviour. By varying the distance between the magnet and the actuator, it is possible to control the applied magnetic field. In addition, low-intensity magnetic field stimulation of the core structure via Joule heating can be used to activate the actuator.

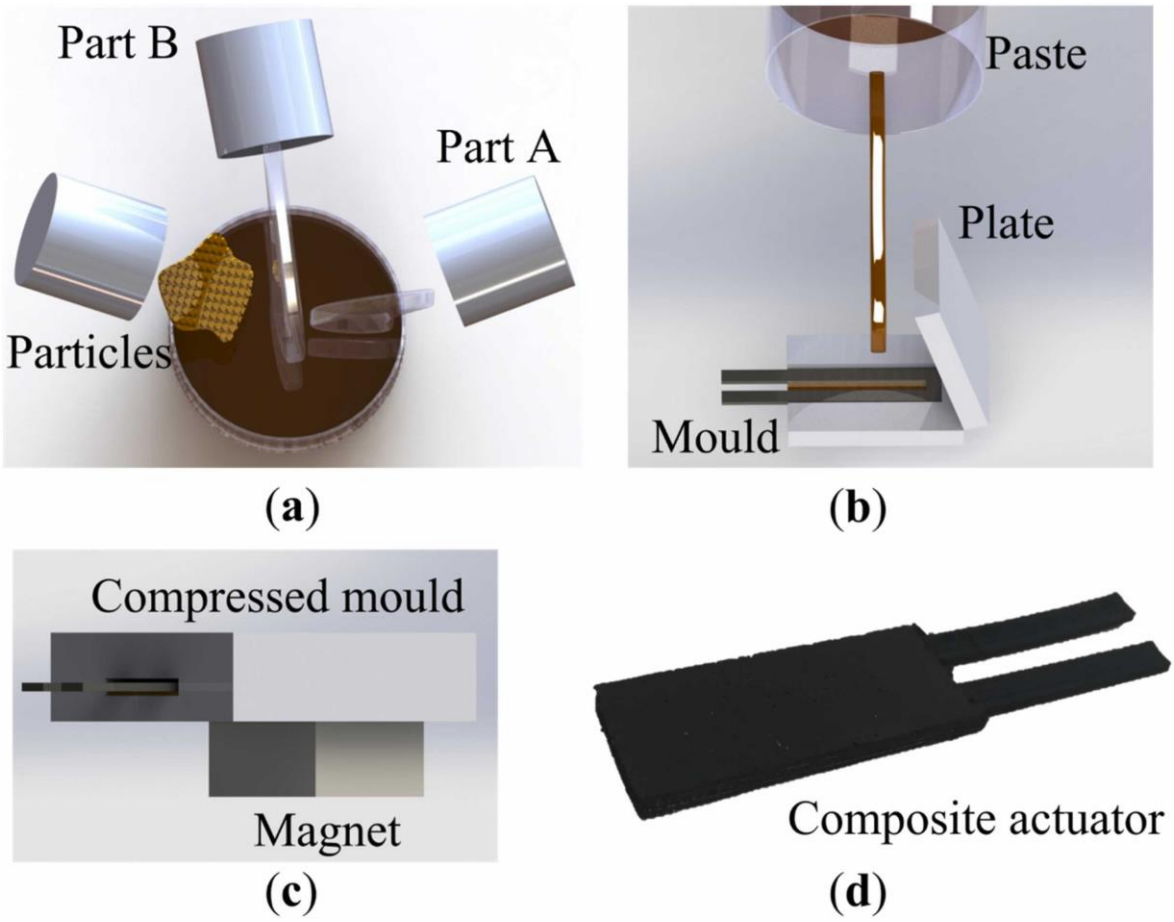

Figure 3.3. (a) Paste preparation: Magnetic particles are mixed with silicone resins to create a homogeneous, viscous paste. (b) Mould casting: To create actuators with exact geometries, the viscous MRE paste is poured into a 3D-printed mould. (c) Magnetisation and curing: The actuator is magnetised by putting neodymium magnets in particular places during the curing process. To guarantee full filling and a flawless surface finish, the mould is then squeezed. (d) Electroactive composite actuator: The final product is an MRE-based electroactive composite actuator.

3.2.4. Dynamic mechanical analysis of core structure

To evaluate the suitability of 4D-printed CPLA for shape memory applications, this study employs a dynamic mechanical analyser (DMA) (e.g., PerkinElmer DMA 8000) to measure its storage modulus. The DMA samples were printed with dimensions of 40 mm x 10 mm x 1 mm and tested at a speed of 70 mm/s. Storage modulus and loss modulus are considered primary determinants of SME in SMPs. Consequently, these properties are critical for evaluating the electro-induced SME behaviour of the 4D-printed CPLA. The influence of particle integration on the CPLA's storage modulus and T_g needs to be considered. 1 Hz frequency was selected to mimic the property changes occurring during shape memory activation (typically associated with temperature fluctuations). The DMA test involves a temperature ramp from 30°C to 100°C at a rate of 2°C per minute.

3.2.5. Measurements and electrical connections

Establishing a mechanically robust connection between the printed CPLA structure and the power source is crucial. This connection needs to be reliable at both room and operational temperatures. However, for most applications, an easily severable connection is desirable. A direct current (DC) power supply was used for these tests. For safety reasons in basic circuits lacking additional protection, 120 VDC was chosen. In this test, crocodile clips were attached to the core structure exposed terminals. The current entering the CPLA structure during activation is measured with a digital multimeter. The data is then collected and analysed using software such as Keithley KickStart. An infrared camera (e.g., FLIR) is employed to monitor the temperature changes within the 4D-printed structure during activation. In order to make sure the structure gets hotter than its T_g, the applied voltage is changed from 60 V to 120 V.

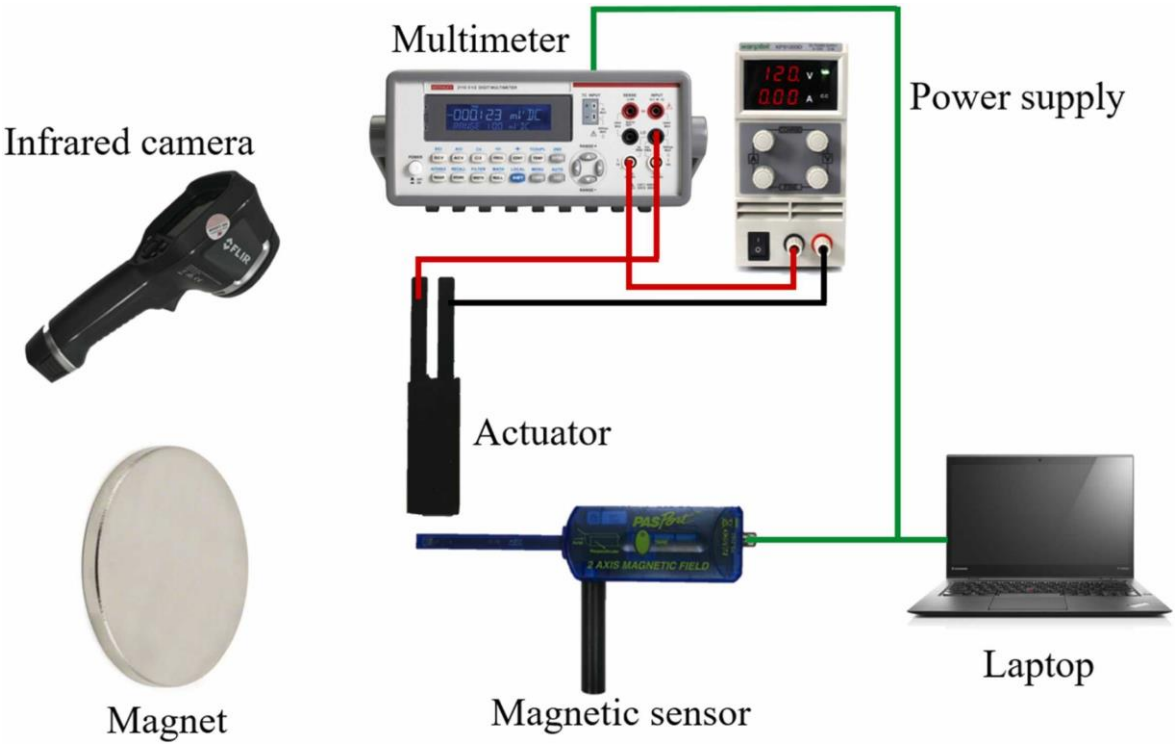

Figure 3.4. A schematic of the data recording system's parts.

3.2.6. Magnetic measurement

In a magneto-thermal characterization, hysteresis loops were measured at room temperature (300 K) using a physical property measurement system at a rate of 2.5 mT/s to investigate the magnetic properties of the magneto-responsive composites. Bending actuation performance was evaluated by measuring the deflection of a cantilever actuator subjected to a lateral magnetic field generated by a circular permanent magnet with a diameter of 60 mm from Magnet Expert Ltd. The field strength was measured to understand its influence on actuator behaviour. Regarding the activation reaction of the actuators, the combined effects of Joule heating and an external magnetic field were examined. The programmed magnetization patterns determined the motion of the actuators under these combined stimuli. The permanent magnet's magnetic field strength was measured using a PASCO Capstone system and a Pasco magnetic field sensor with a 0.01 G resolution probe at 10 Hz. In addition, the magnetic flux density was measured using a portable Gaussmeter from RS Pro. The PASCO software was utilised to examine the trajectory data obtained from the experiments and determine the bending angles and deflections of the composite actuators.

3.2.7. MRE properties

A universal mechanical testing device (Shimadzu AG-X plus machine) was used to assess the mechanical properties of the composites. The ASTM D412 standard was used to test five dog-bone-shaped specimens made of Ecoflex 00-30 silicone material and five specimens that included 70% magnetic particles (N. N. Azmi, et al. 2014). All samples had a gauge length of 33 mm. Comparing the composites' stress response was the aim of the testing. The samples were clamped between jaws and moved at a speed of 500 millimetres per minute.

3.3. Results and discussions

3.3.1. Electroactive performance

The results of the DMA study are shown in **Figures 3.5a and 3.5b**. The T_g for pure PLA is 55 °C, according to earlier research, whereas for CPLA is roughly 75 °C. (Alshebly and Nafea Jan 1, 2022). The inclusion of carbon black shows a marginal increase in the T_g of the composites. This phenomenon is attributed to carbon's role as heterogeneous nucleation sites, promoting a higher crystallization temperature within the PLA matrix. The PLA matrix becomes significantly more rigid as a result of the carbon addition, which causes CPLA to have somewhat greater storage moduli than pure PLA. But as the temperature rises, chain flow takes over and the storage modulus rapidly decreases, making the state rubbery. In contrast, due to increased intermolecular friction within the polymer chains, the loss modulus rises with temperature, resulting in a larger dissipation of energy. At temperatures above T_g, there is less energy lost because this loss modulus peaks close to the material's transition phase and then drops precipitously as molecular activity decreases. Utilising SEM, more research is done on the distribution of carbon particles within the CPLA composite. As illustrated in **Figures 3.5c and 3.5d**, A key component of the material's conductivity characteristics is the uniform dispersion of carbon particles throughout the PLA matrix, as seen in SEM photos of the CPLA filament and structure.

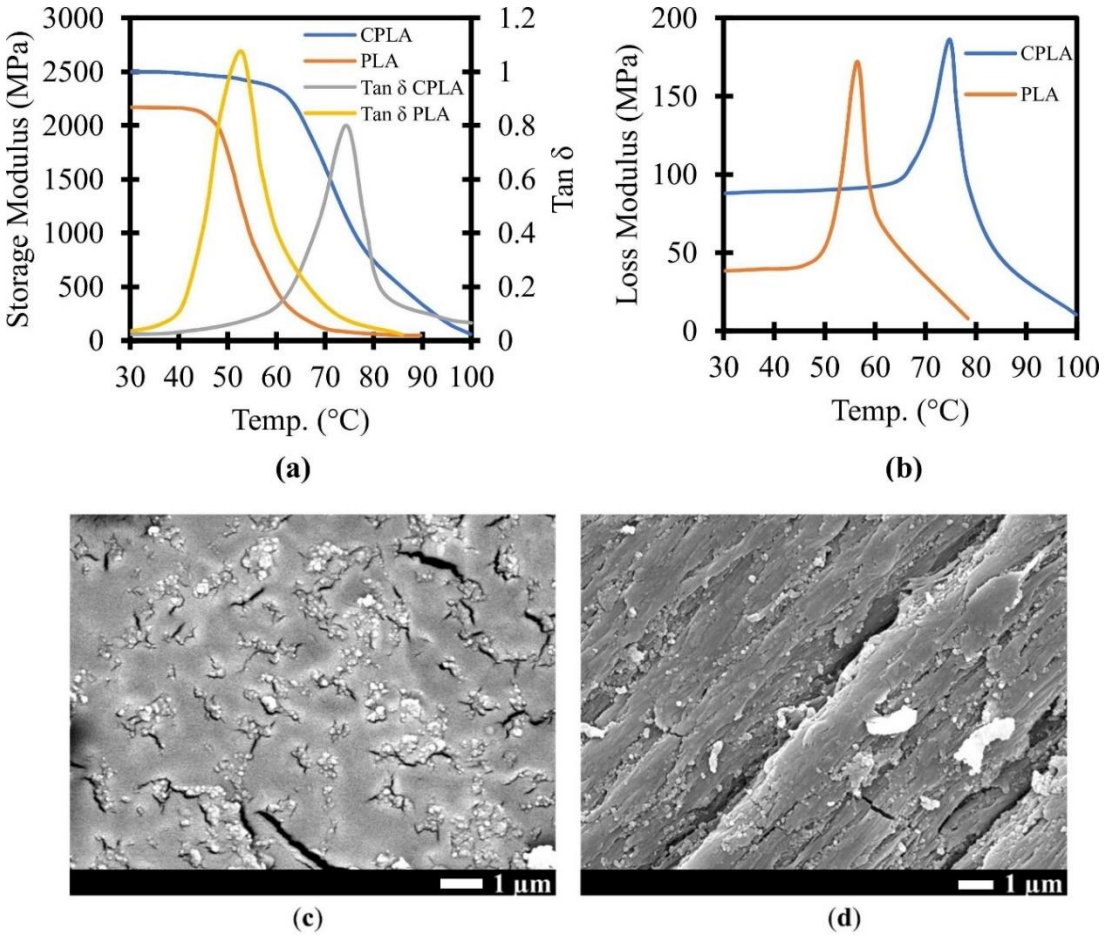

Figure 3.5. DMA results printed samples are shown in (a) and (b). (c) A cross-sectional SEM picture of a CPLA filament. (d) A 3D-printed CPLA sample's SEM picture.

Initial investigations focused on the heating capabilities of 4D-printed CPLA structures and the voltage required for rapid activation and heating. This measurement aimed to determine the optimal voltage for stimulating these structures. Three 3D-printed U-shaped specimens were connected and subjected to heating at different voltages (see **Figure 3.6a**). Temperature-related variations in resistance have been detected in correlation (see **Figure 3.6b**). The data reveals a positive correlation between temperature and voltage with increasing resistance observed at higher values. Throughout the structures' heating and cooling cycles, an infrared camera recorded temperature variations. The temperature profiles are displayed over time at different voltages (see **Figures 3.6c, 3.6d, and 3.6e**).

The U-shaped structure achieved a temperature of 99 °C within 17 seconds when applying a voltage of 120 V. Conversely, the temperature failed to reach the T_g with a 60 V application. The data demonstrates a decrease in current over time with increasing temperature. This phenomenon translates to higher resistance, which subsequently decreases upon cooling the structure (Al-Rubaiai, et al. Sep 18, 2017). As expected, applying a higher voltage resulted in a greater maximum temperature (Garces, I. T. and Ayranci 2020). Following the application of voltage, the printed core structures reached a temperature plateau, signifying an equilibrium state between the energy supplied by Joule heating and the heat lost to the surroundings. Notably, heating at 120 V caused the heating rate to increase and the Young's modulus to fall by 12% as a result. The voltage of 120 V was selected for this investigation since it was important to have a quick response.

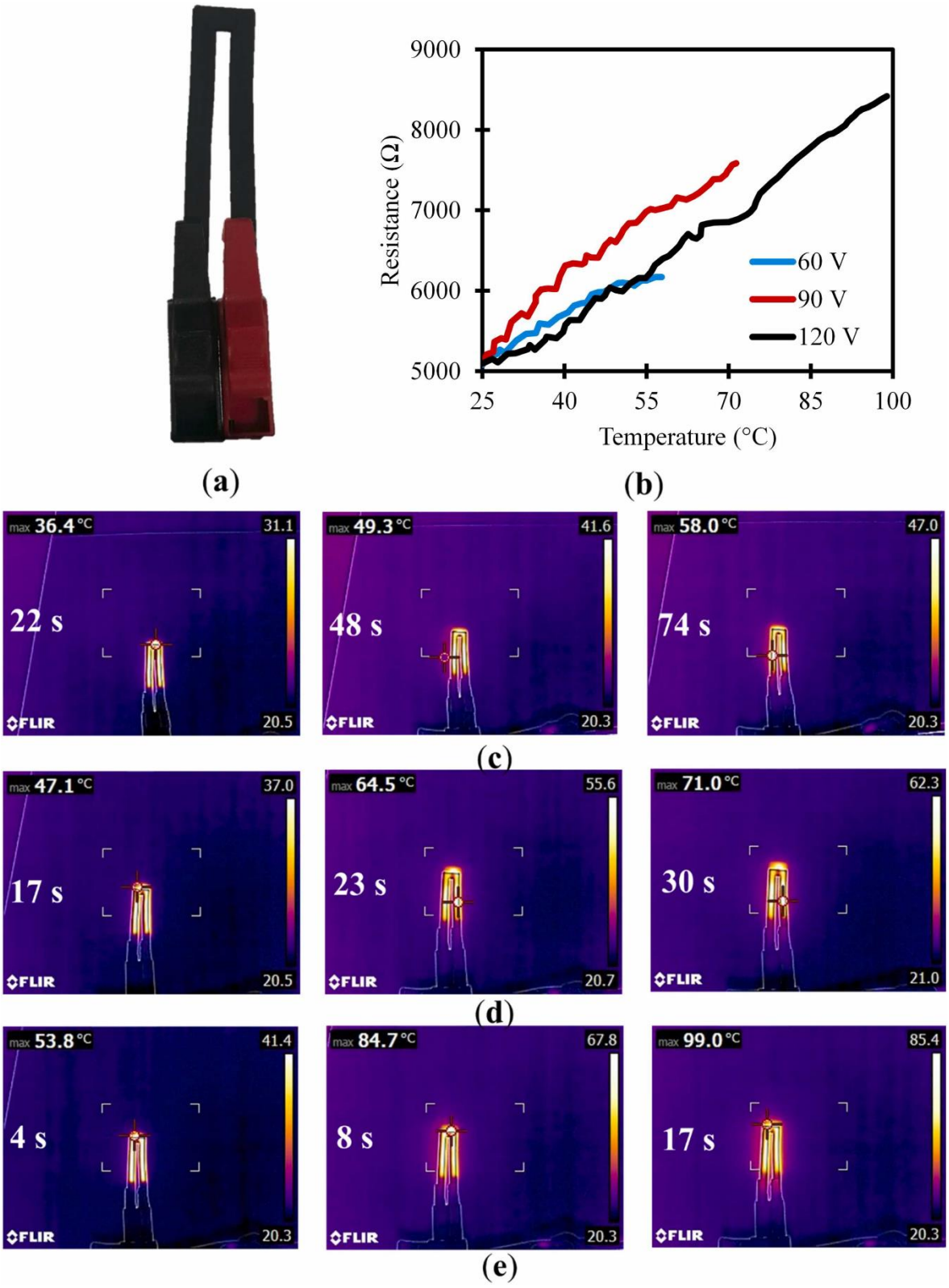

Figure 3.6. (a) A U-shaped structure clamped using crocodile clips. (b) Changes in resistance measured during temperature increase with application of power supply. Distribution of heat inside the U-shaped structure when it is powered by (c) 60 V, (d) 90 V, and (e) 120 V.

The factors influencing printed SMP structures exhibit greater complexity compared to those affecting filaments. The printing process has a minimal impact on the thermal characteristics of the printed structures. However, a slight decrease in the storage modulus of the printed structures was observed (Dong, X., et al. 2022). There are five equal individual layers in this structure, which have a thickness of 1 mm. The principal elements causing deformation are the U-shaped structure's two longer legs, which bend perpendicular to the base.

Equipping the two long legs with wires should theoretically allow for full structure activation. However, the current preferentially travels through the shortest internal path within the structure, leading to a localized temperature increase in this area. Consequently, heat diffusion governs the temperature rise in other parts, resulting in a lower-than-expected thermal conductivity along the direction perpendicular to the two long legs. Conversely, this issue is mitigated due to the structure's narrow width. **Figure 3.7a** showcases the electroactive shape memory capabilities of the U-shaped structures, while **Figure 3.7b** depicts the internal heat distribution. The concentric pattern and smaller size of the specimen contribute to a more uniform internal heat distribution and a lower activation voltage. The 4D-printed structure can revert to its initial form in less than 17 seconds, as evidenced by its shape recovery time. **Figure 3.7c** depicts the correlation between tip bending angle and time during shape recovery. Furthermore, **Figure 3.7d** illustrates the corresponding relationship between tip bending angle and temperature. The findings suggest that the structure reverts to its original shape once the T_g is surpassed.

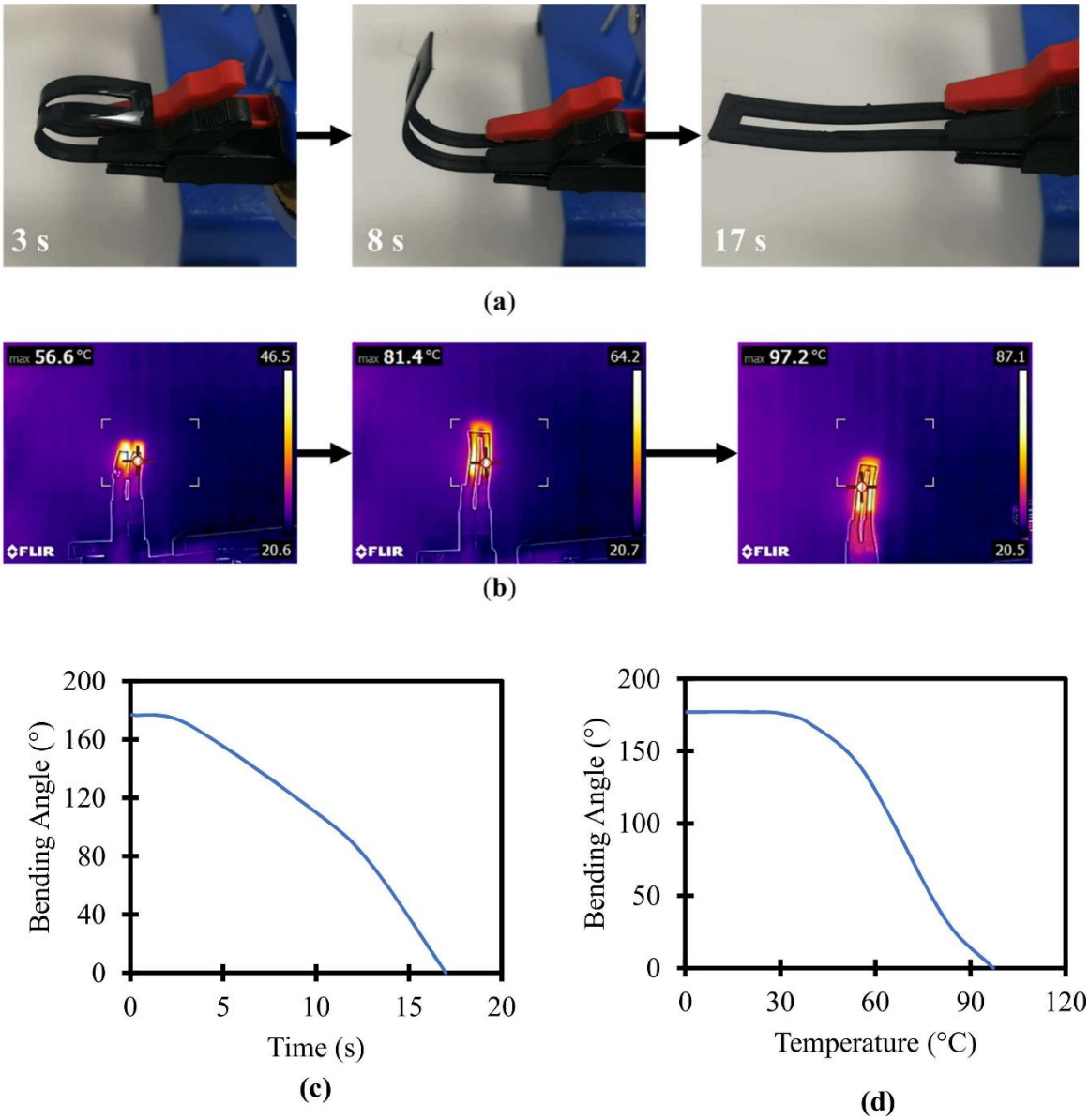

Figure 3.7. (a) A 120 V DC is used to electroactively recover the geometry of a dynamic structure. (b) Heat distribution during the electroactive shape recovery. (c) The tip bending angle against the shape recovery time. (d) A plot showing the temperature-dependent tip bending angle during CPLA form recovery.

3.3.2. MRE-based composite actuator

Figure 3.8a visually confirms the formation of a composite material when UF-S2 particles are incorporated into the polymerized resin mixture. The magnetic response of the particle-filled silicones was evaluated using magnetization curves. The measured magnetic moment, typically achieved under external magnetic fields, is relatively low at approximately 0.3 T. **Figure 3.8b** depicts the magnetization moment of the composite film. The energy lost during magnetic field reversal is represented by the enclosed region of the hysteresis loop. The saturation magnetisation, remanence, and coercivity were found to be 30 emu/g, 10 emu/g, and 0.02 T, respectively, based on this analysis.

The remanence values reported indicate that the magnetic dipoles in magnetic particles can be easily aligned by external magnetic fields and can stay aligned even after the field is removed. The permanent orientation of these dipoles in a single direction necessitates an external field exceeding the material's coercive magnetic field (Carpenter, et al. 2021). This shows that when the resin dries completely, the particles line up with their long axis parallel to the applied field. The elastomer composite exhibits the ability to be repeatedly activated without magnetization loss, provided the driving field remains within the capabilities of common permanent magnets.

Furthermore, tensile testing showed that silicone films containing magnetic particles performed better than pure silicone. This was explained by the composites' increased compliance (refer to **Figure 3.8c**). The data presented represents the median values obtained from five samples for both pure silicone and silicone with magnetic particles. The presence of UF-S2 particles contributes to the enhanced strength observed in the composite films compared to the dog-bone-shaped pure silicone samples.

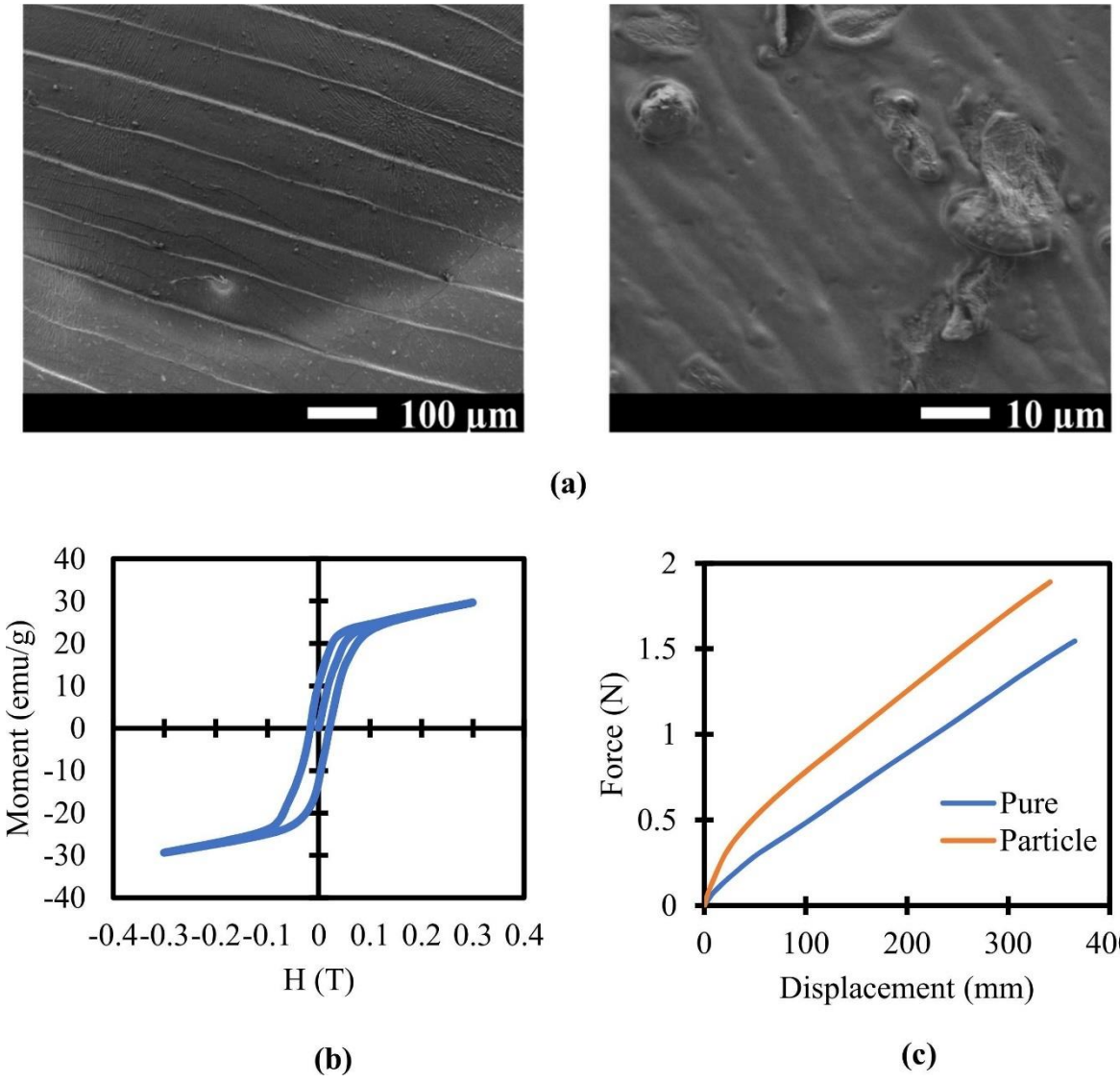

Figure 3.8. (a) SEM images of the UF-S2 particles within the silicone matrix, illustrate their shape and size distribution. (b) The rubber composites' H-field cyclic magnetisation curve, which shows a slow rise from -0.3 T to 0.3 T. (c) The median values of the tensile test results for the silicone composite samples with and without magnetic particles, derived from five samples.

This study investigates the impact of incorporating 4D-printed structures on the stability of MRE actuators. Notably, both sets of actuators (with and without 4D-printed structures) have identical weight and size. As illustrated in **Figures 3.9a and 3.9b**, MRE actuators containing a 4D-printed core exhibit significantly improved stability compared to those lacking the core structure. The reason for this increased stability is thought to be the inadequate stability seen in MREs with a homogenous 2.5 mm thickness. Accuracy and repeatability are increased, and actuator performance is enhanced by the addition of a 4D-printed framework. Furthermore, lowering the total weight reduces material waste and makes it easier to create lighter items.

An illustration of the local flux density is shown in **Figure 3.9c**, and it shows a linear relationship with the magnetisation of the smart composite actuator. The figure highlights a higher concentration of UF-S2 particles at the end of the MRE-based composite. This non-uniform distribution is a consequence of the actuator's magnetization during the curing

process, resulting in a negative value on the image. The actuator's end shows slightly more magnetisation than other locations because magnetic flux naturally concentrates around the magnetising magnet's edges. As a result, less magnetic field is needed to stimulate this end.

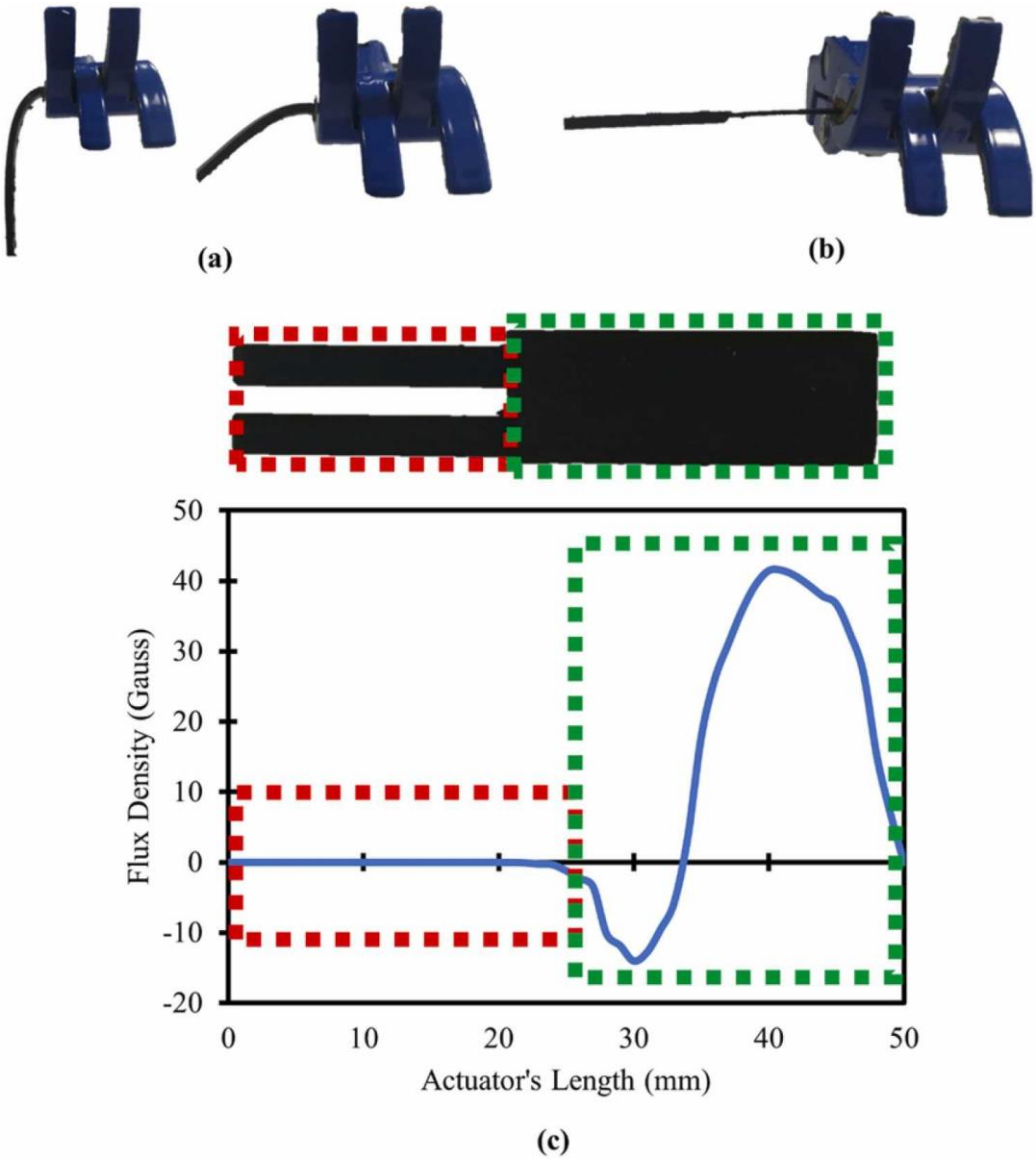

Figure 3.9. (a) MRE composite samples (50 mm and 30 mm). (b) Integrated MRE composite actuator with 4D-printed structure. (c) Magnetic flux density profile in MRE composite actuator. (The red area is the printed core structure and the green area is the MRE elastomer)

The actuator exhibits actuation even under relatively low magnetic field strengths. Experimental data suggests that the composite elastomer can be effectively activated using weak magnetic fields. The actuator clamps on one side due to the substantial force produced by the magnetic field, as illustrated in **Figure 3.10a**.

The actuation process begins with heating the actuator. An electrical current is passed through the actuator, leading to rapid heating. This thermal effect reduces the structural rigidity, enabling magnetic attraction of the actuator as illustrated in **Figure 3.10b**. The actuator then experiences deformation to match the magnetic field, as shown in **Figure 3.10c**. Because the core structure is inherently stiff, the actuator cools to room temperature even after the power source is cut off, as seen in **Figure 3.10d**. This allows the actuator to stay in a bent, stable position when needed.

Joule heating is used to transform the smart actuator back into its original shape. As illustrated in **Figures 3.10e and 3.10f**, heating the 4D-printed core causes the actuator to revert to its original configuration. The heat distribution inside the actuator during the attraction process is shown in **Figure 3.10g**.

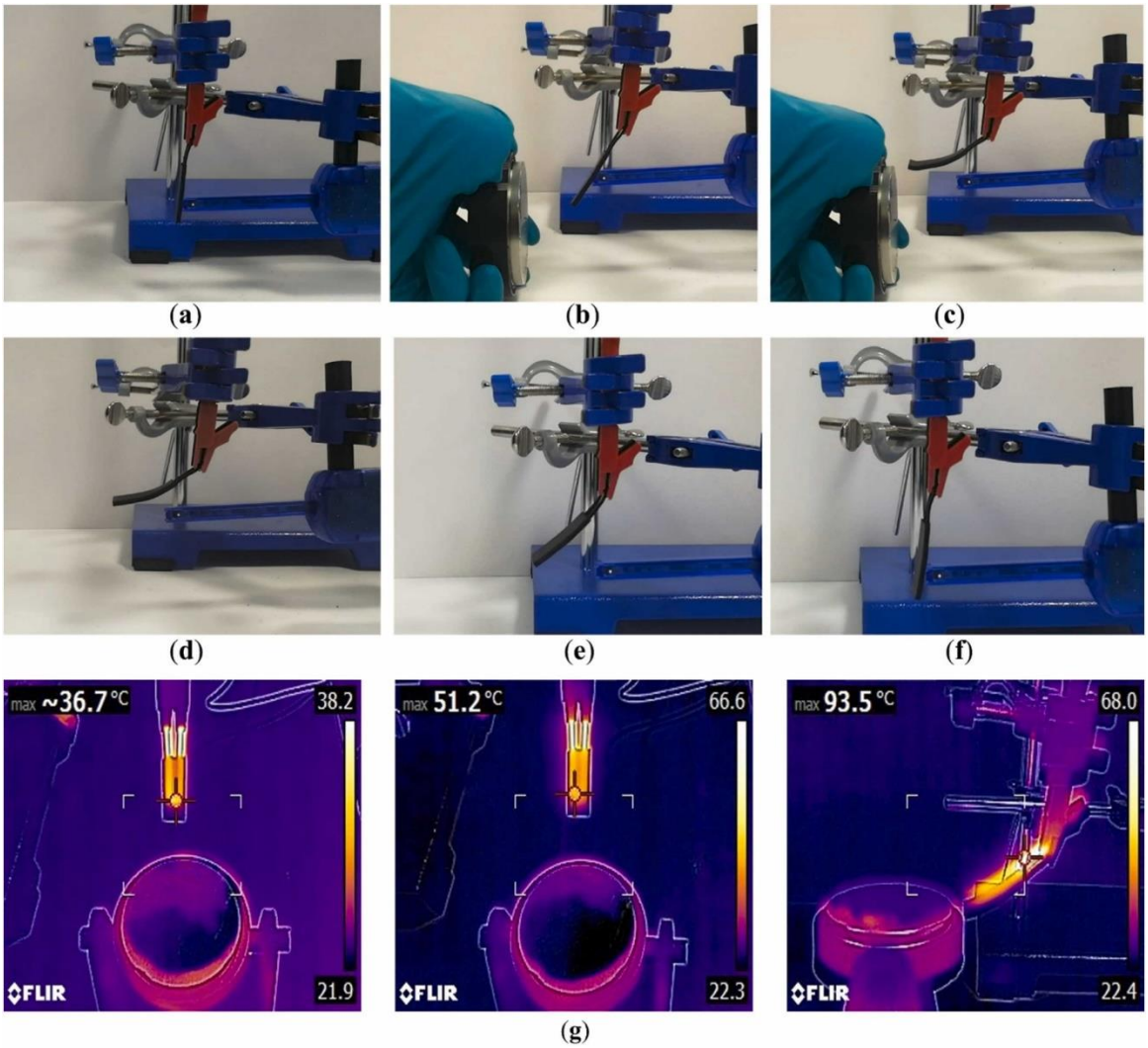

Figure 3.10. (a) Smart actuator in its initial position. (b) Joule heating when the composite encounters a magnet. (c) The maximum bending angle of the actuator is attained as a result of magnetic attraction and concomitant Joule heating. (d) After the magnet is removed, the actuator remains bent. Reactivating the Joule heating process for actuator recovery (e). (f) Restoring the actuator to its initial form in less than eighteen seconds. (g) Profile of the actuator's heat distribution during the periods of magnetic attraction and activation.

The bi-directional actuation capability of the composite actuator is demonstrated in **Figures 3.11a and 3.11b**. This functionality arises from the opposing orientation of magnetic domains at the actuator's ends. The mechanism of this arrangement is to place the actuator along the magnetic flux route that connects the opposite poles of a pair of magnets. A faster shape recovery is facilitated by the magnetic field along this path being orientated in the opposite direction to the field at the actuator's tip. The permanent magnet is rotated and the actuator is heated while it is bent during the actuation process. The magnet begins to reject the composite actuator when the T_g is reached. The actuator's ability to maintain two distinct shapes through the interaction of magnetic fields and Joule heating is supported by the data, which also shows the actuator's bi-stable behaviour.

The magnetisation and mechanical characteristics of the actuator are reflected in its reaction to external magnetic fields. When exposed to magnetic fields, the actuator demonstrates remarkable responsiveness because of the high compliance and magnetic characteristics that the UF-S2 particles impart. During the procedure, the intensity of the magnetic field is also recorded. The strength of the axial field rises with decreasing distance between the magnets. The composite actuator's trajectory pathways, which show how the magnet attracts and repels it, are shown in **Figure 3.11c.** The measured axial strengths for attraction and repulsion are 18 mT and 34 mT, respectively. The higher repulsion field strength is attributed to the closer proximity of the magnet to the actuator during this phase. The maximum bending angles achieved are 80° for attraction and 76° for repulsion. These results suggest the potential for remote programming and control of the actuator.

This finding indicates how well the core structure does its job of improving the MRE's actuator characteristics. Depending on needs and magnetic field strengths, the idea can be modified to create a variety of designs and arrangements. One unit underwent a 200-cycle fatigue test to assess the actuator's performance. A relay switch was used to regulate current on and off cycles. The system's cooling limitations, due to the temperature-dependent nature of CPLA, restrict the dynamic behaviour. Temperature measurements were also recorded using a thermometer to assess any changes after 200 cycles. The results, presented in **Figure 3.11d**, indicate that the temperature remains consistent, with no observable changes. Following the cycling test, the actuator also shows good bonding interaction between the core structure and MRE elastomer. The CPLA structure may melt at temperatures higher than 100 °C for a long time activation.

Figures 3.11e, 3.11f, and 3.11g further detail the actuator's behaviour. The phases of the actuator's tip for attraction and repulsion concerning the strength of the magnetic field are shown in **Figure 3.11e.** The angle and the field strength both rise at the same time as the magnet gets closer to the actuator. The form recovery of the bent actuator with time and temperature is shown in **Figures 3.11f and 3.11g.** After achieving T_g, the actuator takes 18 seconds to return to its original shape. **Figure 3.11h** shows the form recovery percentages for the repelled and attracted stages.

The combination of two stimuli, temperature and magnetic field, facilitates the creation of a bi-stable form more readily than using either stimulus alone. In the absence of a magnetic field, the structure can only be attracted to the desired position without becoming locked. Similarly, Joule heating alone cannot generate new shapes due to the inherent tendency of the structure to recover its original form as the temperature rises. However, the combined application of these stimuli allows for the creation of well-defined and diverse shapes.

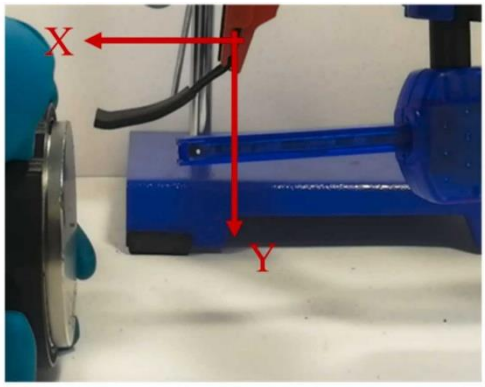
X
Y

(a)

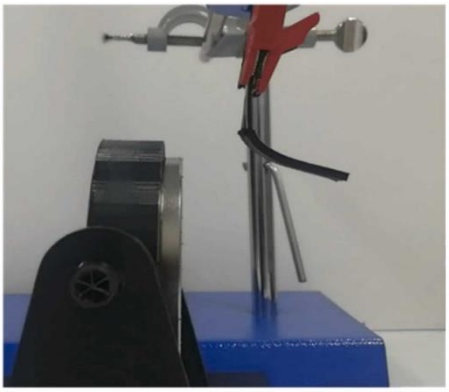

(b)

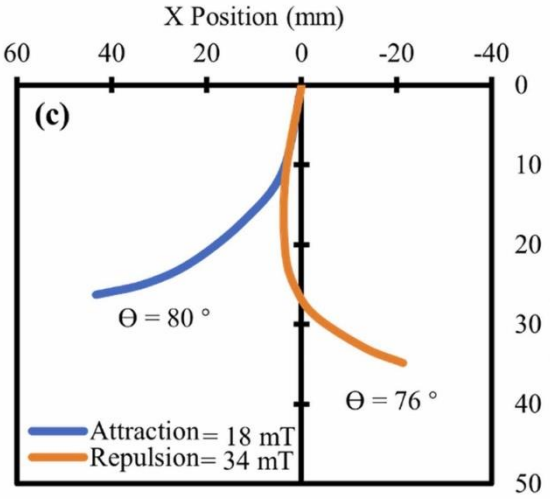
X Position (mm)
60
40
20
0
-20
-40
(c)
Θ = 80 °
Θ = 76 °
Attraction = 18 mT
Repulsion = 34 mT
0
10
20
30
40
50
Y Position (mm)

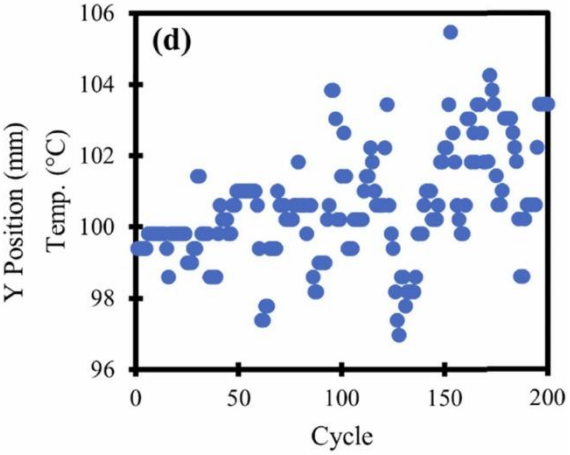
(d)
106
104
102
100
98
96
Temp. (°C)
0
50
100
150
200
Cycle

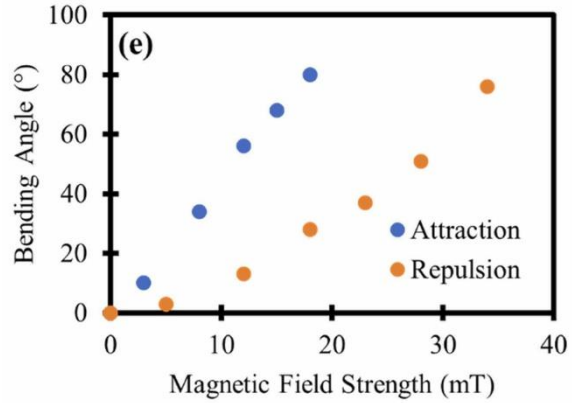
(e)
100
80
60
40
20
0
Bending Angle (°)
Attraction
Repulsion
0
10
20
30
40
Magnetic Field Strength (mT)

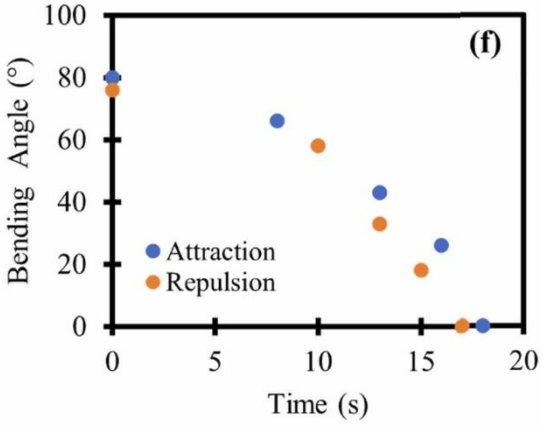
(f)
100
80
60
40
20
0
Bending Angle (°)
Attraction
Repulsion
0
5
10
15
20
Time (s)

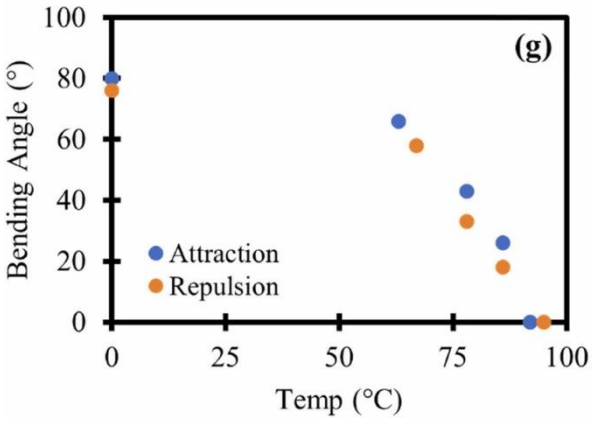
(g)
100
80
60
40
20
0
Bending Angle (°)
Attraction
Repulsion
0
25
50
75
100
Temp (°C)

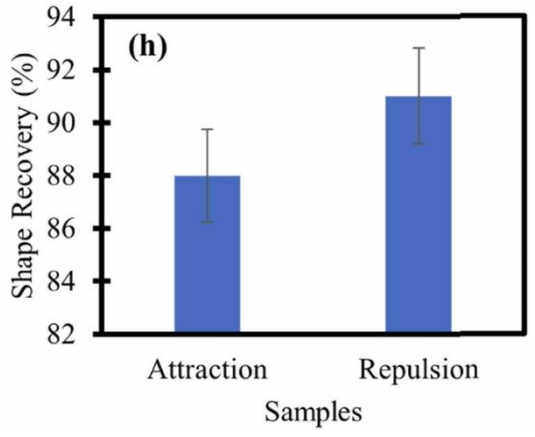
(h)
94
92
90
88
86
84
82
Shape Recovery (%)
Attraction
Repulsion
Samples

Figure 3.11. (a) The actuator's deflection is caused by attraction. (b) Repulsion-induced actuator deflection. (c) The actuator's deflection trajectory throughout the attraction and repulsion processes shows the greatest bending angle. (d) Temperature fatigue cycling test findings. (e) The actuator's tip bending angle is about the applied magnetic field strength under situations of attraction and repulsion. (f) Shape recovery of the tip bending angle of the actuator in both repulsion and attraction circumstances over time. (g) The actuator's tip bending angle shape recovery as a function of temperature. (h) Shape recovery rate in the presence and absence of repulsion.

3.3.3. Applications

The possible uses of MRE-based conductive SMP actuators in mechanical and biological engineering are examined in this section. This composite actuator can be used to build grippers, for instance. Joule heating is the first step in the actuation process, after which the actuator is drawn in by a magnetic field. Following deflection, the actuator is cooled to room temperature. When the magnetic field is removed, the actuator holds its gripped position. The actuator weighs only 1.47 g, but it can sustain and pull masses up to 200 g, as shown in **Figure 3.12a**. Even higher lifting capacities can be reached by adjusting the design and creating larger actuators with this method. Furthermore, a grouping of those devices can be employed as a gripper to pick and position a variety of items with varying geometries. This gripper's capacity to hold a grip for long periods without the need for magnetic fields or other external stimuli is a major advantage.

This actuator's capacity to operate in both directions enables it to reshape the framework during the Joule heating process by particular needs. The actuator is shaped-changeable by using a magnet, which enables it to be used as a hook mechanism similar to an attachment in a system. In this instance, the composite actuator's use as a controlled remote hook is demonstrated using a 3D-printed framework. A target spot that could be challenging to get within the structure can be reached by positioning and bending the actuator. The actuator is then heated by the electrical system and bent and resisted as needed by the introduction of a magnetic field. The actuator secures itself onto the framework or item by using its bent structure as a hook. As long as necessary after cooling, the actuator stays in the deflected position (see **Figure 3.12b**). This feature implies possible uses in biomedical devices for tracheal splints and shattered bone support, among other supporting applications. Such magneto-responsive electroactive actuators have potential applications as well, such as self-deployable stents. These actuators could be used to treat clots in pipes.

In addition, structures manufactured using FDM 4D printing may be employed as a hook device. In this design, the actuator's bending and locking are controlled remotely. Because of its SME and bi-stability, the actuator can be used as an opening and closing locking mechanism. 4D structures are appropriate for customised locking systems due to their remote controllability. A proposed design of the 4D framework is shown in **Figure 3.12c** as a locking mechanism in the form of a hook. The adaptive actuator is activated when the temperature rises over the critical threshold and a magnetic field is applied. The actuator bends and closes the system as a result of attraction or repulsion triggered by this. To build a locking mechanism inside a system, a pair of these devices can be used. The 4D-printed CPLA/UF-

S2 composite actuator has many possible uses, of which the examples examined in this paper merely scratch the surface. Because it is flexible and conformal, this component can be used in mechanical and biological devices that are built with 4D printing technology in the future.

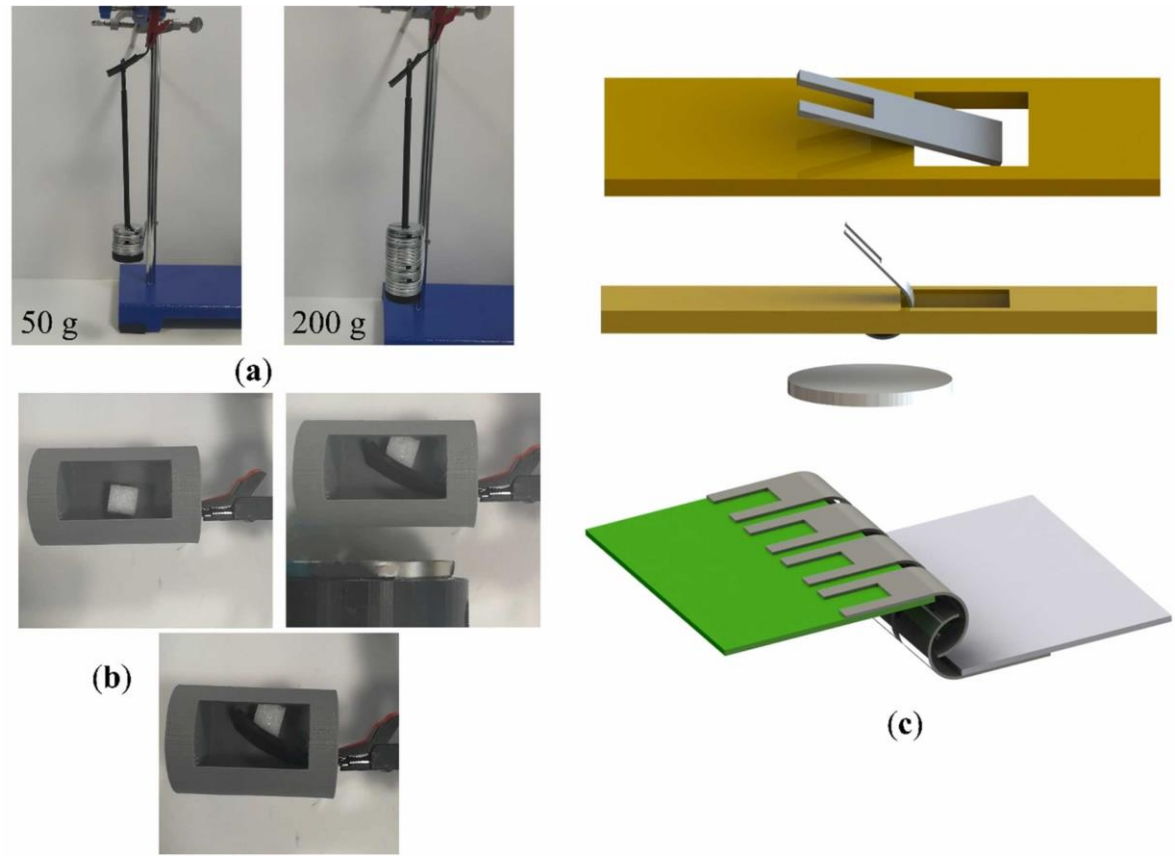

Figure 3.12. (a) The actuator after shape, cooling, and programming, bearing different weights. (b) Activating an actuator that resembles a hook inside a closed system that is integrated into a structure. (c) A schematic representation of the actuator's hook-like locking and releasing mechanism.

3.4. Conclusion

This work described a simple process that combines silicone casting with FDM to create MRE-based electroactive shape memory structures. The primary structural element under research was the CPLA filament. In order to describe the electrical, thermal, and electroactive shape memory behaviour of the filament, the research investigated the Joule heating and SME features of the printed core using a range of input voltages. The stability of MRE-based actuators was greatly improved by integrating 4D printing technology. The study also covered the smart actuator's programming and remote control capabilities, as well as how to achieve form restitution in the presence of magnetic fields and at particular temperatures. The outcomes showed that weak magnetic fields might be used to regulate the actuator.

A thorough analysis of the special composite actuator was carried out, covering its microstructure, shape restoration properties, and response to two stimuli (temperature and magnetic field). Remarkably, when applying a 120 V power source, the 4D-printed core demonstrated quick shape restitution to its initial configuration. Under low external fields, the composite actuator obtained a maximum bending angle of 80° for attraction and 76° for repulsion. The study investigated the bi-directional and bi-stable functions of the actuator. The actuator's suitability for extended use was validated by the cycling test results. The results of the experiment provide strong evidence for the promising potential of 4D-printed MRE composite actuators in a range of mechanical and biomedical applications, such as biomedical devices, grippers, and locking mechanisms. It is anticipated that this research will further the field of 4D printing technology and open up new ways for the design and development of dynamic structures featuring bi-directional, wireless, bi-stable, and shape memory characteristics.

Chapter 4

Sustainable 4D printing of magneto electroactive shape memory polymer composites

This chapter proposes a novel approach using magneto-electroactive SMPCs for 4D printing. These sustainable composites offer remote electrical control, fast response, and multi-stability achieved through high-temperature programming. This allows a single structure to hold multiple designs, reducing material waste. The investigation focuses on composite materials comprised of magnetic polylactic acid (MPLA)/CPLA filled with carbon black. The analysis examines material properties, the composite interface, and the overall mechanical properties of these materials. The research explores the mechanics and magnetic response of SMPCs for FDM printing, paving the way for efficient, multi-shaped structures in various fields. All content is adapted with permission from the article published as follows:

- **Lalegani Dezaki M**, Bodaghi M. Sustainable 4D printing of magneto-electroactive shape memory polymer composites. Int J Adv Manuf Technol 2023;126(1-2):35-4810.1007/s00170-023-11101-0.

This chapter's literature and introduction are covered in **Chapter 2**, where a brief overview of the chapter is also provided.

4.1. Introduction

4D printing offers a novel approach to address challenges in traditional printing processes. These challenges include staircase defects and the need for support structures, which can be eliminated using 4D printing (Zhang, Zhizhou, Demir and Gu 2019, Wickramasinghe, Do and Tran 2020). This technology also reduces material usage, leading to lower production costs and faster printing times. A key advantage of 4D printing is its ability to create shape-morphing structures that can transition from one form to another. A common example involves transforming a flat 2D shape into a desired 3D structure (Ji, et al. 2022, Lee, A. Y., et al. 2020). This allows printing the object in a simpler one-dimensional (1D) form and then manipulating it into the required 2D configuration. The same principle can be applied to convert 2D shapes into 3D structures (Bodaghi, Mahdi, et al. 2019). This technique not only reduces waste by eliminating support structures but also minimizes material usage by enabling the creation of complex shapes from a single structure. As a result, 4D printing contributes to the development of sustainable and cost-effective smart structures.

The application of morphing structures in engineering holds significant promise for increased design efficiency and customization across various industries (Katia Bertoldi, et al. 2017, Robin M. Neville, Fabrizio Scarpa and Alberto Pirrera 2016). These dynamic structures are versatile enough for a wide range of applications since they may be remotely reconfigured to respond to external stimuli without the use of traditional sensor and actuator systems (Bastola and Hossain 2021, Alapan, et al. 2020). Pre-strained domains facilitate rapid, pre-programmed shape changes upon exposure to stimuli. Nevertheless, current methods for fabricating artificially morphing structures frequently have drawbacks, necessitating a trade-off between quick shape changes and complex geometries. Additionally, 3D printing complex structures are typically time-consuming, challenging, and wasteful. Magneto-electroactive SMPCs offer a solution by combining fast response times with shape-shifting capabilities. The mechanical qualities of PLA materials may be adversely affected by hot water programming, which is avoided with this method.

Although magneto/electro-responsive materials have several benefits in 4D printing, there is still no low-cost way to combine magneto-electroactive 4D printing with FDM technology. The constant requirement for a magnetic field to activate and maintain the position of magnetic structures presents another challenge (Lalegani Dezaki and Bodaghi 2022, Lalegani Dezaki and Bodaghi 2023a). Furthermore, the environmental impact and sustainability of magneto-electroactive 4D printing require further investigation. This study addresses these gaps by being the first to integrate CPLA and MPLA materials for 4D printing low-cost, sustainable, bi-stable, reversible, and lightweight composite structures using the FDM process. The created hybrid MM adaptive structure operates in a low magnetic field using a Joule heating approach and makes use of permanent magnets. With this combined-stimulus method, a continuous magnetic field following actuation is not required.

This work presents a new type of composite actuator that can be programmed remotely. Highlighting important facets of green design, putting out a theoretical foundation for sustainability, and providing a thorough explanation of the 4D printing process used to produce shape-memory and shape-morphing objects are the main goals. The construction of highly stable, lightweight, and ecologically friendly 4D-printed magneto-electroactive structures could be facilitated by the suggested model and solution. The study assesses the possible applications of 4D-printed structures' ability to change their shape. In contrast to other studies that concentrated on chemical methods to achieve shape memory, this work controls the structure's topology through 4D printing. The shape memory effect, remote programming, and the setup of this study are shown in **Figure 4.1**. The mechanical characteristics and microstructural elements of CPLA and MPLA are further examined in this study. It also describes the material characteristics and the way that 4D-printed CPLA and MPLA change shape. Finally, it evaluates the actuator's performance.

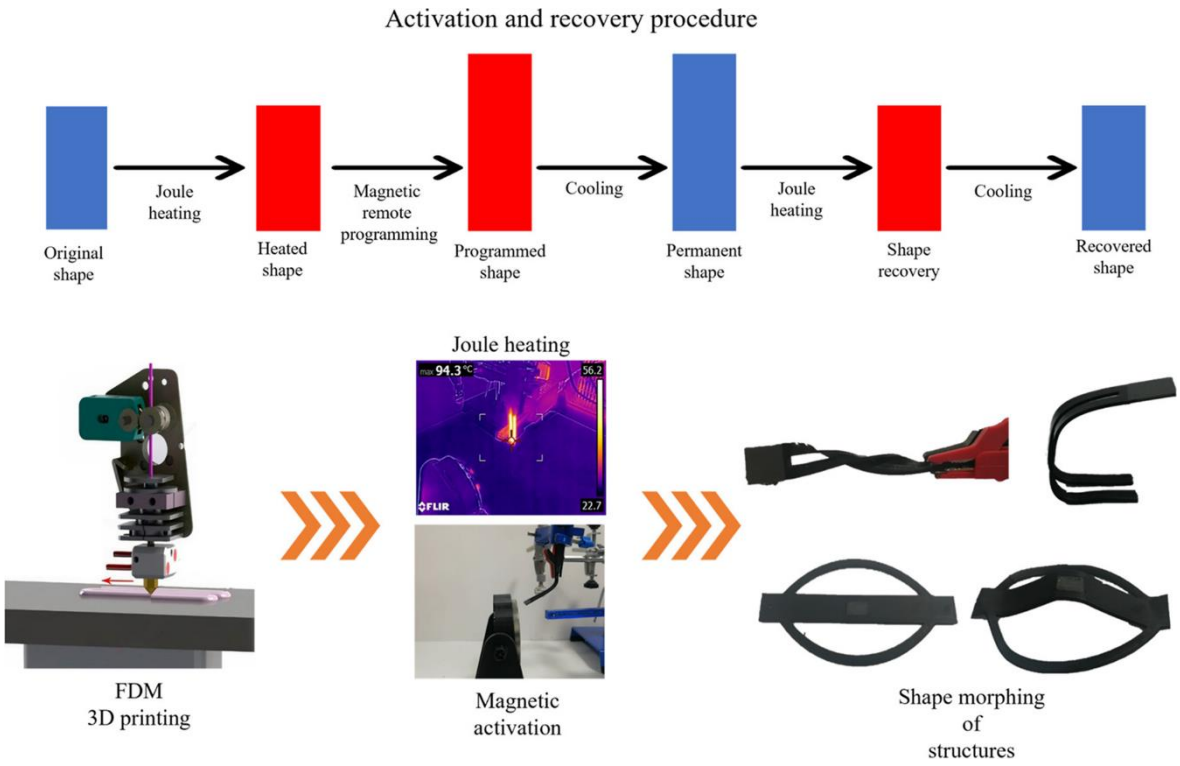

Figure 4.1. The proposed method leverages remote programming through a 4D printing approach. Joule heating elevates the temperature of the structure. A magnetic field is subsequently used to program the heated shape. Ultimately, the intelligent structure gets cooled down without losing its activated status. To recover its original shape, Joule heating is once again employed to activate the actuator.

4.2. Materials and methods

4.2.1. Materials

This study explores the potential of FDM 4D printing for creating objects with diverse material properties and functionalities. Existing thermoplastic filaments, potentially including those with functional additives, can be utilized for this purpose. These properties can be strategically tailored throughout the printed object by adjusting the printing process at specific locations. Two specific filament types were chosen for this investigation: electrically CPLA and MPLA from Proto-Pasta. CPLA offered a commercially available option with a significant SME compared to other popular SMPCs. Its composition includes electrically conductive carbon black (approximately 21 wt%) embedded within the PLA matrix. This made CPLA suitable for low-voltage applications.

MPLA, on the other hand, incorporates metal powder particles (around 250 microns) within a PLA-based resin. Notably, research indicates a substantial decrease in Young's modulus, a measure of stiffness, when MPLA is heated from room temperature to 80°C (Riley, et al. 2020). The study focuses on these materials' mechanical attributes, deformation behaviour, and magnetic properties in order to gain an adequate understanding of the design space. SEM (JSM-7100F LV FEG) and energy-dispersive spectroscopy (EDS) were employed to analyse the microstructure, chemical composition, and particle distribution within 3D-printed samples of CPLA and MPLA. This analysis also assessed the bonding between the co-printed CPLA and MPLA filaments.

4.2.2. Design and printing

This chapter investigated the utilization of a combined material approach using CPLA and MPLA to create both rapid and stable actuators and remotely controlled objects with shape-shifting capabilities. By employing the technique of 4D printing, the aim is to design actuators with the thinnest possible profile while maintaining bi-directional actuation. These adaptive actuators, which have the capacity to both alter and regain their shape, were created using the FDM process (Zafar and Zhao 2020, Thanh Tai Nguyen and Jooyong Kim 2020, Joshi, et al. 2020). An FDM printer equipped with dual nozzles was used to MM printing all structures within this research. **Figure 4.2** showcased the design and construction of the 4D-printed structure, featuring a thickness of 1 mm, developed using SolidWorks software. The core design principle revolved around the phase transitions exhibited by both CPLA and MPLA. The arrangements that were selected allowed for the best possible heat dispersion between the structures. Previous studies have looked at CPLA's resistivity and conductivity characteristics (Beniak, et al. 2022, Stopforth 2021).

Slic3r software was employed to convert the CAD file into a series of .gcode files suitable for 3D printing. Printing parameters, outlined in **Table 4.1**, were established to ensure smooth extrusion from the printer nozzle. A concentric infill strategy was utilized to guarantee internal structural continuity within the printed objects. Finally, the models were merged to enable the printing of both MPLA and CPLA materials within a single structure.

The magnetic properties of the 4D-printed composite construction were analysed using the magnetic flux density on the samples' surfaces in the out-of-plane direction. Preserving the actuator's rigidity and weight while keeping it in place was crucial. In order to reduce the magnetic field and produce a stable design after activation, a structure utilising CPLA and MPLA was designed. The technique was especially well-suited to the development of actuators with the ability to regain their shape and behave in both directions. The distance between the magnet and the 4D-printed actuator could be changed to alter the applied magnetic field. The actuators were activated in accordance by applying a mild magnetic field and utilising Joule heating to activate the 4D-printed structure.

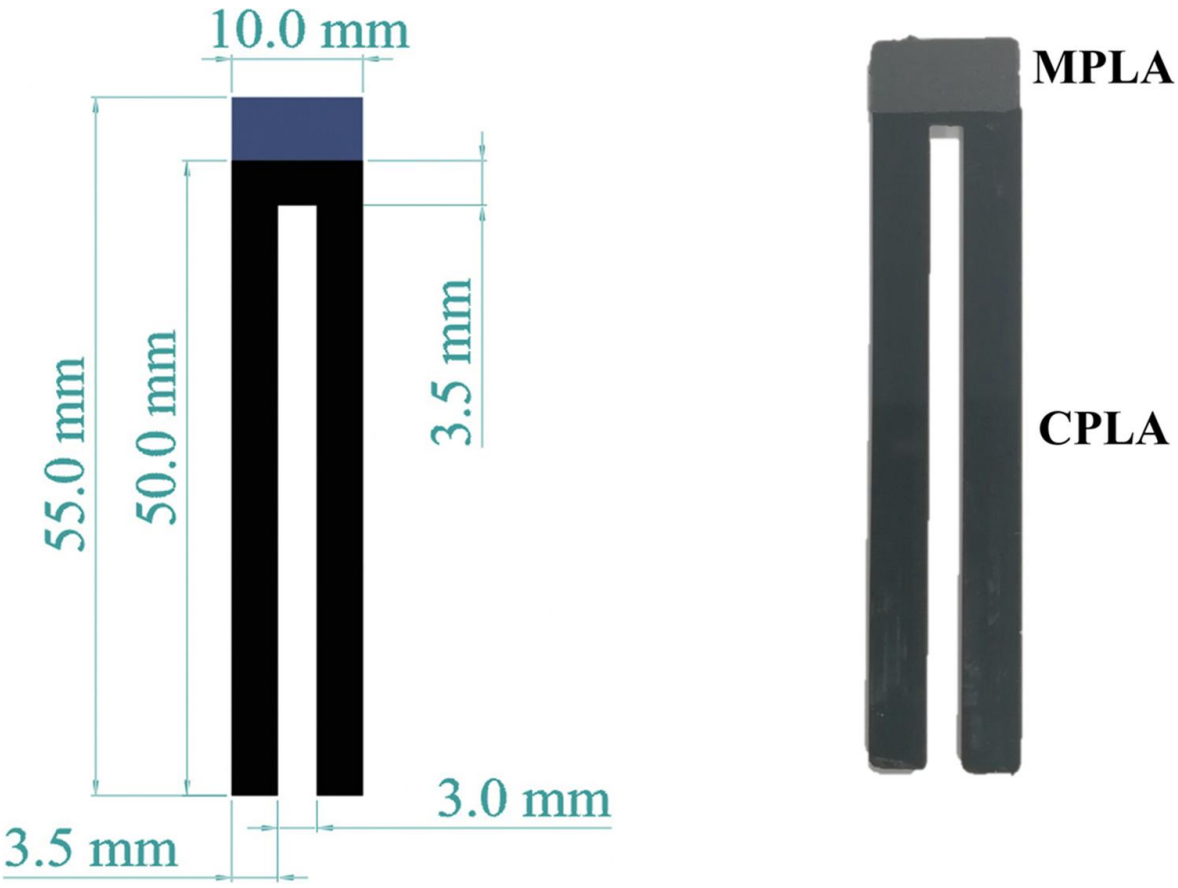

Figure 4.2. Design and fabrication considerations for 4D-printed structures.

Table 4.1. CPLA and MPLA printing settings.

Parameters	Value
Layer height (mm)	0.2
Infill density (%)	100
Infill pattern	Concentric
Extruder temperature (ºC)	210
Bed temperature (ºC)	60
Material flow (%)	100
Printing speed (mm/s)	70

4.2.3. Electrical measurements

This passage described the experimental setup for investigating the SME of 4D-printed specimens. A CPLA material was employed, featuring mechanically reliable connections secured by the power cables at room temperature. These connections were designed to be readily breakable for ease of use in most applications. A DC power supply used the necessary electricity, with a voltage limitation of 120 VDC for unprotected experimental circuits. Common lab practice utilized crocodile clamps and wires for temporary or semi-permanent connections on exposed terminals.

A Keithley digital multimeter was used to measure the current entering the CPLA structure during activation. After that, Keithley Instruments' Keithley KickStart program was used to obtain the relevant data. To evaluate the 4D-printed structures' shape memory capacity, a FLIR infrared camera was utilised. To ensure that the structure heated and rose above its T_g, the applied voltage was gradually increased from 60 V to 120 V. After that, each specimen was wired together, and placed inside the test stand, and the test protocol was followed (see **Figure 4.3**).

Analysing the SME of the 4D-printed actuators was the goal of the experiment. A permanent magnet was used to apply an external force as part of the shape-fixing technique. Even after deactivation (turning off the electricity), the induced deformation persisted above T_g until the specimen cooled and hardened. The shape recovery behaviour was recorded by a video camera and then measured with recovery time and other parameters.

4.2.4. Magnetic field

This investigation explored the deflection behaviour of 4D-printed composite structures under the influence of an external lateral magnetic field. A permanent magnet generated the magnetic field, and the actuator's responsiveness was evaluated by measuring its deflection. Both the magnetic field and the Joule heating activation were applied to the actuators during the experiment (see **Figure 4.3**). A Pasco magnetic field sensor was used to measure the strength of the magnetic field. This sensor boasted a high degree of precision (0.01 G) and a sampling frequency of 10 Hz. The permanent magnet's magnetic strength was measured using a Pasco Capstone system. Software from Pasco was then used to record the motion trajectories of the soft actuators, allowing for subsequent calculation of their deflection.

4.2.5. DMA test

This section investigated the influence of two crucial thermodynamic parameters, storage modulus and T_g, on the SME of 4D-printed PLA-based materials. These parameters were critical for understanding the behaviour of SMPs. A DMA 8000 from PerkinElmer was employed to measure the storage modulus of the printed materials (CPLA, PLA, and MPLA). The test samples were created at a printing speed of 70 mm/s with the same dimensions (40 mm length, 10 mm width, and 1 mm thickness) to guarantee uniformity. A test frequency of 1 Hz was chosen, as it aligned well with the anticipated gradual changes in material properties due to temperature variations. The DMA test sequence was programmed to ramp the temperature from 30°C to 100°C at a controlled rate of 2°C per minute. This temperature range encompassed the expected operating conditions for the shape memory behaviour.

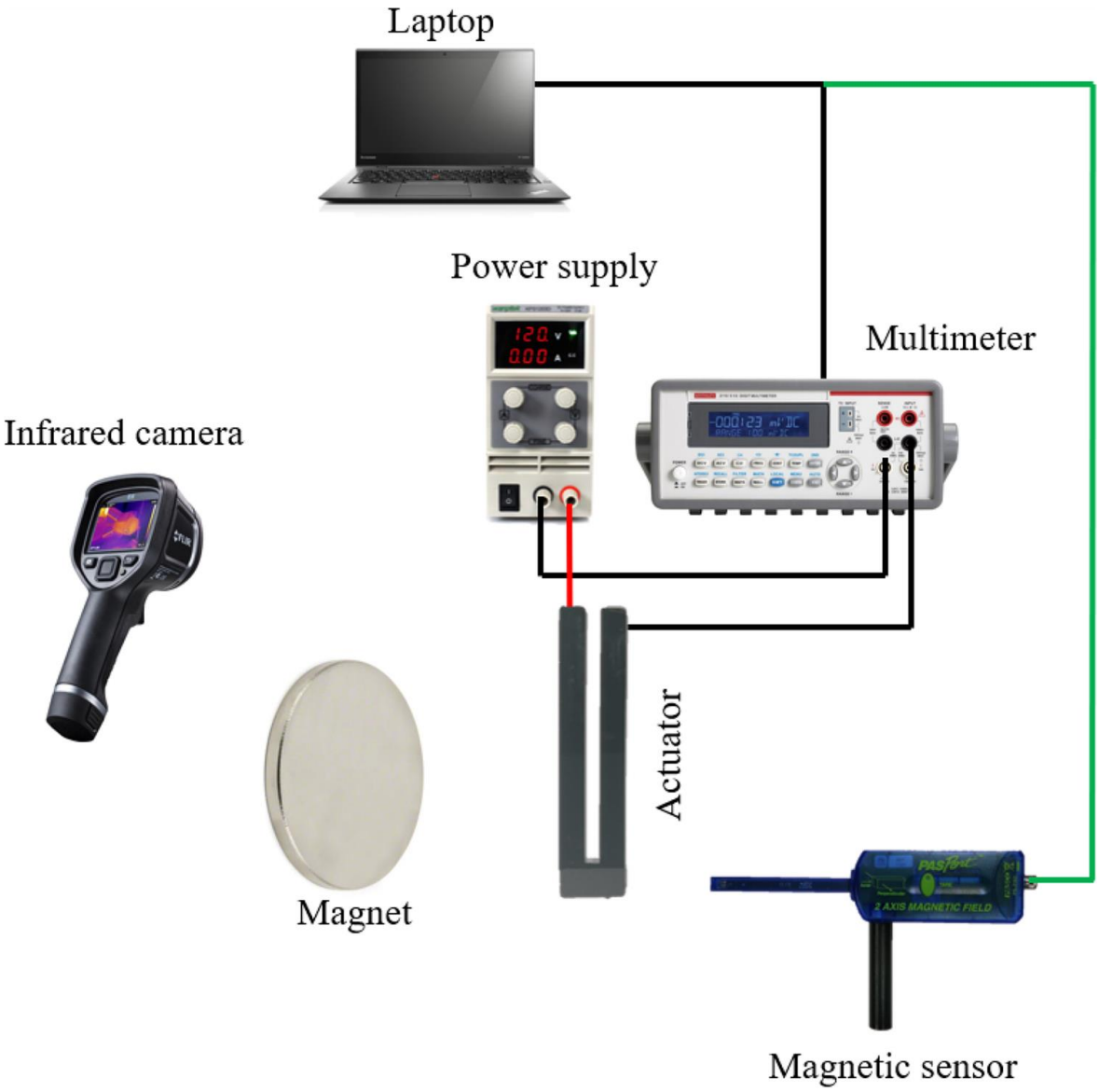

Figure 4.3. Schematic representation of data recording and actuator control.

4.3. Results and discussion

4.3.1. Material properties

Results of the DMA for CPLA, MPLA, and PLA are shown in **Figure 4.4a.** The T_g of the composites rises with the addition of carbon black and iron particles. As a result, it is found that the T_g of MPLA and CPLA are approximately 65°C and 75°C correspondingly. For shape memory behaviour to be induced, the higher T_g requires activation temperatures above these values. The increased crystallisation temperature within the PLA matrix is caused by iron and carbon particles, which are responsible for this phenomenon.

The rigidity of the PLA matrix is increased by the inclusion of carbon and iron, as seen in **Figure 4.4a**. This leads to greater storage moduli for CPLA and MPLA than for pure PLA. However, upon reaching the T_g, chain flow within the material disrupts its rigidity, causing a rapid decline in storage modulus and a transition to a rubbery, viscous state. Conversely, the loss modulus exhibits an opposite trend, increasing as the frictional interactions between polymer chains intensify. As the material approaches the T_g, these molecular activities diminish, leading to a decrease in wasted energy and consequently a reduction in the loss modulus.

CPLA and MPLA microstructures were analysed using SEM analysis, as shown in **Figures 4.4b and 4.4c**. The primary emphasis of this investigation is the dispersion of iron and carbon particles. Additionally, the boundary conditions between these two 3D-printed materials are investigated in this study. When comparing the PLA matrix of the CPLA and MPLA constructions, the SEM pictures show that the carbon and iron particles are evenly distributed throughout. To obtain the appropriate conductivity and magnetic characteristics, this homogeneous dispersion is essential.

Boundary conditions and material interfaces are studied using EDS. Iron particles are visible in the MPLA structure but not in the CPLA portions, **as Figure 4.4d illustrates**. Because of possible layer interaction during printing, very little iron is seen in the border area. On the other hand, no iron particles are found in the CPLA structure's core. Data noise is the cause of the little blue dots seen in the CPLA image. These investigations verify that the iron and carbon black particles have been successfully and uniformly distributed throughout the structure, which is essential for activating actuators.

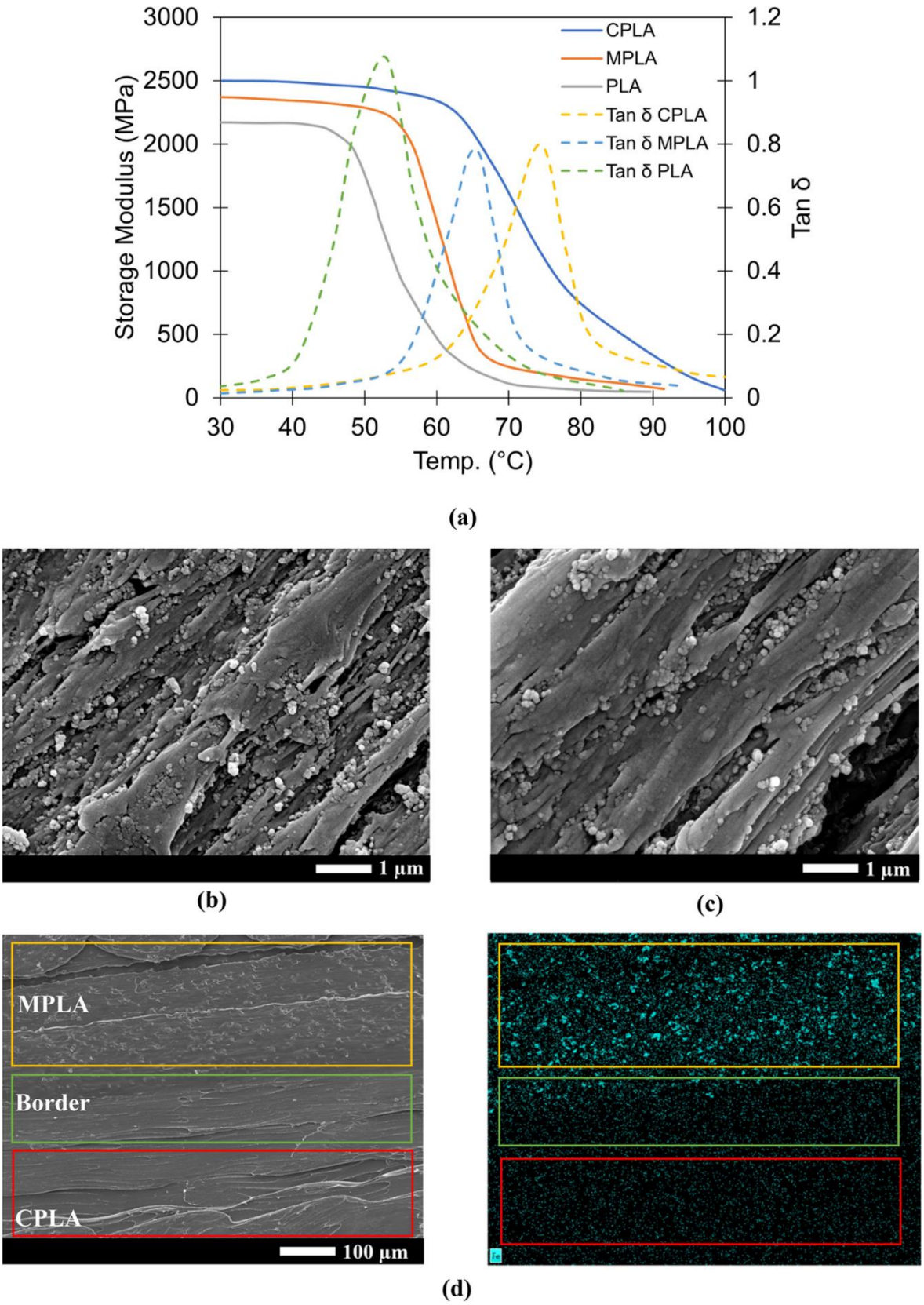

Figure 4.4. (a) DMA evaluations for materials. SEM image of materials created via (b) CPLA and (c) MPLA in 3D printing. (d) SEM and EDS images of the border condition and interface of the MPLA and CPLA that were 3D printed for iron particles. In the CPLA region, no iron particles are seen. (The MPLA is represented by the yellow box, the CPLA and MPLA borders are represented by the green box, and the CPLA is represented by the red box.)

4.3.2. Magneto-electroactive composite actuators

This initial investigation focuses on the thermal response of 4D-printed SMPC actuators when exposed to electrical current. The voltage required for quick activation and heating must be ascertained. This measurement is used to establish the voltage threshold for initiating shape change. **Figure 4.5a** shows how three structures are connected and heated at different voltages (60, 90, and 120 volts). The temperature changes that occur during the heating and cooling cycles are tracked by an infrared camera. **Figures 4.5b, 4.5c, and 4.5d** illustrate the maximum temperature achieved at each respective voltage. It is noteworthy that the structure is successfully heated to a consistent temperature of 104 °C across the sample in 26 seconds by applying 120 V. Conversely, the use of 60 V proves insufficient to reach the T_g of 100 °C. The data further demonstrates an observed decrease in current over time as the temperature rises.

Figure 4.5e details the variation in resistance as a function of temperature, employing a constant voltage of 120 V. The data suggests a positive correlation between resistance, temperature, and applied voltage. Additionally, **Figure 4.5f** presents the time required to reach a stable temperature at various voltage levels. The 4D-printed actuators exhibit a plateau in temperature upon voltage application, indicating an equilibrium established between the Joule heating effect and environmental heat loss. Notably, the specimen heated with 120 V reaches this plateau faster and consequently experiences a more significant reduction in Young's modulus.

It is important to acknowledge that the necessary voltage is contingent upon the specific design of the structure. Therefore, the following section explores methods to stimulate 4D-printed structures using lower voltage inputs. Factors influencing the behaviour of printed magneto-electroactive structures present a greater degree of complexity compared to purely electroactive structures. The structure that is being studied is one millimetre thick and is made up of five similar individual layers. The lengthy legs of the U-shaped structure might theoretically be connected to electrodes to accomplish full energisation. However, the current preferentially follows the path of the smallest resistance within the framework, which raises the local temperature in that area. The remaining portions primarily experience temperature increases due to heat diffusion from this hot spot. Consequently, the thermal conductivity of the structure along the axis perpendicular to the long legs is demonstrably lower than anticipated. Fortunately, this challenge can be mitigated due to the relatively narrow width of the structure.

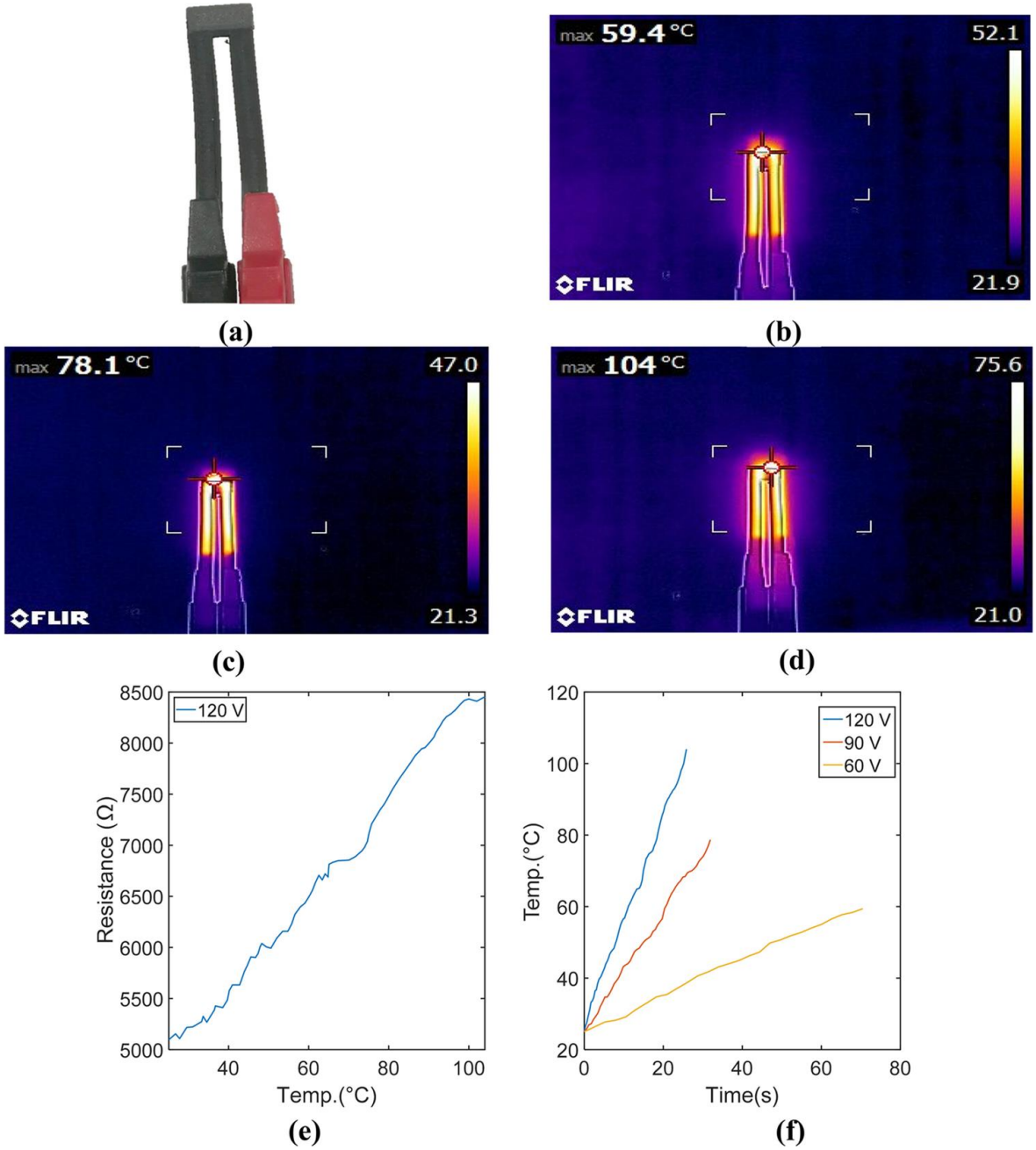

Figure 4.5. (a) The crocodile clippers clamp a structure that was manufactured using a 3D printer. The greatest distribution of heat produced by the 4D-printed actuator at (b) 60 V, (c) 90 V, and (d) 120 V. (e) Resistance varies as the temperature rises. (f) Steady temperature over time at varying input voltages.

The inherent presence of iron particles within the MPLA material allows for low-energy magnetic field activation of the actuator tip. This shows that employing an external magnetic field to actuate the 4D-printed composite construction is feasible. As shown in **Figure 4.6a**, the actuator must have one end clamped due to the significant force of the magnetic field. Heating up the actuator is the first step in the actuation process. The current flow through the structure results in rapid heating, as shown in **Figure 4.6b**. When the storage modulus decreases due to this heating, the actuator is drawn to the magnet and bent to line up within the magnetic field.

The actuator is then allowed to cool to room temperature once the power is turned off. Crucially, due to the inherent strength and rigidity of the SMPC structure, the actuator retains its bent configuration even after the removal of the magnetic field (see **Figure 4.6c**). This SME allows the adaptive structure to achieve a stable bending state without the need for continuous external stimuli. Eventually, the smart actuator is shaped back to its original form via Joule heating. The hot, bi-stable, structure shows almost 100% return to its original shape, as **Figure 4.6d** illustrates.

The smart composite actuator's reaction to an external magnetic field provides evidence of the interaction between its mechanical and magnetic properties. The MPLA material exhibits exceptional magneto-responsiveness in the presence of a magnetic field due to its inherent compliance and magnetic susceptibility. The strength of the magnetic field was also quantified throughout the experiment. As the distance between the magnets decreases, the axial force produced by the magnetic field grows. The relationship between the magnetic attraction force and the bending angle is depicted in **Figure 4.6e**. Furthermore, **Figure 4.6f** illustrates the variation in magnetic field strength over time at various distances. These findings suggest the potential for remote programming and control of the bi-stable composite actuator. Remote shape programming is made easier and bi-stability is achieved with the help of the smart composite actuator. This concept offers the flexibility to be adapted into various shapes and configurations depending on specific requirements and magnetic field intensities.

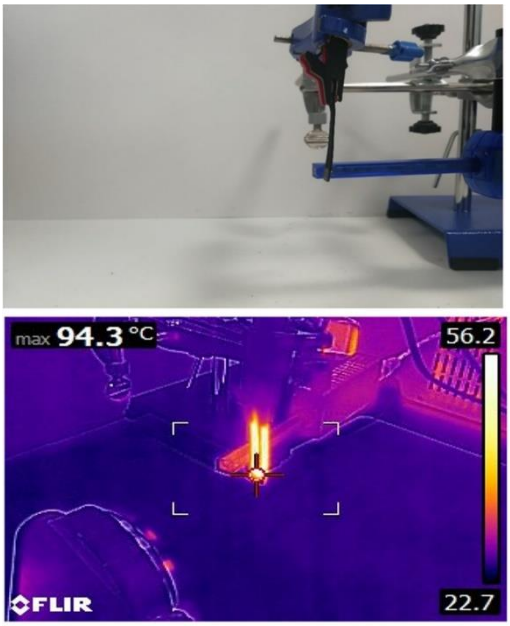
max 94.3 °C
56.2
22.7
FLIR

(a)

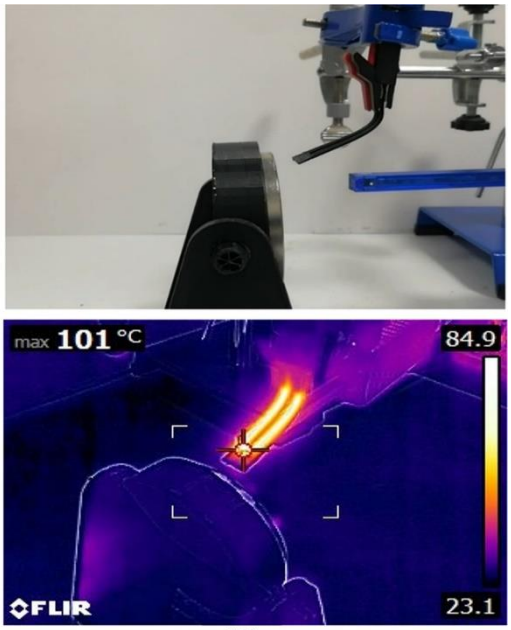
max 101 °C
84.9
23.1
FLIR

(b)

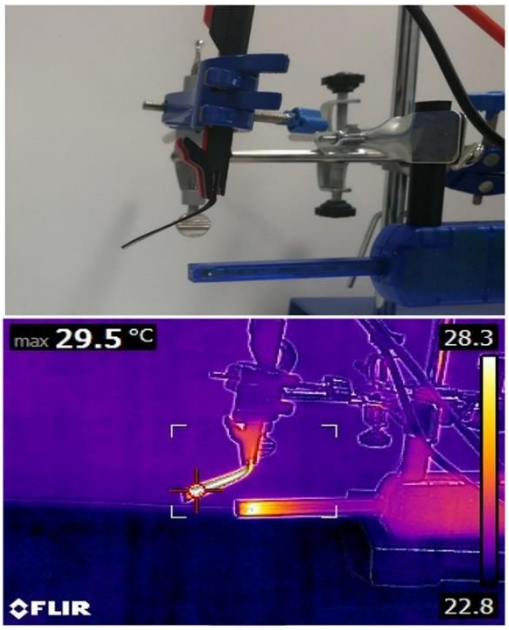
max 29.5 °C
28.3
22.8
FLIR

(c)

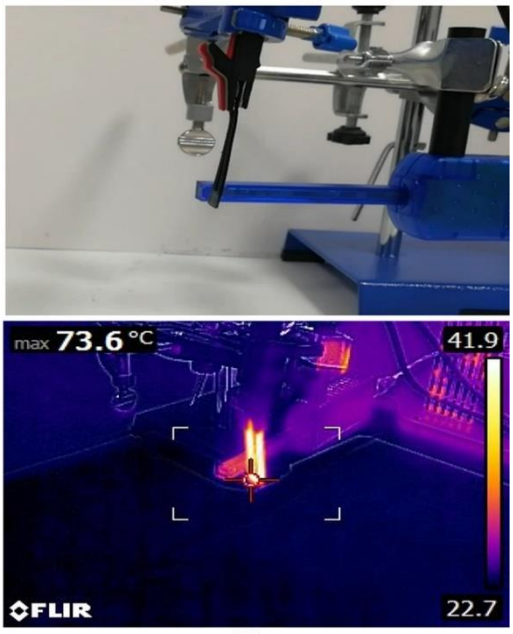
max 73.6 °C
41.9
22.7
FLIR

(d)

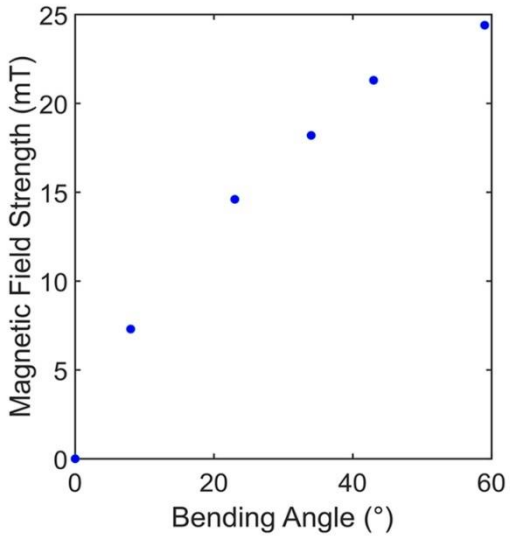
Magnetic Field Strength (mT)
Bending Angle (°)
0
5
10
15
20
25
0
20
40
60

(e)

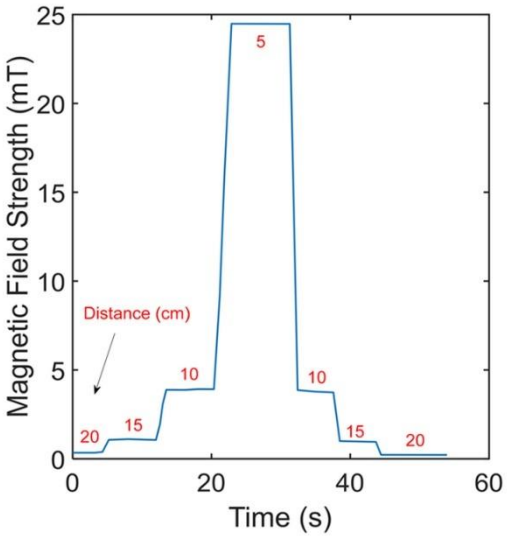
Magnetic Field Strength (mT)
Time (s)
Distance (cm)
20
15
10
5
10
15
20
0
5
10
15
20
25
0
20
40
60

(f)

Figure 4.6. (a) The process of heating the MM printed actuator that is orientated vertically. (b) The temperature and bend angle can be maximised by using magnetic attraction. (c) Cooling the composite actuator after removing the permanent magnet. (d) Joule heating of the actuator regains its original shape after 26 seconds and 100% shape recovery. The deflection of actuators at varying strengths of magnetic fields. (f) A graph displaying magnetic strength against time at different distances.

4.3.3. Modifying shape and sustainability

The integration of electro/magneto active SMPCs unlocks the potential for the creation of multi-stable structures, enabling a single actuator to achieve a multitude of shapes and configurations. By applying a permanent magnet above their T_g, these multi-stable actuators can be made to transition between several programmable configurations. Upon cooling below T_g, the structures solidify and retain their configured shape. This activation cycle, involving Joule heating and a magnetic field, allows for rapid and reversible shape changes. Furthermore, MM printing MPLA and CPLA materials allow for the realisation of complex geometries with localised, pre-programmed deflections.

This method provides a great deal of design flexibility. Basic sheet constructions are easily created, and their overall dimensions and size can be adjusted to meet needs. To ensure uniform heating efficiency throughout the structure, designs should incorporate features that promote equal resistance and thermal conductivity across all regions. This necessitates structures where each segment connected to the power source possesses an identical length. The layer-by-layer nature of the FDM printing process can however lead to variations in heating efficiency. The structure's ability to change shape in response to a magnetic field is demonstrated using the design as a basis. A programming temperature of 80 °C is established for this purpose.

Figure 4.7a illustrates the stable shapes achievable with this technology. A permanent magnet can be used to secure the structure in a variety of user-defined configurations, including twisted or folded forms. Upon application of an electrical current, the structure efficiently reverts to its original form. Compared to conventional robotic devices like pneumatic grippers, which require constant external power to retain a grip on an object, this provides a considerable benefit. Moreover, this method makes it easy to achieve various shape configurations. A key benefit of this technique lies in its ability to program and control multiple shapes within one actuator.

Figure 4.7b shows the fabrication of a flat beam structure to study the SME of SMPC actuators. A DC power supply is connected to two opposing sides of the beam to initiate the form change. The beam is heated to 80 °C by adding a voltage of 60 volts. It is noteworthy that lower voltages can be employed due to improved heat diffusion within the structure. A permanent magnet is positioned above the centre of the beam to induce attraction. A second permanent magnet is then used to generate a magnetic field that rapidly draws the magnetic portion of the beam upwards, causing it to adopt a secondary form. Repeating the heating and reprogramming procedure is necessary to get the final shape that is desired. The structure is cooled after that to produce a stable and permanent configuration.

In addition, the same design ideas are applied to a flat, rectangular construction (**Figure 4.7c**). This building is wired with a 120-volt power supply on all four sides to provide even heat dispersion. Like the previous experiment, two opposing sides are secured, and a permanent magnet is used to initiate shape change in the centre. The sample exhibits near-perfect 100 % shape fixity. Nonetheless, the significant force applied by the magnetic field results in a reduced rate of form restitution. Interestingly, this approach can convert 2D structures into 3D arrangements.

Using FDM 3D printing methods, a 2D pyramidal form actuator is developed and built. This structure is then stimulated using the same methodology as described above. As depicted in **Figure 4.7d**, a final 3D shape is successfully obtained. Upon cooling, the stiffness of the structure dramatically increases, allowing it to retain its achieved form. It does not require constant external energy input or actuation to sustain this locked condition. Remarkably, warming the structure causes it to revert to its initial shape. The combination of multi-stability and the locking mechanism provided by switchable temporary and permanent shapes paves the way for the development of low-energy, remotely controlled actuators.

This novel 4D printing technique using magneto-electroactive SMPCs offers significant advantages over traditional 3D printing methods. A key benefit lies in its ability to achieve a variety of shapes within a single printed sample, thereby minimizing material waste and energy consumption. The inherent challenges associated with 3D printing complex twisted or folded structures, which often require substantial support materials and increased printing time, are effectively addressed by this method.

To illustrate the environmental benefits of this technique, PLA structures are fabricated using 3D printing and compared to their 4D-printed counterparts (see **Figure 4.8**). A clear distinction is observed in terms of material usage and energy expenditure. Traditional 3D printing of diverse shapes necessitates a greater volume of material throughout the process. **Figure 4.8** exemplifies the support structures employed in conventional 3D printing, which significantly contribute to the overall weight of the printed object. While altering the printing angle can potentially reduce the need for support structures, this approach often compromises surface quality and introduces staircase defects. Furthermore, intricate structures inherent to the FDM process invariably necessitate support structures in certain orientations.

In contrast, 4D printing with shape morphing techniques enables the creation of these structures in a 2D shape, ensuring better surface integrity. This translates to reduced printing time and lower energy consumption. Conversely, traditional 3D printing methods often necessitate excessive material usage, particularly for large and bulky structures. Additionally, complex areas and unsupported regions in 3D-printed objects frequently exhibit compromised surface quality and structural integrity. **Figure 4.8** serves as an example, where the unsupported rectangular structure displays poor surface quality on its legs. These issues are significantly mitigated or eliminated by employing 4D printing with SMPC materials. This method allows structures to be printed on a flat sheet and then changed into their final form while maintaining surface and material quality.

This idea has a wide range of possible applications in technical fields. The ability to create smart, adaptable structures opens doors for the development of robotic grippers capable of grasping objects without continuous stimuli. Moreover, this approach offers intriguing

prospects for personalised packaging solutions and intelligent building implementations. Within the packaging industry, this technique can be leveraged to reduce storage space by printing structures in a flat 2D form and activating them later to achieve the desired customized shape. The inherent ability to lock the structure in its final configuration allows for its utilization as a hook-shaped locker, eliminating the need for external stimuli once activated.

Ensuring identical internal printing structures within branches participating in the deformation process and printing accuracy are critical design considerations for 4D-printed magneto-electroactive actuators. The strategic integration of magnetic and electroactive materials facilitates rapid, reversible, and remotely controlled shape changes in 4D-printed composite actuators. The potential for wireless actuation using fields of magnets is demonstrated by the application of CPLA and MPLA. This research paves the way for the development of low-cost, smart, and adaptable structures with multi-stable configurations. The proposed method not only enhances efficiency and minimizes material waste but also fosters the implementation of sustainable design principles by overcoming limitations inherent in traditional 3D printing technologies. Because of its adaptability, this approach can be used to meet special needs in a variety of sectors.

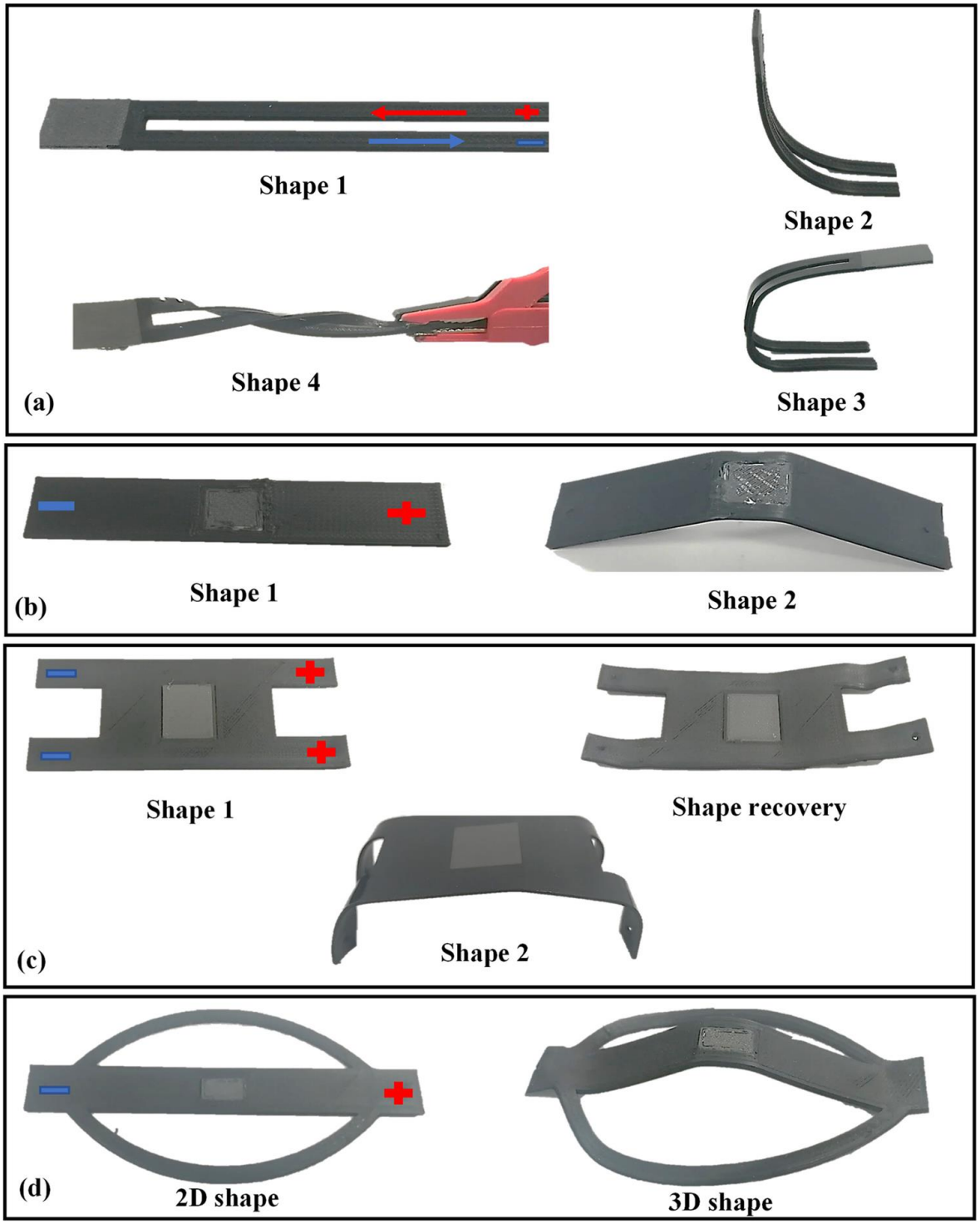

Figure 4.7. (a) Variations in a 2D U-shape using MPLA (grey) and CPLA (black) material. (b) Converting a 1D beam shape into a 2D shape with a 60 V power source and a permanent magnet. (c) A 2D rectangular shape can be converted into a 3D structure with 93% shape recovery by using Joule heating in conjunction with magnetic remote programming. (d) Creating a 3D structure by programming a 2D pyramid.

Figure 4.8. Permanent form structures printed in three dimensions with support.

4.4. Conclusion

This study uses FDM 4D printing technology to create magneto-electroactive smart actuators in a new and affordable way. 4D-printed CPLA and MPLA were the primary core materials under investigation. The magnetic response and Joule heating of the 4D-printed objects were thoroughly assessed. A thorough analysis was conducted to determine how different input voltages affected the structures' electrical, thermal, and electroactive shape memory properties. Methods for programming and remote control of the composite actuator were also established by the study. Additionally, under particular magnetic field and temperature conditions, a shape recovery technique was used. The actuator's behaviour was modulated by applying a low-intensity magnetic field. The microstructural investigation, composite interface assessment, shape recovery evaluation, and dual-stimulus characterisation were performed on the special composite actuator.

Upon activation with a 120V power source, the 4D-printed composite actuator showed a quick form recovery reaction. An actuator's greatest bending angle was 59 degrees when it was exposed to weak external magnetic fields. The shape morphing ability and potential for bi-stable configurations of the actuator were examined in this study. The effectiveness of shape morphing was demonstrated by analysis, which turned a single one- or two-dimensional structure into a variety of 2D and 3D forms. The significant potential of 4D-printed composite actuators for shape-morphing applications was clearly shown by the experimental results. The study also emphasises how the technology may improve sustainability by reducing energy and material waste. It is anticipated that this research will improve the field of 4D printing technology and open up new avenues for the fabrication of controllable functional components with multi-stable configurations, shape restoration capabilities, and environmentally friendly design.

Chapter 5

Shape memory meta-laminar jamming actuators fabricated by 4D printing

A novel design idea for meta-laminar jamming (MLJ) actuators is presented in this chapter. These actuators leverage 4D-printed polyurethane SMP meta-structures, fabricated using 4D printing. The fact that MLJ actuators don't require constant negative air pressure to operate is a major benefit over traditional LJ actuators. The chapter covers a concise overview, the purpose of the research, the techniques utilised to create MLJ actuators, as well as specific outcomes and applications. The following article served as the basis for the chapter. All content is adapted with permission from the article published as follows:

- **Lalegani Dezaki M**, Bodaghi M. Shape memory meta-laminar jamming actuators fabricated by 4D printing. Soft matter 2023;19(12):2186-22310.1039/d3sm00106g.

5.1. Introduction

The novel and adaptable class of soft robotic actuators known as LJ actuators has the potential to revolutionise several fields because of their special qualities as discussed in **Chapter 2**. Since LJ actuators are made of compliant materials and work on the idea of jamming to generate force and motion, they differ from conventional rigid-bodied actuators in this regard (Li, W., et al. May 30, 2021). A basic overview of LJ is given in this introduction, which covers its major features, operational principles, and possible uses.

The usual design of LJ actuators is a stack of thin plates or layers that are freely movable concerning one another (Narang, Vlassak and Howe 2018). Pressurised inflation chambers integrated within the stack force the plates to press against one other, creating a stiff structure. The LJ actuators can contract, elongate, bend, or twist due to the precise actuation pattern that is produced by carefully regulating the pressurisation of several chambers (Narang, et al. 2018).

This work investigates design considerations for LJ actuators. Ideally, LJ actuators should be lightweight yet possess sufficient strength to withstand external shocks while maintaining precise actuation for specific tasks. The continual negative pressure required to maintain the desired position poses a substantial problem for pneumatic LJ actuators, resulting in greater energy consumption from continuous actuation. Therefore, a sustainable design strategy is essential to minimise power consumption. This chapter presents a novel approach to build soft/hard MLJ actuators by combining LJ technology and 4D printing. These MLJ actuators are capable of zero-power holding, shape restoration, and model locking. Actuation is achieved through thermal programming (hot programming for activation and cold programming for shape locking). The design approach focuses on exploiting the contrasting behaviour of the MLJ actuators in jammed and unjammed configurations, an area that has received limited research attention.

The combination of 4D printing and LJ technology paves the way for the development of sustainable LJ sandwich actuators. In order to improve vacuum-based jamming and lower energy consumption, the suggested approach makes use of the 4D-printed core metamaterials. Excellent structural flexibility is provided by the lightweight metamaterial core, and its SME allows the structure to lock into the appropriate position without consuming any power. This method offers several advantages. It enhances reconfigurability

and reusability first and foremost. By only changing the relative rigidity at various points while keeping the core design intact, the actuation behaviour may be changed. Secondly, the SME and locking mechanism significantly reduce the actuator's power consumption. Lastly, a variety of features of the actuators are impressive, such as form recovery, high rigidity, bending and contraction, and shape locking in the appropriate position. These features make them suitable for various applications, such as zero-power lifting and gripping tasks.

5.2. Materials and methods

5.2.1. Concept and model

This work builds upon previous research on FDM printing, LJ actuators, and SMPs to create an FG metamaterial idea. The fundamental concept is to build sustainable, adaptive MLJ actuators by fusing SMPs with LJ technology. One amazing feature of SMPs is their ability to change shape in response to external stimuli and then revert to their original form. The goal of this project is to combine MLJ technology with this programming capability. A typical diagrammatic step-by-step thermomechanical programming methodology for MLJ actuators is shown in **Figure 5.1**.

The SMP metamaterial is first subjected to a low temperature (below the T_g), strain-free, and relaxed conditions. The temperature rises over T_g as a result. Negative pressure is used to put the SMP under the greatest amount of strain during the rubbery phase. After that, the material is cooled down to a low temperature while the vacuum pressure is kept constant. As the rubbery phase returns to the glassy phase, this step creates rigid stresses. At last, the material maintains its pre-strain while its framework is released. The actuator disconnects and stays locked in the position determined by the form of the meta-structure. The actuator core is heated to a high temperature, which releases strain and activates it to return to its permanent form.

The module's integration of PVC films provides control over the actuator's behaviour, allowing it to transition from contraction to bending. In the absence of PVC films, negative air pressure induces contraction and compaction of the actuator. The actuator's shape is locked in both cases until it is heated again. According to the study, the MLJ actuator's metamaterial core is essential for forming MLJ structures and causing an elastic pre-strain, which in turn affects how SMPs behave. This implies that different programming techniques for the metamaterial could result in a variety of pre-strain values. Furthermore, it is determined that printing settings, force levels, material characteristics, and structure dimensions are critical elements to take into account while optimising MLJ actuators.

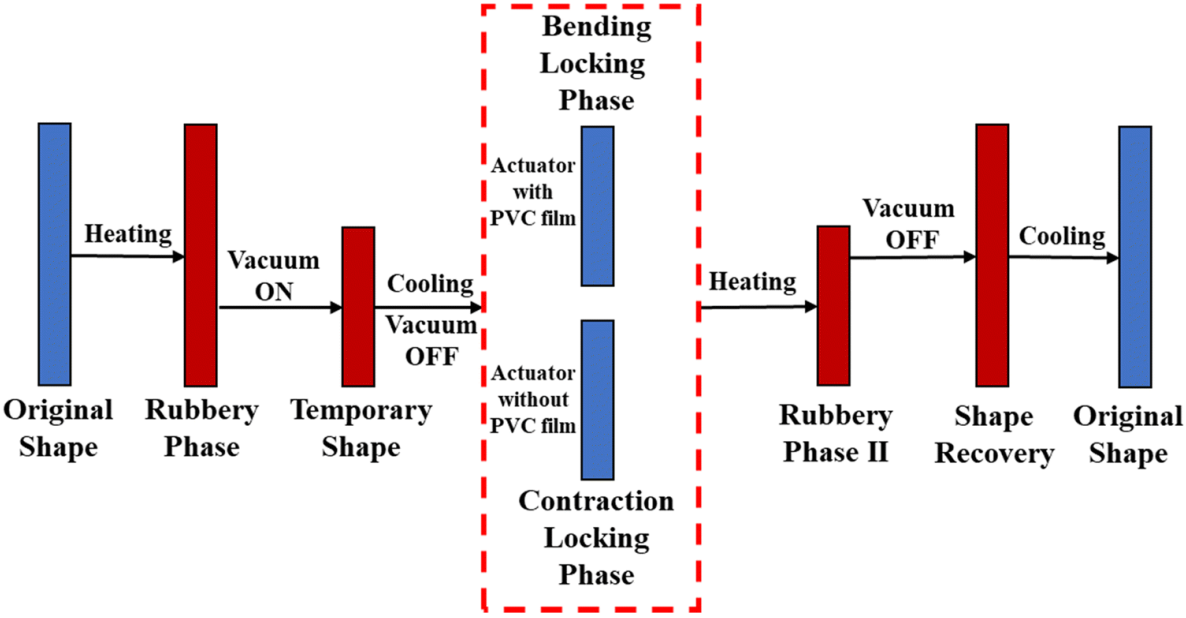

Figure 5.1. The process and idea behind powering on 4D-printed MLJ actuators.

5.2.2. Design and fabrication

A constant design was maintained across all actuator structures to isolate the effects of core geometry. Five distinct lattice geometries were chosen for analysis: honeycomb, circle, rectangle, diamond, and auxetic. These selections prioritised versatility in applications and consistent mechanical behaviour. All models were constructed in SolidWorks© software with identical size and volume (detailed illustrations provided in **Figure 5.2**).

The core structures were 3D printed using the FDM technique using polyurethane SMP-based filaments (1.75 mm diameter) from SMP Techno. The capacity of FDM to create complex SMP structures in compliance with standards proved useful. Using generated tool paths and G-codes written with Slic3r software, samples were made from bottom to top. For reliable core structure manufacture, an open-source 3D printer was used. Printing parameters significantly influenced the quality of SMP metamaterials (Bodaghi, M., Damanpack and Liao 2017, Wang, F., et al. 2023). In order to guarantee uniformity, every sample was printed using the following parameters: 40 mm/s print velocity, 0.2 mm layer height, 5 mm retraction distance, 210 °C nozzle temperature, and 0 °C substrate temperature.

Pneumatics inspired by vacuum-actuated muscles as well as fluid-driven artificial muscles inspired by origami served as inspiration for the actuators' internal designs, with a preference for the latter. The assembly process is depicted in **Figure 5.3**. To activate the core structure, the heating temperature surpassed the material's T_g. Consequently, Easy Composite Ltd.'s thermally resistant nylon PA6 vacuum film was used, which has a maximum operating temperature of 200 °C. A heat sealer was used to seal three sides of the film. The bagging film was placed into the core metamaterials. Within the actuator module, a thin 0.25 mm PVC film was added to regulate its motion (bending or contraction). The intended motion could determine where to place the film. One side of the module had a TPU tube fixed to it,

and Easy Composite Ltd.'s polyisobutylene sealant tape was used to seal the assembly. The actuator's ability to contract or bend was then used to assess how well it performed.

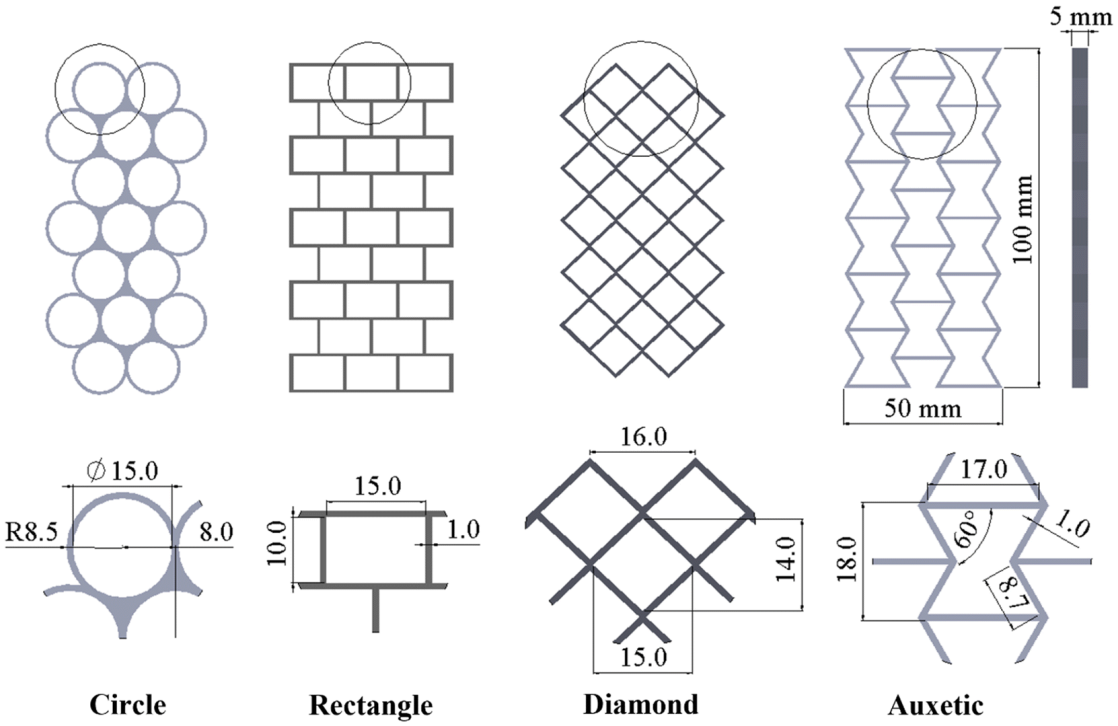

Figure 5.2. Meta-structure core 2D schematic design with details.

5.2.3. DMA test

A PerkinElmer 8000 DMA was employed to characterize the storage modulus of the 3D-printed polyurethane SMP. The test sample was manufactured at a printing speed of 40 mm/s and had the following measurements: 15 mm for length, 1.6 mm for width, and 1 mm for thickness. T_g is a crucial thermodynamic parameter influencing the SME of SMPs. Therefore, evaluating T_g was essential for understanding the shape memory behaviour of the 4D-printed polyurethane. Additionally, the influence of heating on the material's T_g was investigated. In order to depict the slow changes in characteristics brought on by temperature, a test frequency of 1 Hz was selected. A temperature ramp from 25 °C to 85 °C at a rate of 5 °C/min was used in the DMA test program.

5.2.4. Mechanical properties

To evaluate the MLJ actuators' strength and stiffness, a three-point bending test was used. Three configurations were tested: the actuators inside the vacuum bag, the metamaterials by themselves, and the actuators with and without the PVC sheets. For the testing, a Shimadzu AG-X plus machine was used, and TRViewX software was used to collect the results. During the test, samples were fastened on both sides to keep them from moving. The resulting deflection was continually recorded while a constant force rate was applied. A 1 kN load cell was utilised for both the loading and unloading cycles, and the crosshead speed was adjusted to 5 mm/min. Three samples were tested for each configuration. Furthermore, the influence of vacuum pressure on the flexural strength of the actuators was evaluated. The study involved a flexural test under continuous negative pressure application, which facilitated an

examination of the properties of the structures and the actuators' performance in these settings.

In order to improve stability, the sample width was increased to 10 mm and the length was shortened for the compression test, which examined how the structures behaved under load in the context of actuator contraction. Once more, data was acquired using the TRViewX software and the Shimadzu AG-X plus machine. The crosshead speed was maintained at 5 mm/min for both loading and unloading. In order to maintain uniformity and avoid undue deformation, a maximum strain of 10% was implemented on each sample. At temperatures over the T_g, the functionality of the actuators and structures was also examined. The previously specified steps were repeated here. Since this is the temperature at which the actuator starts to contract or bend, 70 °C was selected. Both the three-point bending and compression tests included a heating chamber. When the temperature reached 70 °C, the testing machine's top jaw was designed to drop.

5.2.5. SME

Both bending and contraction circumstances were studied for the SME. At room temperature, the samples were heated to 70 °C. In the instant that followed loading, the samples were quickly chilled to 25 °C. To find the form recovery time and ratio, this heating-cooling cycle was repeated. Following up to three repetitions of the free shape memory test in the contraction and bending modes, shape recovery values for the metamaterials and the MLJ actuators were determined. Examining the shape recovery ratio and time of the metamaterial structures themselves was the first step in the evaluation procedure. Then, when they were incorporated as central components of the MLJ actuators, their shape memory behaviour was evaluated. Equation (5.1) is utilised to determine the form recovery ratio.

$$Recovery\ ratio\ (\%) = \frac{Height\ of\ actuator\ after\ recovery}{Initial\ height\ of\ actuator} * 100 \tag{5.1}$$

5.2.6. Actuators' evaluation

Leakage prevention was crucial, so the modules were sealed. Smart actuator operation was achieved using a Tinkrmind programmable air kit, with a maximum operating vacuum pressure of 1 bar. The output flow between 0 and 1 bar could be precisely controlled using this kit. Throughout the procedure, the negative pressure differentials were observed using a differential pressure manometer. To make sure the structure exceeded its T_g, a heat gun was utilised to activate the SME. Next, by warming the framework and timing its recovery, shape memory and recovery were assessed. The behaviour of the 4D-printed metamaterial was monitored during this procedure using a FLIR infrared camera. A SAUTER 100 N electronic force gauge was used to measure the force produced by each actuator (see **Figure 5.3** for an illustration). The pressure gauge and the actuators were both clamped to one side for uniformity. The movements of the actuators were recorded using a video camera. The motion and trajectory of the smart composite actuators were also recorded and tracked using the PASCO application.

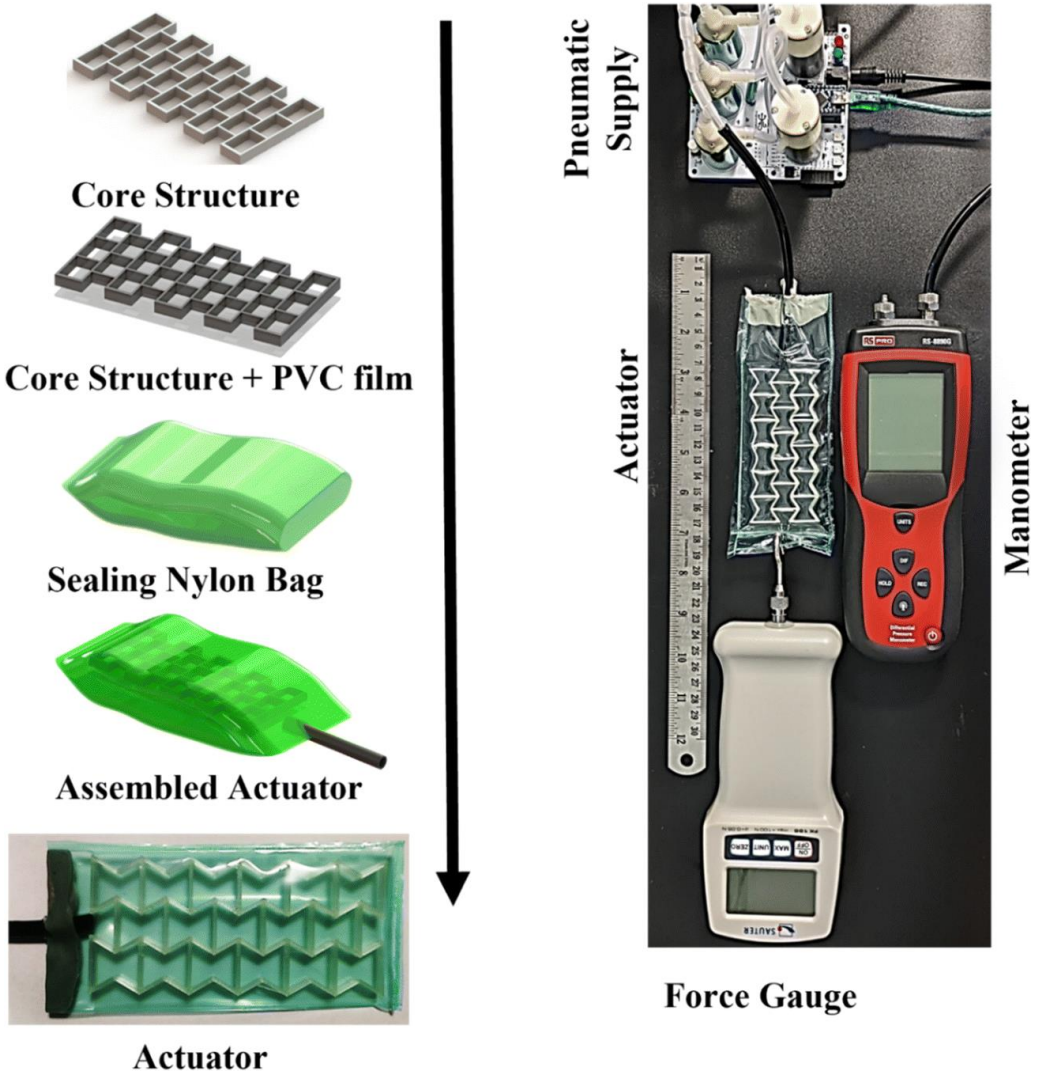

Figure 5.3. The process of constructing MLJ actuators and apparatus to examine their functionality.

5.3. Results and discussion

5.3.1. Three-point bending test

The temperature dependency of the material's tan δ and storage modulus is shown in **Figure 5.4.** Tan δ and the storage modulus show a clear peak and thereafter decline with increasing temperature from 25 °C to 85 °C. This behaviour indicates a limited T_g. Tan δ exhibits a maximum value of 0.8 above 55 °C, followed by a sharp decline to 0.09 at temperatures higher than 60 °C. The storage modulus is roughly 1600 MPa, and after T_g, it significantly drops to 35 MPa. This transition is attributed to chain flow within the material, transforming it from a stiff solid (glassy phase) to a viscous liquid (rubbery phase) with a markedly reduced storage modulus. The prominent peak in the tan δ curve at $T_g \approx 60$ °C signifies the glass transition temperature. This distinctive behaviour implies that, for the printed structure to regain its original shape following deformation due to a thermally induced process, an activation temperature greater than T_g is necessary.

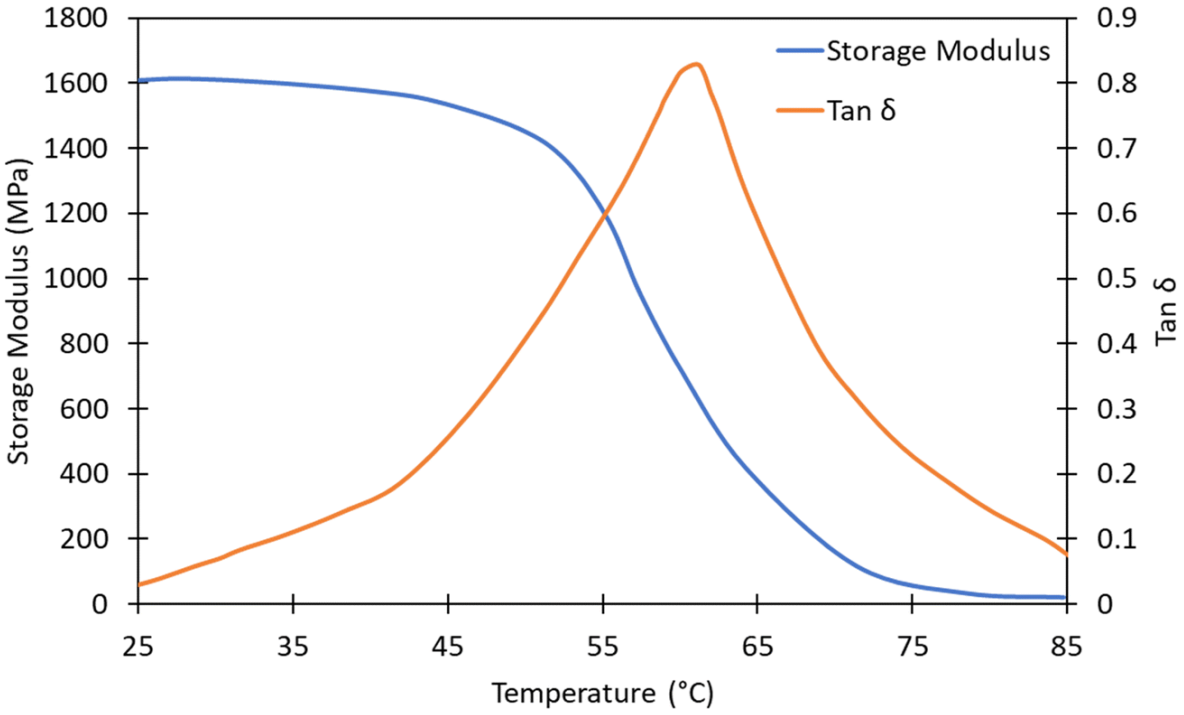

Figure 5.4. The storage modulus and tan δ of the printed SMP were determined by DMA measurements.

Three-point bending and compression experiments were performed at room temperature and 70°C to forecast the mechanical characteristics of MLJ composite actuators under different temperature settings. It is important to comprehend the behaviour and reaction of core structures under three-point bending because of the vacuum jamming actuation mechanism. This test serves a dual purpose: evaluating the behaviour of individual cells and their assembled structures. In essence, it allows for the investigation of core structures' mechanical properties, particularly their bending behaviour within actuator modules. Each test was run three times to verify data dependability, and the median findings were then published. Three-point bending tests on metamaterials and their constructed modules are performed as described in **Figure 5.5**. Interestingly, in both jammed and unjammed states, the core structure shows rigidity. To achieve the best possible structural performance in terms of shape memory behaviour, a minimum cell thickness of 1 mm is also set. For bending

experiments conducted only on metamaterial constructions, the methods used are explicitly shown in **Figure 5.5a**.

Starting the testing process, the samples are loaded up to a 10 mm displacement. The weight is then released, and the testing device moves back to its starting position. A module consisting of a bag, a PVC sheet and a core structure is shown in **Figure 5.5b**. On the other hand, **Figure 5.5c** displays a module that only has a bag and a core lattice structure. A vacuum pump applies a pressure of 0.85 bar to achieve jamming within the structures. Three samples from each module configuration are subjected to the test. The entire procedure is then replicated at an elevated temperature of 70°C to ascertain the mechanical properties of the structures in their rubbery state. These tests aim to elucidate the disparities in properties and behaviour between the different module types. The main structure usually regains its shape at room temperature after the structures and modules are unloaded. There is a residual angle deviation, indicating that this shape recovery is not entirely successful, as seen in **Figure 5.5d**. For every structure, the angle is measured to assess the changes in shape recovery following unloading.

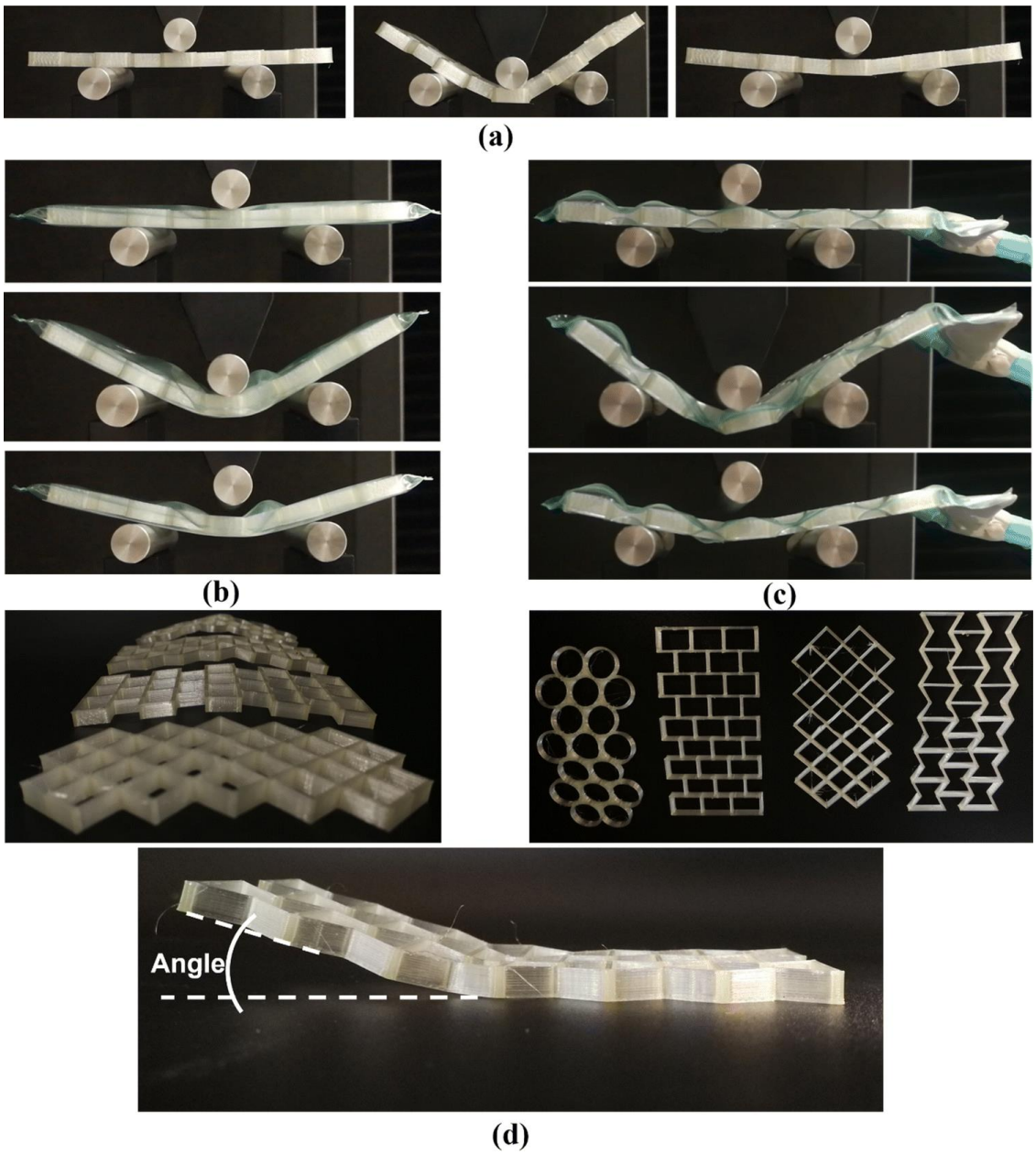

Figure 5.5. Three-point bending tests were conducted on (a) meta-structures, (b) MLJ actuators that were not jammed and had. MLJ actuators with jammed sheets made of PVC, and (c) PVC sheets themselves. (d) Meta-structures that have undergone a three-point bending inspection have their shapes restored.

Various core configurations with advanced bending characteristics for these modules are investigated in a controlled setting. The functioning of each metamaterial component and associated module is shown in Figure 5.6. Because of the glassy state's rigidity, the core structure is essential to keeping the MLJ actuator in its locked shape. The cyclic load graphs for the auxetic, circle, diamond, and rectangle configurations of the structures and modules were obtained by a three-point bending test. The force rises to 75.11 N at a displacement of 6 mm and subsequently falls to 62 N at a 10 mm stroke when the actuator is under vacuum and the core structure is auxetic, as shown in **Figure 5.6a**. However, this generated force drops significantly to 1 to 2 N when the temperature is raised. This reduction occurs because the structure transitions to the rubbery phase at high temperatures, as documented in previous studies (Tao, Xi, et al. 2020, Tao, Ji, et al. 2020). In non-vacuum conditions, the entire

module displays comparable behaviour, emphasising the actuators' reliance on the core framework. Remarkably, the MLJ actuator becomes stiffer even at elevated temperatures when negative pressure is applied. In this case, however, the resultant force is still less than in the glassy phase because of the decreased stiffness. Finally, the results indicate that the structures in the rubbery stage do not absorb any energy.

Similar results are obtained for objects shaped like circles and diamonds (see **Figures 5.6b and 5.6c**). However, the rectangle structure behaves differently. Its load steadily increases to 10 mm without any force drop (see **Figure 5.6d**). The actuators without PVC sheets and bags and those with them produce almost the same amount of power. This demonstrates once more how dependent the actuators are on the central structure. The generated load is higher when a module without a PVC sheet is subjected to a vacuum, though. When the actuators are vacuumed by the pump, the module gets stronger and jams the structure. Elastoplastic behaviour is shown by the structures within a 10 mm stroke.

The maximum produced force for each structure within a 10 mm stroke is shown in **Figure 5.6e.** In all modules, the force is increased by applying negative pressure. On the other hand, modules featuring both bags and PVC sheets show a maximum force that is nearly the same as the structures by themselves. After unloading, the structure is impacted by the module's stiffening due to the applied pressure. Except for rectangles (49.01 ± 1 N), the maximum force is comparable for diamond, auxetic, and circle meta-structures (around 74 ± 1 N). This discrepancy results from cell behaviours that affect how much energy is absorbed. (Hamzehei, et al. 2022, Bodaghi, M., et al. 2020). Improved shape recovery upon unloading is the result of energy absorbed in this region.

A meta-structure's angle following unloading is shown in **Figure 5.6f.** During loading and heating, the performance of shape recovery was evaluated in this experiment. The core structure's reaction to PVC films and the vacuum process was also assessed by measuring the angle. When a PVC sheet or negative pressure is used in place of structures alone, shape recovery improves following unloading. The greatest results (29.67 ± 0.7° for the structure alone and 20.67 ± 0.5°) are obtained by structures shaped like circles. Deformation can be decreased by 47% by applying a negative pressure of 0.85 bar. Auxetic core actuators have an angle of 9.02 ± 0.6° achieved. In tests of three-point bending, auxetic- and rectangle-shaped modules function better when subjected to negative pressure. On the other hand, without changing the generated force, the use of extremely flexible PVC sheets in MLJ actuators reduces meta-structure deformation.

When the temperature increases, other structures exhibit behaviour like the auxetic structure. After T_g, their Young's modulus decreases, which makes them less rigid. As a result, the force created inside a 10 mm displacement is around 1 to 2 N. Nevertheless, the actuator module becomes more rigid when negative pressure is applied, which raises the load correspondingly. Yield strength may be increased by optimising the input vacuum pressure, core thickness, and coefficient of friction between internal components. However, this study prioritizes minimizing force. The ideal structure should bend and contract easily with low force and exhibit good shape recovery after activation. However, design parameter adjustments can introduce challenges. It could take more energy to trigger the actuator when using PVC sheets or a thicker core structure.

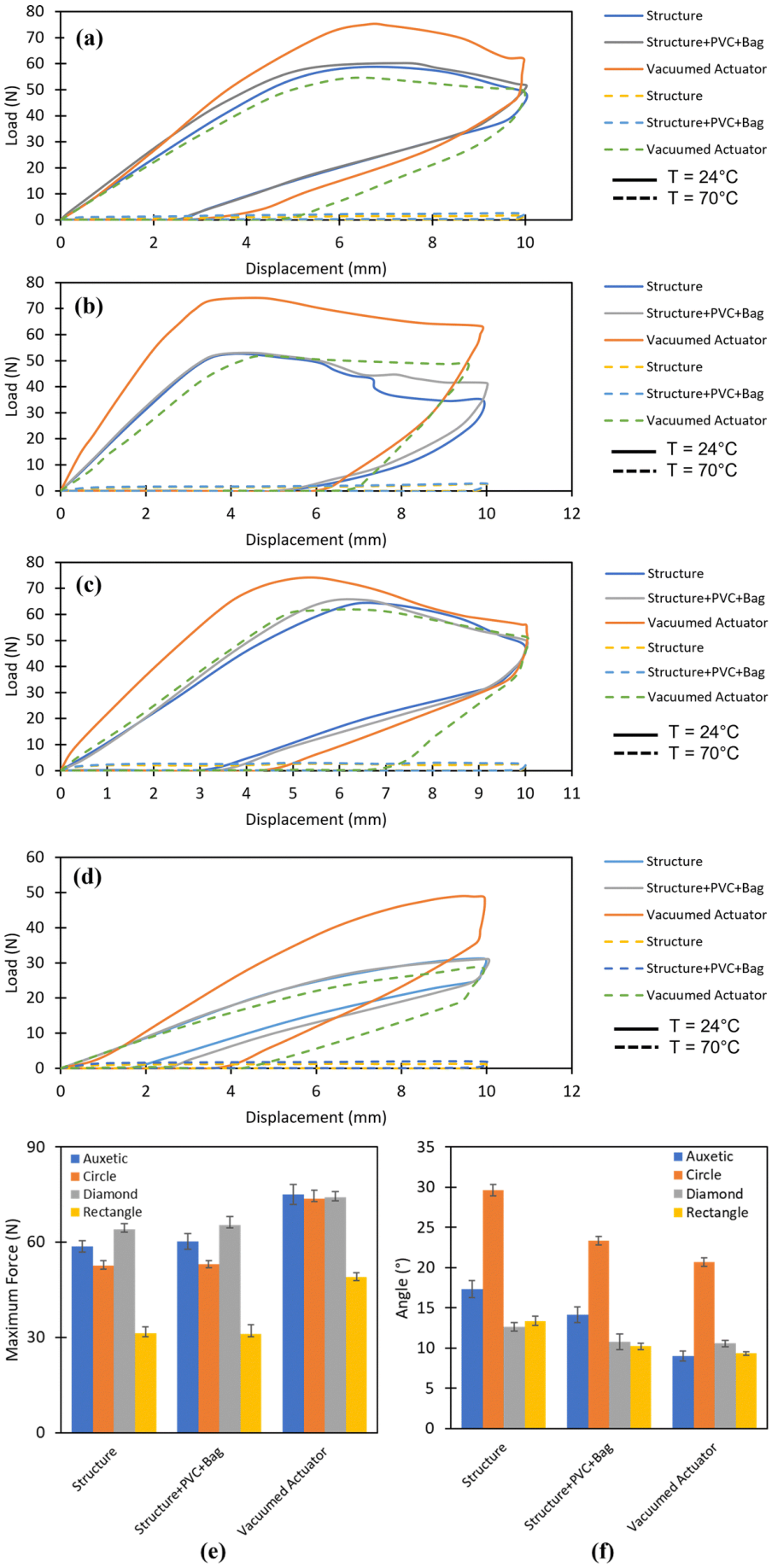

Figure 5.6. Load against displacement of MLJ actuators with the following meta-structures: (a) auxetic; (b) circle; (c) diamond; and (d) rectangle at room temperature and 70 °C. (e)

Achieved the maximum force feasible for different designs. (f) Angle attained in the room temperature three-point bending test after the weight has been unloaded.

5.3.2. Compression test

This study investigates the compressive behaviour of various meta-structures to identify designs that optimize actuator module performance. A key factor influencing actuator functionality is shape recovery after contraction. To avoid compromising this recovery, the compression test is limited to a 10% strain. The ideal meta-structure should distribute applied forces uniformly throughout its structure, thereby minimizing stress concentrations and enhancing shape recovery.

The experiment involved securing each meta-structure sample to the base of a testing apparatus. To simulate a quasi-static mechanical force, a crosshead was used to apply a continuous downward movement of 5 mm/min. Due to the limited compression stroke, the structures were anticipated to exhibit a combination of elastic and elastoplastic behaviour. Force and displacement measurements were used to assess the structural responses of each meta-structure at both room temperature (24°C) and high temperature (70°C). 10% strain was given to each sample's length during the compression test.

The reaction of the meta-structures to compressive force at room temperature is shown graphically in **Figure 5.7a-d.** All structures, except the circular design, demonstrated effective force distribution throughout their entirety. As shown in **Figure 5.7e**, different meta-structure geometries exhibit distinct mechanical properties. The auxetic structures exhibited a loss of stability and buckling behaviour after a 3 mm displacement, despite demonstrating contraction in both vertical and horizontal directions. This contraction is attributed to material densification within the structure upon compression. In contrast, the circular meta-structure displayed concentrated deformation on its upper surface.

The rectangular and diamond-shaped structures exhibited elastic behaviour, with a significant degree of shape recovery after unloading. However, residual stresses within the auxetic structures suggest some energy dissipation due to plastic deformation. This indicates the conversion of a portion of the input energy into kinetic energy via plastic deformation mechanisms. The circular unit cells have a steeper force-displacement curve in both elastic and plastic areas, which is consistent with their increased stiffness in comparison to other architectures. This translates to a lower degree of shape recovery for the circular meta-structure after unloading. Notably, the force experienced by all structures decreased to approximately 1.5 N at the elevated temperature. A substantial drop in 35 MPa Young's modulus is the cause of this decline, which jeopardises the structures' ability to absorb energy. To mimic the usual negative pressure restrictions seen in actuator core architectures, the strain was set at 10 mm. The three-point bending test trends were seen in all the actuators.

The relative stiffness of each meta-structure is indicated by the maximum force measured for each, which is summarised in **Figure 5.7f.** Among the structures tested, diamond-shaped configurations demonstrated the least resistance to force (mean ± SD: 102.94 ± 7.09 N), followed by auxetic and rectangular designs (132.08 ± 6.02 N and 139.45 ± 7.2 N, respectively). Circular structures exhibited the greatest force (183.98 ± 6.4 N). Results from both three-point bending and compression tests revealed that circular meta-structures underperform in comparison to other configurations regarding contraction and flexural

properties. These structures exhibited greater deformation under identical three-point loading conditions and demonstrated increased stiffness, an unfavourable trait for the intended application, in conjunction with suboptimal shape restoration following cyclic compression.

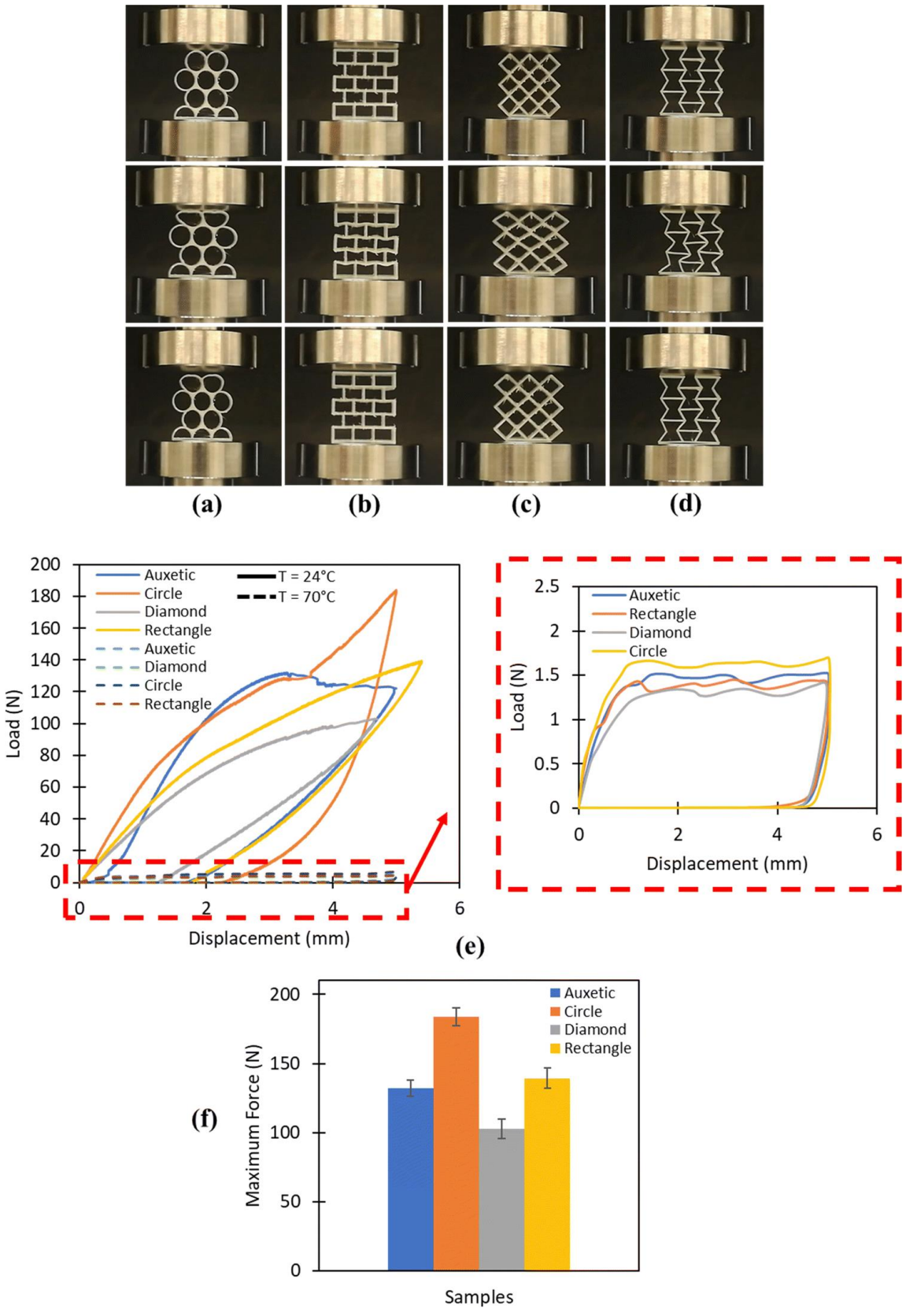

Figure 5.7. The effects of the cyclic compression loads: (a) circles, (b) rectangles, (c) diamonds, and (d) auxetic meta-structures. (e) At room temperature and 70°C, the meta-

structure load is measured against displacement during a single-cycle compression load. (f) Within 10% strain, every design's maximum force is recorded.

5.3.3. SME of core structures

This section investigates the shape recovery behaviour of three types of meta-structures: auxetic, rectangular, and diamond-shaped structures. The experiment employs a two-step process: deformation and recovery. In the deformation stage, the meta-structures are compressed while in their rubbery state (above T_g) and then cooled, fixing their contracted shape. The extent of contraction is measured. Subsequently, the deformed structures are heated to trigger shape recovery, which is documented. **Figure 5.8a** depicts the shape recovery process for a rectangular meta-structure. After compression and cooling, the structure regains its original form upon heating, achieving a 100% shape recovery ratio. Similarly, **Figure 5.8b** demonstrates the recovery sequence for the auxetic meta-structure, which recovers its original shape at 74.6 °C.

Furthermore, the shape recovery of bent meta-structures is evaluated. All structures achieve a maximum bending angle of 30° after heating and application of a load. **Figure 5.8c** showcases the recovery process for the auxetic structure, where it regains its original form upon heating to 66.4 °C. The shaping process is replicated for the remaining components. All materials fully returned to their original state following heat gun application. When heated beyond a specific temperature threshold, the material becomes highly flexible, enabling intricate designs. However, overheating risks material degradation or structural failure.

Figure 5.8d summarizes the recovery behaviour for all structures after compression and bending tests. Shape recovery commences around 60 °C for all specimens. Notably, the recovery temperature range is slightly different for compressed (71 ± 2 °C) and bent structures (68 ± 2 °C). The material's distinctive properties can be attributed to its structural configuration. Its capacity for shock absorption and its response to pressure are instrumental in producing these outcomes (Yousefi, et al. 2023).

Finally, **Figure 5.8e** presents the recovery time for each meta-structure, measured from the start of heating to complete shape restoration. Due to the varying degrees of bending attained during the test, different recovery times are observed. All structural configurations returned to their original state within a 20-second timeframe. The diamond-shaped configuration demonstrated the most rapid recovery, with durations of 13 seconds and 16 seconds for bending and compression, respectively. The possibility of reducing recovery time through increased heating rates is also acknowledged. The investigation culminates in emphasizing the full restoration of the original form in all meta-structures. Their potential utility as fundamental components within actuators is underscored by the exhibited capacities for contraction and flexion.

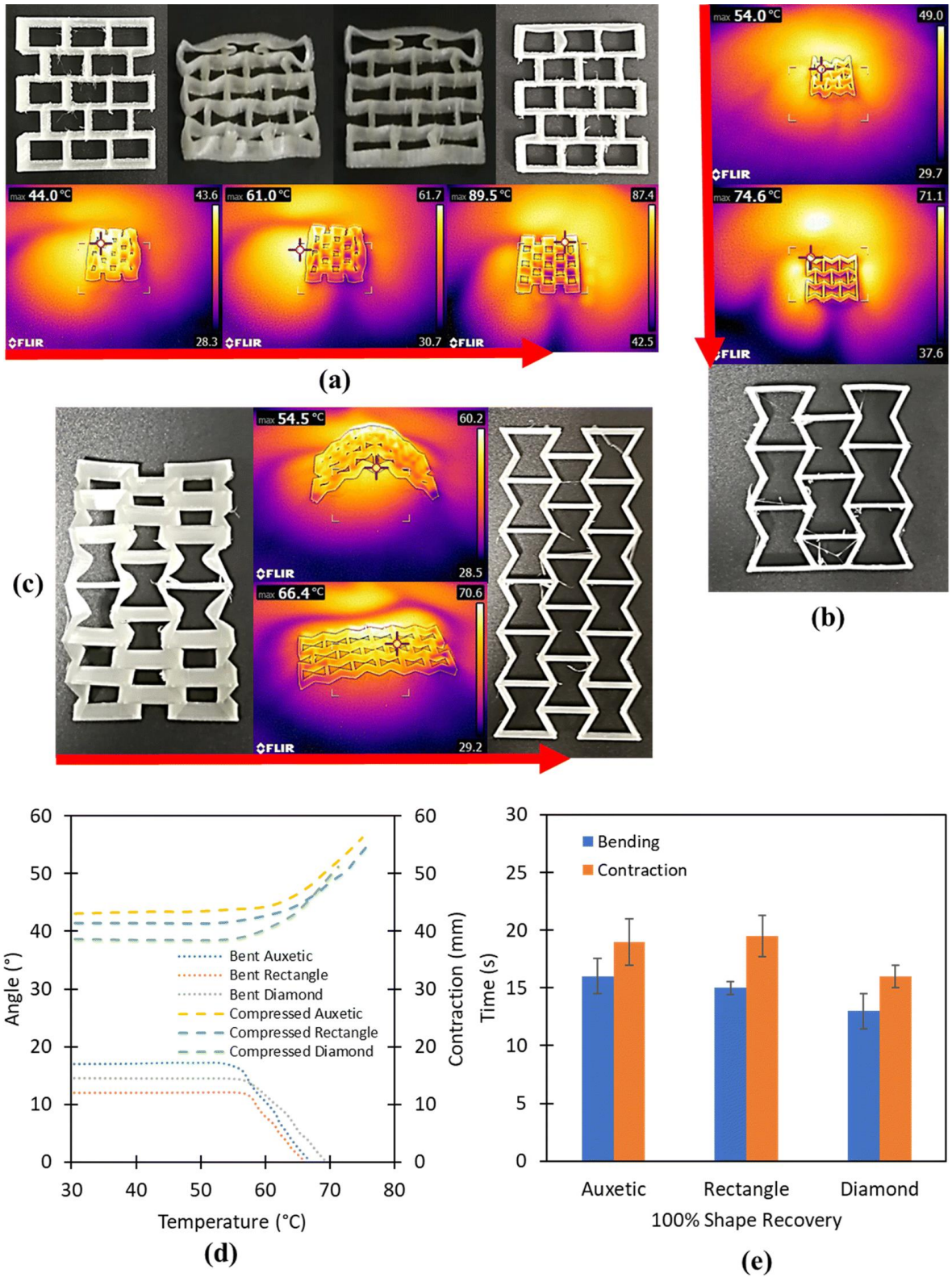

Figure 5.8. (a) Shape recovery of rectangular meta-structures following contraction. This involved compressing the printed specimen and subsequently applying heat. The deformed structure was then heated to restore its original configuration. (b) The recuperation process of auxetic-shaped meta-structures post-contraction. (c) Shape restoration of auxetic structures after undergoing a flexural test. (d) Shape recovery of a specimen group subjected to both flexural and compression testing. (e) The amount of time it takes for all structures to regain their shapes to 100%.

5.3.4. MLJ actuators performance

Figure 5.9a illustrates the process of activating an actuator equipped with an auxetic core. Initially, in a vitreous state, the core inhibits the actuator's ability to contract or flex. Activation is initiated by heating the core, using either hot water or air, to a temperature surpassing the T_g. The low thermal conductivity of the plastic cover necessitates the use of a heat gun to attain the target temperature of 80 °C.

Achieving a uniform phase transition necessitates a heating duration of 30 to 35 seconds for the actuator. An elevated heating rate can expedite this process. Subsequent to activation, the application of negative air pressure, culminating at 0.4 bar, induces contraction due to the core's softened state. The actuator is then cooled to below 50 °C, preserving the contracted configuration while the vacuum source is terminated. As previously elaborated, the actuator reverts to its original shape upon cooling. Releasing the actuator and disconnecting the power supply facilitates the core's return to its initial condition through reheating to 80 °C. The structure subsequently cools to ambient temperature.

Actuators exhibit bending capabilities, as depicted in **Figure 5.9b**. The methodology employed for bending mirrors that of contraction, except a PVC sheet strategically positioned on one side of the core structure to induce controlled bending. The process entails heating and applying a vacuum during stage II, followed by shape fixation in stage III. After this, the actuator reverts to its original form. The achieved bending angles vary across actuators.

The investigation indicates that while actuators can be subjected to increased negative pressures, up to a maximum of 0.8 bar, or utilize thicker core meta-structures, these conditions result in pronounced deformation and compromised shape recovery. While a higher pressure (0.8 bar) results in greater contraction compared to 0.4 bar, complete shape recovery is not achieved. This translates to decreased accuracy and precision in cyclic testing for MLJ actuators. Additionally, twisting and deformation during the vacuum procedure negatively impact the results.

An alternative activation method involves initiating the vacuum first, followed by gradual heating. This subjects the structure to a constant negative pressure (0.4 bar) with increasing temperature, inducing contraction or bending. However, this method exhibits a slower actuation rate compared to the initial approach.

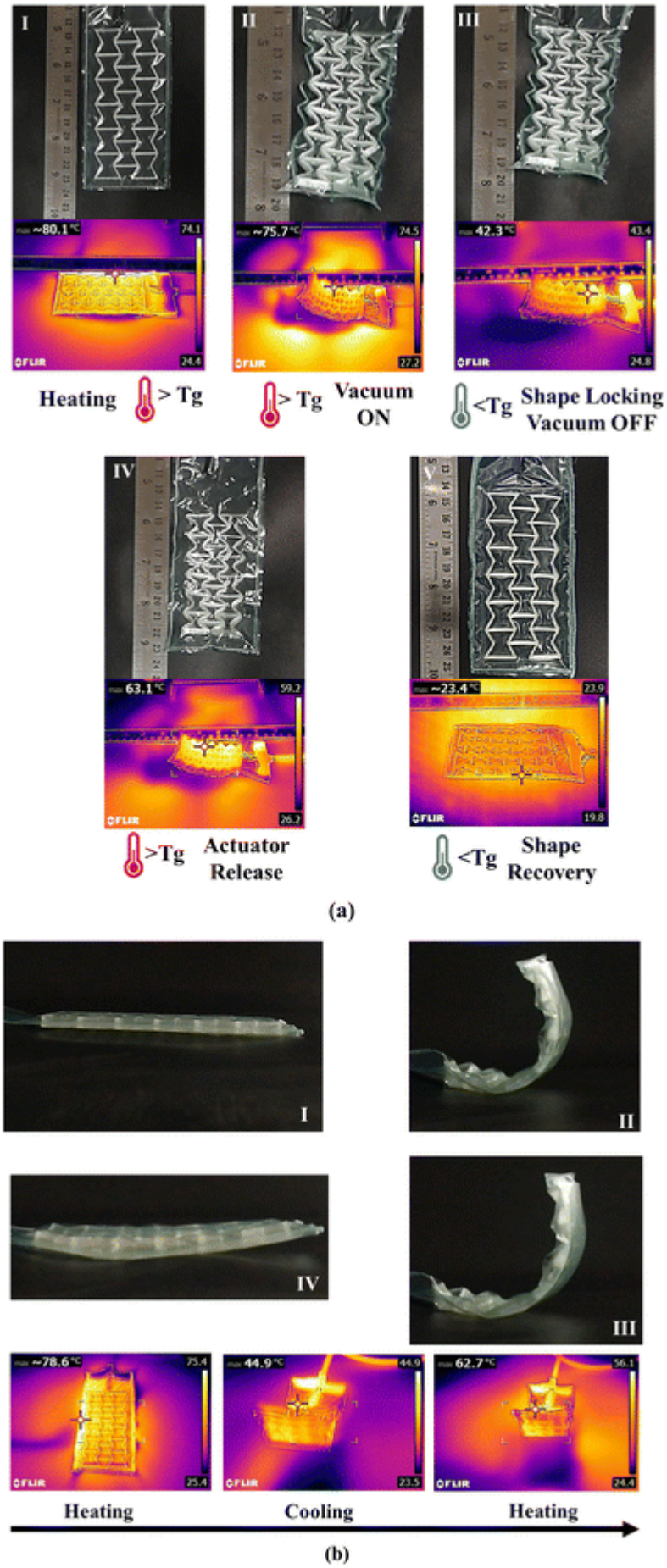

Figure 5.9. The procedures for MLJ activation, shape locking without input power, and shape recovery under (a) contraction and (b) bending conditions.

A comparative study was undertaken to discern performance variations among MLJ actuators equipped with different core structures. The primary aim was to identify the optimal core configuration. All actuators were subjected to identical testing conditions, including a maximum negative pressure of 0.4 bar. Shape recovery was assessed for both bending and contraction deformations. **Figure 5.10a** illustrates the contraction profiles of the actuators subjected to increasing pressure from 0 to 0.4 bar. The auxetic core structure demonstrated the highest contraction reaching a maximum value of 30 mm compared to 25 mm and 21 mm for the rectangular and diamond core actuators, respectively (**Figure 5.10b**). Upon reaching a negative pressure of 0.4 bar, contraction stabilized until shape locking was engaged. It is crucial to emphasize that while increased applied pressure led to enhanced contraction for all actuators, this improvement was accompanied by a reduction in complete shape recovery.

In MLJ actuators, **Figure 5.10b** illustrates the link between contraction and generated force. A linear relationship is evident, with increased contraction directly linked to higher force output. The actuator incorporating the auxetic core structure demonstrated the highest peak force, approaching 8 N. This force value exhibited a gradual decline with rectangular and diamond samples as contraction levels decreased.

The MLJ actuators' tip bending angle data are shown **in Figure 5.10c.** A positive correlation exists between increasing negative pressure and a higher tip angle. As evident in **Figure 5.10d**, the tip angle generally reaches around 60° and continues to rise with increasing pressure. At a negative pressure of 0.4 bar, the auxetic core actuator reaches a tip angle of 120°. Actuators with diamond and rectangular cores reach a maximum tip angle of 100° under the same pressure (see **Figure 5.10e**). These findings show that the auxetic inner modulator performs better since it can bend more under the same amount of applied negative pressure.

The actuators' ability to regain their shape after contraction and bending was also assessed. For actuators with different core architectures, the form recovery ratio is shown in **Figure 5.10f**. Bending results in shape recovery that is greater than that seen following contraction. Contact between the plastic and inner structure is the cause of this discrepancy, which prevents full healing. Notably, the auxetic core structure actuator exhibits a higher shape recovery ratio compared to those with rectangular and diamond cores after contraction. The zero Poisson ratio of the auxetic core, which permits effective energy absorption, explains this occurrence. In contrast to the others, the auxetic core actuator's form recovery also stays constant.

The auxetic core structure actuator was chosen for further evaluation in practical applications. The findings emphasize the dependence of MLJ actuator performance on the core structure, as evidenced by the variations in achieved angles and contractions. It is important to note that reducing the core structure thickness compromises the actuator's capabilities. This happens as a result of the imposed negative air pressure, which makes the plastic coverings stick together. This obstructs the airflow and reduces the performance of the MLJ actuator.

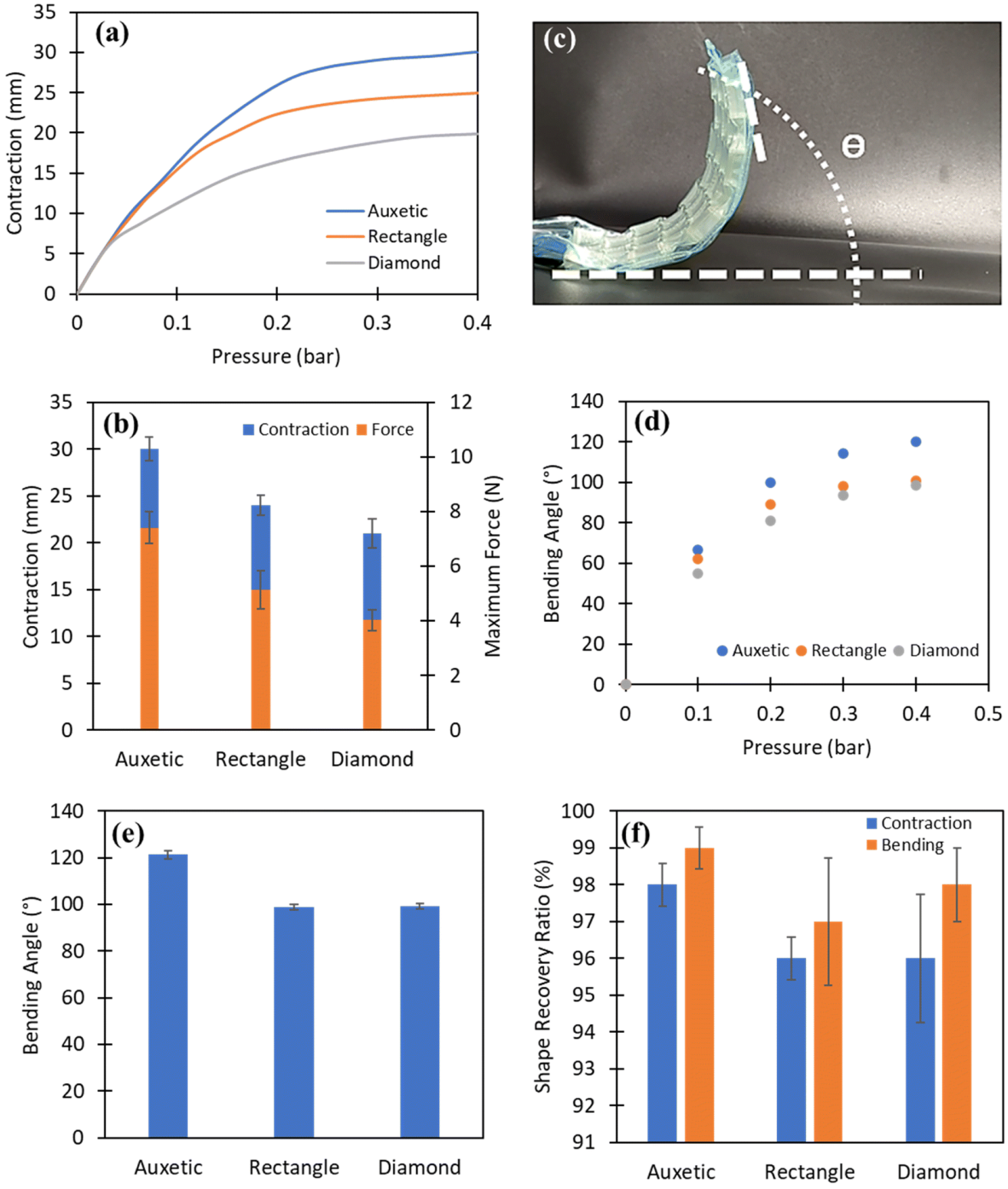

Figure 5.10. (a) The way MLJ actuators contract when there is a negative air pressure of 0 to 0.4 bar. (b) The maximum contraction and force produced for each meta-structure design. (c) Calculating the locked tip bending angle of the MLJ actuators. (d) The MLJ actuators' tip angle following jamming with negative pressure ranging from 0.1 to 0.4 bar. (e) The auxetic, diamond, and rectangular MLJ actuators' maximum bending angle following activation. (f) For all designs, the MLJ actuators' shape recovery ratio follows bending and contraction.

5.3.5. Protentional applications

The performance of an MLJ actuator with an auxetic structure for various applications is evaluated (see **Figure 5.11a**). A key advantage of the MLJ actuator over prior designs is its ability to maintain its activated shape without continuous negative air pressure. This eliminates the need for constant power input during holding tasks. One end of the actuator is secured, while the other end is used for load attachment (see **Figure 5.11b**). The actuator's lifting capability is demonstrated.

The experiment involves heating the actuator to 80°C, triggering a phase transition from glass to rubber. Subsequently, a vacuum is applied, causing the actuator to contract and lift designated weights (100g and 200g). While heavier objects can be lifted, the contraction distance decreases. Furthermore, design modifications and increased negative pressure can enhance contraction, but shape recovery must be carefully controlled to prevent damage.

A significant benefit of the MLJ actuator is its shape-locking ability, which significantly reduces power consumption. This characteristic makes the design more sustainable by removing the requirement for constant power input to maintain the intended configuration. Consequently, less pressure is needed to obtain and maintain the desired shape. For extended grabbing and holding operations, this shape-locking capability reduces battery usage.

The MLJ actuator's superiority lies in its zero-power object-holding capacity. Following object manipulation, the actuator is reheated to regain its original shape, demonstrating its precise operation (see **Figure 5.11c**). The actuators are capable of lifting and gripping objects with different shore toughness without causing harm since they work efficiently as grippers. Actuators are clamped on one end of the experimental arrangement. Applying -0.3 bar negative pressure to both actuators after heating with a heat gun to 80°C is the next step. They bend as a result and grasp the things. The actuators lock into the appropriate clutching position when the negative pressure is deactivated. In order to minimise energy usage over extended operations, this design achieves form-locking and zero-power maintaining.

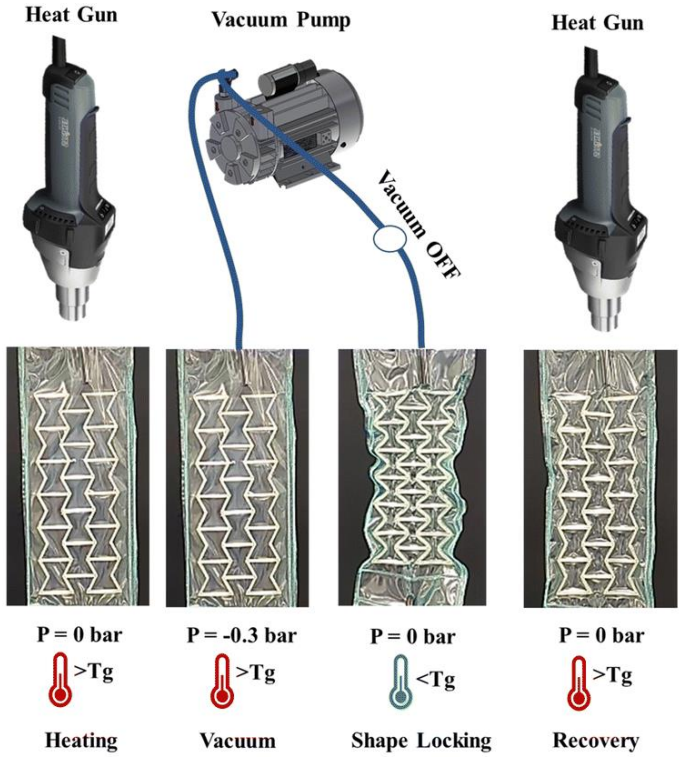
Heat Gun
Vacuum Pump
Heat Gun
Vacuum OFF
P = 0 bar
>Tg
Heating
P = -0.3 bar
>Tg
Vacuum
P = 0 bar
<Tg
Shape Locking
P = 0 bar
>Tg
Recovery

(a)

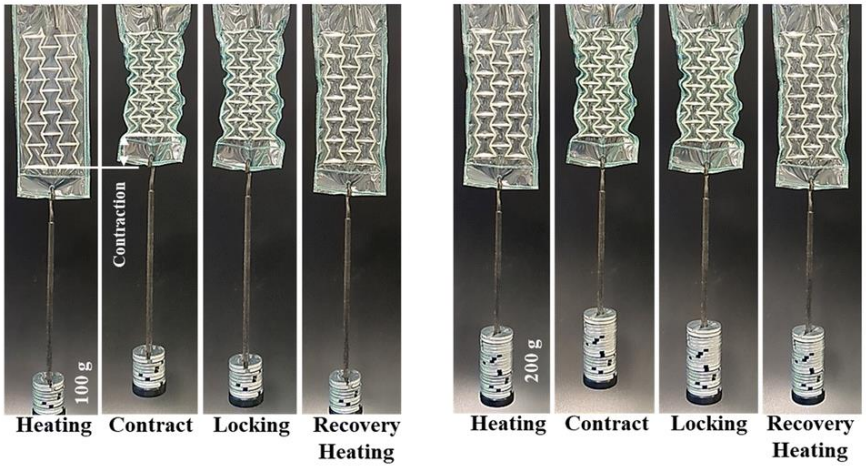
100 g
Contraction
Heating
Contract
Locking
Recovery
Heating
200 g
Heating
Contract
Locking
Recovery
Heating

(b)

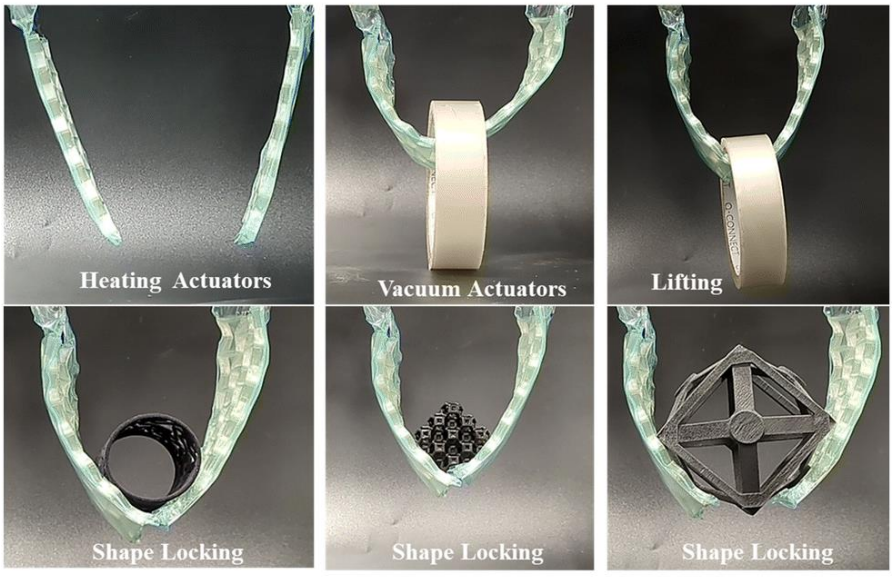
Heating Actuators
Vacuum Actuators
Lifting
Shape Locking
Shape Locking
Shape Locking

(c)

Figure 5.11. (a) A schematic illustration of the MLJ's activation mechanism. (b) The procedure for form-locking without power, actuator shape recovery, and lifting objects while preserving -0.4 bar of air pressure. (c) Grasping and lifting objects of different weights without using any force.

The performance of the actuator in terms of precision, reliability, and shape locking is further investigated in this study. To verify the constancy of an MLJ actuator across several trials, cyclic lifting experiments are carried out with a single actuator (see **Figures 5.12a and 5.12b**). The experiment measures the contraction distance achieved during five lifting cycles with weights of 100g and 200g. The results reveal an average contraction of 50 ± 2 mm for the 100g load and 45 ± 2 mm for the 200g load. Significantly, after each cycle, the actuator maintains its contracted state without requiring additional power input due to the shape-locking property. Heating the MLJ module restores its original form.

The two actuators' trajectory paths are recorded using PASCO Capstone software in order to assess the MLJ actuators' repeatability and precision (see **Figure 5.12c**). The recordings capture both the unjammed and shape-locked (jammed) states of the actuators. A designated target point is then used as a reference to measure repeatability during activation cycles. Both actuators undergo 20 cycles of activation and shape recovery. The achieved positions, as shown in **Figure 5.12d**, consistently fall within ±5 mm of the target point, demonstrating the actuators' high repeatability during activation.

The precise design and intended use of these actuators have a significant impact on their energy consumption. Soft pneumatic actuators' energy consumption is measured using both numerical and experimental methods. Several factors influence the power consumption, including the supplied air pressure, the actuator's size and shape, and the desired motion and force output. Pneumatic actuators are typically regarded as devices that require little power since they run on compressed air instead of electricity or mechanical power (Vanderborght, et al. , Wehner, et al. 2014, Shengda, Wang and Zhu 2021, Luo, et al. 2022).

Maintaining an actuator in a specific position typically requires continuous energy input. Previous research has shown that a constant pressure is necessary for prolonged holding (Shengda, Wang and Zhu 2021, Luo, et al. 2022). These studies focused on the energy consumed during actuator activation. Nevertheless, the current study shows that the MLJ actuator's shape-locked state can be maintained without the need for further power after activation and cooling because of the core structure's SME, greatly lowering the device's overall energy consumption. Although the differences in characteristics make it difficult to directly compare the energy consumption of other actuator models, such as earlier designs and the MLJ actuator, future studies will investigate this topic in controlled settings.

These actuators are perfect for applications where end-effectors need longer holding times because of their shape-locking and zero-power holding capabilities. Future research will explore improvements to the hot programming process by incorporating electroconductive materials and thermally isolated plastics. These materials can potentially reduce activation time by facilitating easier heating, potentially with the use of electroactive SMP materials.

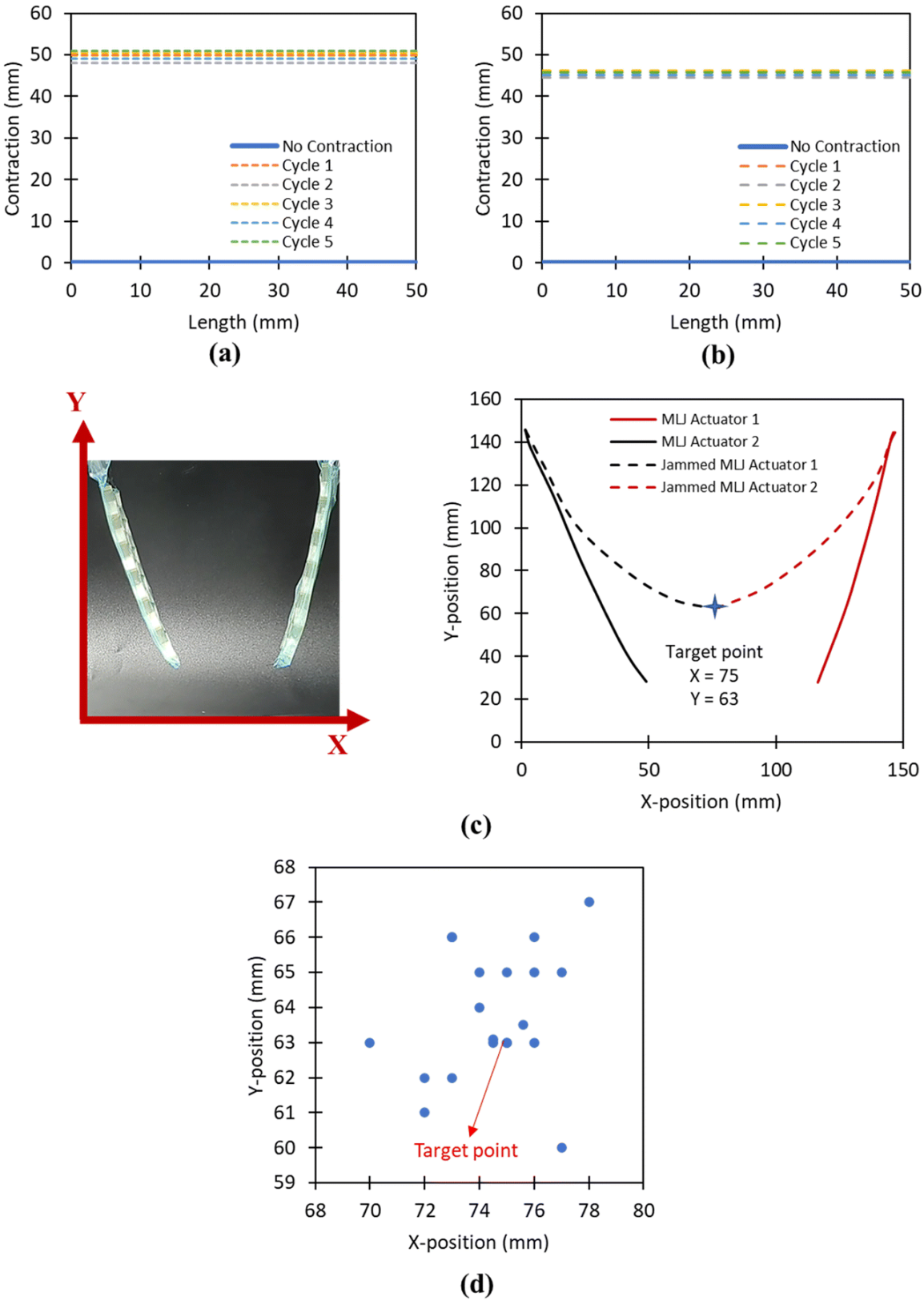

Figure 5.12. Activation and contraction cycles with two different loads: (a) 100 g and (b) 200 g. (c) The trajectory path of the actuator in cases of shape-locking and unjamming. (d) During a 20-cycle interval, the two MLJ gripper actuators' cycle behaviour is dependent on the target point.

5.4. Conclusion

This work effectively illustrates how 4D printing and LJ technologies may be combined to create soft actuators. In order to produce MLJ actuators with form memory and shape-locking capabilities, a unique approach was created. To investigate their properties, the inquiry involved designing and assessing auxetic, diamond, rectangle, and circle meta-structures. Testing for mechanical qualities involved cyclic three-point bending and compression. The meta-structures' shape recovery and SMEs were examined using bending and contraction tests. Additionally, the contraction and bending performance of the MLJ actuators under negative pressure application was studied. The findings show that in terms of bending, contraction, and shape recovery, MLJ actuators with auxetic meta-structures perform better than those with alternative designs. The developed actuators' shape-locking abilities, zero-power holding, and efficient gripping are their main advantages. All in all, this work expedites the manufacture of jamming actuators, clarifies the fundamental physics of LJ and 4D printing technologies, and lays the groundwork for the creation of mechanically flexible actuators and meta-structures. The reduced power consumption inherent to this design holds promise for sustainable actuation.

Chapter 6

4D printing and programming of continuous fibre-reinforced shape memory polymer composites

The study used FDM technology to create CFRC parts with different types of continuous fibres embedded in a biopolymer matrix PLA. The concept and idea of this chapter can be used in all previous works to improve the mechanical properties of smart actuators. The mechanical characteristics, shape memory capabilities, and microstructure of the SMPCs were evaluated using methods such as cold and hot programming. The study emphasises how the strength, lightweight, and usage of biodegradable materials in 4D-printed CFRCs/SMPCs might be advantageous for various applications. Items in mechanical engineering, biomedical science, and human-material interaction are possible applications. The chapter covers a concise overview, the purpose of the research, the techniques utilised to create SMPC actuators, as well as specific outcomes and applications. All content is adapted with permission from the article published as follows:

- **Lalegani Dezaki M**, Bodaghi M. 4D printing and programming of continuous fibre-reinforced shape memory polymer composites. European polymer journal 2024;21010.1016/j.eurpolymj.2024.112988.

6.1. Introduction

Applying continuous fibres during the printing process is a particular way of improving the mechanical properties of SMPs, building on the constraints mentioned in **Chapter 2** and the pertinent research examined in this chapter. Earlier research on the creation and examination of SMPCs reinforced with continuous fibres is covered in **Chapter 2**. Nevertheless, these investigations have mainly concentrated on the mechanical characteristics of printed meta-composite frameworks that are obtained using various kinds of reinforcements. Additionally, these studies evaluated the effectiveness of SMPCs based on critical aspects like shape recovery and SME. Comparative examination of the fibres (AF, FG, and CF) utilised as reinforcing agents in 4D-printed PLA is notably lacking from previous studies. Additionally, much is known about the printed SMPCs' versatility and ultralight nature. Researching material and weight reduction possibilities would encourage ecologically friendly and sustainable design methods. It is important to investigate the unexplored domain of these fibre reinforcements, and this omission draws attention to a worthwhile research opportunity.

In this work, a novel method for printing CF, FG, and AF using FDM in a biocompatible PLA for 4D printing is investigated. The main goal is to use cold and hot programming techniques to unravel the shape memory features that these additively made SMPCs exhibit. This investigation will be further complemented by a rigorous analysis of the microstructure and mechanical performance of the printed composites, specifically focusing on CFRCs. This novel method provides a strong benefit by cutting down on waste production and material use. The resulting parts are not only lighter but also demonstrably stronger, ultimately leading to an improvement in overall quality. Furthermore, the inherent shape recovery capability of these 4D-printed objects facilitates their reusability, aligning seamlessly with the tenets of a circular economy that prioritizes environmentally friendly and sustainable manufacturing practices. This method reduces the amount of material used in the printing process while simultaneously increasing mechanical strength, which is a major step forward for sustainability. In order to go deeper, the study carefully assesses shape

rigidity and restoration behaviour in specimens infused with various fibre types under regulated printing circumstances.

A comprehensive examination is undertaken to gain a deeper understanding of the shape memory response exhibited by 4D-printed SMPCs. This in-depth analysis incorporates a meticulous evaluation of microscopic and SEM images of fractured specimens, with a particular focus on the microstructure and the integration of fibres within the matrix. The results of this study demonstrate the revolutionary potential of SMPCs to revolutionise several manufacturing sectors. A graphic depiction of the application concept made possible by this new approach is provided in **Figure 6.1**. These printed structures' intrinsic reusability results in reduced waste of materials and total usage during the production process. The advantage of these manufactured structures is that they are both observably strong and lightweight. Basically, because of its many features, this method encourages sustainable practices.

Figure 6.1. The 4D printing of SMPCs illustrates their uses in several industries and highlights their sustainability part. Material engineering and design could undergo a radical change because of 4D printing technology.

6.2. Materials and methods

6.2.1. Materials

This investigation necessitates the employment of a matrix material exhibiting SME properties to achieve the desired shape-changing capability. PLA finds extensive use in 4D printing due to its pronounced SME characteristics (Xu, J. and Song 2015). Additionally, PLA filament boasts eco-friendly credentials as a thermoplastic polymer derived from renewable resources (Han, et al. 2022). Moreover, PLA is well known for being easy to use, demanding little work to produce high-quality components—especially when combined with FDM technology (Lee, C. H., et al. 2021). The red PLA filament from 3DGence used in this investigation has a density of 1.24 g/cm^3 and a diameter of 1.75 mm.

CFRCs have been used to improve the mechanical qualities of printed items, even though thermoplastics currently have limits in this area. Several fibre reinforcements, including CF, AF, and FG, show compatibility with FDM printing techniques. No pre- or post-processing is done to the fibres used in this study, which are obtained from Markforged. A constant 0.36 mm diameter is seen in these fibres. The datasheets supplied by the manufacturer contain specific information about their characteristics (Markforged c, Markforged a, Markforged b).

6.2.2. Extruder development

The creation of CFRCs and the specially made extruder created for FDM printers are covered in detail in this section. An industrial Creality Ender 3 V2 3D printer is used in the study. In order to meet the requirements of this study, the printer's stock extruder was modified and assembled. To facilitate the co-deposition of continuous fibres and molten plastic, the extruder's main job is to effortlessly combine them. The design of the extruder adheres to established principles outlined in the references (Matsuzaki, et al. 2016, Khosroupour Arabi and Kordani 2023)

The proposed extruder has an aluminium heated block, heating elements, an aluminium heat drain, and a brass tip, as shown in **Figure 6.2a**. Most notably, to enable CFRC printing, the hot end of the Creality Ender 3 V2 extruder has been rebuilt and reconfigured. Two inlets are featured on this customised extruder: one is for feeding raw PLA filament, and the other is for adding continuous fibres. The thin stainless-steel pipe that passes by the hot block makes sure the fibre doesn't come into contact with the melted plastic until it gets to the nozzle's tip.

Teflon PTFE tubing encircles the brushed stainless steel pipe, acting as insulation to prevent direct contact between the pipe and block. Thus, the PTFE pipe, with its 0.25 W/(m.K) thermal conductivity, effectively shields the pipe from excessive heat. This configuration is required to keep the nozzle from clogging. The fibre that comes from the printed area of the fibres is stretched during printing when the plastic filament is extruded. Along the print route, this force protects the fibre against distortion brought on by motion between the print bed and nozzle. Since the speed of the extruder controls the flow rate of the plastic filament, the ratio of melting plastic to fibres is the same in all samples.

Table 6.1 illustrates the constant printing parameters used for all specimens in this study. Every test sample is produced using the 1.5 mm diameter designed extruder without any clogging problems (Chen, K., et al. 2021, Le Duigou, A., et al. 2019). These prototypes'

geometry is designed with SolidWorks software. The specimen's shape is then saved as an STL file and entered into the Slic3r software to be sliced, after which the processing parameters are adjusted. Owing to the 180° print path change at each end of the length direction, flat CFRCs require a slower printing speed. This modification gives the fibre tension ample time to grow and solidify.

To give further details, the numerical control approach known as G-code is used to take into consideration several variables, such as the nozzle's feed speed, the length of the fibre redirection, and path coding to prevent inconsistencies. Layers of material are stacked according to the printing path of a single layer along the thickness of each composite part. The G-code method for numerical control considers many parameters. These consist of the nozzle's feed speed, the length of the time the extrusion pauses after the fibre is rerouted, and path design to prevent fibre knots.

Table 6.1. CFRCs printing settings.

Parameters	**Value**
Nozzle Diameter (mm)	1.5
Layer Thickness (mm)	0.25
Printing Speed (mm/s)	15
Infill Density (%)	100
Printing Pattern	Linear
Nozzle Temp. (°C)	210
Bed Temp. (°C)	60

6.2.3. DMA test

The T_g and the storage modulus of 4D-printed SMPCs are two essential thermodynamic factors. Before assessing the material's subsequent thermal properties, several characteristics must be assessed. The effects of fibre integration on the employed semi-crystalline PLA's storage modulus and T_g must be investigated. In this work, printed pure PLA and CFRC samples are subjected to thermal analysis using a DMA 8000 PerkinElmer. Beam shape samples (30 mm x 8 mm x 1 mm) were printed. The temperature increases at a rate of 5 °C per minute and a frequency of 1 Hz from 30 °C to 80 °C.

6.2.4. Mechanical properties

The Shimadzu machine is a multipurpose mechanical assessment device that is used to assess the structural characteristics of SMPCs. This device uses an optical camera to track sample displacement and is outfitted with a 50 kN loading cell. Tensile testing specimens for CFRCs and pure PLA are sized following ASTM D3039 and D638 standards, respectively, and are tested at a consistent 2 mm/min (International b, International a). For this tensile testing arrangement, beams with standard parameters of 100 mm in length, 1.5 mm in width, and 0.5 mm in thickness are used. The objective of this methodology is to examine the impact of adding a fibre layer to a PLA on the mechanical properties that emerge. To further investigate their characteristics, specimens are also ready to go through a three-point bending test. The ASTM D790 specifies the physical characteristics of these bending test samples, with a testing speed of 2 mm/min and a prescribed span length of 40 mm (International c). For each required property, five samples are assessed in total, and the average values are then shown. Significantly, to optimise their intrinsic strength, every sample is printed longitudinally. The test specimens and the final printed samples are shown graphically in **Figure 6.2b**. The established methods described in ASTM D790 (Equation (6.1) and Equation (6.2) will be used to calculate the stress and strain for the bending test specimens.

$$\sigma_f = \frac{3FL}{2bd^2} \tag{6.1}$$

$$\epsilon_f = \frac{6Dd}{L^2} \tag{6.2}$$

Here, b is the test sample width, d is the sample thickness, F is the force causing the bending, L is the distance between the supports, and D is the maximum deflection of the beam's centre.

6.2.5. SEM and optical imaging

Using a Leica ICC50 W microscope and a JSM-7100 F LV FEG SEM, the composition of the CFRCs is investigated, and fracture behaviour and fibre incorporation inside the PLA are evaluated. After testing, the printed samples' broken cross-sectional views and interface forms are evaluated. This study aims to evaluate the overall bonding strength of the printed composite and the degree to which the different components are integrated.

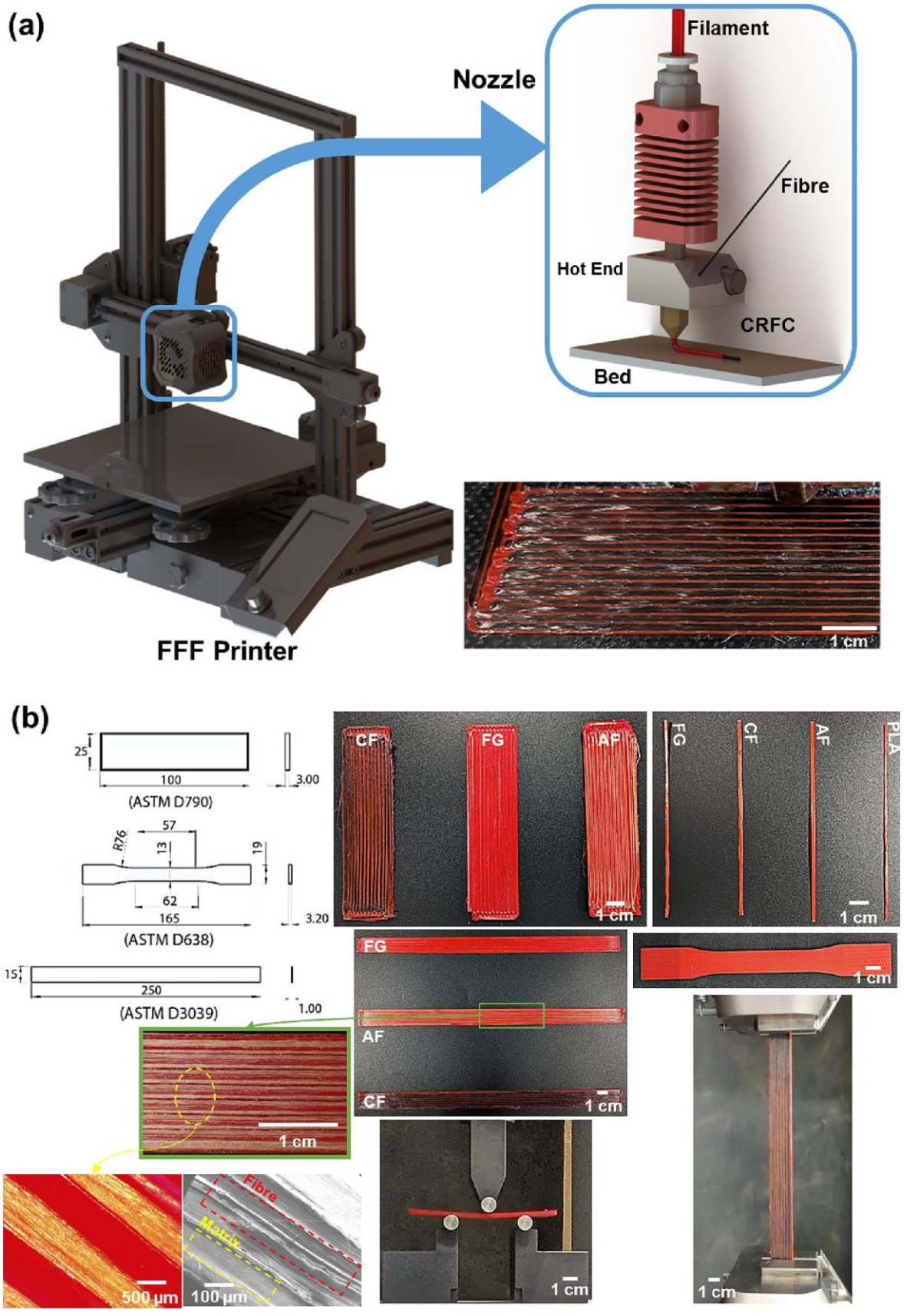

Figure 6.2. (a) A graphic showing the nozzle of an FDM printer and how composite specimens are printed. (b) Pictures of samples and CFRC beams that were made by ASTM guidelines for mechanical testing.

6.2.6. Shape memory properties

The fundamental principle of the SME is theorised to involve the generation of thermal energy. This is because most SMPCs exhibit a response triggered by heat, which is typically applied externally. **Figure 6.3a** details the standard cold and hot programming approaches used to evaluate the form restoration behaviour of printed specimens under heat stimulation (Bodaghi, M., et al. 2020, Soleyman, et al. 2022). Each specimen is built using SolidWorks software to methodically analyse the SME of the manufactured samples. Straightforward beam-shaped specimens are created and then 3D printed with dimensions of 50 mm x 1.5 mm x 0.5 mm.

This study aims to clarify the impact of fibre inclusion on the PLA's SME properties. To evaluate the effect of a single fibre layer inside the PLA matrix, a specific beam is created. A two-layer manufacturing process is used to accomplish this. The first layer is made of PLA that has been infused with the selected fibre, as seen **in Figure 6.3b**. The fibre is then manually removed, leaving just the PLA matrix material in the subsequent layer. This method prevents fibre breakage and ensures a strong binding by encasing the fibre inside the first matrix layer. For every composition of CFPLA, AFPLA, and FGPLA, a total of ten samples are assessed.

Figure 6.3c presents a detailed illustration of the shape memory programming procedure. The hot programming method involves the initial deformation of the specimens within a temperature-controlled heat gun set to a temperature exceeding the T_g. The distorted samples are subsequently cooled to achieve dimensional stability in a twisted state. On the other hand, cold training involves deforming the structures at room temperature and then releasing the force that was applied to stabilise their shape. Ultimately, heating over T_g causes all the beams that were programmed via the hot and cold procedures to revert to their initial forms. Equations (6.3) and (6.4) can be used to determine the specimens' shape fixity and recovery ratio.

$$R_f = Shape\ fixity\ ratio = \frac{\theta_{deformed} - \alpha}{\theta_{deformed}} \times 100\% \tag{6.3}$$

$$R_r = Shape\ recovery\ ratio\ = \frac{\theta_{deformed} - \theta_{unrecovered}}{\theta_{deformed}} \times 100\% \tag{6.4}$$

This study defines the unrecovered angle ($\theta_{unrecovered}$) as the residual sample deformation remaining after stimulation. The maximum temporary deformation achieved is represented by the deformed angle ($\theta_{deformed}$), as illustrated in the unloaded section of **Figure 6.3c**. The experiment involves measuring the average angles of cantilever beams. These beams, fixed at one end and standing upright, are heated with a heat gun to a specific temperature. The process of the beams returning to their original shape is recorded using a video camera, PASCO software, and a thermal imaging camera. A digital thermometer attached to the beam continuously measures its temperature during the cooling and shape recovery phase.

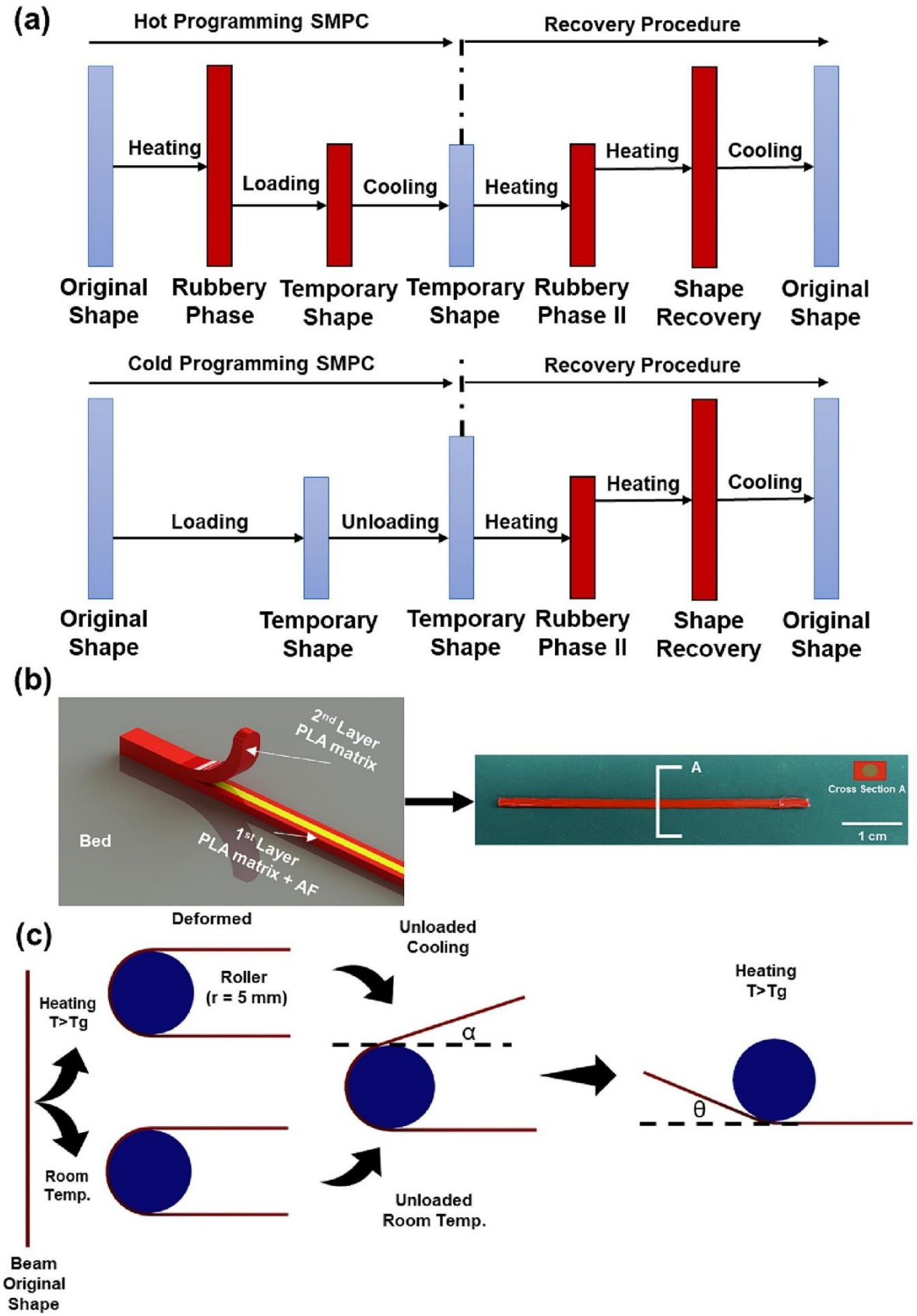

Figure 6.3. (a) The method of configuring the SMPC in both hot and cold environments. (b) The printing process and the final SMPC in cross-section. (c) The procedures for recovering from cold and hot shape programming.

6.3. Results and discussion

6.3.1. Mechanical properties

Standardised tensile and flexural test specimens, as well as basic beams, were made using both PLA and PLA reinforced with continuous fibres to evaluate the efficacy of the created extruder and the structural integrity of the fabricated CFRCs. A resolution of ± 0.25 mm was attained by the technology in terms of printing precision. Fibre content determination followed a well-defined protocol, ensuring consistent fibre distribution throughout the printing path within the print head during co-extrusion with the molten plastic. The amount of weight per unit length was multiplied by the total fibre length, which is directly derived from the tool path length, to determine the fibre content (Hou, et al. 2018). Thus, the ultimate fibre content is represented by the fibre-weight ratio to the composites. The thickness of the layer is a key factor in determining the amount of fibre in the printed CFRCs since it is closely correlated with the path of the tool and the unit volume of the injected polymer matrix. Thus, for printed samples, precise fibre content assessment is essential. The fibre content of the CFPLA, AFPLA, and FGPLA composites was determined to be 18.11%, 17.98%, and 17.86%, in that order. This value directly affects the mechanical characteristics and overall efficiency of the composite, making it a crucial indicator of its composition.

Figure 6.4a shows the outcomes of tensile tests that were performed on printed PLA and CFRCs by ASTM D638 and D3039 standards. Every sample was printed using the same parameters and kept the same amount of fibre. The results show that using printed CFRCs significantly increases strength. The addition of continuous fibres to CFRCs results in a significant improvement in mechanical characteristics when compared to PLA (Zhang, Peng, et al. 2023, Zhu, et al. 2023). CFPLA exhibited the highest strength (average 461 MPa) compared to FGPLA and AFPLA. However, given the intrinsic brittleness of continuous CF, it is significant that these samples showed signs of early crack initiation (Siddiqui, et al. 2023). Both AFPLA and FGPLA showed a strength of about 335 ± 5 MPa, although FGPLA showed a much greater strain at failure than CFPLA and AFPLA. Furthermore, standardised beams underwent tensile tests. To assess the effect of this single layer on physical characteristics, these beams were printed with just one layer of fibre. **Figure 6.4b** shows the outcomes of the tension tests conducted on CFRC and pure PLA beams. The results were consistent with what was seen in the ASTM specimens. Remarkably, in this case, the PLA matrix containing one layer of FG exhibited somewhat greater strength than AFPLA.

In addition, a three-point bending test was employed to evaluate the performance of the fabricated samples (as illustrated in **Figure 6.4c**). Following the outcomes of the tensile tests, CFPLA demonstrated better mechanical characteristics than AFPLA, FGPLA, and pure PLA. Achieving an average stress value of 102 MPa, AFPLA outperformed pure PLA in terms of ultimate tensile strength, which only reached 37 MPa. Because of these materials' intrinsic brittleness and stiffness in comparison to AF, specimens strengthened with CF and FG showed gradual cracking. Among other testing techniques, CFPLA most notably showed remarkable mechanical qualities in tensile and three-point bending analysis. However, when subjected to the same ASTM tensile test circumstances, the breaking strength characteristics of AFPLA and FGPLA seemed equivalent. Noticeably, the ASTM tensile and three-point bending tests revealed that the strength of CFPLA significantly improved, showing increases of 1027.5% and 497.3% in comparison to pure PLA. Although the maximum stress values for AFPLA and FGPLA were still quite similar, there was a noticeable difference when a

flexural test was involved. It's interesting to note that FGPLA showed more strain at the point of fracture during tensile testing, indicating a different physical performance.

The incorporation of fibres into PLA considerably increases its strength (Cersoli, et al. 2021). Interestingly, this method has the added benefit of reducing trash production and material use at the same time. This invention has a lot of potential for practical uses, especially in the field of 4D printing. It makes it easier to produce a variety of items while preserving their mechanical integrity and a smaller material footprint. This development not only improves structural integrity but also makes a significant contribution to ecologically friendly production processes.

As the stress increases, the earliest cracks start inside the layered structure and move down the sample's size, as seen in **Figure 6.4e**. Both layers eventually separate because of this process. Parallel fractures are induced in the layer closest to the applied load point when the propagating interlayer fractures connect. Furthermore, at the lowest layer, which is located below the centre of gravity, tensile fractures occur. Starting from the opposite sides of the specimen, these two different types of fractures gradually move in the direction of one another until total failure. Fiber-matrix debonding, fibre rupture, matrix cracking, and delamination are among the failure modes that were noted throughout the studies. Specifically, the failure sequence is triggered in large part by delamination. Comparatively speaking to the other failure mechanisms, fibre-matrix debonding takes centre stage following delamination. In the tensile test samples, a similar occurrence was noted, as **Figure 6.4f** illustrates. Broken fibres and the matrix were also visible. A strong bonding contact is suggested by the fact that some fibres were able to keep their adherence and remain unbroken.

Sectioning and analysing the fractured area of the CFRCs under a microscope and SEM allowed for a better understanding of the fibre-matrix interface (**Figures 6.4g and 6.4h**). It is evident from the micrographs that void formation is more common at the ends of the fibres. Most likely, during the printing procedure, the melting polymer was distributed unevenly and fibre shrinkage contributed to this issue. A visible fibre pull-out at the cracked area of the bent specimens shows in these photos that the fibre-matrix bond continues until the last crack. The minimum return radius is one of the fundamental limitations preventing the fibre fraction of volume from increasing any further due to inherent manufacturing technique limits. The radius of a fibre is defined as the length of the specimen that a fibre must travel through and circle back upon approaching its destination (Heidari-Rarani, Rafiee-Afarani and Zahedi 2019). Fibre breakage results from the pull-out of the fibres from the matrix if this radius is less than a critical value. As a result, as shown in the SEM images shown in **Figure 6.4h**, a gap inevitably forms between the two parallel fibre routes.

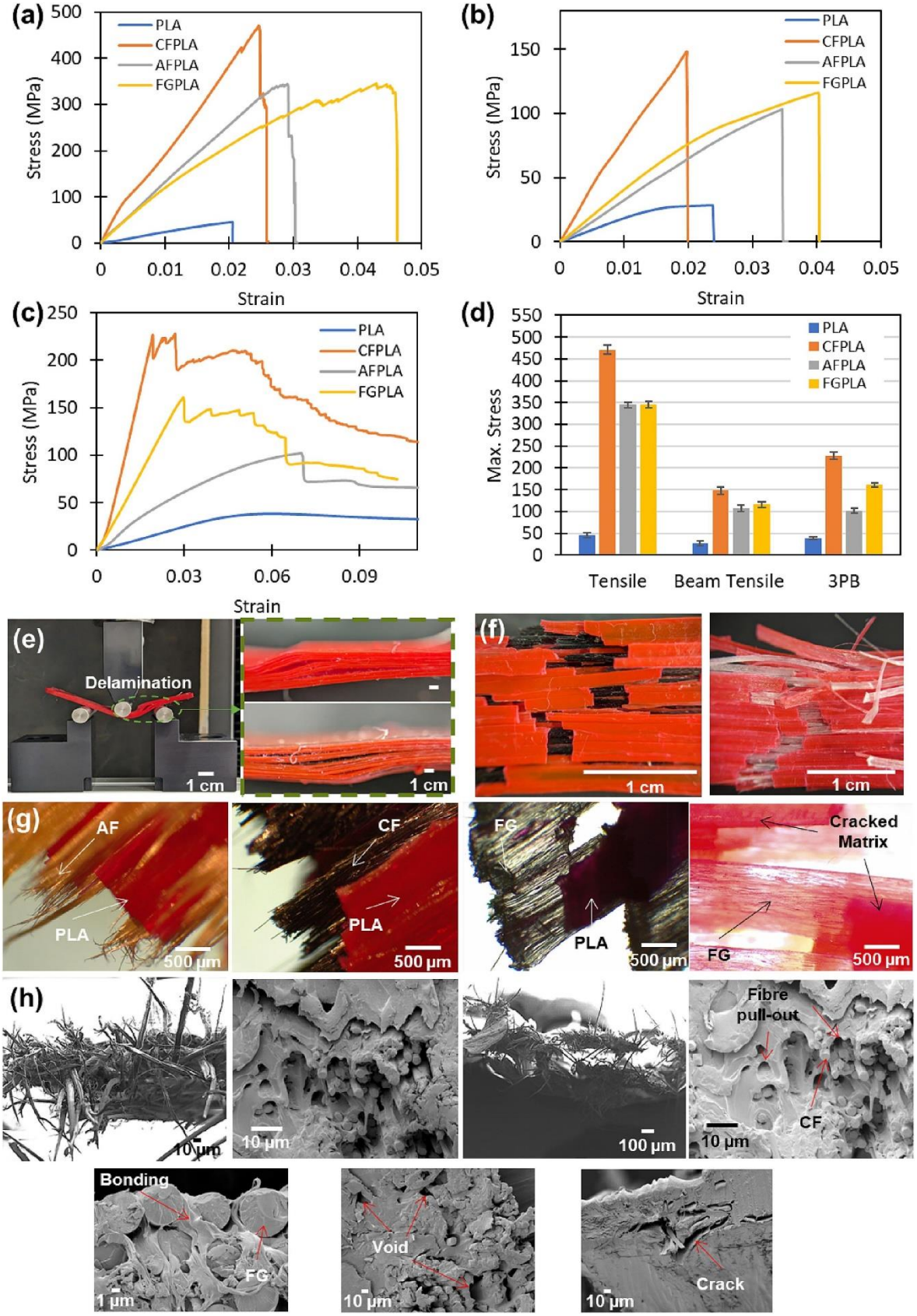

Figure 6.4. Tensile test results for printed CFRC (a) samples produced by ASTM standards and (b) beams were documented. (c) The flexural test results for the PLA and printed CFRCs. (d) Peak stress values for printed CFRCs obtained from flexural and tensile tests. (e) Applying flexural testing to printed CFRCs to check for delamination. (f) Illustrations of printed CFRCs that have partially cracked, yet the fibres inside the matrix have remained

intact. CFRC failure sites are visualised using optical and SEM imaging in images (g) and (h).

A DMA test was performed on all printed materials with the same size and printing settings to investigate the connection between form memory qualities and the mechanical characteristics of SMPCs. The values of tan δ and modulus of storage for pure PLA and SMPCs are shown in **Figure 6.5**. The findings show that SMPCs have a significantly higher storage capacity than PLA. But when compared to PLA, CFRCs have lower tan δ values. The reason for this discovery is that printed CFRCs are by nature stiffer than pure PLA. Consequently, the PLA matrix's entire physical performance, durability, and rigidity are all greatly improved by the integration of fibres. T_g values for AFPLA, FGPLA, and pure PLA vary between 64 °C and 70 °C, respectively, with T_g for CFPLA being the highest at 70 °C. Pure PLA has a T_g of about 61 °C. Following testing, all samples were subjected to temperatures higher than their individual T_g values to guarantee consistent findings in shape-retaining characteristics.

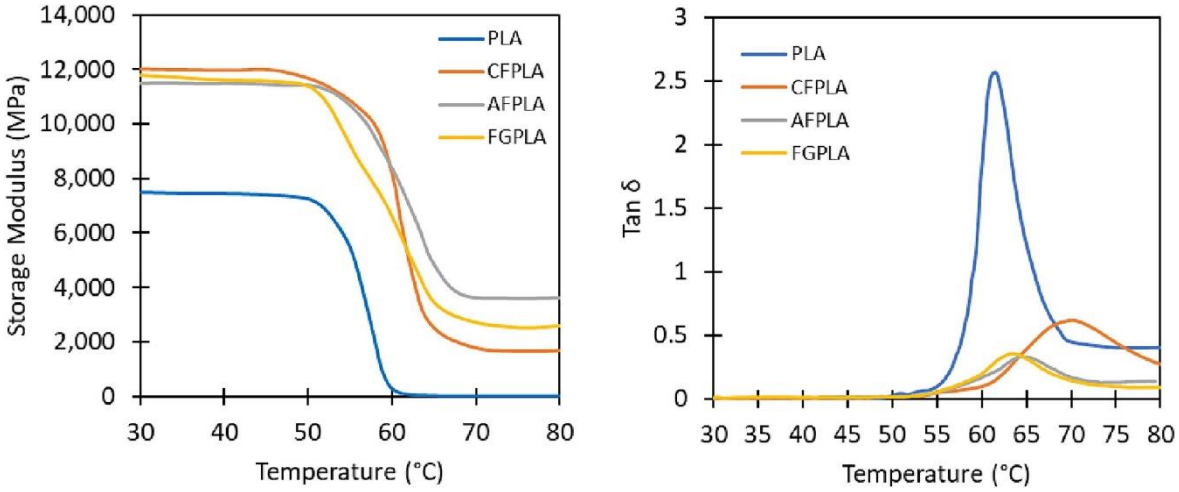

Figure 6.5. DMA results for PLA matrix and printed SMPCs.

6.3.2. Shape memory property

The approach part included both hot and cold programming methods for analysing PLA and SMPC specimens. The purpose of the research was to clarify the impact of adding a fibre layer on the form fixity and recovery properties of SMPCs. The fibres in the PLA caused an obvious rise in sample stiffness during the cold training step. The programmed form and the restored shape that is observed in cold training for FGPLA specimens are shown in **Figure 6.6a**. A gripper was used to measure the shape memory efficiency of the specimens, which were maintained vertically. Temperature readings were recorded using a thermocouple and an infrared camera in tandem. The FGPLA beam tended to revert to its original shape during cold programming, which can be attributed to its higher stiffness in comparison to hot programming, as evidenced by its cold-programmed shape. This tendency consequently affects printed CFRCs' form fixity. The beam was heated by a heating gun that was placed at a certain distance to cause shape return. The sample took on its initial form because of the heat activating the PLA matrix's SME. A comparable approach is used in the hot encoding process, which is shown in **Figure 6.6b**. As will be discussed in more detail below, the samples did, however, display greater shape rigidity because of the intrinsic nature of hot programming. The printed FGPLA's ability to revert to its initial form when heated is demonstrated convincingly by the infrared photographs.

A thorough assessment of their shape restoration and fixity was made possible by using a video camera together with Capstone software to accomplish the trajectory path. In cold and hot programming conditions, **Figures 6.6c and 6.6**d depict the programmed and restored morphologies of the FGPLA. The temperature of every sample was carefully recorded using a thermocouple to guarantee the data's reliability. This was a crucial step in confirming that the test circumstances were consistent. The chart shows the temperature that the thermocouple has been measuring, as shown in **Figure 6.6e**, and shows how it has increased to 70 °C over time. Our experimental setup's validity is further supported by a similar pattern in temperature progress.

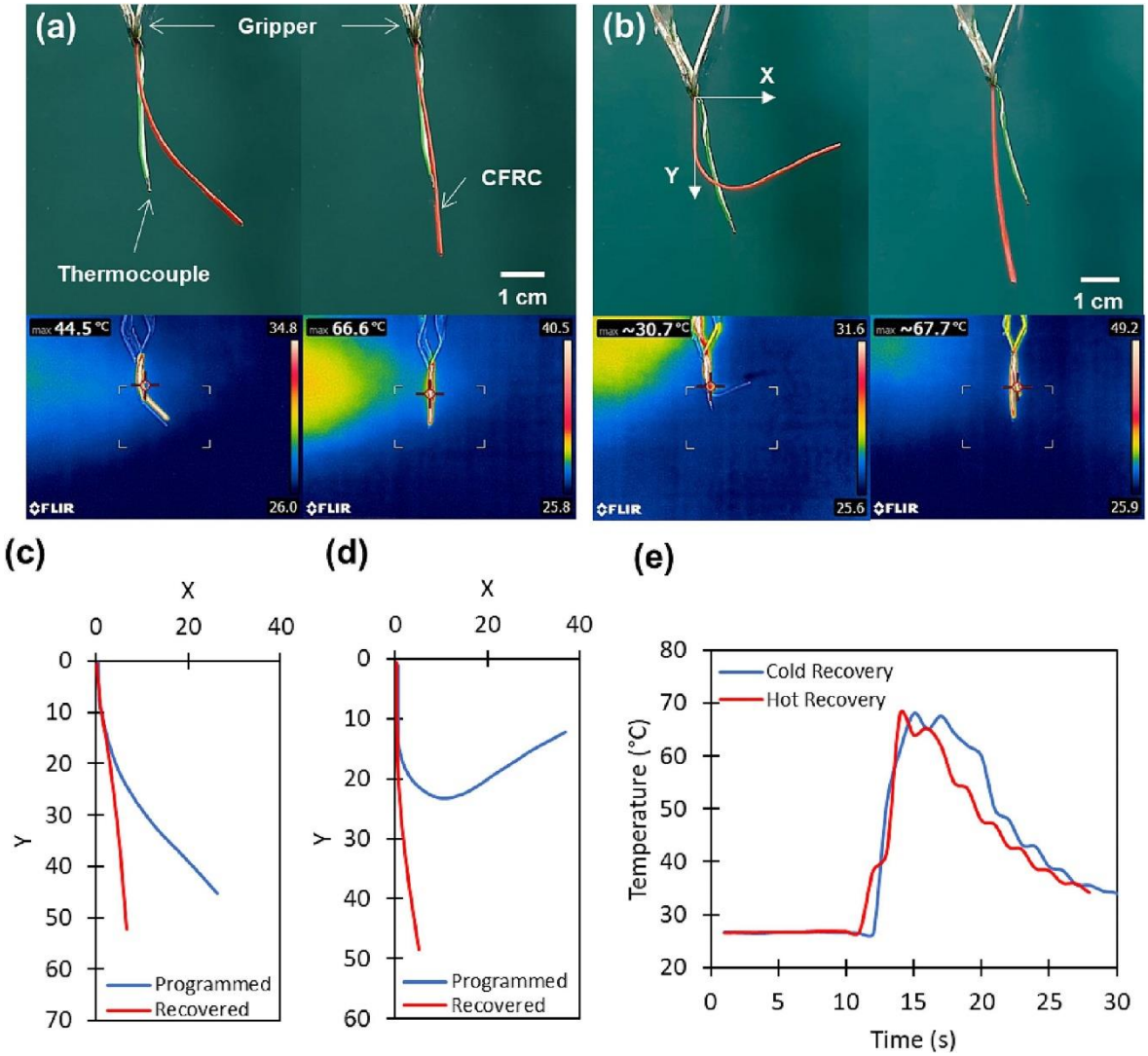

Figure 6.6. (a) Cold-trained FGPLA and recovery form after heating. (b) Hot-trained FGPLA and recovery form after heating. (c) The projection of the FGPLA beam's recovered and fixed shape via cold programming. (d) Using hot programming to project the fixed and recoverable shapes of the FGPLA beam. (e) Temperature monitoring using thermocouples.

Figure 6.7a presents the recorded shape fixity ratios for beams subjected to both cold and hot training. Notably, hot programming yielded a significant improvement in shape retention. For example, with the shift from cold to hot training, the shape fixity ratio in CFPLA and AFPLA increased from 24% to 78% and from 38% to 92%, respectively. Conversely, cold programming resulted in decreased shape fixity due to the enhanced stiffness and strength of the fibre-PLA matrix at ambient temperature. Pure PLA showed the greatest shape fixity of all the materials studied, followed by AFPLA and FGPLA under both hot and cold programming circumstances. The beams printed using CFPLA had the lowest form fixity ratio, which was noteworthy. This phenomenon can be attributed to the increased rigidity and reduced flexibility of the fibres and PLA matrix at room temperature under cold programming.

Figure 6.7b depicts the shape recovery ratio achieved by the 3D-printed SMPC variants. Each data point represents the average result from a set of ten specimens. Notably, PLA beams exhibited superior shape recovery, with impressive ratios of 97.9% (cold training) and 98.3% (hot training). Following closely were the FGPLA composites, achieving 95.3% and 96.1% recovery for cold and hot programming, respectively. CFPLA specimens demonstrated comparable but slightly lower shape recovery compared to FGPLA. This difference can be attributed to the inherent rigidity of CF compared to FG. This stiffness is especially noticeable when CFPLA is cold-trained, which can cause fibre breaking. On the other hand, the shape restoration performance of 3D-printed AFPLA beams was the lowest. When PLA is exposed to AF, its ability to restore its shape is greatly diminished. This is reflected in the notably lower ratios achieved by AFPLA: 81.2% (cold) and 83.2% (hot) (Dong, K., et al. 2021). These results unequivocally show that the shape recovery performance of printed CFRPs is negatively impacted by the fibre integration.

According to this study, the main factor reducing form recovery in PLA that has been 3D printed is the intrinsic structural characteristics of continuous fibres. These fibres might clash with the polymer's natural flexibility when added to the PLA matrix, adding stiffness and rigidity (Dong, K., et al. 2023). This difference in material behaviour can show up as a decrease in the composite's overall elasticity, which makes it more difficult for the material to regain its original shape after deformation. Further hindering shape recovery is the possibility of localised stress concentrations in the material due to misalignment or unequal distribution of the fibres (Zeng, et al. 2022). Additionally, a crucial factor is the bonding strength at the PLA matrix and fibre contact. The ability of the material to restore its original form may be compromised by delamination or separation caused by a weak contact. Consequently, careful consideration of elements including fibre type, orientation, concentration, and processing methods is required to maximise the performance of continuous fibre-reinforced 3D-printed PLA composites.

The study further investigated the shape recovery kinetics of SMPC beams after hot programming. This method was chosen due to its ability to prolong the shape recovery process, facilitating more accurate time measurements (Chen, H., et al. 2021, Liu, Wenbo, Wu and Pochiraju 2018). As depicted in **Figure 6.7c**, CFPLA and FGPLA composites demonstrated faster shape recovery compared to AFPLA and PLA. This can be attributed to the inherent rigidity and brittleness of the fibres in these composites. **Figure 6.7d** quantifies this observation, indicating that PLA requires 8 seconds to recover its shape, whereas CFPLA and FGPLA achieve recovery in only 5.5 and 6.2 seconds, respectively, upon initiating heating. Conversely, AFPLA requires 7 seconds, exhibiting a recovery time closer to PLA. This aligns with the results of the three-point bending test, suggesting a softer nature for AF compared to CF and FG. It is important to acknowledge that while CFRCs exhibit faster recovery kinetics, their overall shape recovery ratio remains lower compared to pure PLA.

The investigation employs a cyclic shape recovery test involving both cold and hot programming cycles, as illustrated in **Figures 6.7e and 6.7f**. Figures 6.7e and 6.7f show how the research uses a cyclic shape restoration test with both cold and hot design cycles. The test makes use of samples that resemble printed beams that go through 20 cycles of programming that alternate between cold and hot, followed by restoration stages. Throughout these cycles, pure PLA constantly exhibits shape recovery, fully recovering its initial shape after each repetition (Wu, et al. 2022). However, CFRCs exhibit a decline in

their form recovery ratio during the cold training phase. Conversely, FGPLA outperforms CFPLA and AFPLA in the hot programming stages of the cyclic test. These observations suggest that SMPCs demonstrate enhanced performance under hot training compared to cold training. This can be attributed to the reduced stiffness of the material during hot shape programming. Additionally, both PLA and the reinforcing fibres exhibit lower brittleness during hot programming, leading to improved shape fixity.

Among the fibre-reinforced PLA composites investigated, FGPLA exhibits better performance in shape restoration as well as cyclic shape restoration, following closely behind pure PLA. CFRC cyclic form recovery can be improved with a 20% applied programming load reduction. FGPLA has more consistent cyclic shape memory qualities than CFPLA, while both demonstrate similar form recovery characteristics. This improved performance also includes mechanical durability, as FGPLA is ranked second in tensile and flexural tests, only behind CFPLA. This is explained by the better bonding that occurs between PLA and FG, as well as the fact that FG is naturally less brittle than CF. Specifically, CF's increased stiffness causes a compatibility problem with the PLA, which lowers CFPLA's ability in cyclic shape memory testing. Thus, given the combined factors of durability, cycle performance, and form recovery, FG is the fibre of choice for a variety of purposes.

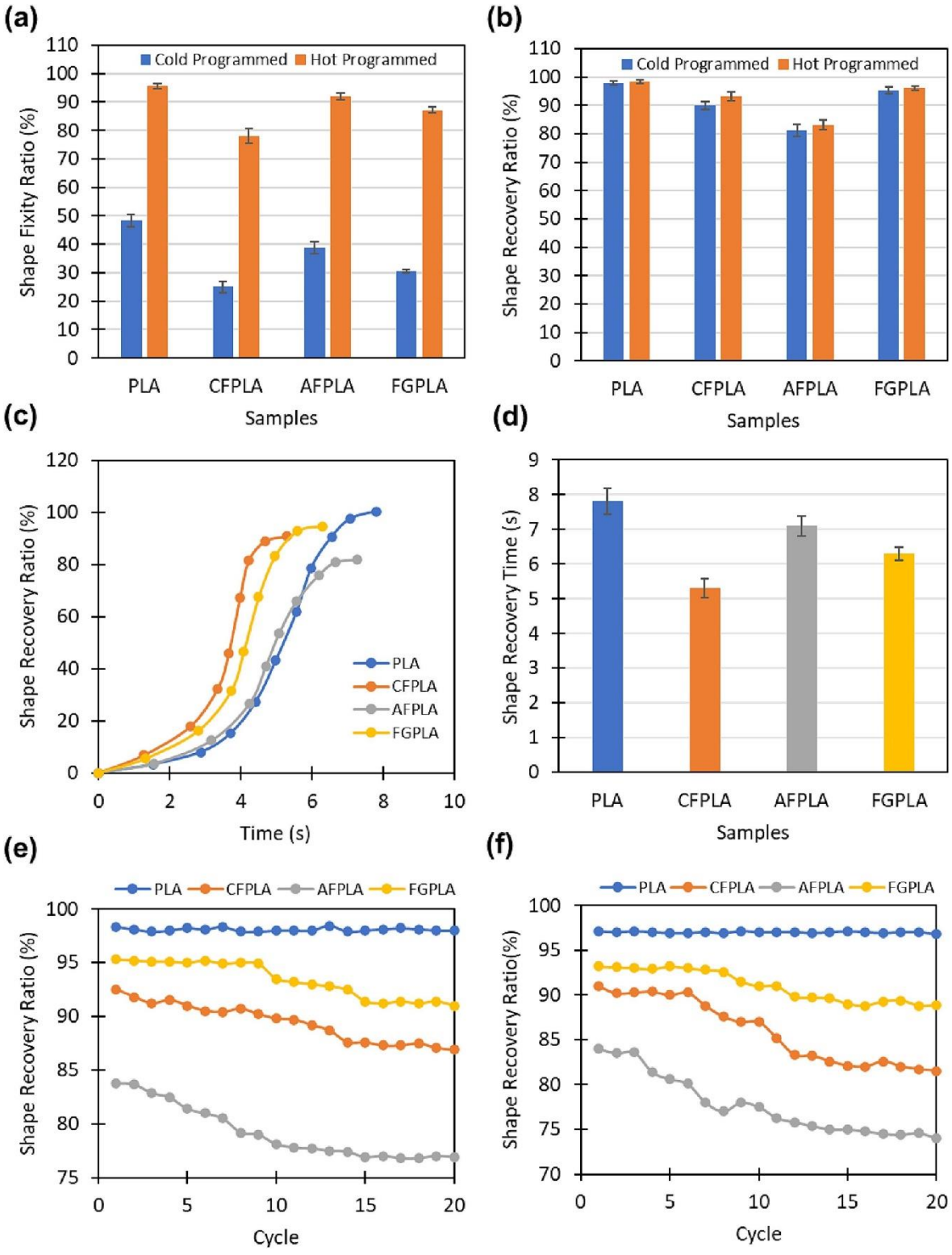

Figure 6.7. (a) The shape fixity for SMPCs trained with cold/hot training. (b) Shape recovery for cold/hot trained SMPCs. (c) How the ability of printed SMPCs and PLA to recover their shape changes during hot processing. (d) Comparison of SMPC and PLA shape recovery times. (e) The repeated ability of cold-processed materials to return to their original shape. (f) The repeated ability of hot-processed materials to return to their original shape.

6.4. Potential applications

6.4.1. Human-material interaction

The field of human-material interaction has witnessed a growing interest in 4D printing technology in recent times (Yu, Yuxuan, et al. 2020, Dezaki, et al. 2024). Developing design concepts that encourage the production of 4D-printed objects that are environmentally friendly is a major focus. The goal of this emphasis is to reduce the amount of materials used and waste produced during the operation. Furthermore, FDM 4D printing technology offers the ability to produce customized and personalized products tailored to specific user needs (Ameta, et al. 2022). This versatility empowers the creation of unique gadgets that closely align with user preferences, ultimately leading to improved pleasure and experience for users. FDM 4D printing presents a cost-effective manufacturing solution due to its emphasis on product reusability. Compared to traditional methods, FDM 4D printing eliminates the need for complex tooling and moulds, streamlining the production process. The accessibility and user-friendliness of non-toxic materials further contribute to the overall suitability and practicality of FDM 4D-printed devices (Nugroho, et al. 2021).

This research explores the development of several designs for human-material interaction applications. These designs prioritize reusability, lightweight construction, and durability. These advantageous properties are achieved through the integration of FG material in a continuous form inside a PLA. The original design, a beam actuator with specified dimensions, is shown in **Figure 6.8a**. The actuator in the form of a hook weighs just 0.36 grammes. After hot form training, the actuator shows that it can lift and hold things up to 500 grammes in weight or keep an item firmly. Notably, this represents a dead load capacity 1385 times greater than the weight of the actuator itself. In contrast, a beam fabricated solely from PLA matrix material would break under such a load during testing. Furthermore, the designed actuator boasts an impressive 94% form recovery upon heating. This enables its reusability in various consumer products across multiple cycles. This reusable element helps create a more sustainable design by reducing the amount of materials used and waste produced.

A locker-style setup for the FGPLA actuator is presented in the article (**Figure 6.8b**). At 0.94 grammes, this locker version has an improved shape restoration rate of 96%. It is important to note that the shape recovery performance in these 3D-printed SMPC products is influenced by parameters like the total thickness of the product and the design shape. The study explores the form programming, form locking, and shape recovery procedures that are involved in these actuators. Although a basic shape-programmed setup is set up, the design allows for the programming to be adjusted and changed as needed. A key component of this design is the use of continuous FG. It makes it possible for the actuator to change into a strong, sturdy locker. Because of its unique design, the locker can cling to an item and then grab hold of something else on the other side of the actuator.

Moreover, this research explores the potential application of FGPLA composites in the field of orthopaedics, specifically focusing on finger splints (Javaid and Haleem 2020). Finger splints are commonly used medical devices designed to immobilize and support fractured or injured fingers, aiding patient recovery and regaining functionality (Zolfagharian, Gregory, et al. 2020). The study proposes a sustainable design for a CFRC finger splint, fabricated using a sheet and tailored to individual patients (**Figure 6.8c**). The first design, the hot

shaping procedure, the shape recovery that followed, and the ultimate form that was restored are all shown in the figure. With an outstanding shape restoration rate of almost 95%, this lightweight splint (2.79 grams) is made to be reused several times. The design notably excludes a top layer matrix cover so that the behaviour of the fibres after shaping and recovery may be observed. Following recovery, there is some fibre fragmentation in the bent region, as seen in **Figure 6.8c**. The reusability and mechanical strength of the splint are unaffected by this fragmentation, thanks to the intrinsic fibre qualities and the robust PLA-FG link.

The splint supports the palm and finger joints by moulding itself to the shape of the wounded finger. Because of its flexible design, it fits a variety of fingers that are smaller than the one shown securely. Furthermore, the splint's transparent material makes it simple to watch the damaged area, which aids in evaluating the degree of healing. The study acknowledges the potential for utilising other thermoplastics in this application by modifying printing settings. However, a crucial consideration lies in employing materials that exhibit SME to ensure reusability, a key feature for finger splints. Furthermore, creating a solid connection between continuous fibres and the PLA is difficult, especially when changing the nature of the matrix.

There are major sustainability benefits when SMPCs are used in products used for human-material interaction. One key advantage lies in reduced material consumption without sacrificing strength. CFRCs are excellent choices for a variety of applications due to their remarkable strength-to-weight ratio. With SMPCs, durable objects may be produced with a significantly smaller material footprint than with typical materials like metals or solid plastics. This is accomplished by taking advantage of continuous fibre's natural strength. The reduction of material utilisation is essential in the current environmentally conscious period where resource conservation is of utmost importance. Additionally, 3D-printed SMPCs' shape recovery properties enable product reusability, which lowers waste materials. The packaging aspect of 4D-printed SMPCs is another advantage in terms of sustainability. Because of the 2D sheet printing method used, products can be transported in minimal and compact packaging. As a result, this lowers the cost of transportation procedures as well as packaging materials. This reduces the environmental effect of packaging and transportation.

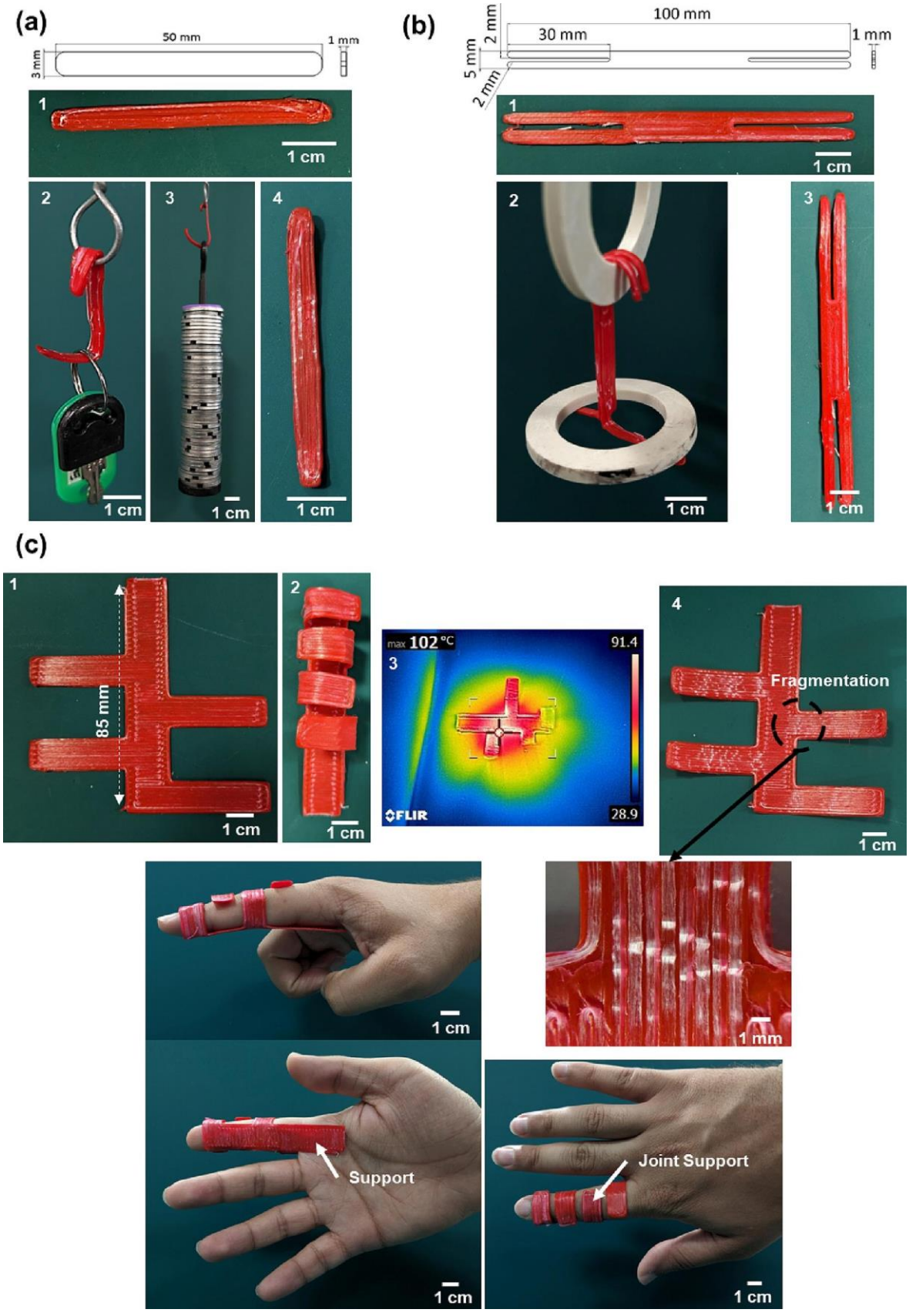

Figure 6.8. (a) Figures 1-4 show pictures of the composite actuator holder together with the processes for hot shape training, applications, and form recovery. (b) Pictures depict the numbered restoration and form programming procedures in addition to the printed locker. (c) 1. A picture of the finger splint from SMPC. 2. CFRC splint that is adjustable. 3. An infrared picture was captured while the form was being recovered. 4. The ultimate form of

the recovered finger splint, shows evidence of FG fibre fragmentation. The purpose of the finger splint is to provide support for the pointing finger joint.

6.4.2. Cellular meta-composite

Lattice or cellular structures possess several inherent advantages, including minimal weight, excellent specific strength, and high stiffness (Kaur, Han and Kim 2017). These properties have led to extensive research on their applications across various fields (Nazir, et al. 2019). Hierarchical arrangements within lattice structures demonstrate the ability to withstand significant loads. These specialized structures, due to their exceptional strength-to-weight ratio, have found success in diverse building applications (Siddique, et al. 2022). A prime example of lightweight components, honeycomb structures have attracted a lot of research and development attention because of their many possible uses (Isaac and Duddeck 2022, Ghazlan, et al. 2020, Saufi, et al. 2021, Bodaghi, Mahdi, et al. 2023). A 2D honeycomb structure (see Figure 6.9) was developed to evaluate the effectiveness of cold training and form recovery in CFRCs. The periodic loading graphs and compression stages for this framework are shown accordingly.

The compression examination was applied samples and a 50 kN load cell moving at two millimetres per minute. The construction is subjected to repeated compression up to 80% of its beginning height (62 mm), as **Figure 6.9a** illustrates. The graphic also shows the structure's following full emptying. The same protocol is used on an additional specimen, but with a maximum strain of 50%, to examine the effects of low loading on the structure (**Figure 6.9b**). The frameworks are compressed, then heated above their T_g to cause form recovery and rise to their initial height. In this test, the form recovery ratio is obtained by dividing the restored height by the initial height.

Following the heating and shape recovery stages, the results of the cyclic compression tests were meticulously analysed (**Figures 6.9c-e**). The results of the periodic compression tests performed up to 50% and 80% strain, respectively, are shown in **Figures 6.9c and 6.9d.** Furthermore, the findings of form recovery for frameworks that underwent sequential thermo-mechanical loading are shown in **Figure 6.9e.** The form recovery ability of the structure drops to 92% when it is loaded to 80% strain, according to the data. The fact that the structure can't completely return to its previous form indicates that performance has been weakened. This is explained by the substantial displacement that occurs during loading, which causes internal PLA matrix fractures and plastic deformation inside the sample. Additionally, at this strain level, the structure's performance and form recovery gradually decline with each successive cycle, as shown in **Figure 6.9c.**

In comparison, the form recovery after heating reaches about 96% when the structure is squeezed up to 50% strain. Constant fibres within the meta-composite structure are responsible for this amazing healing. For the 50% strain case, the compression test and shape recovery findings that follow show that the results stay for cycles two and three. This implies that because of its great shape memory qualities and enhanced performance under these loading circumstances, the structure shows exceptional reusability.

A further benefit of the created cellular structures is their capacity to absorb substantial quantities of energy during compaction without undergoing undue stress (Yin, H., et al. 2023, Hedayati, Yousefi and Bodaghi 2022). Their capacity to experience significant compressive

distortion at a particular stress threshold helps them achieve this capacity. The basic idea underlying energy absorption in meta-composite materials is their ability to change impact force into a variety of different types of energy. These processes include breakage, mechanical difficulties, and elastic or plastic distortion. Based on the force-displacement graph, the absorbed and dissipated energy are shown in Figure 6.10a. The investigation of the structures' specific energy absorption (SEA) and energy absorption (EA) is part of this broader examination. Equations 6.5 and 6.6 below offer the results of the calculations for EA and SEA.

$$EA = \int_0^d F_{(x)} d_x \tag{6.5}$$

$$SEA = \frac{EA}{m} \tag{6.6}$$

The area under the force-displacement graph's load-displacement curve is used to quantify EA inside structures. In this formula, d denotes the total deformation encountered, and F(x) is the force applied as a function of displacement (x). By integrating the load-displacement curve from zero displacement to the greatest distortion point, the total energy absorption may be ascertained. Next, SEA is computed by dividing the specimen's weight by the total absorbed energy value. The findings of the SEA measurement in the cellular SMPC specimens are shown in **Figure 6.10b**. After the first cycle, the SEA values for samples compressed by 80% show a considerable decrease. On the other hand, samples compacted to 50% strain show a rather moderate drop in SEA, with values staying around 0.055. The wasted energy exceeds the absorbed energy in both structures under investigation. Both the PLA material's plastic hardening qualities and the lattice structure itself are responsible for this phenomenon. Consequently, more energy is left as heat instead of being retained by the substance. The form memory qualities seen at lower compressive strains allow the design to remain successful for reusability despite this finding.

Cellular structures, due to their advantageous properties such as lightweight design and outstanding energy absorption capabilities, are widely employed in various industries including automotive, marine, and aerospace sectors. The weight of the sandwich development and its energy absorption capability are important factors to consider in real-world applications. Therefore, it is conceivable to develop SMP meta-composite structures with important applications across varied sectors by carefully increasing the number of unit cells within the design. These constructions provide a special blend of lightweight and strong strength. Because of their exceptional strength-to-weight ratios, the resultant polymers can completely transform the area of material engineering. This creates opportunities for new applications. The creation of safer, more efficient, and environmentally sustainable solutions across a wide range of sectors.

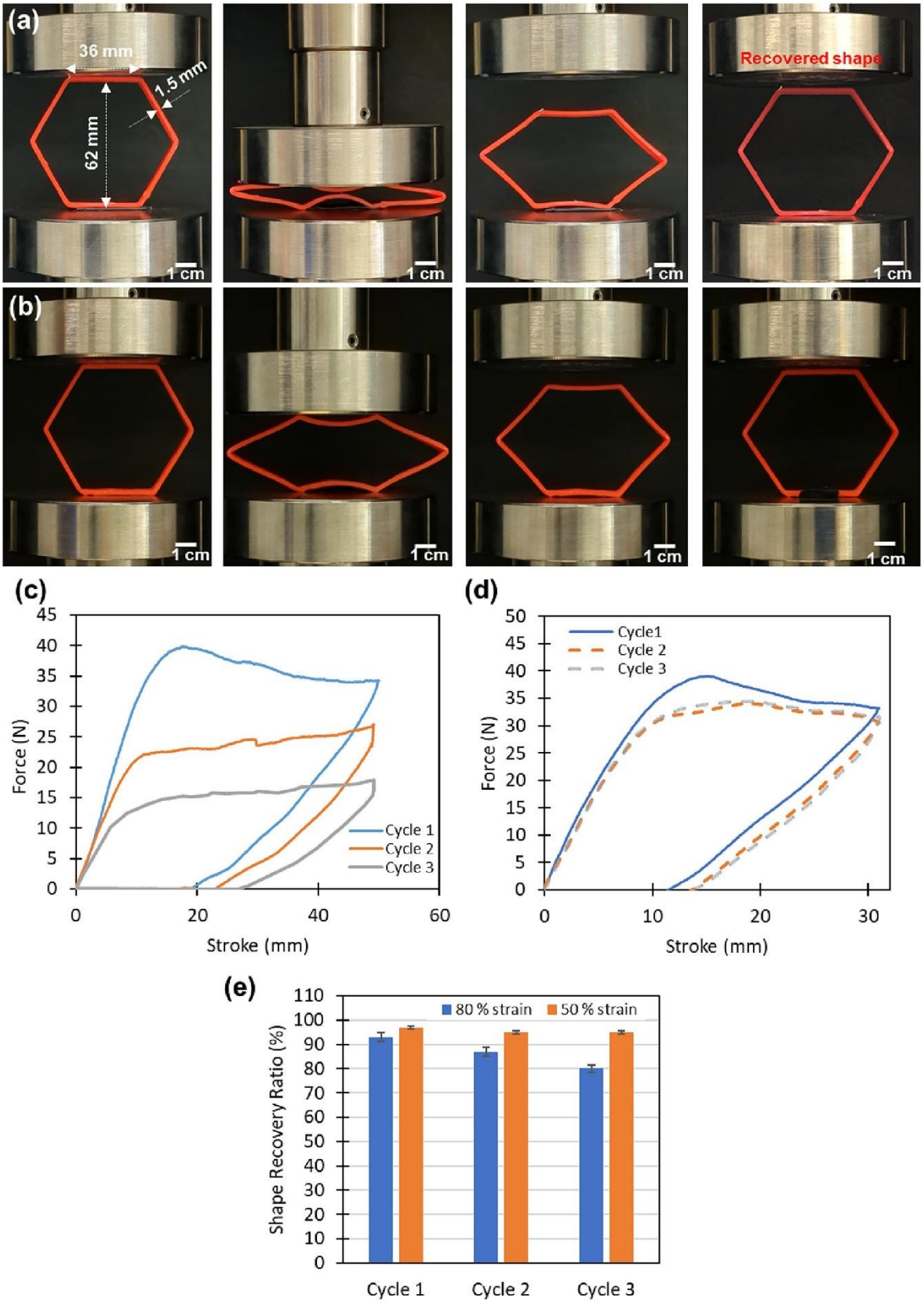

Figure 6.9. (a) Honeycomb compression test up to 80% strain. (b) The phases of loading/unloading SMPC honeycomb up to 50% strain. (c) Force versus stroke obtained after shape recovery with heating to 80% strain, during cyclic loading on a single sample. (d) Force versus stroke values obtained after shape recovery with heating up to 50% strain during cyclic loading on a single sample. (e) The cyclic compression test after heating the sample.

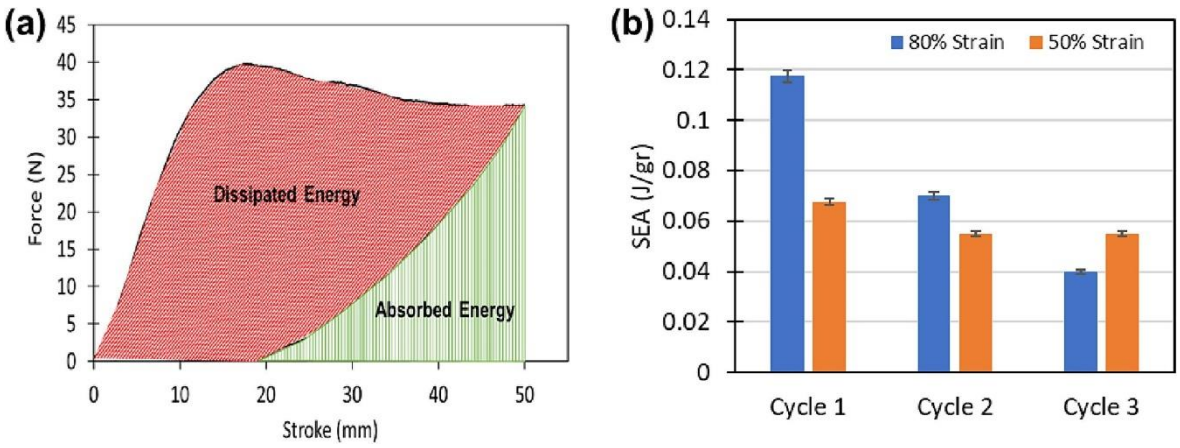

Figure 6.10. (a) How energy is distributed between absorption and dissipation from the first cycle to 80% strain. (b) In cyclic compression testing, SEA was found at 50% and 80% strain levels.

6.5. Conclusion

This research investigates the use of FDM 3D/4D printing to create 4D-printed CFRC structures. The goal is to produce lightweight, strong, and reusable products by incorporating various continuous fibres into a polymer matrix. The study modified a standard 3D printer to simultaneously print different fibre types (CF, AF, and FG) within a PLA material. Tensile and flexural testing showed that adding fibres significantly improved the strength and stiffness of the printed parts compared to pure PLA. However, the shape-changing abilities of the CFRCs were slightly reduced. This method facilitates reusability, which supports sustainable design principles. Because of their innate strength and stiffness, SMPCs showed quicker shape recovery periods. Due to its greater shape recovery ratio and consistent performance, FG outperformed the other tested fibres. Functional prototypes that demonstrated the usefulness of this technology were created. Innovative and eco-friendly items can be made with 4D-printed composites since they reduce the need for raw materials and allow for shape customisation. To reach their full potential, future research should focus on increasing the complexity and capabilities of these materials.

Chapter 7

Conclusion and future work

7.1. Conclusion

This final chapter summarizes the key discoveries made during this doctoral research project. This thesis centres on the exciting potential of combining FDM 4D printing technology with the field of soft actuators. By merging these two areas, the study investigates the development of 4D-printed composite actuators with unique capabilities. It also explores potential areas for future research in the rapidly developing field of 4D-printed composite actuators. This dissertation leverages the convergence of design, 3D/4D printing, and SMPs/SMPCs unique ability to modulate their SME and mechanical properties. By employing 4D printing with SMPs/SMPCs, distinct functional structures or actuators are presented for diverse applications. This thesis focused on the development of next-generation shape memory composite actuators. These actuators aimed to achieve two key advancements including integration of a secondary stimulus and enhanced mechanical properties. Here is a brief look at the findings in each chapter.

Chapter 1 establishes a foundational understanding by introducing the core principles of 3D and 4D printing technologies. It provides a general overview of the 4D printing field. Subsequently, the chapter identifies a significant challenge hindering the advancement of 4D printing with SMPCs specifically in the context of smart composite actuators. This identification serves as the key justification for the research undertaken in this dissertation. The chapter then outlines the overarching objective of exploring the possibilities of FDM 4D printing with SMPCs. This exploration ultimately aims to develop 4D-printed smart composite actuators and structures with enhanced functionalities. Finally, a concise overview of the dissertation's structure is provided, guiding the reader through the subsequent chapters.

This thesis breaks new ground by presenting a comprehensive systematic review of 4D printing in **Chapter 2**. This review sheds light on the significance of 4D printing technology and its potential benefits. The chapter explores the commonly used FDM process for creating dynamic structures and actuators using both 3D/4D printing. Furthermore, the chapter analyses the advantages of FDM compared to other 3D printing technologies, specifically focusing on why FDM is well-suited for 4D printing composite actuators. A key finding of this review is the in-depth exploration of SMPs and SMPCs. It delves into how and why SMPCs can be particularly effective in developing composite actuators. The chapter explores the concept and applications of SMPCs, highlighting their potential in various fields. It then discusses how FDM 4D printing of SMPCs can be used to create composite actuators that respond to magnetic, electric, and pneumatic stimuli. Finally, the chapter summarizes the current state of FDM 4D printing for composite actuators, identifying limitations and challenges found in previous research.

A unique design for high-performance, bi-stable actuators that combined MRE composites and 4D-printed conductive SMPCs was introduced in **Chapter 3.** These actuators offered several advantages, including remote control, rapid movement, adaptability to uneven surfaces, and safe interaction with humans. Traditional MREs, despite their benefits, suffered from limited stability due to their softness and the constant need for a magnetic field for actuation and positioning. This research addressed these limitations by introducing a new concept. The proposed design incorporated strontium ferrite magnetic particles within

silicone resins and integrated a core made of 4D-printed CPLA. This innovative approach resulted in a lightweight, bi-stable actuator with programmable magnetic patterns. A key feature of this design was its ability to maintain its actuated position without external stimuli. The research demonstrated the actuator's remarkable capabilities through a series of tests. Despite its weight of only 1.47 grams, the actuator could hold and lift objects up to 200 grams. This discovery has the potential to significantly advance the field of smart composite actuators with remotely controlled shape-memory functions, as there is a lack of equivalent concepts in the literature currently in publication. Applications in the realms of biomedicine and mechanics appeared to be promising for this invention.

Chapter 4 proposed a new approach that utilized magneto-electroactive SMPCs combined with 4D printing technology to achieve a high degree of design flexibility with sustainable structures. These composites offered several advantages, including the ability to be triggered by electricity, controlled remotely, and respond rapidly. Several stable shapes could be achieved and repeatedly switched between by programming these 4D-printed SMPC structures at high temperatures. This allowed for a single structure to embody multiple designs, eliminating material waste. Understanding FDM methods, magnetism, and SMPC mechanics were necessary for understanding the fundamental idea. The research investigated MPLA and CPLA composites, focusing on their microstructure, interfacial properties, and mechanical behaviour. Characterization studies were employed to manipulate the structures with a low magnetic field. The shape-morphing potential of these magneto-electroactive SMPC structures was then investigated in this work. Using FDM, MPLA and CPLA adaptive structures that could change their shape from 1D/2D to 2D/3D by applying a magnetic field were 3D printed. These switchable multi-stable structures have the potential to decrease material waste, consume less energy, and boost efficiency across a range of industries, including packaging.

The field of soft robotics is gaining significant momentum due to its ability to create robots that are flexible, adaptable, and inherently safer than traditional rigid robots. **Chapter 5** introduces a novel concept of MLJ actuators. These actuators leverage 4D-printed SMP meta-structures, offering a sustainable alternative to conventional LJ technology. A key advantage of MLJ actuators lies in their ability to function without requiring continuous negative air pressure for stimulation, unlike traditional LJ actuators. The study examines several SMP meta-structure designs that are made with 4D printing, such as diamond, circular, rectangular, and auxetic shapes. Flexural and compression tests are used to evaluate mechanical qualities. Through hot air programming, SMEs and the shape recovery capabilities of the MLJ actuators and meta-structures are examined. Notably, auxetic meta-structure core MLJ actuators exhibit improved contraction and bending performance as well as full shape recovery following stimulation. Even while supporting 200 grammes of weight, these environmentally friendly MLJ actuators can regain and lock their shape without the need for external power. This translates to the potential for manipulation of objects with varying shapes and weights without requiring constant power. The versatility of these actuators makes them promising candidates for applications such as grippers and end-effectors in robotic systems.

Chapter 6 explored the potential of FDM-based 4D printing for creating programmable bio-SMPCs CFRC structures. Using FDM technology, experiments were conducted to fabricate lightweight CFRC parts with a PLA reinforced with various continuous fibres like CF, AF,

and FG. Using cold and hot programming approaches, the SMPCs' microstructure, mechanical attributes, and shape memory qualities were assessed. The research found that continuous fibres significantly enhanced mechanical properties. Compared to pure PLA, tensile strength increased by over 1027.5% and three-point bending strength by nearly 497.3%. The study also investigated the impact of continuous fibres on shape recovery and fixity ratios in 4D-printed SMPCs. It was observed that these ratios decreased with the addition of fibres. The results of this study demonstrated the capability of 4D-printed CFRCs for a variety of uses from mechanical to human-material interaction. Furthermore, by lowering waste and material consumption, the reusable nature of these lightweight constructions improved sustainability.

The created actuators are triggered by a variety of stimuli, such as electricity, heat, magnetic fields, and pneumatic systems. The use of magneto-electro active actuators, in conjunction with pneumatic air supply, allows for remote programming of the actuators. This advancement makes it possible to control the actuators more easily, providing the functionality of two-way composite actuators. These actuators can thus be manipulated remotely, responding to specific signals from magnetic or electrical sources, or adjustments in pneumatic pressure, to achieve desired movements or tasks. This remote programmability not only increases the flexibility and efficiency of the actuators but also broadens their application potential in various fields. Meanwhile, by integrating CFRC actuators into these existing systems, it is possible to significantly enhance their strength and stiffness. The inclusion of CFRC actuators improves the overall performance of composite actuators across all these activation methods. This translates to actuators capable of handling heavier loads, withstanding greater forces, and maintaining their shape under pressure, even when activated through various stimuli.

7.2. Future works

This work successfully demonstrated the feasibility of 4D printing for composite smart actuator fabrication. It further expanded upon this concept by encompassing the entire process, including the creation, analysis, modelling, and control of these 4D-printed actuators. However, there remains significant potential for the development and modelling of novel 4D-printed actuators with a focus on minimizing environmental impact. The following section details potential avenues for future research in this area. Employing a CFRC actuator with electro-magneto responsive characteristics. This design has the potential to simultaneously enhance the mechanical properties of the actuator and improve its remote controllability. Also, CFRCs offer significant advantages when incorporated into pneumatic composite actuators or LJ actuators. Specifically, their use can lead to the development of actuators with increased rigidity and strength. Furthermore, the combination of Joule heating CFRCs with jamming technology presents a promising avenue for improved performance. This approach has the potential to enhance remote programmability and achieve on-demand shape modifications.

The key to achieving successful development in robotic actuators lies in the ability to generate complex shapes using materials that respond to external stimuli. This can be further enhanced by integrating various types of SMPCs such as those responsive to light or magnetic fields. The incorporation of these micro- and nano-scale structures during the 4D printing process of SMP-based components presents a promising direction for the creation

of intelligent robotic actuators. The development of novel heating elements alongside the strategic positioning and shaping of these elements can significantly improve control over deformation timing, leading to enhanced remote actuation capabilities under thermal stimuli. Additionally, exploring alternative heating methods such as induction and microwave could be beneficial in evaluating a wider range of combinations between stimuli and smart materials.

Despite significant advancements in 4D-printed soft actuators and robots, particularly in miniaturization, the commercialization of 4D-printed smart materials remains elusive. This technology holds immense promise for the future of biomedical applications, including the development of micro-scaled robots for minimally invasive surgery, micro-stents, smart scaffolds, and adaptive drug-releasing reservoirs. However, from a biomedical perspective, the transition from 3D-printed to 4D-printed robotics is still in its early stages. Future research efforts should prioritize the material science of smart materials to enhance the morphological behaviour of actuators and sensors. Additionally, further exploration is warranted in the field of high-performance, multi-functional coupling-actuated soft actuators due to their potential applications in various emission control methods and their effectiveness in mitigating airborne pollutants.

Significant research efforts are still required to realize the full potential of 4D printing technology and make it as ubiquitous in soft robotics applications as 3D printing technology. This can be achieved by exploring novel smart materials with diverse functionalities and by developing advanced micro-fabrication techniques. The advancement of 4D-printed actuators holds great promise for transforming robotic applications within the fields of bioengineering and medicine. 4D printing technology holds immense promise for the future, and focused research holds the key to unlocking its full potential in the field of soft robotics within the next few years.

References

Aberoumand, M., Soltanmohammadi, K., Rahmatabadi, D., et al., 2023. 4D Printing of Polyvinyl Chloride (PVC): A Detailed Analysis of Microstructure, Programming, and Shape Memory Performance. *Macromolecular Materials and Engineering,* , 2200677.

Ai, C., Chen, Y., Xu, L., et al., 2021. Current Development on Origami/Kirigami-Inspired Structure of Creased Patterns toward Robotics. *Advanced Engineering Materials,* 23 (10), 2100473-n/a. Available at: https://onlinelibrary.wiley.com/doi/abs/10.1002/adem.202100473.

Aktaş, B., Narang, Y.S., Vasios, N., et al., 2021. A Modeling Framework for Jamming Structures. *Advanced Functional Materials,* 31 (16), n/a. Available at: https://onlinelibrary.wiley.com/doi/abs/10.1002/adfm.202007554.

Alapan, A., Karacakol, K., Guzelhan, G., et al., 2020. Reprogrammable shape morphing of magnetic soft machines. *Science Advances,* 6 (38), eabc6414. Available at: https://www.ncbi.nlm.nih.gov/pubmed/32948594.

Al-Rubaiai, M., Pinto, T., Torres, D., et al., Sep 18, 2017. Characterization of a 3D-Printed Conductive PLA Material With Electrically Controlled Stiffness. In: American Society of Mechanical Engineers, .

Alshebly, Y.S. and Nafea, M., Jan 1, 2022. Joule Heating Activation of 4D Printed Conductive PLA Actuators. In: Piscataway: The Institute of Electrical and Electronics Engineers, Inc. (IEEE), .

Ameta, K.L., Solanki, V.S., Haque, S., et al., 2022. Critical appraisal and systematic review of 3D & 4D printing in sustainable and environment-friendly smart manufacturing technologies. *Sustainable Materials and Technologies,* 34, e00481. Available at: https://dx.doi.org/10.1016/j.susmat.2022.e00481.

Andreu, A., Su, P., Kim, J., et al., 2021. 4D printing materials for vat photopolymerization. *Additive Manufacturing,* 44, 102024. Available at: https://dx.doi.org/10.1016/j.addma.2021.102024.

Ang, B.W.K. and Chen-Hua Yeow, Sep 2017. Print-it-Yourself (PIY) glove: A fully 3D printed soft robotic hand rehabilitative and assistive exoskeleton for stroke patients. In: IEEE, pp. 1219-1223 Available at: https://ieeexplore.ieee.org/document/8202295 .

Arif, Z.U., Khalid, M.Y., Sheikh, M.F., et al., 2022. Biopolymeric sustainable materials and their emerging applications. *Journal of Environmental Chemical Engineering,* 10 (4), 108159. Available at: https://dx.doi.org/10.1016/j.jece.2022.108159.

Aufa, A.N., Ismail, Z., and Zaki Hassan, M., 2023. Emerging trends in 4d printing of hydrogels in the biomedical field: A review. *Materials Today : Proceedings,* Available at: https://dx.doi.org/10.1016/j.matpr.2023.01.101.

Ausanio, G., Iannotti, V., Ricciardi, E., et al., 2014. Magneto-piezoresistance in Magnetorheological elastomers for magnetic induction gradient or position sensors. *Sensors and Actuators A: Physical,* 205, 235-239. Available at: https://www.sciencedirect.com/science/article/pii/S0924424713005128.

Baechle-Clayton, M., Loos, E., Taheri, M., et al., 2022. Failures and Flaws in Fused Deposition Modeling (FDM) Additively Manufactured Polymers and Composites. *Journal of Composites Science*, 6 (7), 202. Available at: https://search.proquest.com/docview/2693974836.

Bastola, A.K. and Hossain, M., 2021. The shape – morphing performance of magnetoactive soft materials. *Materials & Design*, 211, 110172. Available at: https://www.sciencedirect.com/science/article/pii/S0264127521007279.

Bazli, M., Ashrafi, H., Rajabipour, A., et al., 2023. 3D printing for remote housing: Benefits and challenges. *Automation in Construction*, 148, 104772. Available at: https://dx.doi.org/10.1016/j.autcon.2023.104772.

Beniak, J., Šooš, Ľ, Križan, P., et al., 2022. Resistance and Strength of Conductive PLA Processed by FDM Additive Manufacturing. *Polymers*, 14 (4), 678. Available at: https://www.ncbi.nlm.nih.gov/pubmed/35215591.

Bernat, J., Gajewski, P., Kapela, R., et al., 2022. Design, Fabrication and Analysis of Magnetorheological Soft Gripper. *Sensors (Basel, Switzerland)*, 22 (7), 2757. Available at: https://www.ncbi.nlm.nih.gov/pubmed/35408370.

Bodaghi, M., Damanpack, A.R., and Liao, W.H., 2017. Adaptive metamaterials by functionally graded 4D printing. *Materials & Design*, 135, 26-36. Available at: https://dx.doi.org/10.1016/j.matdes.2017.08.069.

Bodaghi, M., Serjouei, A., Zolfagharian, A., et al., 2020. Reversible energy absorbing meta-sandwiches by FDM 4D printing. *International Journal of Mechanical Sciences*, 173, 105451. Available at: https://dx.doi.org/10.1016/j.ijmecsci.2020.105451.

Bodaghi, M., Namvar, N., Yousefi, A., et al., 2023. Metamaterial boat fenders with supreme shape recovery and energy absorption/dissipation via FFF 4D printing. *Smart Materials and Structures*, 32 (9), 95028. Available at: https://iopscience.iop.org/article/10.1088/1361-665X/acedde.

Bodaghi, M., Noroozi, R., Zolfagharian, A., et al., 2019. 4D Printing Self-Morphing Structures. *Materials*, 12 (8), 1353. Available at: https://www.ncbi.nlm.nih.gov/pubmed/31027212.

Bonifacich, F.G., Lambri, O.A., Recarte, V., et al., 2021. Magnetically tunable damping in composites for 4D printing. *Composites Science and Technology*, 201, 108538. Available at: https://dx.doi.org/10.1016/j.compscitech.2020.108538.

Bowen, J.J., Rose, M.A., and Morin, S.A., 2021. Surface molding of multi-stimuli-responsive microgel actuators. *MRS Bulletin*, 46 (4), 337-344. Available at: https://link.springer.com/article/10.1557/s43577-021-00077-5.

Calì, J., Calian, D.A., Amati, C., et al., 2012. 3D-printing of non-assembly, articulated models. *ACM Transactions on Graphics*, 31 (6), 1-8. Available at: https://search.proquest.com/docview/1506377201.

Carpenter, J.A., Eberle, T.B., Schuerle, S., et al., 2021. Facile Manufacturing Route for Magneto-Responsive Soft Actuators. *Advanced Intelligent Systems*, 3 (8), n/a. Available at: https://onlinelibrary.wiley.com/doi/abs/10.1002/aisy.202000283.

Carrell, J., Gruss, G., and Gomez, E., 2020. Four-dimensional printing using fused-deposition modeling: a review. *Rapid Prototyping Journal*, 26 (5), 855-869. Available at: https://www.emerald.com/insight/content/doi/10.1108/RPJ-12-2018-0305/full/html.

Cerbe, F., Mahlstedt, D., Sinapius, M., et al., 2023. Relationship between programming stress and residual strain in FDM 4D printing. *Progress in Additive Manufacturing*, Available at: https://doi.org/10.1007/s40964-023-00477-w.

Cersoli, T., Yelamanchi, B., MacDonald, E., et al., 2021. 3D printing of a continuous fiber-reinforced composite based on a coaxial Kevlar/PLA filament. *Composites and Advanced Materials*, 30, 263498332110000. Available at: https://journals.sagepub.com/doi/full/10.1177/26349833211000058.

Chaudhary, V., Mantri, S.A., Ramanujan, R.V., et al., 2020. Additive manufacturing of magnetic materials. *Progress in Materials Science*, 114, 100688. Available at: https://dx.doi.org/10.1016/j.pmatsci.2020.100688.

Chen, H., Zhang, F., Sun, Y., et al., 2021. Electrothermal shape memory behavior and recovery force of four-dimensional printed continuous carbon fiber/polylactic acid composite. *Smart Materials and Structures*, 30 (2), 25040. Available at: https://iopscience.iop.org/article/10.1088/1361-665X/abd912.

Chen, K., Yu, L., Cui, Y., et al., 2021. Optimization of printing parameters of 3D-printed continuous glass fiber reinforced polylactic acid composites. *Thin-Walled Structures*, 164, 107717. Available at: https://dx.doi.org/10.1016/j.tws.2021.107717.

Chen, M., Gao, M., Bai, L., et al., 2023. Recent Advances in 4D Printing of Liquid Crystal Elastomers. *Advanced Materials (Weinheim)*, 35 (23), e2209566-n/a. Available at: https://onlinelibrary.wiley.com/doi/abs/10.1002/adma.202209566.

Chen, Q., Han, L., Ren, J., et al., 2020. 4D Printing via an Unconventional Fused Deposition Modeling Route to High-Performance Thermosets. *ACS Applied Materials & Interfaces*, 12 (44), 50052-50060. Available at: http://dx.doi.org/10.1021/acsami.0c13976.

Cheng, Y., Li, J., Qian, X., et al., 2021. 3D printed recoverable honeycomb composites reinforced by continuous carbon fibers. *Composite Structures*, 268, 113974. Available at: https://dx.doi.org/10.1016/j.compstruct.2021.113974.

Cho, J.W., Kim, J.W., Jung, Y.C., et al., 2005. Electroactive Shape-Memory Polyurethane Composites Incorporating Carbon Nanotubes. *Macromolecular Rapid Communications*, 26 (5), 412-416. Available at: https://api.istex.fr/ark:/67375/WNG-6V796HZ6-G/fulltext.pdf.

Chung, H., Parsons, A.M., and Zheng, L., 2021. Magnetically Controlled Soft Robotics Utilizing Elastomers and Gels in Actuation: A Review. *Advanced Intelligent Systems*, 3 (3), n/a. Available at: https://onlinelibrary.wiley.com/doi/abs/10.1002/aisy.202000186.

Cole, T. and Tang, S., 2022. Liquid metals as soft electromechanical actuators. *Materials Advances*, 3 (1), 173-185. Available at: https://doi.org/10.1039/d1ma00885d.

CORREA, D., MENGES, A., SHEIL, B., et al., 2017. FUSED FILAMENT FABRICATION FOR MULTI-KINEMATIC-STATE CLIMATE-RESPONSIVE APERTURE. In: FUSED FILAMENT FABRICATION FOR MULTI-KINEMATIC-STATE CLIMATE-

RESPONSIVE APERTURE*Fabricate 2017*. UCL Press, pp. 190-195. Available at: http://www.jstor.org/stable/j.ctt1n7qkg7.30.

Cremonini, A., Sol, J.A.H.P., Schenning, A.P.H.J., et al., 2023. The Interplay between Different Stimuli in a 4D Printed Photo-, Thermal-, and Water-Responsive Liquid Crystal Elastomer Actuator. *Chemistry : A European Journal*, , e202300648. Available at: https://www.ncbi.nlm.nih.gov/pubmed/37051945.

de Kergariou, C., Le Duigou, A., Perriman, A., et al., 2023. Design space and manufacturing of programmable 4D printed continuous flax fibre polylactic acid composite hygromorphs. *Materials & Design*, 225, 111472. Available at: https://dx.doi.org/10.1016/j.matdes.2022.111472.

de León, E.H., Valle-Pérez, A.U., Khan, Z.N., et al., 2023. Intelligent and smart biomaterials for sustainable 3D printing applications. *Current Opinion in Biomedical Engineering*, 26, 100450. Available at: https://dx.doi.org/10.1016/j.cobme.2023.100450.

de Oliveira Barros, A., Hasan Kashem, M.N., Luna, D., et al., 2022. Magnetic properties of PDMS embedded with strontium ferrite particles cured under different magnetic field configurations. *AIP Advances*, 12 (3), 035121-7. Available at: http://dx.doi.org/10.1063/9.0000338.

Demoly, F. and André, J., 2022. *4D Printing 1 : Between Disruptive Research and Industrial Applications*. Newark: John Wiley & Sons, Inc. Available at: https://library.biblioboard.com/viewer/8ccdfff6-13ac-4ebc-bf8c-55de4136e631.

Demoly, F., Dunn, M.L., Wood, K.L., et al., 2021. The status, barriers, challenges, and future in design for 4D printing. *Materials & Design*, 212, 110193. Available at: https://dx.doi.org/10.1016/j.matdes.2021.110193.

Dey, A. and Yodo, N., 2019. A Systematic Survey of FDM Process Parameter Optimization and Their Influence on Part Characteristics. *Journal of Manufacturing and Materials Processing*, 3 (3), 64. Available at: https://search.proquest.com/docview/2548645902.

Dezaki, M.L., Zolfagharian, A., Demoly, F., et al., 2024. Human–Material Interaction Enabled by Fused Filament Fabrication 4D Printing. *Advanced Engineering Materials*, Available at: https://doi.org/10.1002/adem.202301917.

Díez, A.G., Tubio, C.R., Etxebarria, J.G., et al., 2021. Magnetorheological Elastomer-Based Materials and Devices: State of the Art and Future Perspectives. *Advanced Engineering Materials*, 23 (6), n/a. Available at: https://onlinelibrary.wiley.com/doi/abs/10.1002/adem.202100240.

Ding, Z., Weeger, O., Qi, H.J., et al., 2018. 4D rods: 3D structures via programmable 1D composite rods. *Materials & Design*, 137, 256-265. Available at: https://dx.doi.org/10.1016/j.matdes.2017.10.004.

Dong, K., Ke, H., Panahi-Sarmad, M., et al., 2021. Mechanical properties and shape memory effect of 4D printed cellular structure composite with a novel continuous fiber-reinforced printing path. *Materials & Design*, 198, 109303. Available at: https://dx.doi.org/10.1016/j.matdes.2020.109303.

Dong, K., Wang, Y., Wang, Z., et al., 2023. Reusability and energy absorption behavior of 4D printed continuous fiber-reinforced auxetic composite structures. *Composites.Part A, Applied Science and Manufacturing*, 169, 107529. Available at: https://dx.doi.org/10.1016/j.compositesa.2023.107529.

Dong, X., Zhang, F., Wang, L., et al., 2022. 4D printing of electroactive shape-changing composite structures and their programmable behaviors. *Composites. Part A, Applied Science and Manufacturing*, 157, 106925. Available at: https://dx.doi.org/10.1016/j.compositesa.2022.106925.

Doostmohammadi, H., Baniassadi, M., Bodaghi, M., et al., 2024. 4D Printing of Magneto-Thermo-Responsive PLA/PMMA/Fe3O4 Nanocomposites with Superior Shape Memory and Remote Actuation. *Macromolecular Materials and Engineering*, n/a, 2400090. Available at: https://doi.org/10.1002/mame.202400090.

Ehrmann, G. and Ehrmann, A., 2021. 3D printing of shape memory polymers. *Journal of Applied Polymer Science*, 138 (34), 50847-n/a. Available at: https://onlinelibrary.wiley.com/doi/abs/10.1002/app.50847.

El-Atab, N., Mishra, R.B., Al-Modaf, F., et al., 2020. Soft Actuators for Soft Robotic Applications: A Review. *Advanced Intelligent Systems*, 2 (10), 2-n/a. Available at: https://onlinelibrary.wiley.com/doi/abs/10.1002/aisy.202000128.

Espalin, D., Alberto Ramirez, J., Medina, F., et al., 2014. Multi-material, multi-technology FDM: exploring build process variations. *Rapid Prototyping Journal*, 20 (3), 236-244. Available at: https://www.emerald.com/insight/content/doi/10.1108/RPJ-12-2012-0112/full/html.

Fallah, A., Asif, S., Gokcer, G., et al., 2023. 4D printing of continuous fiber-reinforced electroactive smart composites by coaxial additive manufacturing. *Composite Structures*, 316, 117034. Available at: https://dx.doi.org/10.1016/j.compstruct.2023.117034.

Fitzgerald, S.G., Delaney, G.W., and Howard, D., 2020. A Review of Jamming Actuation in Soft Robotics. *Actuators*, 9 (4), 104. Available at: https://doaj.org/article/068799e8e0ca49e2844dc0a2ebf3bd14.

Ford, S. and Minshall, T., 2019. Invited review article: Where and how 3D printing is used in teaching and education. *Additive Manufacturing*, 25, 131-150. Available at: https://dx.doi.org/10.1016/j.addma.2018.10.028.

Fu, C., Xia, Z., Hurren, C., et al., 2022. Textiles in soft robots: Current progress and future trends. *Biosensors & Bioelectronics*, 196, 113690. Available at: https://dx.doi.org/10.1016/j.bios.2021.113690.

Gao, Y., Huang, X., Mann, I.S., et al., 2020. A Novel Variable Stiffness Compliant Robotic Gripper Based on Layer Jamming. *Journal of Mechanisms and Robotics*, 12 (5) Available at: http://dx.doi.org/10.1115/1.4047156.

Garces, I.T. and Ayranci, C., 2020. Active control of 4D prints: Towards 4D printed reliable actuators and sensors. *Sensors and Actuators A: Physical*, 301, 111717. Available at: https://www.sciencedirect.com/science/article/pii/S0924424719315213.

Garces, I.T. and Ayranci, C., 2021. Advances in additive manufacturing of shape memory polymer composites. *Rapid Prototyping Journal*, 27 (2), 379-398. Available at: https://www.emerald.com/insight/content/doi/10.1108/RPJ-07-2020-0174/full/html.

Ge, Q., Qi, H.J., and Dunn, M.L., 2013. Active materials by four-dimension printing. *Applied Physics Letters*, 103 (13), 131901.

George, E., Liacouras, P., Rybicki, F.J., et al., 2017. Measuring and Establishing the Accuracy and Reproducibility of 3D Printed Medical Models. *Radiographics*, 37 (5), 1424-1450. Available at: https://www.ncbi.nlm.nih.gov/pubmed/28800287.

Gerez, L., Gao, G., Dwivedi, A., et al., 2020. A Hybrid, Wearable Exoskeleton Glove Equipped With Variable Stiffness Joints, Abduction Capabilities, and a Telescopic Thumb. *IEEE Access*, 8, 173345-173358. Available at: https://ieeexplore.ieee.org/document/9201268.

Ghazlan, A., Nguyen, T., Ngo, T., et al., 2020. Performance of a 3D printed cellular structure inspired by bone. *Thin-Walled Structures*, 151, 106713. Available at: https://dx.doi.org/10.1016/j.tws.2020.106713.

Gu, J., Lin, Y., Cui, Q., et al., 2022. PneuMesh: Pneumatic-driven Truss-based Shape Changing System. In: pp. 1-12.

Hamzehei, R., Zolfagharian, A., Dariushi, S., et al., 2022. 3D-printed bio-inspired zero Poisson's ratio graded metamaterials with high energy absorption performance. *Smart Materials and Structures*, 31 (3), 035001. Available at: https://dx.doi.org/10.1088/1361-665X/ac47d6.

Han, W.B., Yang, S.M., Rajaram, K., et al., 2022. Materials and Fabrication Strategies for Biocompatible and Biodegradable Conductive Polymer Composites toward Bio-Integrated Electronic Systems. *Advanced Sustainable Systems*, 6 (2), 2100075. Available at: https://doi.org/10.1002/adsu.202100075.

Hao, Y., Zhang, S., Fang, B., et al., 2022. A Review of Smart Materials for the Boost of Soft Actuators, Soft Sensors, and Robotics Applications. *Chinese Journal of Mechanical Engineering*, 35 (1), 37-16. Available at: https://link.springer.com/article/10.1186/s10033-022-00707-2.

Hartmann, F., Baumgartner, M., and Kaltenbrunner, M., 2021. Becoming Sustainable, The New Frontier in Soft Robotics. *Advanced Materials (Weinheim)*, 33 (19), e2004413-n/a. Available at: https://onlinelibrary.wiley.com/doi/abs/10.1002/adma.202004413.

Hedayati, R., Yousefi, A., and Bodaghi, M., 2022. Sandwich structures with repairable cores based on truncated cube cells. *Composites.Part B, Engineering*, 243, 110124. Available at: https://dx.doi.org/10.1016/j.compositesb.2022.110124.

Heidari-Rarani, M., Rafiee-Afarani, M., and Zahedi, A.M., 2019. Mechanical characterization of FDM 3D printing of continuous carbon fiber reinforced PLA composites. *Composites.Part B, Engineering*, 175, 107147. Available at: https://dx.doi.org/10.1016/j.compositesb.2019.107147.

Hong, K.Y., Jeong, H.L., Nasrallah, F., et al., May 2015. A soft exoskeleton for hand assistive and rehabilitation application using pneumatic actuators with variable stiffness. In: IEEE, pp. 4967-4972 Available at: https://ieeexplore.ieee.org/document/7139889 .

Hosseinzadeh, M., Ghoreishi, M., and Narooei, K., 2023. 4D printing of shape memory polylactic acid beams: An experimental investigation into FDM additive manufacturing process parameters, mathematical modeling, and optimization. *Journal of Manufacturing Processes,* 85, 774-782. Available at: https://dx.doi.org/10.1016/j.jmapro.2022.12.006.

Hou, Z., Tian, X., Zhang, J., et al., 2018. 3D printed continuous fibre reinforced composite corrugated structure. *Composite Structures,* 184, 1005-1010. Available at: https://dx.doi.org/10.1016/j.compstruct.2017.10.080.

Hu, D., Zhang, J., Yang, Y., et al., Jul 2020. A Novel Soft Robotic Glove with Positive-negative Pneumatic Actuator for Hand Rehabilitation. In: IEEE, pp. 1840-1847 Available at: https://ieeexplore.ieee.org/document/9158826 .

Hu, G. and Bodaghi, M., 2023. Direct Fused Deposition Modeling 4D Printing and Programming of Thermoresponsive Shape Memory Polymers with Autonomous 2D-to-3D Shape Transformations. *Advanced Engineering Materials,* 25 (19).

Huang, X., Panahi-Sarmad, M., Dong, K., et al., 2021. Tracing evolutions in electro-activated shape memory polymer composites with 4D printing strategies: A systematic review. *Composites.Part A, Applied Science and Manufacturing,* 147, 106444. Available at: https://dx.doi.org/10.1016/j.compositesa.2021.106444.

Hwang, D., Barron, 3., Edward J, Haque, A.B.M.T., et al., 2022. Shape morphing mechanical metamaterials through reversible plasticity. *Science Robotics,* 7 (63), eabg2171. Available at: https://www.ncbi.nlm.nih.gov/pubmed/35138882.

Ibrahimi, M., Paternò, L., Ricotti, L., et al., 2021. A Layer Jamming Actuator for Tunable Stiffness and Shape-Changing Devices. *Soft Robotics,* 8 (1), 85-96. Available at: https://www.liebertpub.com/doi/abs/10.1089/soro.2019.0182.

International, A., a. ASTM D3039. Standard Test Method for Tensile Properties of Polymer Matrix Composite Materials.

International, A., b. ASTM D638-14. Standard Test Method for Tensile Properties of Plastics.

International, A., c. ASTM D790. Standard Test Methods for Flexural Properties of Unreinforced and Reinforced Plastics and Electrical Insulating Materials. , 12.

Isaac, C.W. and Duddeck, F., 2022. Current trends in additively manufactured (3D printed) energy absorbing structures for crashworthiness application - a review. *Virtual and Physical Prototyping,* 17 (4), 1058-1101. Available at: https://www.tandfonline.com/doi/abs/10.1080/17452759.2022.2074698.

Iwasaki, H., Lefevre, F., Damian, D.D., et al., 2020. Autonomous and Reversible Adhesion Using Elastomeric Suction Cups for In-Vivo Medical Treatments. *IEEE Robotics and Automation Letters,* 5 (2), 2014-2021. Available at: https://ieeexplore.ieee.org/document/8977313.

J. Morrow, S. Hemleben, and Y. Menguc, 2017. Directly Fabricating Soft Robotic Actuators With an Open-Source 3-D Printer. *IEEE Robotics and Automation Letters*, 2 (1), 277-281.

Javaid, M. and Haleem, A., 2020. Significant advancements of 4D printing in the field of orthopaedics. *Journal of Clinical Orthopaedics and Trauma*, 11, S485-S490. Available at: https://dx.doi.org/10.1016/j.jcot.2020.04.021.

Javaid, M., Haleem, A., Singh, R.P., et al., 2022. Significance of 4D printing for dentistry: Materials, process, and potentials. *Journal of Oral Biology and Craniofacial Research (Amsterdam)*, 12 (3), 388-395. Available at: https://dx.doi.org/10.1016/j.jobcr.2022.05.002.

Jeong, H.Y., Lee, E.C., Ha, S., et al., 2019. Multistable Thermal Actuators Via Multimaterial 4D Printing. *Advanced Materials Technologies*, 4 (3), n/a. Available at: https://onlinelibrary.wiley.com/doi/abs/10.1002/admt.201800495.

Ji, Q., Chen, M., Wang, X.V., et al., 2022. Optimal shape morphing control of 4D printed shape memory polymer based on reinforcement learning. *Robotics and Computer-Integrated Manufacturing*, 73, 102209. Available at: https://www.sciencedirect.com/science/article/pii/S0736584521000922.

Jiachen Zhang, Onaizah, O., Middleton, K., et al., 2017. Reliable Grasping of Three-Dimensional Untethered Mobile Magnetic Microgripper for Autonomous Pick-and-Place. *IEEE Robotics and Automation Letters*, 2 (2), 835-840. Available at: https://ieeexplore.ieee.org/document/7833089.

Jing, X., Mi, H., Peng, X., et al., 2015. The morphology, properties, and shape memory behavior of polylactic acid/thermoplastic polyurethane blends. *Polymer Engineering and Science*, 55 (1), 70-80. Available at: https://api.istex.fr/ark:/67375/WNG-J29QBTB2-5/fulltext.pdf.

Jones, T.J., Jambon-Puillet, E., Marthelot, J., et al., 2021. Bubble casting soft robotics. *Nature (London)*, 599 (7884), 229-233. Available at: https://www.ncbi.nlm.nih.gov/pubmed/34759362.

Joseph Arockiam, A., Subramanian, K., Padmanabhan, R.G., et al., 2022. A review on PLA with different fillers used as a filament in 3D printing. *Materials Today : Proceedings*, 50, 2057-2064. Available at: https://dx.doi.org/10.1016/j.matpr.2021.09.413.

Joshi, S., Rawat, K., C, K., et al., 2020. 4D printing of materials for the future: Opportunities and challenges. *Applied Materials Today*, 18, 100490. Available at: https://dx.doi.org/10.1016/j.apmt.2019.100490.

Ka ergis, L., Mitkus, R., and Sinapius, M., 2019. Influence of fused deposition modeling process parameters on the transformation of 4D printed morphing structures. *Smart Materials and Structures*, 28 (10), 105042. Available at: https://iopscience.iop.org/article/10.1088/1361-665X/ab3d18.

Kabir, S.M.F., Mathur, K., and Seyam, A.M., 2020. A critical review on 3D printed continuous fiber-reinforced composites: History, mechanism, materials and properties. *Composite Structures*, 232, 111476. Available at: https://dx.doi.org/10.1016/j.compstruct.2019.111476.

Kafle, A., Luis, E., Silwal, R., et al., 2021. 3D/4D Printing of Polymers: Fused Deposition Modelling (FDM), Selective Laser Sintering (SLS), and Stereolithography (SLA). *Polymers*, 13 (18), 3101. Available at: https://www.ncbi.nlm.nih.gov/pubmed/34578002.

Kantaros, A., Ganetsos, T., and Piromalis, D., 2023a. 3D and 4D Printing as Integrated Manufacturing Methods of Industry 4.0. *American Journal of Engineering and Applied Sciences,* 16 (1), 12-22.

Kantaros, A., Ganetsos, T., and Piromalis, D., 2023b. 4D Printing: Technology Overview and Smart Materials Utilized. *Journal of Mechatronics and Robotics,* 7 (1), 1-14.

Katia Bertoldi, Vincenzo Vitelli, Johan Christensen, et al., 2017. Flexible mechanical metamaterials. *Nature Reviews. Materials,* 2 (11), 17066. Available at: https://e-archivo.uc3m.es/bitstream/10016/25772/1/flexible_NRM_2017_ps.pdf.

Kaur, M., Han, S.M., and Kim, W.S., 2017. Three-dimensionally printed cellular architecture materials: perspectives on fabrication, material advances, and applications. *MRS Communications,* 7 (1), 8-19. Available at: https://dx.doi.org/10.1557/mrc.2016.62.

Khalid, M.Y., Arif, Z.U., Ahmed, W., et al., 2022. Recent trends in recycling and reusing techniques of different plastic polymers and their composite materials. *Sustainable Materials and Technologies,* 31, e00382. Available at: https://dx.doi.org/10.1016/j.susmat.2021.e00382.

Khalid, M.Y., Arif, Z.U., Ahmed, W., et al., 2022. 4D printing: Technological developments in robotics applications. *Sensors and Actuators.A.Physical.,* 343, 113670. Available at: https://dx.doi.org/10.1016/j.sna.2022.113670.

Khalid, M.Y., Arif, Z.U., Noroozi, R., et al., 2022. 4D printing of shape memory polymer composites: A review on fabrication techniques, applications, and future perspectives. *Journal of Manufacturing Processes,* 81, 759-797. Available at: https://dx.doi.org/10.1016/j.jmapro.2022.07.035.

Khosroupour Arabi, M. and Kordani, N., 2023. 3D-printing of Continuous Fiber: A review of processes, materials and properties. *Polymer-Plastics Technology and Materials,* 62 (12), 1525-1559. Available at: https://www.tandfonline.com/doi/abs/10.1080/25740881.2023.2222793.

Kuang, X., Roach, D.J., Wu, J., et al., 2019. Advances in 4D Printing: Materials and Applications. *Advanced Functional Materials,* 29 (2), 1-n/a. Available at: https://onlinelibrary.wiley.com/doi/abs/10.1002/adfm.201805290.

Kumar, S., Singh, R., Singh, T., et al., 2019. Multimaterial printing and characterization for mechanical and surface properties of functionally graded prototype. *Proceedings of the Institution of Mechanical Engineers. Part C, Journal of Mechanical Engineering Science,* 233 (19-20), 6741-6753. Available at: https://journals.sagepub.com/doi/full/10.1177/0954406219867984.

Kwon, J., Choi, I., Park, M., et al., 2022. Selectively Stiffening Garments Enabled by Cellular Composites. *Advanced Materials Technologies,* 7 (9), n/a. Available at: https://onlinelibrary.wiley.com/doi/abs/10.1002/admt.202101543.

Lalegani Dezaki, M., Ariffin, M.K.A.M., Serjouei, A., et al., 2021. Influence of Infill Patterns Generated by CAD and FDM 3D Printer on Surface Roughness and Tensile Strength Properties. *Applied Sciences*, 11 (16), 7272. Available at: https://search.proquest.com/docview/2564650762.

Lalegani Dezaki, M. and Bodaghi, M., 2024. 4D printing and programming of continuous fibre-reinforced shape memory polymer composites. *European Polymer Journal*, 210 Available at: https://dx.doi.org/10.1016/j.eurpolymj.2024.112988.

Lalegani Dezaki, M. and Bodaghi, M., 2023a. Magnetorheological elastomer-based 4D printed electroactive composite actuators. *Sensors and Actuators. A. Physical.*, 349, 114063. Available at: https://dx.doi.org/10.1016/j.sna.2022.114063.

Lalegani Dezaki, M. and Bodaghi, M., 2023b. A Review of Recent Manufacturing Technologies for Sustainable Soft Actuators. *International Journal of Precision Engineering and Manufacturing-Green Technology*, 10 (6), 1661-1710. Available at: https://link.springer.com/article/10.1007/s40684-023-00533-4.

Lalegani Dezaki, M. and Bodaghi, M., 2023c. Shape memory meta-laminar jamming actuators fabricated by 4D printing. *Soft Matter*, 19 (12), 2186-223. Available at: https://www.ncbi.nlm.nih.gov/pubmed/36880606.

Lalegani Dezaki, M. and Bodaghi, M., 2023d. Sustainable 4D printing of magneto-electroactive shape memory polymer composites. *International Journal of Advanced Manufacturing Technology*, 126 (1-2), 35-48. Available at: https://link.springer.com/article/10.1007/s00170-023-11101-0.

Lalegani Dezaki, M. and Bodaghi, M., 2022. Soft Magneto-Responsive Shape Memory Foam Composite Actuators. *Macromolecular Materials and Engineering*, 307 (11), n/a. Available at: https://onlinelibrary.wiley.com/doi/abs/10.1002/mame.202200490.

Lalegani Dezaki, M., Bodaghi, M., Serjouei, A., et al., 2023. Soft Pneumatic Actuators with Controllable Stiffness by Bio-Inspired Lattice Chambers and Fused Deposition Modeling 3D Printing. *Advanced Engineering Materials*, 25 (6), n/a. Available at: https://onlinelibrary.wiley.com/doi/abs/10.1002/adem.202200797.

Lalegani Dezaki, M. and Mohd Ariffin, M.,Khairol Anuar, 2020. The Effects of Combined Infill Patterns on Mechanical Properties in FDM Process. *Polymers*, 12 (12), 2792. Available at: https://www.ncbi.nlm.nih.gov/pubmed/33255897.

Lalegani Dezaki, M., Mohd Ariffin, M.,Khairol Anuar, and Hatami, S., 2021. An overview of fused deposition modelling (FDM): research, development and process optimisation. *Rapid Prototyping Journal*, 27 (3), 562-582. Available at: https://www.emerald.com/insight/content/doi/10.1108/RPJ-08-2019-0230/full/html.

Le Duigou, A., Barbé, A., Guillou, E., et al., 2019. 3D printing of continuous flax fibre reinforced biocomposites for structural applications. *Materials & Design*, 180, 107884. Available at: https://dx.doi.org/10.1016/j.matdes.2019.107884.

Le Duigou, A., Chabaud, G., Scarpa, F., et al., 2019. Bioinspired Electro-Thermo-Hygro Reversible Shape-Changing Materials by 4D Printing. *Advanced Functional Materials*, 29 (40), n/a. Available at: https://onlinelibrary.wiley.com/doi/abs/10.1002/adfm.201903280.

Le Duigou, A., Correa, D., Ueda, M., et al., 2020. A review of 3D and 4D printing of natural fibre biocomposites. *Materials & Design*, 194, 108911. Available at: https://dx.doi.org/10.1016/j.matdes.2020.108911.

Lee, A.Y., Zhou, A., An, J., et al., 2020. Contactless reversible 4D-printing for 3D-to-3D shape morphing. *Virtual and Physical Prototyping*, 15 (4), 481-495. Available at: https://doi.org/10.1080/17452759.2020.1822189.

Lee, C.H., Padzil, F.N.B.M., Lee, S.H., et al., 2021. Potential for Natural Fiber Reinforcement in PLA Polymer Filaments for Fused Deposition Modeling (FDM) Additive Manufacturing: A Review. *Polymers*, 13 (9), 1407. Available at: https://www.ncbi.nlm.nih.gov/pubmed/33925266.

Leist, S.K. and Zhou, J., 2016. Current status of 4D printing technology and the potential of light-reactive smart materials as 4D printable materials. *Virtual and Physical Prototyping*, 11 (4), 249-262. Available at: https://www.tandfonline.com/doi/abs/10.1080/17452759.2016.1198630.

Li, G. and Wang, A., 2016. Cold, warm, and hot programming of shape memory polymers. *Journal of Polymer Science.Part B, Polymer Physics*, 54 (14), 1319-1339. Available at: https://agris.fao.org/agris-search/search.do?recordID=US201600175243.

Li, J., Li, M., Ji, J., et al., 2023. All-in-One Print: Designing and 3D Printing Dynamic Objects Using Kinematic Mechanism Without Assembly. In: pp. 1-15.

Li, M., Chen, J., Shi, M., et al., 2019. Electroactive anti-oxidant polyurethane elastomers with shape memory property as non-adherent wound dressing to enhance wound healing. *Chemical Engineering Journal (Lausanne, Switzerland : 1996)*, 375, 121999. Available at: https://dx.doi.org/10.1016/j.cej.2019.121999.

Li, M., Pal, A., Aghakhani, A., et al., 2022. Soft actuators for real-world applications. *Nature Reviews. Materials*, 7 (3), 235-249. Available at: https://www.ncbi.nlm.nih.gov/pubmed/35474944.

Li, W., Guo, X., Fang, F., et al., May 30, 2021. Amplifying Laminar Jamming for Soft Robots by Geometry-Induced Rigidity. In: Piscataway: IEEE, pp. 11907-11912.

Lin, D., Yang, F., Gong, D., et al., 2023. Bio-inspired magnetic-driven folded diaphragm for biomimetic robot. *Nature Communications*, 14 (1), 163. Available at: https://www.ncbi.nlm.nih.gov/pubmed/36631471.

Lin, Y., Yang, G., Liang, Y., et al., 2020. Controllable Stiffness Origami “Skeletons” for Lightweight and Multifunctional Artificial Muscles. *Advanced Functional Materials*, 30 (31), n/a. Available at: https://onlinelibrary.wiley.com/doi/abs/10.1002/adfm.202000349.

Liu, G., Xiong, Y., and Zhou, L., 2021. Additive manufacturing of continuous fiber reinforced polymer composites: Design opportunities and novel applications. *Composites Communications*, 27, 100907. Available at: https://dx.doi.org/10.1016/j.coco.2021.100907.

Liu, H., Wang, F., Wu, W., et al., 2023. 4D printing of mechanically robust PLA/TPU/Fe3O4 magneto-responsive shape memory polymers for smart structures. *Composites. Part B, Engineering*, 248, 110382. Available at: https://dx.doi.org/10.1016/j.compositesb.2022.110382.

Liu, W., Chen, H., Ge, M., et al., 2018. Electroactive shape memory composites with TiO2 whiskers for switching an electrical circuit. *Materials & Design*, 143, 196-203. Available at: https://dx.doi.org/10.1016/j.matdes.2018.02.005.

Liu, W., Wu, N., and Pochiraju, K., 2018. Shape recovery characteristics of SiC/C/PLA composite filaments and 3D printed parts. *Composites.Part A, Applied Science and Manufacturing*, 108, 1-11. Available at: https://dx.doi.org/10.1016/j.compositesa.2018.02.017.

Liu, Y. and Chou, T.-., 2020. Additive manufacturing of multidirectional preforms and composites: from three-dimensional to four-dimensional. *Materials Today Advances*, 5, 100045. Available at: https://dx.doi.org/10.1016/j.mtadv.2019.100045.

Liu, Y., Shang, S., Mo, S., et al., 2021. Soft actuators built from cellulose paper: A review on actuation, material, fabrication, and applications. *Journal of Science. Advanced Materials and Devices*, 6 (3), 321-337. Available at: https://dx.doi.org/10.1016/j.jsamd.2021.06.004.

Liu, Y., Lv, H., Lan, X., et al., 2009. Review of electro-active shape-memory polymer composite. *Composites Science and Technology*, 69 (13), 2064-2068. Available at: https://dx.doi.org/10.1016/j.compscitech.2008.08.016.

Luo, J., Jiang, P., Li, X., et al., 2022. A Soft Self-Stable Actuator and Its Energy-Efficient Grasping. *Actuators*, 11 (4).

Maraveas, C., Bayer, I.S., and Bartzanas, T., 2022. 4D printing: Perspectives for the production of sustainable plastics for agriculture. *Biotechnology Advances*, 54, 107785. Available at: https://dx.doi.org/10.1016/j.biotechadv.2021.107785.

Markforged, a. *Aramid Fibre (Kevlar®)*. Available at: https://markforged.com/materials/continuous-fibers/kevlar.

Markforged, b. *Carbon Fibre*. Available at: https://markforged.com/materials/continuous-fibers/continuous-carbon-fiber.

Markforged, c. *Fibreglass*. Available at: https://markforged.com/materials/continuous-fibers/fiberglass.

Mather, P.T., Luo, X., and Rousseau, I.A., 2009. Shape Memory Polymer Research. *Annual Review of Materials Research*, 39 (1), 445-471. Available at: http://dx.doi.org/10.1146/annurev-matsci-082908-145419.

Mathur, V., Agarwal, P., Srinivasan, V., et al., 2023. Facet of 4D printing in biomedicine. *Journal of Materials Research*, 38 (1), 2-18. Available at: https://link.springer.com/article/10.1557/s43578-022-00779-9.

Matsuzaki, R., Ueda, M., Namiki, M., et al., 2016. Three-dimensional printing of continuous-fiber composites by in-nozzle impregnation. *Scientific Reports*, 6 (1), 23058. Available at: https://www.ncbi.nlm.nih.gov/pubmed/26965201.

Maurya, M.R., Sadasivuni, K.K., Cabibihan, J., et al., 2022. Modern Approach Towards Additive Manufacturing and 4D Printing: Emerging Industries, Challenges and Future Scope. In: Modern Approach Towards Additive Manufacturing and 4D Printing: Emerging Industries, Challenges and Future Scope*Shape memory composites based on polymers and*

metals for 4D printing. Switzerland: Springer International Publishing AG, pp. 389-412. Available at: http://ebookcentral.proquest.com/lib/SITE_ID/reader.action?docID=6992904&ppg=401.

McLellan, K., Sun, Y., and Naguib, H.E., 2022. A review of 4D printing: Materials, structures, and designs towards the printing of biomedical wearable devices. *Bioprinting,* 27, e00217. Available at: https://dx.doi.org/10.1016/j.bprint.2022.e00217.

Mehrpouya, M., Vahabi, H., Janbaz, S., et al., 2021. 4D printing of shape memory polylactic acid (PLA). *Polymer (Guilford),* 230, 124080. Available at: https://dx.doi.org/10.1016/j.polymer.2021.124080.

Meng, H. and Li, G., 2013. A review of stimuli-responsive shape memory polymer composites. *Polymer (Guilford),* 54 (9), 2199-2221. Available at: https://dx.doi.org/10.1016/j.polymer.2013.02.023.

Meng, Q. and Hu, J., 2009. A review of shape memory polymer composites and blends. *Composites. Part A, Applied Science and Manufacturing,* 40 (11), 1661-1672. Available at: https://dx.doi.org/10.1016/j.compositesa.2009.08.011.

Mishra, V., Negi, S., and Kar, S., 2023. FDM-based additive manufacturing of recycled thermoplastics and associated composites. *Journal of Material Cycles and Waste Management,* 25 (2), 758-784. Available at: https://link.springer.com/article/10.1007/s10163-022-01588-2.

Mitchell, A., Lafont, U., Hołyńska, M., et al., 2018. Additive manufacturing — A review of 4D printing and future applications. *Additive Manufacturing,* 24, 606-626. Available at: https://dx.doi.org/10.1016/j.addma.2018.10.038.

Mitkus, R., Cerbe, F., and Sinapius, M., 2022. 2 - 4D printing electro-induced shape memory polymers. In: M. BODAGHI, and A. ZOLFAGHARIAN, eds., *Smart materials in additive manufacturing.* Elsevier, pp. 19-51. Available at: https://www.sciencedirect.com/science/article/pii/B9780323954303000026.

Mohammadi, M., Kouzani, A.Z., Bodaghi, M., et al., 2023. 3D-Printed Phase-Change Artificial Muscles with Autonomous Vibration Control. *Advanced Materials Technologies,* .

Momeni, F., M.Mehdi Hassani.N, S., Liu, X., et al., 2017. A review of 4D printing. *Materials & Design,* 122, 42-79. Available at: https://dx.doi.org/10.1016/j.matdes.2017.02.068.

Moradi, M., Lalegani Dezaki, M., Kheyri, E., et al., 2023. Simultaneous FDM 4D printing and magnetizing of iron-filled polylactic acid polymers. *Journal of Magnetism and Magnetic Materials,* 568, 170425. Available at: https://dx.doi.org/10.1016/j.jmmm.2023.170425.

Muthe, L.P., Pickering, K., and Gauss, C., 2022. A Review of 3D/4D Printing of Poly-Lactic Acid Composites with Bio-Derived Reinforcements. *Composites.Part C, Open Access,* 8, 100271. Available at: https://dx.doi.org/10.1016/j.jcomc.2022.100271.

Muzaffar, A.K., Ahamed, M.B., Deshmukh, K., et al., 2020. Chapter 4 - 3D and 4D printing of pH-responsive and functional polymers and their composites. In: Chapter 4 - 3D and 4D printing of pH-responsive and functional polymers and their composites*3D and 4D printing*

of polymer nanocomposite materials. United States: Elsevier Inc, pp. 85-117. Available at: https://dx.doi.org/10.1016/B978-0-12-816805-9.00004-1.

N. N. Azmi, M. N. A. Ab Patar, S. N. A. Mohd Noor, et al., 2014. Testing standards assessment for silicone rubber. In: *2014 International Symposium on Technology Management and Emerging Technologies*, pp. 332-336.

Nachimuthu, M. and P.K., R., 2023. Inkjet four-dimensional printing of shape memory polymers: a review. *Rapid Prototyping Journal*, 29 (3), 437-446. Available at: https://search.proquest.com/docview/2780351797.

Narang, Y.S., Degirmenci, A., Vlassak, J.J., et al., 2018. Transforming the Dynamic Response of Robotic Structures and Systems Through Laminar Jamming. *IEEE Robotics and Automation Letters*, 3 (2), 688-695. Available at: https://ieeexplore.ieee.org/document/8141952.

Narang, Y.S., Vlassak, J.J., and Howe, R.D., 2018. Mechanically Versatile Soft Machines through Laminar Jamming. *Advanced Functional Materials*, 28 (17), 1707136. Available at: https://doi.org/10.1002/adfm.201707136.

Nazir, A., Abate, K.M., Kumar, A., et al., 2019. A state-of-the-art review on types, design, optimization, and additive manufacturing of cellular structures. *International Journal of Advanced Manufacturing Technology*, 104 (9-12), 3489-3510. Available at: https://link.springer.com/article/10.1007/s00170-019-04085-3.

Nezhad, I.S., Golzar, M., Behravesh, A.h., et al., 2022. Comprehensive study on shape shifting behaviors in FDM-based 4D printing of bilayer structures. *International Journal of Advanced Manufacturing Technology*, 120 (1-2), 959-974. Available at: https://link.springer.com/article/10.1007/s00170-022-08741-z.

Nugroho, W.T., Dong, Y., Pramanik, A., et al., 2021. Smart polyurethane composites for 3D or 4D printing: General-purpose use, sustainability and shape memory effect. *Composites.Part B, Engineering*, 223, 109104. Available at: https://dx.doi.org/10.1016/j.compositesb.2021.109104.

Oladapo, B.I., Kayode, J.F., Akinyoola, J.O., et al., 2023. Shape memory polymer review for flexible artificial intelligence materials of biomedical. *Materials Chemistry and Physics*, 293, 126930. Available at: https://dx.doi.org/10.1016/j.matchemphys.2022.126930.

Orozco, F., Horvat, D., Miola, M., et al., 2023. Electroactive Thermo-Pneumatic Soft Actuator with Self-Healing Features: A Critical Evaluation. *Soft Robotics*, 10 (4), 852-859. Available at: https://www.liebertpub.com/doi/abs/10.1089/soro.2022.0170.

Pacillo, G.A., Ranocchiai, G., Loccarini, F., et al., 2021. Additive manufacturing in construction: A review on technologies, processes, materials, and their applications of 3D and 4D printing. *Material Design & Processing Communications*, 3 (5), n/a. Available at: https://onlinelibrary.wiley.com/doi/abs/10.1002/mdp2.253.

Palaniyappan, S., Annamalai, G., Sivakumar, N.k., et al., 2023. Development of functional gradient multi-material composites using Poly Lactic Acid and walnut shell reinforced Poly Lactic Acid filaments by fused filament fabrication technology. *Journal of Building Engineering*, 65, 105746. Available at: https://dx.doi.org/10.1016/j.jobe.2022.105746.

Palaniyappan, S., Veeman, D., Sivakumar, N.K., et al., 2022. Development and optimization of lattice structure on the walnut shell reinforced PLA composite for the tensile strength and dimensional error properties. *Structures (Oxford)*, 45, 163-178. Available at: https://dx.doi.org/10.1016/j.istruc.2022.09.023.

Parandoush, P. and Lin, D., 2017. A review on additive manufacturing of polymer-fiber composites. *Composite Structures*, 182, 36-53. Available at: https://dx.doi.org/10.1016/j.compstruct.2017.08.088.

Patel, R., Desai, C., Kushwah, S., et al., 2022. A review article on FDM process parameters in 3D printing for composite materials. *Materials Today : Proceedings*, 60, 2162-2166. Available at: https://dx.doi.org/10.1016/j.matpr.2022.02.385.

Pei, E. and Loh, G.H., 2018. Technological considerations for 4D printing: an overview. *Progress in Additive Manufacturing*, 3 (1-2), 95-107. Available at: https://link.springer.com/article/10.1007/s40964-018-0047-1.

Pei, E., Loh, G.H., Harrison, D., et al., 2017. A study of 4D printing and functionally graded additive manufacturing. *Assembly Automation*, 37 (2), 147-153. Available at: https://www.emerald.com/insight/content/doi/10.1108/AA-01-2017-012/full/html.

Peng, B., Yang, Y., Ju, T., et al., 2021. Fused Filament Fabrication 4D Printing of a Highly Extensible, Self-Healing, Shape Memory Elastomer Based on Thermoplastic Polymer Blends. *ACS Applied Materials & Interfaces*, 13 (11), 12777-12788. Available at: http://dx.doi.org/10.1021/acsami.0c18618.

Peng, X. and Wang, H., 2018. Shape changing hydrogels and their applications as soft actuators. *Journal of Polymer Science. Part B, Polymer Physics*, 56 (19), 1314-1324. Available at: https://onlinelibrary.wiley.com/doi/abs/10.1002/polb.24724.

Pereira, T., Kennedy, J.V., and Potgieter, J., 2019. A comparison of traditional manufacturing vs additive manufacturing, the best method for the job. *Procedia Manufacturing*, 30, 11-18.

Pingale, P., Dawre, S., Dhapte-Pawar, V., et al., 2023. Advances in 4D printing: from stimulation to simulation. *Drug Delivery and Translational Research*, 13 (1), 164-188. Available at: https://link.springer.com/article/10.1007/s13346-022-01200-y.

Pinho, A.C., Buga, C.S., and Piedade, A.P., 2020. The chemistry behind 4D printing. *Applied Materials Today*, 19, 100611. Available at: https://dx.doi.org/10.1016/j.apmt.2020.100611.

Popescu, D., Zapciu, A., Amza, C., et al., 2018. FDM process parameters influence over the mechanical properties of polymer specimens: A review. *Polymer Testing*, 69, 157-166. Available at: https://dx.doi.org/10.1016/j.polymertesting.2018.05.020.

Quiñonez, P.A., Ugarte-Sanchez, L., Bermudez, D., et al., 2021. Design of Shape Memory Thermoplastic Material Systems for FDM-Type Additive Manufacturing. *Materials*, 14 (15), 4254. Available at: https://search.proquest.com/docview/2558846847.

Rafiee, M., Farahani, R.D., and Therriault, D., 2020. Multi-Material 3D and 4D Printing: A Survey. *Advanced Science*, 7 (12), 1902307-n/a. Available at: https://onlinelibrary.wiley.com/doi/abs/10.1002/advs.201902307.

Rahmatabadi, D., Aberoumand, M., Soltanmohammadi, K., et al., 2023. 4D Printing-Encapsulated Polycaprolactone–Thermoplastic Polyurethane with High Shape Memory Performances. *Advanced Engineering Materials*, 25 (6), 2201309-n/a. Available at: https://onlinelibrary.wiley.com/doi/abs/10.1002/adem.202201309.

Ram Kishore, S., Sridharan, A.P., Chadha, U., et al., 2023. Natural fiber biocomposites via 4D printing technologies: a review of possibilities for agricultural bio-mulching and related sustainable applications. *Progress in Additive Manufacturing*, .

Rastogi, P. and Kandasubramanian, B., 2019. Breakthrough in the printing tactics for stimuli-responsive materials: 4D printing. *Chemical Engineering Journal (Lausanne, Switzerland : 1996)*, 366, 264-304. Available at: https://dx.doi.org/10.1016/j.cej.2019.02.085.

Razzaq, M.Y., Gonzalez-Gutierrez, J., Farhan, M., et al., 2023. 4D Printing of Electroactive Triple-Shape Composites. *Polymers*, 15 (4), 832. Available at: https://www.ncbi.nlm.nih.gov/pubmed/36850116.

Regassa Hunde, B. and Debebe Woldeyohannes, A., 2022. Future prospects of computer-aided design (CAD) – A review from the perspective of artificial intelligence (AI), extended reality, and 3D printing. *Results in Engineering*, 14, 100478. Available at: https://dx.doi.org/10.1016/j.rineng.2022.100478.

Ren, L., Wu, Q., Liu, Q., et al., 2023. Stiffness-tunable and self-sensing integrated soft machines based on 4D printed conductive shape memory composites. *Materials & Design*, 228, 111851. Available at: https://dx.doi.org/10.1016/j.matdes.2023.111851.

Riley, K.S., Ang, K.J., Martin, K.A., et al., 2020. Encoding multiple permanent shapes in 3D printed structures. *Materials & Design*, 194, 108888. Available at: https://dx.doi.org/10.1016/j.matdes.2020.108888.

Robin M. Neville, Fabrizio Scarpa, and Alberto Pirrera , 2016. Shape morphing Kirigami mechanical metamaterials. *Scientific Reports*, 6 (1), 1-31067. Available at: https://www.ncbi.nlm.nih.gov/pubmed/27491945.

Roudný, P. and Syrový, T., 2022. Thermal conductive composites for FDM 3D printing: A review, opportunities and obstacles, future directions. *Journal of Manufacturing Processes*, 83, 667-677. Available at: https://dx.doi.org/10.1016/j.jmapro.2022.09.026.

Sadasivuni, K.K., Deshmukh, K., and AlAli AlMaadeed, M., 2019. 3D and 4D printing of pH-responsive and functional polymers and their composites. In: 3D and 4D printing of pH-responsive and functional polymers and their composites*3D and 4D printing of polymer nanocomposite materials*. United States: Elsevier, .

Saufi, S.A.S.A., Zuhri, M.Y.M., Dezaki, M.L., et al., 2021. Compression Behaviour of Bio-Inspired Honeycomb Reinforced Starfish Shape Structures Using 3D Printing Technology. *Polymers*, 13 (24), 4388. Available at: https://www.ncbi.nlm.nih.gov/pubmed/34960939.

Shahbazi, M., Jäger, H., Ettelaie, R., et al., 2023. Multimaterial 3D printing of self-assembling smart thermo-responsive polymers into 4D printed objects: A review. *Additive Manufacturing*, 71, 103598. Available at: https://dx.doi.org/10.1016/j.addma.2023.103598.

Shengda, Y., Wang, T., and Zhu, S., 2021. Research on energy consumption of fiber-reinforced fluidic soft actuators. *Smart Materials and Structures*, 30 (2), 025036. Available at: https://dx.doi.org/10.1088/1361-665X/abd7e6.

Siddique, S.H., Hazell, P.J., Wang, H., et al., 2022. Lessons from nature: 3D printed bio-inspired porous structures for impact energy absorption – A review. *Additive Manufacturing*, 58, 103051. Available at: https://dx.doi.org/10.1016/j.addma.2022.103051.

Siddiqui, S.F., Archer, A., Fandetti, D., et al., 2023. Cryogenic tensile performance of 3D printed onyx–continuous carbon fiber composites. *Rapid Prototyping Journal*, .

Skfivan, V., Sodomka, O., and Mach, F., Apr 2019. Magnetically Guided Soft Robotic Grippers. In: IEEE, pp. 126-130.

Soleyman, E., Rahmatabadi, D., Soltanmohammadi, K., et al., 2022. Shape memory performance of PETG 4D printed parts under compression in cold, warm, and hot programming. *Smart Materials and Structures*, 31 (8), 85002. Available at: https://iopscience.iop.org/article/10.1088/1361-665X/ac77cb.

Solomon, I.J., Sevvel, P., and Gunasekaran, J., 2021. A review on the various processing parameters in FDM. *Materials Today : Proceedings*, 37, 509-514. Available at: https://dx.doi.org/10.1016/j.matpr.2020.05.484.

Song, X., He, W., Chen, P., et al., 2021. Fused deposition modeling of poly (lactic acid)/almond shell composite filaments. *Polymer Composites*, 42 (2), 899-913. Available at: https://onlinelibrary.wiley.com/doi/abs/10.1002/pc.25874.

Spiegel, C.A., Hackner, M., Bothe, V.P., et al., 2022. 4D Printing of Shape Memory Polymers: From Macro to Micro. *Advanced Functional Materials*, 32 (51), 2110580-n/a. Available at: https://onlinelibrary.wiley.com/doi/abs/10.1002/adfm.202110580.

Stopforth, R., 2021. Conductive polylactic acid filaments for 3D printed sensors: Experimental electrical and thermal characterization. *Scientific African*, 14, e01040. Available at: https://dx.doi.org/10.1016/j.sciaf.2021.e01040.

Subash, A. and Kandasubramanian, B., 2020. 4D printing of shape memory polymers. *European Polymer Journal*, 134, 109771. Available at: https://dx.doi.org/10.1016/j.eurpolymj.2020.109771.

Sun, Y., Wan, Y., Nam, R., et al., 2019. 4D-printed hybrids with localized shape memory behaviour: Implementation in a functionally graded structure. *Scientific Reports*, 9 (1), 18754-13. Available at: https://www.ncbi.nlm.nih.gov/pubmed/31822764.

Sun, Z., Guo, Z., and Tang, W., 2019. Design of wearable hand rehabilitation glove with soft hoop-reinforced pneumatic actuator. *Journal of Central South University*, 26 (1), 106-119. Available at: https://link.springer.com/article/10.1007/s11771-019-3986-x.

Tamburrino, F., Graziosi, S., and Bordegoni, M., 2019. The influence of slicing parameters on the multi-material adhesion mechanisms of FDM printed parts: an exploratory study. *Virtual and Physical Prototyping*, 14 (4), 316-332. Available at: https://www.tandfonline.com/doi/abs/10.1080/17452759.2019.1607758.

Tao, R., Ji, L., Li, Y., et al., 2020. 4D printed origami metamaterials with tunable compression twist behavior and stress-strain curves. *Composites Part B: Engineering*, 201, 108344. Available at: https://www.sciencedirect.com/science/article/pii/S135983682033393X.

Tao, R., Xi, L., Wu, W., et al., 2020. 4D printed multi-stable metamaterials with mechanically tunable performance. *Composite Structures*, 252, 112663. Available at: https://www.sciencedirect.com/science/article/pii/S0263822320325897.

Tawk, C. and Alici, G., 2021. A Review of 3D-Printable Soft Pneumatic Actuators and Sensors: Research Challenges and Opportunities. *Advanced Intelligent Systems*, 3 (6), 2000223-n/a. Available at: https://onlinelibrary.wiley.com/doi/abs/10.1002/aisy.202000223.

Thanh Tai Nguyen and Jooyong Kim, 2020. 4D-Printing — Fused Deposition Modeling Printing and PolyJet Printing with Shape Memory Polymers Composite. *Fibers and Polymers*, 21 (10), 2364-2372. Available at: https://link.springer.com/article/10.1007/s12221-020-9882-z.

Tibbits, S., 2014. 4D Printing: Multi-Material Shape Change. *Architectural Design*, 84 (1), 116-121. Available at: https://api.istex.fr/ark:/67375/WNG-454CNDVK-L/fulltext.pdf.

Tripathi, H., Pandey, G.C., Dubey, A., et al., 2021. Superparamagnetic Manganese Ferrite and Strontium Bioactive Glass Nanocomposites: Enhanced Biocompatibility and Antimicrobial Properties for Hyperthermia Application. *Advanced Engineering Materials*, 23 (1), n/a. Available at: https://onlinelibrary.wiley.com/doi/abs/10.1002/adem.202000275.

van Manen, T., Janbaz, S., and Zadpoor, A.A., 2017. Programming 2D/3D shape-shifting with hobbyist 3D printers. *Materials Horizons*, 4 (6), 1064-1069. Available at: https://www.narcis.nl/publication/RecordID/oai:tudelft.nl:uuid:a963bc3e-9f7c-4c5c-bfac-9fa514b535f4.

van Vilsteren, S.J.M., Yarmand, H., and Ghodrat, S., 2021. Review of magnetic shape memory polymers and magnetic soft materials. *Magnetochemistry*, 7 (9), 123. Available at: https://search.proquest.com/docview/2576446163.

Vanderborght, B., Björn Verrelst, Ronald, V.H., et al., Exploiting Natural Dynamics to Reduce Energy Consumption by Controlling the Compliance of Soft Actuators. *The International Journal of Robotics Research*, 25 (4), 343-358. Available at: https://doi.org/10.1177/0278364906064566.

Vyavahare, S., Teraiya, S., Panghal, D., et al., 2020. Fused deposition modelling: a review. *Rapid Prototyping Journal*, 26 (1), 176-201. Available at: https://www.emerald.com/insight/content/doi/10.1108/RPJ-04-2019-0106/full/html.

Wan, X., Luo, L., Liu, Y., et al., 2020. Direct Ink Writing Based 4D Printing of Materials and Their Applications. *Advanced Science*, 7 (16), n/a. Available at: https://onlinelibrary.wiley.com/doi/abs/10.1002/advs.202001000.

Wang, F., Luo, F., Huang, Y., et al., 2023. 4D Printing Via Multispeed Fused Deposition Modeling. *Advanced Materials Technologies*, 8 (2), n/a. Available at: https://onlinelibrary.wiley.com/doi/abs/10.1002/admt.202201383.

Wang, G., Cheng, T., Do, Y., et al., Apr 21, 2018. Printed Paper Actuator. In: New York, NY, USA: ACM, pp. 1-12.

Wang, G., Zhu, K., Zhou, L., et al., 2023a. Blow Molding Artifacts with PneuFab Method. In: pp. 1-4.

Wang, G., Zhu, K., Zhou, L., et al., 2023b. PneuFab: Designing Low-Cost 3D-Printed Inflatable Structures for Blow Molding Artifacts. In: pp. 1-17.

Wang, H., Zhang, Z., Fu, K., et al., 2023. Four-Dimensionally Printed Continuous Carbon Fiber-Reinforced Shape Memory Polymer Composites with Diverse Deformation Based on an Inhomogeneous Temperature Field. *Polymers*, 15 (18), 3740. Available at: https://search.proquest.com/docview/2869546558.

Wang, J., Wang, Z., Song, Z., et al., 2019. Programming Multistage Shape Memory and Variable Recovery Force with 4D Printing Parameters. *Advanced Materials Technologies*, 4 (11), 1900535-n/a. Available at: https://onlinelibrary.wiley.com/doi/abs/10.1002/admt.201900535.

Wang, L., Zhang, F., Du, S., et al., 2023. Advances in 4D printed shape memory composites and structures: Actuation and application. *Science China.Technological Sciences*, 66 (5), 1271-1288. Available at: https://link.springer.com/article/10.1007/s11431-022-2255-0.

Wang, Q., Sun, X., Cobb, S., et al., 2016. 3D printing system: an innovation for small-scale manufacturing in home settings? - early adopters of 3D printing systems in China. *International Journal of Production Research*, 54 (20), 6017-6032. Available at: https://www.tandfonline.com/doi/abs/10.1080/00207543.2016.1154211.

Wang, W., Ping, P., Chen, X., et al., 2006. Polylactide-based polyurethane and its shape-memory behavior. *European Polymer Journal*, 42 (6), 1240-1249. Available at: https://dx.doi.org/10.1016/j.eurpolymj.2005.11.029.

Wang, X., Wu, L., Fang, B., et al., 2020. Layer jamming-based soft robotic hand with variable stiffness for compliant and effective grasping. *Cognitive Computation and Systems*, 2 (2), 44-49. Available at: http://digital-library.theiet.org/content/journals/10.1049/ccs.2020.0003.

Wang, Y., Li, L., Hofmann, D., et al., 2021. Structured fabrics with tunable mechanical properties. *Nature (London)*, 596 (7871), 238-243. Available at: https://www.ncbi.nlm.nih.gov/pubmed/34381233.

Wang, Z., Cai, L., Jiang, X., et al., 2023. 4DCurve: A Shape-Changing Fabrication Method Based on Curved Paths with a 3D Printing Pen. In: pp. 1-7.

Wehner, M., Tolley, M.T., Mengüç, Y., et al., 2014. Pneumatic Energy Sources for Autonomous and Wearable Soft Robotics. *Soft Robotics*, 1 (4), 263-274. Available at: https://doi.org/10.1089/soro.2014.0018.

Wen, Z. and Li, M., 2021. Compressive Properties of Functionally Graded Bionic Bamboo Lattice Structures Fabricated by FDM. *Materials*, 14 (16), 4410. Available at: https://search.proquest.com/docview/2565372203.

Wickramasinghe, S., Do, T., and Tran, P., 2020. FDM-Based 3D Printing of Polymer and Associated Composite: A Review on Mechanical Properties, Defects and Treatments. *Polymers*, 12 (7), 1529. Available at: https://search.proquest.com/docview/2424096162.

Willemstein, N., van der Kooij, H., and Sadeghi, A., 2022. 3D printing of soft fluidic actuators with graded porosity. *Soft Matter*, 18 (38), 7269-7279. Available at: https://search.proquest.com/docview/2721220188.

Wu, P., Yu, T., Chen, M., et al., 2022. Effect of printing speed and part geometry on the self-deformation behaviors of 4D printed shape memory PLA using FDM. *Journal of Manufacturing Processes*, 84, 1507-1518. Available at: https://dx.doi.org/10.1016/j.jmapro.2022.11.007.

Xavier, M.S., Tawk, C.D., Zolfagharian, A., et al., 2022. Soft Pneumatic Actuators: A Review of Design, Fabrication, Modeling, Sensing, Control and Applications. *IEEE Access*, 10, 59442-59485. Available at: https://ieeexplore.ieee.org/document/9785890.

Xu, J. and Song, J., 2015. 10 - Polylactic acid (PLA)-based shape-memory materials for biomedical applications. In: L. YAHIA, ed., *Shape memory polymers for biomedical applications.* Woodhead Publishing, pp. 197-217. Available at: https://www.sciencedirect.com/science/article/pii/B9780857096982000106.

Xu, T., Zhang, J., Salehizadeh, M., et al., 2019. Millimeter-scale flexible robots with programmable three-dimensional magnetization and motions. *Science Robotics*, 4 (29) Available at: https://www.ncbi.nlm.nih.gov/pubmed/33137716.

Yang, B., Baines, R., Shah, D., et al., 2021. Reprogrammable soft actuation and shape-shifting via tensile jamming. *Science Advances*, 7 (40), eabh2073. Available at: https://www.ncbi.nlm.nih.gov/pubmed/34597130.

Yang, H., 2019. *GeoMatries: Machine Learning-Empowered Simulation for 4D Printing and Morphing Materials Design*. Carnegie Mellon University. Available at: https://explore.openaire.eu/search/publication?articleId=dedup_wf_001::501feb0ee5da0fb48e5c25138b437959.

Yang, Y. and Jiao, P., 2023. Nanomaterials and nanotechnology for biomedical soft robots. *Materials Today Advances*, 17, 100338. Available at: https://dx.doi.org/10.1016/j.mtadv.2022.100338.

Yang, Z., Yang, H., Cao, Y., et al., 2023. Magnetically Actuated Continuum Medical Robots: A Review. *Advanced Intelligent Systems*, 5 (6), n/a. Available at: https://onlinelibrary.wiley.com/doi/abs/10.1002/aisy.202200416.

Yarali, E., Baniasadi, M., Zolfagharian, A., et al., 2022. Magneto-/ electro-responsive polymers toward manufacturing, characterization, and biomedical/ soft robotic applications. *Applied Materials Today*, 26, 101306. Available at: https://dx.doi.org/10.1016/j.apmt.2021.101306.

Yin, H., Zhang, W., Zhu, L., et al., 2023. Review on lattice structures for energy absorption properties. *Composite Structures*, 304, 116397. Available at: https://dx.doi.org/10.1016/j.compstruct.2022.116397.

Yin, R., Wang, D., Zhao, S., et al., 2021. Wearable Sensors-Enabled Human–Machine Interaction Systems: From Design to Application. *Advanced Functional Materials,* 31 (11), n/a. Available at: https://onlinelibrary.wiley.com/doi/abs/10.1002/adfm.202008936.

Yousefi, A., Jolaiy, S., Lalegani Dezaki, M., et al., 2023. 3D-Printed Soft and Hard Meta-Structures with Supreme Energy Absorption and Dissipation Capacities in Cyclic Loading Conditions. *Advanced Engineering Materials,* 25 (4), 2201189. Available at: https://doi.org/10.1002/adem.202201189.

Yu, W.W., Zhang, J., Wu, J.R., et al., 2017. Incorporation of graphitic nano-filler and poly(lactic acid) in fused deposition modeling. *Journal of Applied Polymer Science,* 134 (15), np-n/a. Available at: https://onlinelibrary.wiley.com/doi/abs/10.1002/app.44703.

Yu, Y., Wang, J., Han, X., et al., 2023. Fiber-Shaped Soft Actuators: Fabrication, Actuation Mechanism and Application. *Advanced Fiber Materials (Online),* 5 (3), 868-895. Available at: https://link.springer.com/article/10.1007/s42765-022-00254-4.

Yu, Y., Liu, H., Qian, K., et al., 2020. Material characterization and precise finite element analysis of fiber reinforced thermoplastic composites for 4D printing. *Computer Aided Design,* 122, 102817. Available at: https://dx.doi.org/10.1016/j.cad.2020.102817.

Yu, Y., Qian, K., Yang, H., et al., 2022. Hybrid IGA-FEA of fiber reinforced thermoplastic composites for forward design of AI-enabled 4D printing. *Journal of Materials Processing Technology,* 302, 117497. Available at: https://dx.doi.org/10.1016/j.jmatprotec.2022.117497.

Yuan, C., Lu, T., and Wang, T.J., 2022. Mechanics-based design strategies for 4D printing: A review. *Forces in Mechanics,* 7, 100081. Available at: https://dx.doi.org/10.1016/j.finmec.2022.100081.

Yue, C., Li, M., Liu, Y., et al., 2021. Three-dimensional printing of cellulose nanofibers reinforced PHB/PCL/Fe3O4 magneto-responsive shape memory polymer composites with excellent mechanical properties. *Additive Manufacturing,* 46, 102146. Available at: https://dx.doi.org/10.1016/j.addma.2021.102146.

Zafar, M.Q. and Zhao, H., 2020. 4D Printing: Future Insight in Additive Manufacturing. *Metals and Materials International,* 26 (5), 564-585. Available at: https://link.springer.com/article/10.1007/s12540-019-00441-w.

Ze, Q., Kuang, X., Wu, S., et al., 2020. Magnetic Shape Memory Polymers with Integrated Multifunctional Shape Manipulation. *Advanced Materials,* 32 (4), 1906657. Available at: https://doi.org/10.1002/adma.201906657.

Zeenat, L., Zolfagharian, A., Sriya, Y., et al., 2023. 4D Printing for Vascular Tissue Engineering: Progress and Challenges. *Advanced Materials Technologies,* .

Zeng, C., Liu, L., Bian, W., et al., 2022. Temperature-dependent mechanical response of 4D printed composite lattice structures reinforced by continuous fiber. *Composite Structures,* 280, 114952. Available at: https://dx.doi.org/10.1016/j.compstruct.2021.114952.

Zeng, C., Liu, L., Bian, W., et al., 2021. Bending performance and failure behavior of 3D printed continuous fiber reinforced composite corrugated sandwich structures with shape

memory capability. *Composite Structures*, 262, 113626. Available at: https://dx.doi.org/10.1016/j.compstruct.2021.113626.

Zeng, C., Liu, L., Bian, W., et al., 2020. 4D printed electro-induced continuous carbon fiber reinforced shape memory polymer composites with excellent bending resistance. *Composites.Part B, Engineering*, 194, 108034. Available at: https://dx.doi.org/10.1016/j.compositesb.2020.108034.

Zhang, C., Li, X., Jiang, L., et al., 2021. 3D Printing of Functional Magnetic Materials: From Design to Applications. *Advanced Functional Materials*, 31 (34), n/a. Available at: https://onlinelibrary.wiley.com/doi/abs/10.1002/adfm.202102777.

Zhang, F., Wang, L., Zheng, Z., et al., 2019. Magnetic programming of 4D printed shape memory composite structures. *Composites Part A: Applied Science and Manufacturing*, 125, 105571. Available at: https://dx.doi.org/10.1016/j.compositesa.2019.105571.

Zhang, F., Wen, N., Wang, L., et al., 2021. Design of 4D printed shape-changing tracheal stent and remote controlling actuation. *International Journal of Smart and Nano Materials*, 12 (4), 375-389. Available at: https://www.tandfonline.com/doi/abs/10.1080/19475411.2021.1974972.

Zhang, F., Xia, Y., Wang, L., et al., 2018. Conductive Shape Memory Microfiber Membranes with Core–Shell Structures and Electroactive Performance. *ACS Applied Materials & Interfaces*, 10 (41), 35526-35532. Available at: http://dx.doi.org/10.1021/acsami.8b12743.

Zhang, P., Sun, S., Duan, J., et al., 2023. Line width prediction and mechanical properties of 3D printed continuous fiber reinforced polypropylene composites. *Additive Manufacturing*, 61, 103372. Available at: https://dx.doi.org/10.1016/j.addma.2022.103372.

Zhang, Q., Pardo, M., Rudich, Y., et al., 2019. Chemical Composition and Toxicity of Particles Emitted from a Consumer-Level 3D Printer Using Various Materials. *Environmental Science & Technology*, 53 (20), 12054-12061. Available at: http://dx.doi.org/10.1021/acs.est.9b04168.

Zhang, Q., Kuang, X., Weng, S., et al., 2021. Shape-Memory Balloon Structures by Pneumatic Multi-material 4D Printing. *Advanced Functional Materials*, 31 (21), 2010872-n/a. Available at: https://onlinelibrary.wiley.com/doi/abs/10.1002/adfm.202010872.

Zhang, Q., Yan, D., Zhang, K., et al., 2015. Pattern Transformation of Heat-Shrinkable Polymer by Three-Dimensional (3D) Printing Technique. *Scientific Reports*, 5 (1), 8936. Available at: https://www.ncbi.nlm.nih.gov/pubmed/25757881.

Zhang, Q., Zhang, K., and Hu, G., 2016. Smart three-dimensional lightweight structure triggered from a thin composite sheet via 3D printing technique. *Scientific Reports*, 6 (1), 22431. Available at: https://www.ncbi.nlm.nih.gov/pubmed/26926357.

Zhang, Y., Qiao, J., Zhang, G., et al., 2021. Prediction of deformation and failure behavior of continuous fiber reinforced composite fabricated by additive manufacturing. *Composite Structures*, 265, 113738. Available at: https://dx.doi.org/10.1016/j.compstruct.2021.113738.

Zhang, Z., Demir, K.G., and Gu, G.X., 2019. Developments in 4D-printing: a review on current smart materials, technologies, and applications. *International Journal of Smart and*

Nano Materials, 10 (3), 205-224. Available at: https://www.tandfonline.com/doi/abs/10.1080/19475411.2019.1591541.

Zhao, Q., Qi, H.J., and Xie, T., 2015. Recent progress in shape memory polymer: New behavior, enabling materials, and mechanistic understanding. *Progress in Polymer Science*, 49-50, 79-120. Available at: https://dx.doi.org/10.1016/j.progpolymsci.2015.04.001.

Zhao, W., Zhang, F., Leng, J., et al., 2019. Personalized 4D printing of bioinspired tracheal scaffold concept based on magnetic stimulated shape memory composites. *Composites Science and Technology*, 184, 107866. Available at: https://dx.doi.org/10.1016/j.compscitech.2019.107866.

Zhu, W., Li, S., Peng, Y., et al., 2023. Effect of continuous fiber orientations on quasi-static indentation properties in 3D printed hybrid continuous carbon/Kevlar fiber reinforced composites. *Polymers for Advanced Technologies*, 34 (5), 1565-1574. Available at: https://onlinelibrary.wiley.com/doi/abs/10.1002/pat.5991.

Zolfagharian, A., Gharaie, S., Kouzani, A.Z., et al., 2022. Silicon-based soft parallel robots 4D printing and multiphysics analysis. *Smart Materials and Structures*, 31 (11), 115030. Available at: https://iopscience.iop.org/article/10.1088/1361-665X/ac976c.

Zolfagharian, A., Gregory, T.,M., Bodaghi, M., et al., 2020. Patient-specific 3D-Printed Splint for Mallet Finger Injury. *International Journal of Bioprinting*, 6 (2), 259. Available at: https://search.proquest.com/docview/2667808510.

Zolfagharian, A., Kouzani, A.Z., Khoo, S.Y., et al., 2016. Evolution of 3D printed soft actuators. *Sensors and Actuators. A. Physical.*, 250, 258-272. Available at: https://dx.doi.org/10.1016/j.sna.2016.09.028.

Zolfagharian, A., Mahmud, M.A.P., Gharaie, S., et al., 2020. 3D/4D-printed bending-type soft pneumatic actuators: fabrication, modelling, and control. *Virtual and Physical Prototyping*, 15 (4), 373-402. Available at: https://www.tandfonline.com/doi/abs/10.1080/17452759.2020.1795209.